

Copyright

by

Manuel A. Pacheco

1998

**Mass Transfer, Kinetics and Rate-based Modeling of Reactive
Absorption**

by

Manuel Antonio Pacheco, B.S., M.S

Dissertation

Presented to the Faculty of the Graduate School of

The University of Texas at Austin

in Partial Fulfillment

of the Requirements

for the Degree of


Doctor of Philosophy

The University of Texas at Austin

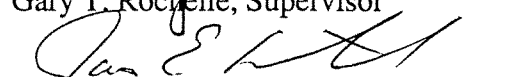
May, 1998

Mass Transfer, Kinetics and Rate-based Modeling of Reactive Absorption

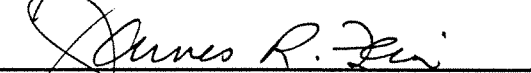
Approved by
Dissertation Committee:




Gary T. Rochelle, Supervisor




James E. Critchfield



James R. Fair



William Koros



Kamy Sepehrnoori

Dedication

To my family, especially to my wife Mary and my son Emmanuel.

Acknowledgements

I see Graduate School as an ideal way of expanding our horizon of knowledge not only on the specific area of our research, but also on other fascinating areas. Therefore, I would like to start recognizing a few professors that, through the courses they taught and their philosophy of teaching, made an important contribution not only to my humble background of knowledge, but also to my point of view about excellence in teaching, something that I love very much: Dr. Robert Schechter (Surface Phenomena), Dr. Roger Bonnecaze (Fluid Flow and Heat Transfer), Dr. Isaac Sanchez (Advanced Thermodynamics) and Dr. William Koros (Mass Transfer). Also, I would like to thank Dr. Delbert Ottmers for giving me the opportunity to be his TA and to give a few lectures for his class of Unit Operations. I enjoyed very much the interaction with him and the students.

I am grateful to Dr. Gary Rochelle for his guidance and patience, and for allowing me to work with him during the last three years. I am also grateful to the other members of my committee. I especially appreciate the different opportunities I had to discuss issues related to my research with Dr. James Critchfield. Through discussions with Dr. James Fair, I had a better understanding on different issues related to trayed and packed column modeling. Being the supervisor of my Master's thesis, I will always be grateful to Dr. Fair for trusting on me to conduct our research project and for believing on my

potential. I benefited a lot from graduate courses taught by Dr. Koros and Dr. Sepehrnoori on Mass Transfer and Applied Numerical Methods, respectively.

I would like to thank Aspen Technology for allowing me to use Aspen Plus® and RATEFRAC® and to Dr. Sivasubramanian at Aspen Tech for his technical assistance.

I appreciate the interaction with fellow graduate students, especially Sanjay Bishnoi, Lia Arthur, Paul Chisholm, Joe DeVincentis and Sho Kaganoi. Sho and I spent many hours in the lab working together and I believe that our team work was very beneficial. Sho's great sense of humor made me enjoy much more the long hours of work in the lab.

I would like to thank my friend Castor Gonzalez, his wife Efi and their family for being such a wonderful people and for making family life much more enjoyable in Austin, especially during the first few years of my experience as graduate students. Special recognition goes to my dear friend Hoshang Subawalla who was my office mate during my experience as a Master's student. Hoshang is not only an outstanding chemical engineer, but most importantly he is a person anybody should be proud of to have as a friend.

Our good friend Sr. Mary Jo Swift (Daughter of Charity) deserves a very special word. During our stay in Austin Sr. Mary Jo brought my wife, Marisol, and myself a lot closer to the teachings of our church. Being my wife's coworker for sometime and our friend, Sr. Mary Jo became our role model because of her hard working nature, sense of responsibility, faith and altruism.

This work was completed under the financial support of Intevp. The diligence of the people of the department of Human Resources in taking care of the needs of my family and my own's is greatly appreciated.

To my parents I own too many things to mention here, but above all the education, good example and kindness I have received from them have made an important influence on me. Most importantly I would like to thank the patient ones: my wife, Mary, and my now one-month old son, Emmanuel. They always understood that I frequently had to spend some extra time on my work, without much complaint on their part. My wife is a caring mother for my son which has made the time I spend at work much more enjoyable.

Mass Transfer, Kinetics and Rate-based Modeling of Reactive Absorption

Publication No. _____

Manuel Antonio Pacheco, Ph.D.

The University of Texas at Austin, 1998

Supervising Professor: Gary T. Rochelle

A mass transfer model was developed to describe the rates of mass transfer of reactive absorbing gases. This model is based on the Danckwerts surface renewal model and uses the concept of time-mean concentrations. The diffusion of reactants and products through the liquid boundary layer, reversibility and interaction between the different chemical reactions is accounted for by the model. The model was applied to reactive absorption of CO₂ into diglycolamine and methyldiethanolamine and blends of these reactive solvents. The electrolyte NRTL thermodynamic model was used to account for the non-ideality of the gas-liquid systems. The model was validated using rates of mass transfer measured in a wetted-wall column reactor at 25°C to 100°C with CO₂ loading varying from 0.015 to 0.55 moles CO₂/moles of reactive solvent. It was found that the reversibility of the chemical reactions affects the mass transfer rate at temperatures as low as 60°C. The interaction between the diffusion of reactants

and products, the reversibility of the chemical reactions, and the electrolyte interaction parameter $\tau(\text{water, DGACOO}^-\text{-MDEAH}^+)$ was found to be crucial for predicting the mass transfer rates, especially at temperatures above 60°C.

The mass transfer model was integrated to simulate the selective absorption of H_2S from a gas stream containing CO_2 using aqueous methyldiethanolamine. A general framework was developed to model the transport processes that take place during reactive absorption when both rate and equilibrium-controlled reactions occur in the liquid phase. A rate-based distillation column module, RATEFRAC[®], was used for the column integration. The Maxwell-Stefan approach to multicomponent mass transfer and the enhancement factor theory were utilized. It was found that in packed columns CO_2 absorption is controlled by diffusion with fast chemical reactions; in trayed columns it is controlled primarily by physical absorption. Gas-film resistance is never significant for CO_2 absorption. For H_2S absorption gas and liquid-film resistances are important, and diffusion of bisulfide controls the liquid-film resistance. Heat effects produce temperature bulges which can cause equilibrium “pinches” at the maximum temperature. This gives an optimum packing height for the H_2S removal. Trayed columns perform better than packed columns for H_2S removal, primarily because of the larger number of mass transfer units; however, this conclusion is subject to the accuracy of the models used for estimating the mass transfer coefficients and interfacial area for mass transfer in the contactors.

RATEFRAC[®] is property of Aspen Technology Inc. and Koch Engineering Company Inc.

Table of Contents

List of Tables	xv
List of Figures.....	xviii
Chapter 1. Introduction.....	1
1.1. Interfacial Mass Transfer and Chemical Reactions.....	3
1.2 Gas Treating with Aqueous Alkanolamines.....	5
1.3 Scope and Overview of the dissertation	8
1.4 Nomenclature.....	12
1.5 References.....	12
Chapter 2. Mass and Heat Transfer with Chemical Reactions.....	15
2.1. Introduction.....	15
2.2. Fick's Law and Maxwell-Stefan Approaches to Mass Transfer	15
2.2.1 Mass Transfer Coefficients.....	18
2.2.2 Relationship Between Diffusive Fluxes and Molar Fluxes	21
2.2.3 Effective Diffusivity Methods	22
2.3. Mass Transfer Interaction Effects.....	24
2.4. Effect of Chemical Reactions on Mass Transfer.....	26
2.4.1 The Maxwell-Stefan Approach for Mass Transfer in Gas-Liquid Reactive Systems	26
2.4.2 Gas-Liquid Reactions and Surface Renewal Theory.....	30
2.5 Kinetics of Gas-liquid Reactions: Reactive Absorption of CO ₂ and H ₂ S in Aqueous Alkanolamines	35
2.5.1 Chemistry of CO ₂ -alkanolamine Systems	35
2.5.2 Chemistry of H ₂ S-alkanolamine Systems.....	38
2.6 Non-Isothermal Gas Absorption: Interfacial Heat Transfer	39
2.7 Temperature Bulges and Reactive Absorption.....	42
2.8 Nomenclature.....	46
2.9 References.....	48

Chapter 3. Packed and Trayed Column Modeling.....	51
3.1. Introduction.....	51
3.2. Trayed Column Hydrodynamics.....	51
3.2.1 Mass Transfer Characteristics.....	56
3.2.2 Flooding Condition.....	60
3.3. Packed Column Hydrodynamics	61
3.3.1. Loading and Flooding Conditions	64
3.3.2. Mass Transfer Characteristics.....	69
3.4. Comparison Between Trays and Packing Performance.....	71
3.5 Nomenclature.....	75
3.6 References.....	79
Chapter 4. Reactive Absorption with Reversible Chemical Reactions: Experimental Methods and Contactor Characterization.....	81
4.1. Introduction.....	81
4.2. Rate Measurements in the Wetted-wall Column.....	85
4.3. Column Characterization.....	89
4.3.1. Liquid-Film Mass Transfer Coefficients	90
4.3.2. Gas-Film Mass Transfer Coefficients.....	96
4.3.3. Marangoni Effects	101
4.4. Conclusions.....	105
4.5 Nomenclature.....	106
4.6. References.....	108
Chapter 5. Reactive Absorption with Reversible Chemical Reactions: Model Development and Validation	111
5.1 Introduction.....	111
5.2 Reactive System Studied	114
5.3 Model Development	115
5.3.1 Mass Balance of Molecular CO ₂	120
5.3.2 Total CO ₂ Diffusion-Reaction	121
5.3.3 Mass Balance for the Reactive Solvents.....	123
5.3.4 Charge Flux	124

5.3.5 Mass Balance of Carbamate	125
5.3.6 Mass Transfer Resistance at the Vapor Phase	127
5.3.7 Numerical Solution.....	127
5.4 Results and Discussion	128
5.4.1 Approach.....	128
5.4.2 Reactive Absorption into Aqueous Solutions of MDEA.....	129
5.4.3 Reactive Absorption into Aqueous Solutions of DGA.....	133
5.4.4 Reactive Absorption into Aqueous Solutions of Mixtures of MDEA and DGA	136
5.4.5. Effect of Individual Reactions on the Mass Transfer Enhancement and Equilibrium Approach.....	144
5.4.6. Diffusion of Reactants and Products	152
5.4.7. Calculated Mass Transfer Enhancement: Contribution of the DGA Reaction	154
5.5 Conclusions.....	159
5.6 Nomenclature.....	160
5.7 References.....	161
Chapter 6. Rate-Based Modeling of Reactive Absorption Columns.....	166
6.1 Introduction.....	166
6.2. Mass Transfer Model.....	169
6.2.1 Reactive System.....	169
6.2.2 Mass Transfer at the Liquid Boundary Layer: Point Modeling	171
6.3 Physical and Transport Properties	176
6.4 Configurations of Contactors Studied and Feed Composition	177
6.5 Modeling Approach.....	178
6.6 Results and Discussion	183
6.6.1 Modeling of Packed Columns	183
6.6.2 Comparison Between Trayed and Packed Columns.....	198
6.7 Conclusions.....	203
6.8 Nomenclature.....	204
6.9 References.....	207

Chapter 7. Conclusions and Future Directions	211
7.1 Conclusions.....	211
7.1.1 Reaction-Diffusion Modeling and Validation	211
7.1.2. Rate-based Modeling of Reactive Absorption Columns	213
7.2. Recommendations on Future Directions	215
7.2.1 Reaction-Diffusion Studies.....	215
7.2.2 Modeling of Reactive Absorption Columns.....	217
Appendix A. Experimental Rate Measurements of Reactive Absorption of CO ₂	220
Appendix B. Thermo-Physical and Transport Properties.....	227
B.1. System MDEA-water-CO ₂	227
B.1.1 Viscosity of the Solution.....	227
B.1.2. Density of the Solution	228
B.1.3. Diffusivity of CO ₂ in the Solution	229
B.1.4. Diffusivity of MDEA in the Solution	232
B.1.5. Solubility of CO ₂ in the Solution.....	234
B.2. System DGA-water-CO ₂	237
B.2.1. Viscosity of DGA Solutions	238
B.2.2. Density of DGA Solutions.....	238
B.2.3. Diffusivity of CO ₂ in the Solution.....	238
B.2.4. Diffusivity of DGA in DGA Solutions	239
B.2.5. Solubility of CO ₂ in the Solution	241
B.3. System DGA-MDEA-water-CO ₂	242
B.4. Properties for the Vapor Phase.....	243
B.4.1. Diffusion Coefficient of CO ₂	243
B.4.2. Density of the Gas Phase	244
B.4.2. Viscosity of the Gas Phase.....	245
B.5. Nomenclature.....	245
B.6. References.....	247

Appendix C. Solution of Diffusion-Reaction Equations for Reactive Absorption: Parallel Reactions	249
C.1. Approximate Solution	249
C.2. Comparison Between Numerical and Approximate Solutions	262
C.3. Comparison between MCFLUX and this work for the system DGA-MDEA-water-CO ₂	270
C.4. Solution of the diffusion-reaction equation assuming instantaneous reaction for the fast reaction	272
C.5. Comparison between the enhancement factor model used in this work and that used by Glasscock and Rochelle (1993)	273
C.6. Nomenclature	275
C.7. References	277
Appendix D. Equilibrium Calculations for the System DGA-MDEA-water-CO ₂	278
References	282
Vita	291

List of Tables

Table 4.1. Experimental data for k_{L,CO_2}^o and theoretical calculations.....	95
Table 4.2. Experimental conditions and results in the measurement of k_g in the reactor.	100
Table 5.1. Experimental Conditions for the Rate Measurements. System MDEA-water- CO_2	129
Table 5.2. Experimental Conditions for the Rate Measurements. System DGA-water- CO_2	133
Table 5.3. Experimental Conditions for the Rate Measurements. System DGA-MDEA-water- CO_2	136
Table 5.4. Results of the regression of $D_{p,r}$ and $\tau(\text{water, DGACOO}^-\text{-MDEAH}^+)$ for the system DGA-MDEA- H_2O - CO_2	141
Table 6.1. Characteristics of the packed and trayed columns.....	177
Table 6.2. Composition of the reactive solvent and feed vapor stream, L/G =0.823 mole/mole.....	178
Table 6.3. Comparison between the performance of trayed and packed columns.....	199
Table A.1. Rate data of reactive absorption of CO_2 into aqueous MDEA solutions. 35wt% MDEA/65wt% water.	220
Table A.2. Rate data of reactive absorption of CO_2 into aqueous MDEA solutions. 50wt% MDEA/50wt% water.	220

Table A.3. Rate data of reactive absorption of CO ₂ into aqueous diglycolamine solutions. 50wt% DGA/50wt% water.....	222
Table A.4. Rate data of reactive absorption of CO ₂ into aqueous diglycolamine solutions. 25wt% DGA/75wt% water.....	222
Table A.5. Rate data of reactive absorption of CO ₂ into aqueous solutions of DGA and MDEA. 5wt% DGA-45wt% water/50wt% water. Temperature: 40°C.....	222
Table A.6. Rate data of reactive absorption of CO ₂ into aqueous solutions of DGA and MDEA. 5wt% DGA-45wt% water/50wt% water. Temperature: 60°C.....	223
Table A.7. Rate data of reactive absorption of CO ₂ into aqueous solutions of DGA and MDEA. 5wt% DGA-45wt% water/50wt% water. Temperature: 80°C.....	224
Table A.8. Rate data of reactive absorption of CO ₂ into aqueous solutions of DGA and MDEA. 5wt% DGA-45wt% water/50wt% water. Temperature: 100°C.....	225
Table A.9. Rate data of reactive absorption of CO ₂ into aqueous solutions of DGA and MDEA. 15wt% DGA-35wt% water/50wt% water. Temperature: 40°C.....	225
Table A.10. Rate data of reactive absorption of CO ₂ into aqueous solutions of DGA and MDEA. 15wt% DGA-35wt% water/50wt% water. Temperature: 80°C.....	226

Table A.11. Rate data of reactive absorption of CO ₂ into aqueous solutions of DGA and MDEA. 15wt% DGA-35wt% water/50wt% water. Temperature: 100°C.....	226
Table B.1. Correlations and Source of Data for Physical and Transport Properties for the System MDEA-water-CO ₂	227
Table B.2. Parameters needed for the correlation of Licht and Weiland (1989).	229
Table B.3. Correlations and Source of Data for Physical and Transport Properties for the System DGA-water-CO ₂	237
Table B.4. Experimental values of viscosity of CO ₂ and N ₂ (Source: Reid et al. 1988).....	245
Table C.1 Comparison between the numerical solution and approximate approach.....	263

List of Figures

Figure 1.1. Representation of the mass transfer processes found in reactive absorption. The curves in the liquid film represent concentration profiles.....	4
Figure 1.2 Structure of the most commonly used amines.	7
Figure 2.1. Diffusion flux for binary and ternary systems as a function of the composition gradient. Representation taken from Taylor and Krishna (1993).....	25
Figure 2.2. Qualitative representation of the temperature profiles predicted by Equations 2.72 assuming linear profiles ($N_k = a + bz$) for the interfacial fluxes. $N_{\text{gas}} = 0.028 + 0.035z'$ (kmol/m ² hr) and $N_{\text{water}} = 0.04 - 0.08z'$ (kmol/m ² hr).....	45
Figure 3.1. Interfacial areas on trays predicted by Scheffe and Weiland (1987) for valve trays and Miyahara et al. (1990) on sieve trays.....	60
Figure 3.2. Qualitative relationship between the liquid holdup and the phase loads in a packed column.....	67
Figure 3.3. Sample calculation of mass transfer coefficients and interfacial area on a tray and packing segment. $0.77 < L/G$ (mole/mole) < 5.4. Superficial liquid velocity: 10.6 kg/m ² sec. Weir height: 0.0508 m. Column diameter: 1.68 m. $P_{\text{tot}} = 20$ atm. 1.5'' Pall rings.	73
Figure 4.1. Detailed diagram of the wetted-wall column contactor.	86
Figure 4.2. Flow Diagram of the Experimental Set up.....	87

Figure 4.3. Desorption of CO ₂ from water in the wetted wall column. Temperature: 50°C. Total pressure: 100 psig; k_{L,CO_2}^o determined: 9.63E-5 m/sec.	92
Figure 4.4. Comparison between experimentally measured and calculated physical mass transfer coefficients of CO ₂ in the wetted-wall column. Measurements of desorption from water and ethylene glycol solutions.....	94
Figure 4.5. Experimental data and correlation of the gas-film mass transfer coefficient in the wetted-wall column.	101
Figure 5.1. Second-order rate constant for the reaction between CO ₂ and MDEA.....	130
Figure 5.2. Effect of the reversibility of the reaction between CO ₂ and MDEA on the enhancement of the mass transfer. Experimental data for 35 and 50 wt% MDEA at 0.7 to 7.4 atm CO ₂ in the wetted-wall column.	131
Figure 5.3. Comparison between the calculated and measured interfacial fluxes of CO ₂ for the system MDEA-water-CO ₂	132
Figure 5.4. Second-order rate constant for the reaction between CO ₂ and DGA.....	134
Figure 5.5. Comparison between the experimental and measured interfacial fluxes of CO ₂ for the system DGA-water- CO ₂	135

Figure 5.6. Sensitivity of calculated CO ₂ flux (N _{CO₂}) to values (P _j) of the rate constants, diffusion coefficients of reactants and products, and thermodynamic interaction parameters. 5wt% DGA/45wt% MDEA, 40°C.....	137
Figure 5.7. Sensitivity of calculated CO ₂ flux (N _{CO₂}) to values of the diffusion coefficients of reactants and products (D _{p,r}), and thermodynamic interaction parameter τ (water, DGACOO ⁻ -MDEAH ⁺). 5wt% DGA/45wt% MDEA.	138
Figure 5.8. Diffusivities of reactants and products obtained from the measured interfacial mass transfer rates of CO ₂ for the system DGA-MDEA-water- CO ₂	139
Figure 5.9. Parameter τ (water, DGACOO ⁻ -MDEAH ⁺) of the electrolyte NRTL model obtained from the experimental CO ₂ fluxes for the system DGA-MDEA-water-CO ₂	140
Figure 5.10. Comparison between the measured and calculated fluxes of CO ₂ for the system DGA-MDEA-water-CO ₂	142
Figure 5.11. Effect of the reversibility of the chemical reactions for the system DGA-MDEA-water-CO ₂ . 50 wt% total reactive solvent. ..	143
Figure 5.12. Individual approach to interfacial equilibrium for the DGA-CO ₂ and MDEA-CO ₂ reaction and comparison with the overall interfacial equilibrium. 50 wt% total reactive solvent, both 5wt%DGA-45wt%MDEA and 15wt%DGA-35wt%MDEA.....	145

Figure 5.13. Comparison between the interfacial mass transfer rates of CO ₂ predicted considering the DGA-CO ₂ reaction as instantaneous and as rate-controlled.....	149
Figure 5.14. Effect of the DGA regeneration by the MDEA-CO ₂ reaction on the interfacial mass transfer rate of CO ₂	150
Figure 5.15. Difference between the interfacial and liquid bulk concentration for the fast reactant, DGA.....	151
Figure 5.16. Contribution of the fluxes of the reaction products to the interfacial CO ₂ flux.....	153
Figure 5.17. Calculated enhancement factors for CO ₂ under low mass transfer driving force ($P_{CO_2} = 1.05P_{CO_2}^*$) for reactive absorption of CO ₂ into aqueous MDEA and blends of MDEA and DGA. $k_{L,CO_2}^o = 4.E-3$ cm/sec.	155
Figure 5.18. Approach to equilibrium at the interface under low mass transfer driving force ($P_{CO_2} = 1.05P_{CO_2}^*$) for reactive absorption of CO ₂ into aqueous MDEA and blends of MDEA and DGA. $k_{L,CO_2}^o = 4.E-3$ cm/sec.	156
Figure 5.19. Effect of mass transfer driving force on the mass transfer enhancement for reactive absorption of CO ₂ into a aqueous mixture of 5 wt% DGA and 45 wt% MDEA. $k_{L,CO_2}^o = 4.E-3$ cm/sec.	157
Figure 5.20. Effect of mass transfer driving force on the approach to equilibrium at the interface. System: 5 wt% DGA and 45 wt% MDEA. $k_{L,CO_2}^o = 4.E-3$ cm/sec.....	158

Figure 6.1. Approach used for modeling reactive absorption with RATEFRAC®	180
Figure 6.2. Interfacial mass transfer rates for the packed column described in Table 6.1.	184
Figure 6.3. Profiles of enhancement factors calculated for the packed column described on Table 6.1. $L/G = 0.823$ moles/moles. Total packing height: 8 m.	185
Figure 6.4. Concentration gradient of bisulfide and fluxes of H_2S and bisulfide. Packed column described on Table 6.1. $L/G = 0.823$ mole/mole. Total packing height: 8 m.	186
Figure 6.5. Temperature profiles calculated for the packed column described on Table 6.1. Total packing height 8 m. $L/G = 0.823$ moles/moles.	188
Figure 6.6. Contribution of the different heat effects on the temperature profile. Packed column described in Table 6.1.	189
Figure 6.7. Detailed results on the point modeling. Packed column described in Table 6.1	193
Figure 6.8. Murphree vapor-phase efficiencies for CO_2 and H_2S . Packed column described in Table 6.1.	192
Figure 6.9. H_2S performance of the packed absorber described in Table 6.1. 15 non-equilibrium segments.	194
Figure 6.10. Liquid-side mass transfer resistance and gas-side mass transfer coefficients for the packed column described in Table 6.1.	195

Figure 6.11. H ₂ S pinch at the temperature bulge. Packed column described in Table 6.1 and conditions of the reactive solvent and vapor feed described in Table 6.2. Packing height 8 m. Squares □,■: operating curves (P _{H₂S}), circles ○,●: equilibrium curves (P [*] _{H₂S}).....	197
Figure 6.12. H ₂ S pinch at the top of the absorber. Packed column described in Table 6.1 and conditions of the reactive solvent and vapor feed described in Table 6.2. Packing height: 8 m. Squares □,■: operating curves (P _{H₂S}), circles ○,●: equilibrium curves (P [*] _{H₂S}).....	198
Figure 6.13. Representation of the approach to pinch for H ₂ S. Trayed and packed columns with same overall removal of CO ₂ . The packed and trays columns are described in Table 6.1. Squares □,■: operating curves (P _{H₂S}), circles ○,●: equilibrium curves (P [*] _{H₂S}).....	201
Figure 6.14. Comparison of the enhancement factors for CO ₂ and H ₂ S for trays and packed columns. Contactors with the same overall removal of CO ₂	202
Figure B.1. Diffusivity of N ₂ O in aqueous MDEA solutions.....	230
Figure B.2. Diffusion coefficients of CO ₂ in pure water.....	231
Figure B.3. Diffusion coefficients of N ₂ O in pure water.....	232
Figure B.4. Diffusion coefficients of MDEA in MDEA solutions measured by Snijder et al. (1993).	233
Figure B.5. Henry's Law Constant of N ₂ O in Pure Water.	235
Figure B.6. Henry's law constant of CO ₂ in pure water.....	235
Figure B.7. Henry's law constant of N ₂ O in different MDEA solutions. Data from Al-Ghawas et al. (1989).....	236

Figure B.8. Henry's law constant of N_2O in 50wt% MDEA.....	237
Figure B.9. Viscosity of aqueous DGA solutions. Jefferson Chemical Company. Technical Bulletin (1970).	238
Figure B.10. Density of aqueous solutions of DGA. Jefferson Chemical Company. Technical Bulletin (1970).	239
Figure B.11. Diffusion coefficients of DEA and DGA at 25°C.	240
Figure B.12. Comparison between the experimental diffusivities of DEA and the predicted diffusivities of DGA.	241
Figure B.13. Henry's constant of CO_2 in aqueous DGA solutions. Calculated using experimental data for H_{N_2O} from Littel (1991) and the N_2O - CO_2 analogy.....	242
Figure C.1. Predictions of enhancement factors, liquid-phase reactant gradients and approach to equilibrium at the interface.....	259
Figure C.2. Effect of the Hatta number for the slower reaction on the mass transfer enhancement and interfacial equilibrium.	260
Figure C.3. Concentration gradients obtained from the numerical and approximate solutions. Case 1 presented in Table C.1. $\theta =$ 0.0101.	264
Figure C.4. Concentration gradients obtained from the numerical and approximate solutions. Case 4 presented in Table C.1. $\theta = 0.754$..	265
Figure C.5. Concentration gradient for the diffusing gas A and equilibrium concentrations for each reaction obtained from the numerical solution. Case 4 presented in Table C.1. $\theta = 0.754$	266

Figure C.6. Concentration gradient for the diffusing gas A and equilibrium concentrations for each reaction obtained from the numerical solution. Case 2 presented in Table C.1. $\theta = 0.155$	267
Figure C.7. Effect of the slower reaction on the regeneration of the faster reactant and equilibrium limitation for the faster reaction.	269
Figure C.8. Mass transfer enhancement of component A predicted by the approximate solution of the diffusion-reaction equations.	270
Figure C.9. Enhancement factors for component A predicted using the approach by DeCoursey (1992) and Glasscock and Rochelle (1993) for a second order reversible reaction. Varying equilibrium constant.	274
Figure C.10. Enhancement factors for component A predicted using the approach by DeCoursey (1992) and Glasscock and Rochelle (1993) for a second order reversible reaction. Varying Hatta number.....	275
Figure D.1 Comparison between calculated equilibrium partial pressures of CO_2 for the systems 50wt% MDEA and 5wt% DGA-45wt% MDEA.....	278
Figure D.2 Comparison between calculated equilibrium partial pressures of CO_2 for the systems 50wt% MDEA and 15wt% DGA-35wt% MDEA.....	279
Figure D.3. Concentrations of free DGA for the systems 5 wt% DGA-45 wt% MDEA and 15 wt% DGA-35 wt% MDEA as predicted by the electrolyte NRTL model.....	280

Figure D.4. Concentrations of free MDEA for the systems 5 wt% DGA-45 wt% MDEA and 15wt% DGA-35wt% MDEA as predicted by the electrolyte NRTL model.	281
---	-----

Chapter 1

Introduction

Processes where mass transfer is accompanied by chemical reactions are frequently encountered in practical applications under the form of reactive absorption or reactive distillation. Zarzycki and Chacuk (1993) divided these processes into two categories:

i) Processes where mass transfer and the chemical reactions occur consecutively, that is one process follows the other. An example of this type of situation is a catalytic reaction in which the reactants first have to diffuse into the active sites of the catalyst, and then a chemical reaction takes place followed by the diffusion of the products from the catalyst surface to the bulk phase.

ii) Processes where mass transfer and the chemical reactions occur simultaneously. In this situation the mass transfer is coupled closely with the chemical reactions and both of these processes take place in the same fluid volume. An illustration is the absorption of gaseous components in a liquid phase followed by chemical reactions between these components and other species in the liquid phase. In this phenomenon the chemical reactions in the liquid phase occur simultaneously with the diffusion of the reaction reactants and products between the vapor-liquid interface and the liquid bulk. The interfacial rates of mass transfer of the gaseous components are affected by the rates of the chemical reactions in the liquid phase. Another example of this situation occurs in catalytic

distillation where reactants and products diffuse through the pores of the catalyst pellets and simultaneous reactions take place (Subawalla, 1997).

Reactive absorption processes are mainly used in two broad areas:

ii.1) The first is to remove one or more undesired components from a gas or vapor stream. An example of this is the removal of CO_2 from gases in ammonia production. Another example is the removal of different acid gases, such as CO_2 , H_2S and COS from natural gas streams to meet the gas specification.

In some processes it is desired to remove only one of several active components present in the gas. This process is called selective absorption. In this process differences in gas solubilities and/or reaction rates in the liquid are utilized to accomplish the desired selectivity.

ii.2) The other aim of reactive absorption is to produce a particular component in the liquid phase. In this case one or more gases are absorbed, chemical reactions between the absorbed gases and a liquid reactant take place to produce the desired chemical species. Often this type of reactive process occur in the presence of a solid catalyst. An illustration of a process without catalyst is the production of detergents by absorption and reaction of SO_2 in fatty alcohols. Another example is the chemical absorption of oxides of nitrogen (NO , NO_2 and N_2O_4) in water to yield a product of 60% by weight of nitric acid (Carberry, 1976).

In the present work the phenomena of mass and heat transfer accompanied with chemical reactions present in gas absorption processes are studied. In this chapter an overview is given on the effects of the chemical reactions on the mass

and heat transfer processes. The scope of the work is presented and an overall description is given on the theoretical and experimental parts of this dissertation.

1.1. INTERFACIAL MASS TRANSFER AND CHEMICAL REACTIONS

When interfacial mass transfer of an absorbing gas is accompanied by mass transfer and diffusion of reactants and reaction products through the boundary layer, the interfacial mass transfer rate is affected by the rate of the chemical reaction and the rate of diffusion of reactants and products. The true driving force for mass transfer is the chemical potential gradient, however, in practice mole fractions or partial pressure gradients are preferred as a way of defining driving forces. Figure 1.1 is a schematic representation of the different mass transfer resistances that can be found in reactive absorption. The diffusive flux of the absorbing gas from the vapor bulk to the vapor-liquid interface is determined by:

$$J = k_g (P_b - P_i) \quad (1.1)$$

while the diffusive flux at the liquid side is defined by:

$$J = \frac{E k_L^0}{H} (P_i - P^*) \quad (1.2)$$

In Equation 1.2, P^* is the partial pressure of the absorbing gas in equilibrium with the liquid bulk. In this expression for the interfacial flux the enhancement factor (E) is introduced. The enhancement factor is defined as the ratio of the interfacial flux of the transferring gas when chemical reactions take place, to the interfacial flux in the absence of chemical reactions but with the same driving force and same hydrodynamic conditions. The enhancement factor

can be determined from the fundamentals of mass transfer coupled with chemical reactions and it quantifies the following effects on the interfacial flux:

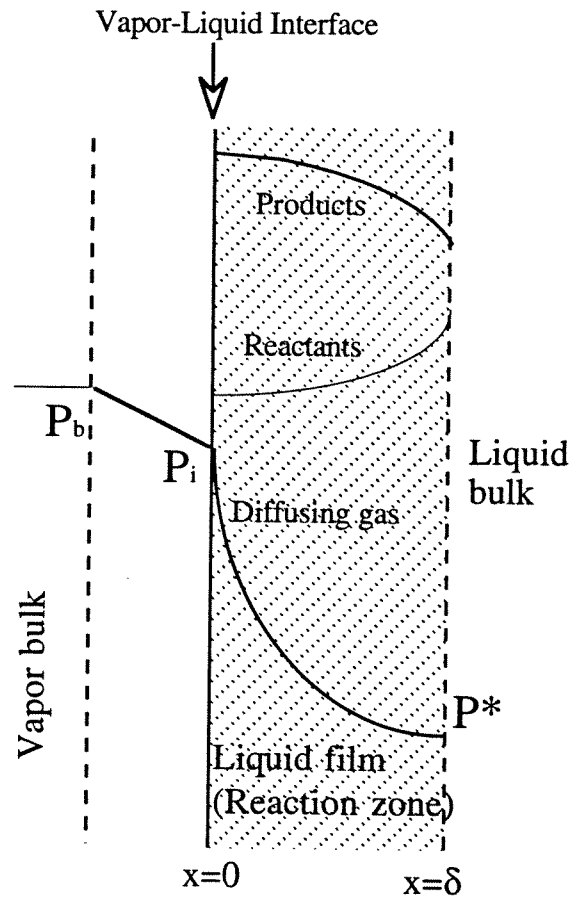


Figure 1.1. Representation of the mass transfer processes found in reactive absorption. The curves in the liquid film represent concentration profiles.

- i. Kinetics of the chemical reactions that take place at the reaction zone (liquid film).
- ii. Diffusion of reactants and reactions products through the reaction zone.
- iii. Reversibility of the chemical reactions.
- iv. Hydrodynamics at the interface.

Due to the condition of continuity of the flux of the absorbing gas at the vapor-liquid interface, Equations 1.1 and 1.2 can be combined giving:

$$J = \frac{P_b - P^*}{\frac{1}{k_g} + \frac{H}{E k_L^o}} \quad (1.3)$$

Equation 1.3 is similar to the equivalent relationship for non-reactive systems, except for the presence of the enhancement factor. Equation 1.3 establishes that the chemical reactions can have two well differentiated effects on the interfacial mass transfer:

- i. Non-equilibrium effect: This effect is caused by the rate of the reactions (and consumption of the diffusing gas) which tend to create a sharper concentration gradient at the vapor-liquid interface and therefore a greater mass transfer enhancement. The non-equilibrium effect is reflected on E.
- ii. Equilibrium effect: Due to the consumption of the diffusing gas in the reaction zone, another effect of the chemical reactions is to decrease the partial pressure of the absorbing gas in equilibrium with the liquid bulk which in turns increases the driving force for mass transfer. The equilibrium effect is reflected on P^* .

1.2 GAS TREATING WITH AQUEOUS ALKANOLAMINES

Among the applications of reactive absorption, gas treating is of great importance. This term is used to describe the separation from gases of acidic impurities such as acid gases (CO_2 , H_2S , SO_2), organic sulfur compounds, and certain other impurities. Acid gas removal generally refers to removal of CO_2 and

H₂S which often occur in large concentrations (1 - 20%) in industrial processes such as hydrogen manufacture, ammonia production and natural gas purification.

The common process for acid gas treating is an absorption/stripping system using aqueous solutions of alkanolamines as a solvent. In this process the acid gas is contacted countercurrently with the amine solution in the absorber where mass transfer with simultaneous chemical reactions between the acid impurities and the amine solution occurs. The amine solution which now contains the acid gases is sent to the top of the stripper where a reduced pressure and a steam heated reboiler create the conditions to reverse the absorption reactions. The stripped amine solution is then recycled back to the top of the absorber.

The alkanolamines most commonly used in industrial applications are monoethanolamine (MEA), diethanolamine (DEA), methyldiethanolamine (MDEA), β,β' -hydroxyaminoethyl ether (or diglycolamine: DGA) and triethanolamine (TEA). TEA was one of the first amines used in the gas treating industry, but it has been largely replaced by other solvents like MDEA. Figure 1.2 shows the structure of these amines.

Even though the bases of the gas treating process are fairly old, both design and operation of acid gas treating plants is very much an art. Fundamental data and a better understanding of the mechanisms that govern the processes of mass transfer with chemical reaction are needed. In a recent article, Abry and Dupart (1995) concluded that it is no longer acceptable to operate amine plants with huge safety margins on circulation rate and energy input and, therefore, optimization is almost imperative. To achieve this goal it is required to have

models capable of predicting the performance of the absorber/stripper system.

The present work represents an attempt to accomplish this objective.

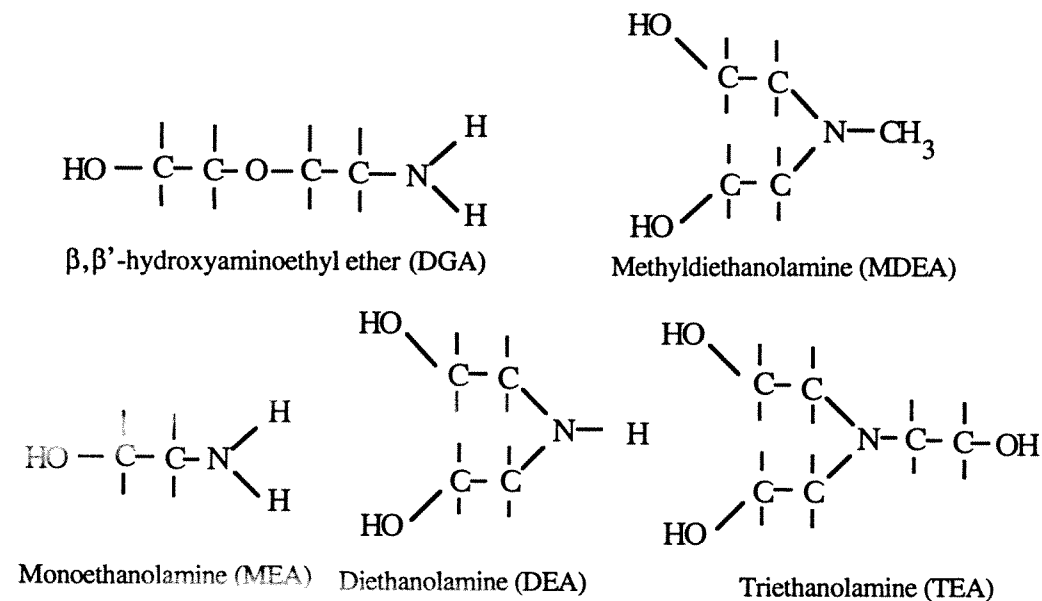


Figure 1.1 Structure of the most commonly used amines.

In this dissertation the system β,β'-hydroxyaminoethyl ether (commercial name diglycolamine, DGA)- methyldiethanolamine (MDEA)-water-CO₂ was chosen for the gas-liquid reaction kinetic studies and the system MDEA-water-H₂S-CO₂ was used for the rate-based modeling of mass transfer with chemical reactions in industrial scale absorbers.

The use of diglycolamine (DGA) for the purpose of acid gas removal was patented by Blohm and Riesenfeld in 1955. DGA has the same molecular weight as diethanolamine (DEA), a secondary amine. However, it has the reactivity of primary amines, like MEA, but with a much lower vapor pressure. Therefore, DGA can be used in more concentrated solutions than other solvents with similar

reactivity with the potential decrease in the solvent flow rate. It has been shown also (Martin et al. 1978) that the equilibrium partial pressure of CO_2 over aqueous DGA solutions is significantly lower than that over MEA solutions which would create a more favorable driving force for mass transfer for DGA. MDEA, a tertiary amine, is a chemical solvent extensively used in industrial applications for the selective removal of H_2S from gas streams containing CO_2 and H_2S .

It has been shown (Meissner et al., 1983; Chakravarty et al., 1985) that the use of blends of primary or secondary amines with tertiary amines combines the favorable properties of fast CO_2 reaction with primary or secondary amines and the low heat of reaction of tertiary amines which makes the blend easier to strip. These characteristics of the system DGA-MDEA were the motivation for its selection.

1.3 SCOPE AND OVERVIEW OF THE DISSERTATION

In this dissertation the general problem of mass transfer accompanied with multiple reversible chemical reactions is addressed. A diffusion-reaction model ("point model") was developed in order to determine the degree of enhancement of the interfacial mass transfer rates due to the chemical reactions. This model is based on the Danckwerts surface renewal theory (Danckwerts, 1970). This model takes into account the reversibility of the chemical reactions, the effect of the diffusion of reactants and reaction products through the reaction zone, the thermodynamic non-ideality of the vapor-liquid system and the mass transfer resistance at the vapor side.

This model was validated using experimental measurements of rates of reactive absorption of CO_2 into aqueous methyldiethanolamine (MDEA), β,β' -hydroxyaminoethyl ether (DGA) and mixtures of DGA and MDEA. A sensitivity analysis was performed to determine the controlling mechanism of the mass transfer under a wide range of conditions. Depending on the controlling mechanism, reaction rate constants, diffusion coefficients of reactants and products through the reaction zone, or thermodynamic interaction parameters were regressed from experimental fluxes.

Previous contributions such as the work of Versteeg et al. (1989, 1990), Glasscock (1990), and Littel et al. (1991) were based on the rigorous modeling of diffusion-reaction phenomena accounting for complex processes like the effect of electrostatic potential gradient on the diffusion of ionic species. This dissertation was aimed at developing a simpler but realistic representation of the reaction-diffusion process for its implementation on an integrated rate-based model for industrial absorbers. The experimental conditions used in the validation of this point model were also unique with respect to previous contributions because higher temperature and higher CO_2 loading were studied. Experimental vapor-liquid-equilibrium or rate data have not been previously reported for the system DGA-MDEA-water- CO_2 .

The reaction-diffusion model was used in the rate-based simulation of reactive absorption of CO_2 and H_2S into aqueous methyldiethanolamine using both trayed and packed columns. This rate-based modeling was performed combining the Generalized Maxwell-Stefan (GMS) equations and the enhancement factor theory. The GMS equations were used to calculate the

physical interfacial fluxes of the reacting gases and the enhancement factors were used to account for the effects of the chemical reactions. The interaction between heat and mass transfer effects was studied and a rigorous description of the thermodynamics was implemented using the electrolyte NRTL model.

In previous contributions on rate-based modeling of reactive absorption, specific assumptions have been introduced. Sivasubramanian (1985) neglected the effect of the reversibility of the rate-controlled gas-liquid reactions when calculating the enhancement of the interfacial fluxes. Blauwhoff et al. (1985) integrated a reaction-diffusion model for the simulation of trayed absorbers and cascades of trickle bed reactors. They assumed thermal equilibrium between the gas and liquid leaving the tray or segment of the column when solving the heat balance. These researchers also adjusted the correlations for estimating mass transfer coefficients in order to obtain “realistic” values of k_g and k_L^0 . However, these researchers made an important contribution when comparing an interactive and a non-interactive mass transfer model for the simultaneous absorption of two gases. Tomcej and Otto (1986) developed a model based on tray efficiencies that incorporates the effect of the tray hydrodynamics and chemical kinetics. The reversibility of the chemical reactions was neglected and pseudo-first order kinetics was assumed. Carey (1990) and Carey et al. (1991) accounted for the reversibility of the reactions but a simplified description of the thermodynamics was used. Chakravarty (1992) attempted to use RATEFRAC[®], the rate-based separation model of Aspen Plus, to simulate the absorber/stripper system used in acid gas treating processes. At that time RATEFRAC[®] did not have the flexibility and capability that was later developed to link with user FORTRAN routines.

Therefore, not much success was achieved in this effort, but Chakravarty established an good precedent for the present project.

In this dissertation two major areas can be differentiated, besides the literature review (Chapters 2 and 3). The first area (Chapters 4 and 5) corresponds to the development and validation of the diffusion-reaction model described above. Chapter 4 describes the experimental methods and procedures used to measure the reactive absorption rates of CO_2 in the wetted-wall column contactor for the two reactive systems studied. Chapter 4 also presents the theory used for the characterization of the contactor with respect to the resistance to the mass transfer at the vapor and liquid phases. The effect of Marangoni instabilities on interfacial mass transfer is also addressed. Chapter 5 describes the development of the diffusion-reaction model as well as the algorithm used for the model solution. Results on the sensitivity study of reaction kinetics, diffusion phenomena and thermodynamic parameters on interfacial fluxes are also presented along with the results of the non-linear parameter regression.

Chapter 6 deals with the implementation of the diffusion-reaction model in the rate-based simulation of reactive absorption columns. The interaction between heat and mass transfer effects are studied in detail. Two reaction regimes are studied, equilibrium-controlled reactions and rate-controlled reactions in both trayed and packed columns. The difference between these two type of contactors with respect to the mass transfer mechanism is also presented. Conclusions and recommendations for future contributions are summarized in Chapter 7.

1.4 NOMENCLATURE

- H: Henry's constant ($\text{atm m}^3/\text{kmol}$).
J: Diffusive flux ($\text{kmol}/\text{m}^2 \text{ sec}$).
 k_g : Mass transfer coefficient in the gas phase ($\text{kmol}/\text{m}^2 \text{ sec atm}$).
 $k_{L,i}^o$: Physical mass transfer coefficient of species i in the liquid phase (m/sec).
P: Partial pressure (atm).
x: Spatial coordinates defined in the liquid film.

Greek Letters:

- δ : Liquid film (reaction zone) thickness (m).

Superscripts:

- *: At equilibrium.

Subscripts:

- b: At the vapor bulk.
i: At the vapor-liquid interface.

1.5 REFERENCES

- Abry, R. G. F., Dupart, M. S., "Amine Plant Troubleshooting and Optimization," *Hydrocarbon Processing*, April 1995, 41.
- Blauwhoff, P. M. M., Kamphuis, B., van Swaaij, W. P. W., Westerterp, K. R., "Absorber Design in Sour Natural Gas Treatment Plants: Impact of Process Variables on Operation and Economics," *Chem. Eng. Process.*, 1985, 19,1.
- Blohm, C. L., Riesenfeld, F. C., U.S. Patent 2712978, July 12, 1955.
- Carberry, J. J., *Chemical and Catalytic Reaction Engineering*. McGraw-Hill Inc., New York, 1976.
- Carey, T. R., "Rate-Based Modeling of Acid Gas Absorption and Stripping Using Aqueous Alkanolamine Solutions". M. S. Thesis, The University of Texas at Austin, 1990.

- Carey, T. R., Hermes, J. E., Rochelle, G. T., "A Model of Acid Gas Absorption/Stripping Using Methyldiethanolamine with Added Acid," *Gas Separation and Purification*, **1991**, 5, 95.
- Chakravarty, S., "Absorption of Carbon Dioxide in Aqueous Blends of Diethanolamine and Methyldiethanolamine". M. S. Thesis, The University of Texas at Austin, 1992.
- Chakravarty, T., Phukan, U., Weiland, R. H., "Reaction of Acid Gases with Mixtures of Amines," *Chem. Eng. Prog.* April **1985**, 32.
- Danckwerts, P. V., *Gas Liquid Reactions*. McGraw-Hill Inc., New York, 1970.
- Glasscock, D. A., "Modelling and Experimental Study of Carbon Dioxide Absorption into Aqueous Alkanolamines". Ph.D Dissertation, The University of Texas at Austin, 1990.
- Littel, R. J., Filmer, B., Versteeg, G. F., Van Swaaij, W. P. M., "Modeling of Simultaneous Absorption of H_2S and CO_2 in Alkanolamine Solutions: The Influence of Parallel and Consecutive Reversible Reactions and the Coupled Diffusion of Ionic Species," *Chem. Engng. Sci.* **1991**, 46, 2313.
- Martin, J. L., Otto, F. D., Mather, A. E., "Solubility of Hydrogen Sulfide and Carbon Dioxide in a Diglycolamine Solution," *J. Chem. Eng. Data*, **1978**, 23, 163.
- Meissner, R. E., Wagner, U., "Low-energy Process Recovers CO_2 ," *Oil & Gas Journal*, Feb. **1983**, 55.
- Sivasubramanian, M. S., "The Heat and Mass Transfer Rate Approach for the Simulation and Design of Acid Gas Treating Units". Ph.D. Dissertation. Clarkson University. December, 1985.
- Subawalla, H. E., "Modeling, Simulation and Design of Reactive Distillation Columns," Ph.D Dissertation, The University of Texas at Austin, 1997.
- Tomcej, R. A., Otto, F. D., "Improved Design of Amine Treating Units by Simulation Using Personal Computers," Presented at the World Congress of Chemical Engineering, Tokyo, Japan, 1986.
- Versteeg, G. F., Kuipers, J. A. M., van Beckum, F. P. H., van Swaaij, W. P. M., "Mass Transfer with Complex Reversible Chemical Reactions-I. Single Reversible Chemical Reaction," *Chem. Engng. Sci.* **1989**, 44, 2295.
- Versteeg, G. F., Kuipers, J. A. M., van Beckum, F. P. H., van Swaaij, W. P. M., "Mass Transfer with Complex Reversible Chemical Reactions-II. Parallel Reversible Chemical Reactions," *Chem. Engng. Sci.* **1990**, 45, 183.

Zarzycki, R., Chacuk, A., *Absorption, Fundamentals and Applications*. Pergamon Press. Oxford, Great Britain, 1993.

Zheng, Y., Xu, X., "Study of Catalytic Distillation Processes. Part II. Simulation of Catalytic Distillation Processes-Quasi Homogeneous and Rate-Based Model," *Trans. IChemE.*, **1992**, 70, Part A, 465.

Chapter 2

Mass and Heat Transfer with Chemical Reactions.

2.1. INTRODUCTION

In this chapter the theory of mass and heat transfer accompanied with chemical reactions in gas-liquid systems is reviewed. The Fick's law and Maxwell-Stefan approaches to mass transfer will be compared and discussed in detail. The effects of chemical reactions on mass transfer with emphasis on the mass transfer enhancement and thermal effects will be reviewed. Also, the chemistry of the reactions between CO_2 and H_2S with alkanolamines will be described. Previous work in these areas is discussed.

2.2. FICK'S LAW AND MAXWELL-STEFAN APPROACHES TO MASS TRANSFER

Fick's law of diffusion establishes that for a binary system where components 1 and 2 are present and where u_1 and u_2 represent the velocity of transfer of components 1 and 2, the diffusive flux J_1 of species 1 is related to the mole fraction gradient by the constitutive relation:

$$J_1 = c_1(u_1 - u) = -c_t D_{12} \nabla x_1 \quad (2.1)$$

where u is the molar average velocity of the mixture ($u = x_1 u_1 + x_2 u_2$). Equation 2.1 defines the Fick's diffusion coefficient D_{12} . Since $\nabla x_1 = -\nabla x_2$ and the sum of the diffusive fluxes is zero, it can be shown that for a binary system $D_{12} = D_{21} = D$.

Besides Fick's law of diffusion, the Generalized Maxwell-Stefan Equations (GMS) can be used to express the mass transfer fluxes in terms of the

driving force. The GMS equations for a binary system can be derived from a force balance on a control volume containing components 1 and 2. Considering that the force exerted on any molecular species i is balanced by friction between the diffusing species, the following expression is obtained (Krishna and Wesselingh 1997):

$$-\frac{d\mu_1}{dz} = \frac{RT}{\mathfrak{D}} x_2 (u_1 - u_2) \quad (2.2)$$

where z is the spatial coordinate of the diffusion path. The term RT/\mathfrak{D} on the right hand side of Equation 2.2 may be interpreted to be the drag coefficient. With this definition, the Maxwell-Stefan diffusivity \mathfrak{D} has the physical significance of an inverse drag coefficient and has units of m^2/sec .

Using the definition for the fluxes $N_1 = c_1 x_1 u_1$, the following expression can be derived:

$$-\frac{x_1}{RT} \nabla_{T,p} \mu_1 = \frac{x_2 N_1 - x_1 N_2}{c_1 \mathfrak{D}} = \frac{x_2 J_1 - x_1 J_2}{c_1 \mathfrak{D}} \quad (2.3)$$

In this expression the chemical potential gradient can be written in terms of the activity coefficients for a non-ideal mixture. Since $\mu_1 = \mu_1^\circ + RT \ln(\gamma_1 x_1)$, the left term in Equation 2.3 can be expressed as follows:

$$-\frac{x_1}{RT} \nabla_{T,p} \mu_1 = -\left(1 + x_1 \frac{\partial \ln \gamma_1}{\partial x_1}\right) \nabla x_1 = -\Gamma \nabla x_1 \quad (2.4)$$

where the thermodynamic factor Γ reflects the non-ideal behaviour of the system. Combining Equations 2.3 and 2.4, and the relationship $J_1 \equiv N_1 - x_1 N_2$, the following equation for the diffusive flux is obtained:

$$J_1 = -c_1 \mathfrak{D} \Gamma \nabla x_1 \quad (2.5)$$

which combined with Equation 2.1 leads to a relationship between the Fick diffusivity D and the Maxwell-Stefan diffusivity:

$$D = \Theta \Gamma \quad (2.6)$$

Equation 2.6 establishes that the Fick diffusivity is a combination of drag effects (reflected on Θ) and thermodynamic non-ideality effects (reflected on Γ). Moreover, it indicates that for a thermodynamically ideal mixture ($\Gamma=1$) the Maxwell-Stefan diffusivity and Fick diffusivity are identical.

Equation 2.3 can be generalized for a multicomponent system with n components:

$$-\frac{x_i}{RT} \nabla_{T,p} \mu_i = \sum_{j=1, j \neq i}^n \frac{x_j N_i - x_i N_j}{c_i \Theta_{i,j}} = \sum_{j=1, j \neq i}^n \frac{x_j J_i - x_i J_j}{c_i \Theta_{i,j}}; \quad i = 1, 2, \dots, n \quad (2.7)$$

These Equations are the Maxwell-Stefan diffusion equations for multicomponent systems. From Equation 2.7 a generalized Fick's formulation to multicomponent systems can be derived establishing in this way a further comparison between the two theories.

For a multicomponent system, the thermodynamic factors Γ_{ij} that relate chemical potentials and activity coefficients can be derived as follows:

$$\frac{x_i}{RT} \nabla_{T,p} \mu_i = \sum_{j=1}^{n-1} \Gamma_{ij} \nabla x_j, \quad \Gamma_{ij} = \delta_{ij} + x_i \frac{\partial \ln \gamma_i}{\partial x_j}; \quad i = 1, 2, \dots, n-1 \quad (2.8)$$

Equation 2.8 can be combined with Equation 2.7 to represent the Maxwell-Stefan diffusion equations for multicomponent systems in $(n-1)$ -dimensional matrix form:

$$-c_i [\Gamma] (\nabla x) = [B] (J) \text{ or } (J) = -c_i [B]^{-1} [\Gamma] (\nabla x) \quad (2.9)$$

where the symbols $[]$ and $()$ represent matrices and vectors respectively. The elements of the matrix $[B]$ can be derived from Equation 2.7 as follows:

$$B_{ii} = \frac{X_i}{D_{in}} + \sum_{\substack{k=1 \\ k \neq i}}^n \frac{X_k}{D_{ik}}, \quad B_{ij(i \neq j)} = -X_i \left(\frac{1}{D_{ij}} - \frac{1}{D_{in}} \right); \quad i, j = 1, 2, \dots, n-1 \quad (2.10)$$

Analogous to the binary case (Equation 2.6), a matrix of Fick diffusivities can be defined considering Equation 2.9, i.e.,

$$(J) = -c_t[B]^{-1}[\Gamma](\nabla x) = -c_t[D](\nabla x) \quad (2.11)$$

where $[D] = [B]^{-1}[\Gamma]$. Equation 2.11 constitutes the proper generalization of the Fick formulation (Equation 2.1) to multicomponent mixtures. The elements D_{ij} of the matrix of Fick diffusivities $[D]$ are not to be confused with the binary diffusion coefficients in Equation 2.1; they may take positive or negative values and, in general, they are not symmetric ($D_{ij} \neq D_{ji}$).

2.2.1 Mass Transfer Coefficients

Another form of expressing the molar flux of component i in a multicomponent system is by using mass transfer coefficients, instead of diffusivities as represented by Equations 2.10 and 2.11. The mass transfer coefficient is defined by Bird et al. (1960) as:

$$k_o = \lim_{N_1 \rightarrow 0} \left(\frac{N_{1o} - x_{1o} N_t}{c_t(x_{1o} - x_{1i})} \right) = \lim_{N_1 \rightarrow 0} \left(\frac{J_{1o}}{c_t \Delta x_1} \right) \quad (2.12)$$

where the driving force for mass transfer Δx_1 is taken as the difference between the mole fraction at the bulk phase and that at the vapor liquid interface. The fluxes used in Equation 2.12 are the bulk fluxes and the mass transfer coefficient

obtained is the bulk phase mass transfer coefficient. An analogous relation exists for interface mass transfer coefficients.

During the process of mass transfer through the interface, the composition and velocity profiles are affected by the diffusion process. In Equation 2.12 the mass transfer coefficient is defined for the limit of vanishingly small mass transfer rates ($N_1, N_2 \rightarrow 0$) in order to avoid introducing these distortions in the definitions of the mass transfer coefficient. The mass transfer coefficients defined by Equation 2.12 are called low-flux or zero-flux mass transfer coefficients. The low-flux mass transfer coefficients are the ones that are usually available from correlations of mass transfer data. These correlations, which are empirical, are usually obtained under conditions of low mass transfer rates. Under the conditions of finite transfer rates,

$$k_o^* = \left(\frac{N_{1o} - x_{1o}N_t}{c_t(x_{1o} - x_{1i})} \right) = \left(\frac{J_{1o}}{c_t \Delta x_1} \right) \quad (2.13)$$

where the superscript \bullet indicates that the mass transfer coefficient corresponds to conditions of finite mass transfer rates.

For the calculation of the mass transfer rate (flux), the finite flux mass transfer coefficient k_o^* is needed. This coefficient is related to the zero-flux coefficient by the general relation:

$$k_o^* = k_o \Xi_o \quad (2.14)$$

with Ξ_o being the correction factor that accounts for the effect of finite fluxes on k_o . The correction factor depends on the composition profiles and total mass transfer rates and, consequently, it is directly related to the model used to describe the hydrodynamics of the mass transfer process.

In multicomponent systems, the mass transfer rates of each species are better expressed in matrix form:

$$(J_o) = (N) - (x_b)N_t = c_t [k_o^*](x_b - x_i) \quad (2.15)$$

where $[k_o^*]$ is a matrix of finite flux mass transfer coefficients. The finite flux mass transfer coefficients are related to the low flux coefficients by a relation equivalent to Equation 2.14

$$[k_o^*] = [k_o][\Xi_o] \quad (2.16)$$

Equation 2.15 is equivalent to Equation 2.9, except that Equation 2.15 defines the diffusion fluxes using mass transfer coefficients. The formulation given by Equation 2.15 is more useful from the practical point of view because it avoids the use of the film thickness. Similarly as it was defined for Equation 2.9, the elements of the matrix of low-flux mass transfer coefficients $[k]$ are given by the following relationships:

$$[k] = [R]^{-1} \quad (2.17)$$

with the elements of matrix $[R]$ being

$$R_{ii} = \frac{x_i}{K_{in}} + \sum_{\substack{k=1 \\ k \neq i}}^n \frac{x_k}{K_{ik}} ; R_{ij(i \neq j)} = -x_i \left(\frac{1}{K_{ij}} - \frac{1}{K_{in}} \right) \quad (2.18)$$

In principle, κ_{ij} , the low-flux mass transfer coefficient for the pair i-j, is defined by $\kappa_{ij} = \bar{D}_{ij}/\delta$, where δ is the film thickness. However, in practice the low-flux mass transfer coefficients are often calculated from empirical correlations to avoid the estimation of the film thickness.

2.2.2 Relationship Between Diffusive Fluxes and Molar Fluxes

So far in this chapter attention has been focused on the determination of the diffusive fluxes J_i . However, in practical applications the molar fluxes N_i are needed because they appear in the equations that govern the mass and energy balances in a given process. For a system with n components there are only $n-1$ independent diffusive fluxes J_i , but all n molar fluxes N_i are independent. Therefore, even if the diffusive fluxes are known, an additional condition has to be defined in order to determine the molar fluxes. The problem of determining the molar fluxes from the diffusive fluxes has been called the bootstrap problem. This additional condition required is sometimes an assumption or a condition imposed for the particular system. For instance in multicomponent distillation equimolar counterdiffusion is sometimes assumed. This assumption establishes that the total molar flux vanishes, i.e., $N_t = 0$. This assumption makes the molar fluxes equal to the respective diffusive fluxes for all the components. Another example corresponds to reactive systems where the ratio of the component molar fluxes can be specified by the stoichiometry of a chemical reaction.

In general these conditions on the mass transfer rates, either governed by the particular system or assumed for convenience, leads to a representation of the molar fluxes in the following form

$$(N) = [\beta](J) \quad (2.19)$$

where $[\beta]$ is called the bootstrap matrix. The departure of the bootstrap matrix from the identity matrix indicates the importance of the convective term $x_i N_i$ in

the mass transfer process. Equation 2.15 and 2.19 can be combined to express the vector of molar fluxes in terms of the mass transfer coefficients:

$$(N) = c_t [\beta_o][k_o^*](x_b - x_i) = c_t [\beta_o][k_o][\Xi_o] (x_b - x_i) \quad (2.20)$$

The formulation of the mass transfer problem represented by Equation 2.20 is quite complex and rigorous calculations require intensive matrix algebra especially for systems with a large number of components. An alternative formulation based on simpler constitutive relations leads to the pseudo-binary or effective diffusivity approach which is the subject of the next section.

2.2.3 Effective Diffusivity Methods

The effective diffusivity in a multicomponent system can be *defined* by a relationship analogous to Equation 2.1:

$$J_i = -c_t D_{i,eff} \nabla x_i \text{ or } N_i = -c_t D_{i,eff} \nabla x_i + x_i \sum_{j=1}^n N_j \quad (2.21)$$

Solving Equation 2.21 for ∇x_i and equating the result to the composition gradient obtained from the Maxwell-Stefan theory (Equation 2.7 for an ideal solution), the following relationship between effective diffusivity and the Maxwell-Stefan diffusivities is obtained (Bird et al. 1960):

$$D_{i,eff} = \frac{N_i - x_i N_t}{N_i \sum_{\substack{j=1 \\ j \neq i}}^n \frac{x_j}{D_{ij}} - x_i \sum_{\substack{j=1 \\ j \neq i}}^n \frac{N_j}{D_{ij}}} \quad (2.22)$$

This complicated relationship indicates that, in principle, the effective diffusion coefficients are not bounded, i.e., they can be negative as well as positive. This in turns implies that the effective diffusion coefficients as defined by Equation 2.22 do not, in general, have the physical significance of a diffusion

coefficient in a binary system. However, in practical applications Equation 2.22 is rarely used and, instead, correlations based on experimental data or simpler approximations are employed.

Other simpler relationships between the effective diffusion coefficients and the Maxwell-Stefan binary diffusion coefficients have been used. For instance Taylor et al. (1993) reports the relationship

$$\frac{1}{D_{i,\text{eff}}} = \frac{x_i}{D_{in}} + \sum_{\substack{k=1 \\ k \neq i}}^n \frac{x_k}{D_{ik}} \quad (2.23)$$

which corresponds to $D_{i,\text{eff}} = 1/B_{ii}$ with B_{ii} determined by Equations 2.10. This approximation is equivalent to neglecting the off-diagonal elements of the matrix [B] in the calculation of the diffusive fluxes using Equation 2.9.

The diffusive flux can be also defined in terms of effective mass transfer coefficients by an expression similar to Equation 2.21

$$J_i = c_i k_{i,\text{eff}} (x_b - x_i) \quad (2.24)$$

Like its multicomponent counterpart the effective mass transfer coefficient is defined in principle as $k_{i,\text{eff}} = D_{i,\text{eff}}/\delta$, but in practice the effective mass transfer coefficients are calculated from empirical correlations using effective diffusivities. When there is a need to compare mass transfer rates calculated from an effective diffusivity approach to those calculated by a more rigorous multicomponent formulation like the GMS approach, the effective mass transfer coefficients are calculated from binary mass transfer coefficients using relationships equivalent to Equation 2.23, but substituting diffusivities by mass transfer coefficients, i.e.,

$$\frac{1}{k_{i,\text{eff}}} = \frac{x_i}{K_{\text{in}}} + \sum_{\substack{k=1 \\ k \neq i}}^n \frac{x_k}{K_{ik}} \quad (2.25)$$

Frank et al. (1995) used a relationship similar to Equation 2.25 to estimate effective mass transfer coefficients when comparing the GMS and pseudo-binary approaches to mass transfer.

2.3. MASS TRANSFER INTERACTION EFFECTS

Equations 2.9 or 2.11 indicate that the diffusive flux of a given species in a multicomponent system not only depends on the driving force to mass transfer for that species, but also on the driving force of the other species as well. This indicates that under certain circumstances multicomponent system can behave quite differently compared to binary systems. Moreover, Equation 2.19 shows that depending on the magnitude of the off-diagonal elements of the bootstrap matrix $[\beta]$, the molar flux of a given species can be significantly affected by the diffusive flux of the other species present in the system.

Krishna and Wesselingh (1997) summarize three different phenomena that can occur in multicomponent systems. Figure 2.1 is a schematic representation of the differences between binary and multicomponent diffusion. These situations were originally anticipated by Toor (1957):

Osmotic Diffusion: Diffusion of a component despite the absence of a driving force.

Reverse Diffusion: Diffusion of a component in a direction opposite to that governed by its driving force.

Diffusion Barrier: Zero or vanishingly small diffusion flux despite the presence of a large driving force.

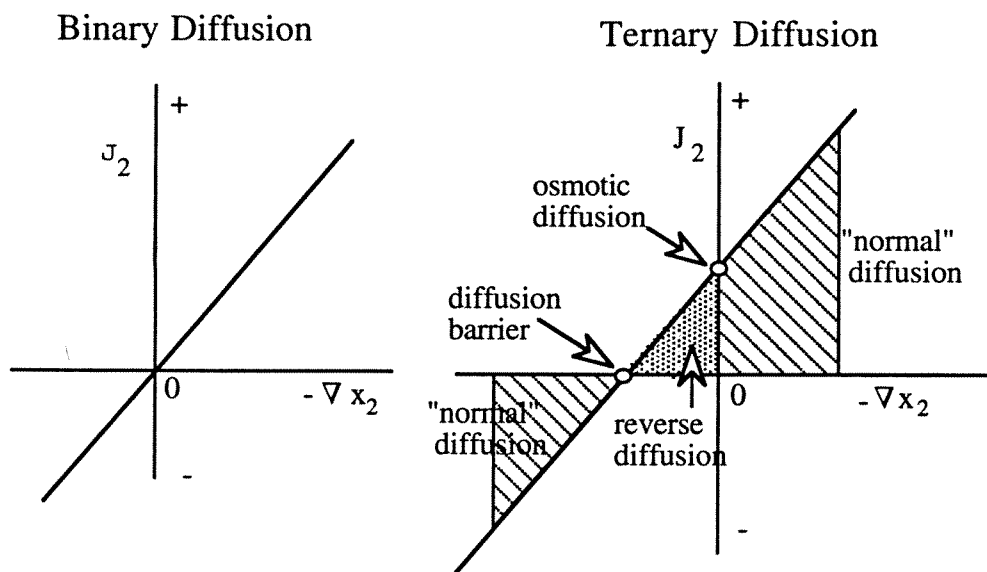


Figure 2.1. Diffusion flux for binary and ternary systems as a function of the composition gradient. Representation taken from Taylor and Krishna (1993).

The importance of the interaction effects on mass transfer depends on the specific conditions of each system and it is difficult to establish a general criteria to determine when the diffusional interactions are unimportant and, therefore, when an effective diffusivity approach can be used. Krishna and Wesselingh (1997) indicate that interaction phenomena occur routinely in multicomponent mass transfer processes like absorption and distillation. In mass transfer equipments, such as trayed and packed columns, the driving force of a given component Δx_i could change sign along the column. This is likely especially for components with intermediate volatility. For such components the driving force

should assume vanishingly small values at some position. When this situation occurs, the flux of that component is strongly influenced by the fluxes of the others. This in turns leads to the “odd” behavior described above, i.e., reverse and osmotic transport, and transport barrier. Under these circumstances the component efficiencies are unbounded and can assume values greater than 100% and of either sign.

2.4. EFFECT OF CHEMICAL REACTIONS ON MASS TRANSFER

2.4.1 The Maxwell-Stefan Approach for Mass Transfer in Gas-Liquid Reactive Systems

Vanni and Baldi (1991), Valerio and Vanni (1994) and Frank et al. (1995) have studied the problem of mass transfer with simultaneous chemical reactions when the mass transfer problem is described by the GMS approach. These researchers compared the predictions of the more rigorous multicomponent approach with estimates of interfacial mass transfer rates using a pseudo-binary approach based on Fickian diffusion. The film model was adopted by these researchers to describe the hydrodynamics at the interface. Frank et al (1995) studied a more general situation where a chemical reaction of the following form takes place in the liquid phase:



with a reaction rate given by $R(\text{kmol/m}^3 \text{ sec}) = k_2[A]^a[B]^b - k_{2,r}[C]^c[D]^d$.

The conservation equation for the liquid phase is given by

$$\frac{dN_i}{d\eta} = v_i R \delta \quad (2.27)$$

where η is the dimensionless distance in the film defined as $\eta=x/\delta$. When a thermodynamic ideal solution is assumed, an expression equivalent to Equation 2.7 can be used to relate the molar fluxes of the different components with the concentration driving force:

$$\frac{dx_i}{d\eta} = \sum_{j=1}^n \frac{x_j N_i - x_i N_j}{c_i \kappa_{i,j}} \quad (2.28)$$

The system of differential Equations 2.27 and 2.28 along with the appropriate boundary conditions can be solved numerically. Frank and coworkers compared molar fluxes for the diffusing gas (component A) calculated using this numerical solution with the interfacial fluxes obtained using the enhancement factor approach based on Fickian diffusion:

$$N_A = E_A N_{A, \text{ without reaction}} \quad (2.29)$$

This comparison was performed only for irreversible reactions of the form $A \rightarrow C$ (first order) and $A+B \rightarrow C$ (1,1 order). The enhancement factor for the diffusing gas was calculated using relationships between the Hatta number and the enhancement factor derived for the case when Fick's formulation for mass transfer is used. The Hatta number is expressed by:

$$Ha = \frac{\sqrt{k_1 D_{A,eff}}}{k_{A,eff}} \quad (2.30)$$

where k_1 is the first order or pseudo-first order reaction rate constant. The effective mass transfer coefficient $k_{A,eff}$ was estimated using a relationship similar to Equation 2.25. The interfacial mass transfer flux in the absence of chemical reactions was calculated using an approximate analytical solution of the GMS

equations (Equations 2.28). Comparison between the two theories indicated that even when the Maxwell-Stefan theory is used to describe the mass transfer process, the enhancement factor follows the same functionality with respect to the Hatta number as is derived on the basis of Fick's law. This result was obtained using a wide range of conditions with respect to diffusion kinetics (both equal and different binary mass transfer coefficients) and reaction kinetics. Mass transfer with a reversible chemical reaction was also modeled using the GMS approach, but no comparison was made with the enhancement factor theory.

The work of Vanni and Baldi (1991) is somewhat similar to the contribution of Frank et al. (1995), but they assumed that the reaction product is soluble in both the liquid and vapor phases. These researchers derived approximate expressions for the enhancement factors that account for the diffusion interactions in the framework of the Maxwell-Stefan theory. Valerio and Vanni (1994) addressed the problem of mass transfer accompanied with chemical reactions in non-ideal multicomponent systems. The effect of non-ideal diffusion kinetics and the implications of thermodynamic non-ideality on reaction kinetics and diffusion kinetics were evaluated for first order and instantaneous reactions. The Maxwell-Stefan diffusivities are calculated from infinite dilution diffusion coefficients corrected for composition effects for concentrated solutions. This composition dependence of the Maxwell-Stefan diffusivities is one source of non-ideality on the diffusion kinetics. The other source of non-ideality on the diffusion kinetics arises from the use of chemical potential gradients rather than molar composition gradients as the driving force for mass transfer. This effect of non-ideal thermodynamics on the kinetics of diffusion is reflected on the matrix

[Γ] (see Equations 2.8 and 2.9). To evaluate the matrix of thermodynamic factors [Γ], a model that relates the activity coefficient of the different components with compositions is needed. Valerio and Vanni (1994) adopted the multicomponent Margules model.

Valerio and Vanni (1994) defined three different ranges for the infinite dilution activity coefficients of component i in component j (γ_{ij}^∞) in order to study the effect of thermodynamic non-ideality on the predictions of the interfacial fluxes of the diffusing gas. For *moderately* non-ideal systems ($0.2 < \gamma_{ij}^\infty < 5$) the difference between the interfacial flux of the diffusing gas calculated considering the non-ideal thermodynamics to that neglecting the effect of the non-ideality was always less than 10%. This range of γ_{ij}^∞ is representative of several actual systems with significant non-ideal behaviour. For systems where the thermodynamic non-ideality was even more significant ($0.05 < \gamma_{ij}^\infty < 20$), the difference between the calculated interfacial fluxes was usually less than 15%. In these calculations the thermodynamic non-ideality of the solution affected not only the diffusion kinetics but also the reaction kinetics.

The effect of the composition dependence on the GMS diffusion coefficients was shown to be negligible even in concentrated solutions. Only when the infinite dilution diffusion coefficients differ by more than a factor of four from each other, the interfacial flux of the diffusing gas is affected by more than 15% with respect to the ideal situation. The authors indicated that for most gas-liquid systems the infinite dilution diffusion coefficients do not differ from each other by more than a factor of two. Under this condition the diffusional non-

ideality accounts for less than 3% of the interfacial flux. Therefore, the surprising conclusion of the work by Valerio and Vanni (1994) is that non-ideal diffusion and non-ideal thermodynamics affect the interfacial fluxes in gas-liquid reactive systems only in very highly non-ideal solutions, excluding most systems of practical interest.

2.4.2 Gas-Liquid Reactions and Surface Renewal Theory

Different models have been developed in order to describe the interfacial hydrodynamics of gas-liquid systems. Film theory, penetration and surface renewal theories, and eddy diffusivity theories are among the models more commonly studied and used. A thorough comparison between these models was conducted by Glasscock and Rochelle (1989). Both penetration and surface renewal theories are unsteady-state theories and are generally accepted as being more accurate than film theory for mass transfer at turbulent gas-liquid interfaces (Danckwerts, 1970; Glasscock and Rochelle, 1989). In the present work the Danckwerts surface renewal theory was adopted in the reaction-diffusion modeling to describe the hydrodynamics at the vapor-liquid interface.

The Danckwerts model of mass transfer is one of the surface-renewal models that take as their basis the replacement at intervals of elements of liquid at the surface by liquid from the interior which has the local mean bulk concentration. Thus, the surface-renewal models visualize the surface of an agitated liquid or a liquid flowing over a packing, as a mosaic of elements which have been exposed to the gas for different lengths of time (or have different “ages”), and which will therefore be absorbing at different specific rates. The

Danckwerts model assumes that the chance of an element of surface being replaced with fresh liquid is independent of the length of time for which it has been exposed. This leads to a distribution of surface “ages” in which the fraction of the surface which at any given instant has been exposed to the surface for times between θ and $(\theta + d\theta)$ is $se^{-s\theta}d\theta$. Where s is the fraction of the area of surface which is replaced with fresh liquid in unit time.

If N is the instantaneous rate of absorption per unit area of surface which has been exposed for time θ , the average rate of absorption into the surface is the value of N averaged over all elements of the surface, having ages between 0 and ∞ :

$$\bar{N} = s \int_0^{\infty} N_{(\theta)} e^{-s\theta} d\theta \quad (2.31)$$

For physical absorption the rate of mass transfer of species A per unit area of surface is $([A]_i - [A]_o) \sqrt{D_A / \pi \theta}$ (Danckwerts, 1970). Therefore, the average mass transfer rate is given by:

$$\begin{aligned} \bar{N} &= ([A]_i - [A]_o) s \sqrt{D_A / \pi} \int_0^{\infty} \frac{e^{-s\theta}}{\sqrt{\theta}} d\theta \\ \bar{N} &= ([A]_i - [A]_o) \sqrt{D_A s} \end{aligned} \quad (2.32)$$

From this equation it can be seen that in Danckwerts model the physical mass transfer coefficient is given by $k_L^o = \sqrt{D_A s}$.

Similarly as the average rate of absorption is given by Equation 2.31, the average concentration of a given component at a distance x below the surface is

$$[\bar{A}]_{(x)} = s \int_0^{\infty} [A]_{(x,\theta)} e^{-s\theta} d\theta \quad (2.33)$$

where $[A]_{(x,\theta)}$ is the instantaneous concentration at a distance x below the vapor-liquid interface at time θ after first exposure of the surface to the gas. Equations 2.31 and 2.33 represent the “s-multiplied” Laplace transform of the instantaneous absorption rate and instantaneous concentration, respectively. DeCoursey and Thring (1989) and DeCoursey (1992) used the property that the time-mean fluxes and concentrations are equal to the respective “s-multiplied” Laplace transform in order to simplify the solution of the diffusion-reaction equations using the Danckwerts surface renewal model for the interfacial hydrodynamics.

For physical absorption, the mass balance of the diffusing gas A can be expressed as:

$$D_A \frac{\partial^2 [A]}{\partial x^2} - \frac{\partial [A]}{\partial t} = 0 \quad (2.34)$$

with the initial and boundary conditions:

$$[A] = [A]_o \quad ; \quad x > 0, t = 0$$

$$[A] = [A]_i \quad ; \quad x = 0, t > 0$$

$$[A] = [A]_o \quad ; \quad x \rightarrow \infty, t > 0$$

where $[A]_o$ and $[A]_i$ are the concentrations at the liquid bulk and vapor-liquid interface, respectively.

Applying the s-multiplied Laplace transform to Equation 2.34, the following expression is obtained:

$$D_A \frac{d^2 [\bar{A}]}{dx^2} - s\{[\bar{A}] - [A]_o\} = 0 \quad (2.35)$$

with

$$[\bar{A}] = [A]_i \quad ; \quad x = 0, t > 0$$

$$[\bar{A}] = [A]_0 \quad ; \quad x \rightarrow \infty, t > 0$$

where the time-mean concentration $[\bar{A}]$ is given by Equation 2.33.

The solution of Equation 2.35 is

$$[\bar{A}] - [A]_0 = ([A]_i - [A]_0) \exp\left\{-\frac{xk_{LA}^0}{D_A}\right\} \quad (2.36)$$

Similarly, when a first order reaction ($R = k_1[A]$) takes place in the liquid phase with the initial and boundary conditions:

$$[A] = 0 \quad ; \quad x > 0, t = 0$$

$$[A] = [A]_i \quad ; \quad x = 0, t > 0$$

$$[A] = 0 \quad ; \quad x \rightarrow \infty, t > 0$$

the solution of the diffusion-reaction equation is the following

$$[\bar{A}] = [A]_i \exp\left\{-\frac{x E_A k_{LA}^0}{D_A}\right\} \quad (2.37)$$

where the enhancement factor for the interfacial flux of A, E_A , is given by:

$$E_A = \sqrt{1 + \frac{k_1 D_A}{k_{LA}^0}} \quad (2.38)$$

The results given by Equations 2.36 and 2.37 led DeCoursey and Thring (1989) and DeCoursey (1992) to consider that an approximate solution of the governing diffusion-reaction equation for a reversible second-order chemical reaction of the form



can be given by:

$$[\bar{A}] - [A]_o = ([A]_i - [A]_o) \exp \left\{ -\frac{x E_A k_{LA}^o}{D_A} \right\} \quad (2.40)$$

where E_A , the enhancement factor for the interfacial flux of A, accounts not only for the effect of the forward chemical reaction, but also for the reversibility and the diffusion limitations of the reactants and reaction products. The functionality of E_A with respect to the diffusion and reaction kinetics, and the equilibria is found in such a way that Equation 2.40 satisfies exactly the diffusion-reaction equation at the interface, but only approximately elsewhere. Further details on this method are given in Chapter 5. Equation 2.40 is exact in value and slope at the interface and liquid bulk for a second-order reaction, but it deviates from the true profile inbetween. The diffusion-reaction equation is satisfied exactly at the interface but only approximately elsewhere because, under most conditions, the reaction rate and diffusion processes closest to the interface has the greatest influence on the mass transfer enhancement. Also the condition of zero flux at the interface of the reactants (different from A) and reaction products, makes their gradient close to zero at the interface.

Equation 2.40 provides the appropriate representation of the interfacial flux, as

$$\bar{N}_A = -D_A \left(\frac{d[\bar{A}]}{dx} \right)_{x=0} = E_A k_{LA}^o ([A]_i - [A]_o) \quad (2.41)$$

where it was assumed that the interfacial molar flux of the diffusing gas is equal to its diffusive flux. This assumption is justified considering that, under most

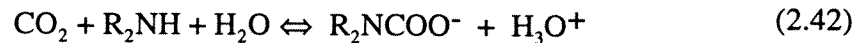
conditions, the mole fraction of the absorbing gas in the liquid phase is quite low which makes the contribution of the convective term ($x_A N_i$) negligible.

2.5 KINETICS OF GAS-LIQUID REACTIONS: REACTIVE ABSORPTION OF CO₂ AND H₂S IN AQUEOUS ALKANOLAMINES

2.5.1 Chemistry of CO₂-alkanolamine Systems

When reacting with CO₂, sterically unhindered primary and secondary alkanolamines form stable carbamate ions. On the other hand, since tertiary alkanolamine molecules do not have the N-H bonds, their reaction with CO₂ produces only bicarbonate and carbonate ions.

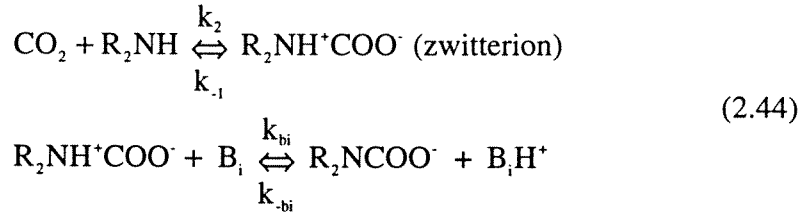
Primary amines like MEA or DGA are noted for their fast reaction rates with CO₂. Secondary amines like DEA have intermediate reaction rates, and finally MDEA, being a tertiary amine, has much slower reaction rate with CO₂. Primary and secondary amines react with CO₂ to form a carbamate:



Depending on the stability of the carbamate, it may revert to bicarbonate:



Danckwerts (1979) proposed that the carbamate formation may involve the formation of an intermediate zwitterion (a locally ionic, net neutral, molecule). Blauwhoff et al. (1984) reported that this mechanism can be used to reconcile much of the kinetic data available, especially for DEA. Critchfield et al. (1987) introduced reversibility into this mechanism. This mechanism is as follows:



where B_i designates any species in solution that can act as a base to abstract the proton from the zwitterion in the second reaction step. When the pseudo-steady state approximation for the zwitterion is applied, the following expression is obtained for the rate of reaction of CO_2 (Critchfield and Rochelle, 1987):

$$R_{\text{CO}_2} = \frac{k_2[\text{R}_2\text{NH}]\{[\text{CO}_2] - [\text{CO}_2]^*\}}{1 + \frac{k_{-1}}{\sum k_{bi}[\text{B}_i]}} \tag{2.45}$$

In Equation 2.45, $[\text{CO}_2]^*$ is the equilibrium concentration of CO_2 and the summation is over all the bases in solution. For the amine system, the species that can abstract the proton from the zwitterion (B_i) are OH^- , water and the amines themselves.

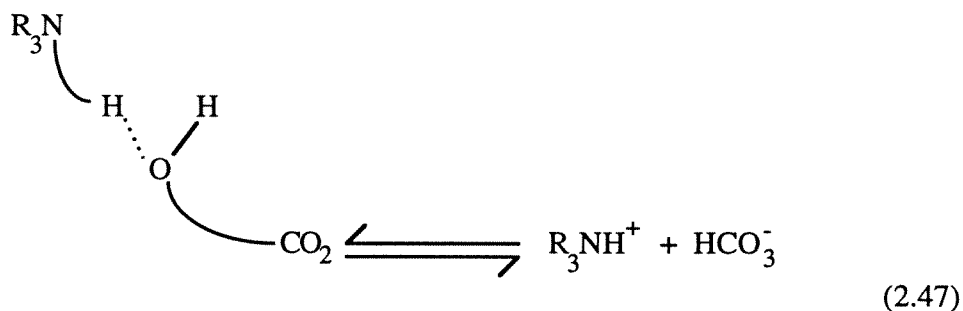
When the rate of the second step represented in Equation 2.44 is much faster than the reverse rate of the zwitterion formation (that is, when step 1 is the controlling mechanism), the rate expression 2.45 reduces to:

$$R_{\text{CO}_2} = k_2[\text{R}_2\text{NH}]\{[\text{CO}_2] - [\text{CO}_2]^*\} \tag{2.46}$$

In this work, it was found that the simplified expression 2.46 describes the experimental data within the experimental uncertainty and it was used to represent the rate of the reaction between DGA and CO_2 . A rate expression equivalent to Equation 2.46 was used by Hagewiesche et al. (1995) to describe the rate of

reaction between MEA and CO₂ when modeling reactive absorption of CO₂ in unloaded solutions of MEA and MDEA.

Tertiary amines, unlike primary and secondary amines, cannot form carbamates and so they react with CO_2 by acting as a source of hydroxide, but there is evidence that the enhanced CO_2 absorption rates in tertiary amine solutions cannot be explained with the hydroxide reaction alone. Donaldson and Nguyen (1980) proposed that the enhanced absorption rates can be explained by a base catalysis of the CO_2 hydration. The essence of this catalysis is assumed to be a hydrogen bonding between the free amine and water which increases the reactivity of water towards CO_2 :



For the specific reaction between CO₂ and MDEA, different researchers (Critchfield, 1988; Versteeg et al., 1990; Glasscock, 1990; Rinker et al., 1995) agree that a second order reversible reaction describes the experimental data. In the present work the following rate expression was used:

$$R_{\text{CO}_2} = k_{21}[\text{R}_3\text{N}][\text{CO}_2] - k_{2r}[\text{R}_3\text{NH}^+][\text{HCO}_3^-] = k_{21}[\text{R}_3\text{N}] \{[\text{CO}_2] - [\text{CO}_2]^*\} \quad (2.48)$$

When a mixture of chemical solvents is used, the equilibrium concentration of CO_2 , $[\text{CO}_2]^*$, is that which makes the total reaction rate equal to

zero. For instance, for an aqueous solution of a primary and tertiary amine, the reaction rate of CO_2 can be expressed as:

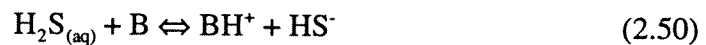
$$R_{\text{CO}_2} = (k_{2,p}[\text{R}_2\text{NH}] + k_{2,t}[\text{R}_3\text{N}])\{[\text{CO}_2] - [\text{CO}_2]^*\} \quad (2.49)$$

with $[\text{CO}_2]^*$ defining, therefore, a global equilibrium. This concept will be described in more detail in Chapter 5.

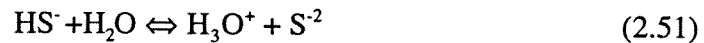
2.5.2 Chemistry of H_2S -alkanolamine Systems

The chemical behavior of H_2S with primary, secondary or tertiary alkanolamines is essentially the same. When H_2S reacts with alkanolamines there is only a proton transfer and therefore the chemical reaction is essentially instantaneous with respect to mass transfer. This instantaneous reaction with H_2S and a slow rate-controlled reaction with CO_2 make tertiary alkanolamines effective solvents for the selective removal of H_2S from gas streams containing CO_2 and H_2S .

When H_2S reacts with a base B, the following proton transfer reaction occurs to form bisulfide (Astarita et al., 1983):



where a base B can be water, hydroxide ions and amines. The second dissociation to form sulfide ions (S^{2-}) can usually be neglected because the equilibrium constant for the reaction



is about 10^{-14} . Therefore, HS^- largely dominates the H_2S equilibrium.

2.6 NON-ISOTHERMAL GAS ABSORPTION: INTERFACIAL HEAT TRANSFER

When modeling processes such as gas absorption and distillation it is essential to consider the transport across the phase boundary and the continuity of mass and energy flux. Gas absorption is a typical exothermal process. In some absorption systems the temperature rise is not significant and therefore isothermal operation can be assumed. However, in some processes of physical absorption and in most reactive absorption situations the thermal effects are large and the heat released can be responsible for a significant increase of the temperature of the liquid and vapor (Zarzycki and Chacuk, 1993). These thermal effects in turn affect the transport and physico-chemical properties and therefore the mass transfer kinetics.

The theory presented in this section on interfacial transport has been developed by Krishna (1977) and Taylor and Krishna (1993). Though the analysis given below is developed for liquid-vapor interface transport, the formalism is generally valid for all two-phase systems.

At the vapor-liquid interface we have continuity of the component molar fluxes:

$$N_i^L = N_i = N_i^V \quad (2.52)$$

and of the total molar fluxes:

$$N_t^L = N_t = N_t^V \quad (2.53)$$

where N_i^L and N_i^V are the normal components of the molar flux N_i at the interface. These fluxes are composed of diffusive and convective contributions as

$$N_i^L = J_i^L + x_i N_t^L = N_i = J_i^V + y_i N_t^V = N_i^V \quad (2.54)$$

We also have continuity of the energy flux across the vapor-liquid interface:

$$E^v = E^l = E \quad (2.55)$$

where E^v and E^l are the normal components of the energy flux at the interface.

The energy flux can be defined as follows:

$$E = q + \sum_{i=1}^n \bar{H}_i N_i \quad (2.56)$$

where q represents the purely conductive heat flux and the second term accounts for the convective enthalpy transfer due to the diffusing species. The conductive heat flux q plays a role analogous to the molar diffusion fluxes J_i .

Considering Equation 2.55, the energy transfer across the interface can be expressed as:

$$q^v + \sum_{i=1}^n N_i^v \bar{H}_i^v(T^v) = q^l + \sum_{i=1}^n N_i^l \bar{H}_i^l(T^l) \quad (2.57)$$

with the conductive heat fluxes in the two phases given by:

$$q^v = h_v(T^v - T^I) \quad (2.58)$$

$$q^l = h_l(T^I - T^l) \quad (2.59)$$

where h_v and h_l are the heat transfer coefficients in the vapor and liquid respectively, and T^I is the temperature at the vapor-liquid interface.

There is a close relationship between the interfacial mass and energy fluxes. This relationship can be visualized rewriting Equation 2.57 as follows:

$$q^l - q^v = \sum_{i=1}^n (\bar{H}_i^v - \bar{H}_i^l) N_i = \sum_{i=1}^n \lambda_i N_i$$

$$\begin{aligned}
&= \sum_{i=1}^n \lambda_i J_i^V + \sum_{i=1}^n \lambda_i y_i N_t \\
&= \sum_{i=1}^n \lambda_i J_i^L + \sum_{i=1}^n \lambda_i x_i N_t \quad (2.60) \\
&= \sum_{i=1}^{n-1} (\lambda_i - \lambda_n) J_i^V + \lambda_y N_t \\
&= \sum_{i=1}^{n-1} (\lambda_i - \lambda_n) J_i^L + \lambda_x N_t
\end{aligned}$$

where

$$\lambda_i = \bar{H}_i^V - \bar{H}_i^L; \lambda_y = \sum_{i=1}^n \lambda_i y_i; \lambda_x = \sum_{i=1}^n \lambda_i x_i \quad (2.61)$$

Considering Equations 2.54 and 2.60, the following relation can be found for the total flux:

$$N_t = -\frac{J_i^L - J_i^V}{x_i - y_i} = \frac{q^L - q^V}{\lambda_y} - \frac{\sum_{k=1}^{n-1} (\lambda_k - \lambda_n) J_k^V}{\lambda_y} \quad (2.62)$$

in a similar form an expression for the total flux can be obtained using the liquid-phase diffusion fluxes:

$$N_t = -\frac{J_i^L - J_i^V}{x_i - y_i} = \frac{q^L - q^V}{\lambda_x} - \frac{\sum_{k=1}^{n-1} (\lambda_k - \lambda_n) J_k^L}{\lambda_x} \quad (2.63)$$

Now the total flux can be eliminated from Equations 2.54 using Equation 2.62 to give:

$$N_i = J_i^V - y_i \sum_{k=1}^{n-1} \Lambda_k J_k^V + y_i \frac{\Delta q}{\lambda_y} \quad (2.64)$$

where the following parameters were defined:

$$\Lambda_k = (\lambda_k - \lambda_y)/\lambda_y ; \Delta q = q^L - q^V \quad (2.65)$$

Equation 2.64 can be written in matrix notation as:

$$(N) = [\beta^V](J^V) + (y)\Delta q/\lambda_y \quad (2.66)$$

where the matrix $[\beta^V]$ has the elements

$$\beta_{i,k}^V = \delta_{i,k} - y_i \Lambda_k ; \quad i,k = 1,2,\dots,n-1 \quad (2.67)$$

and where $\delta_{i,k}$ is the Kronecker delta.

An expression equivalent to Equation 2.66 can be written in terms of the liquid-phase diffusion fluxes:

$$(N) = [\beta^L](J^L) + (x)\Delta q/\lambda_x \quad (2.68)$$

Equations 2.66 and 2.68 along with Equation 2.63 constitute a general framework to describe simultaneous heat and mass interfacial transport. The use of this model for the interfacial transport avoids the introduction of assumptions like equimolar counterdiffusion ($N_t = 0$) which could lead to significant error especially for systems where the enthalpies of absorption (vaporization) of the transferring species are significantly different from each other. This model also demonstrates that the mass transfer rates are strongly coupled with the heat effects in the description of the transport processes across interfaces.

2.7 TEMPERATURE BULGES AND REACTIVE ABSORPTION

In countercurrent reactive absorption processes the enthalpy change due to absorption and reaction of the diffusing gases can cause a significant rise of the temperature of the liquid especially towards the bottom of the column where the interfacial fluxes are usually larger. Consequently, the liquid solvent (e.g., water)

vaporizes. This increase in the temperature of the liquid is accompanied by an increase of the temperature of the vapor as well due mainly to the contribution of the conductive heat transfer. However, towards the top of the column the vapor encounters a cooler incoming solvent, and therefore the vapor tends to condense. This interaction between convective enthalpy transfer of the diffusing gases, the enthalpy of vaporization-condensation of the liquid solvent, and the conductive heat transfer between the vapor and liquid phases, can lead to the development of a temperature bulge at some point along the column.

Different researchers (Raal and Khurana, 1973; Astarita et al., 1983; Krishnamurthy et al., 1986) have reported the existence of significant heat effects and temperature bulges both in physical and reactive absorption processes. Astarita et al. (1983), for instance, illustrated a case of simultaneous absorption of CO₂ and H₂S in a solution of monoethanolamine/diethylene glycol/water. With a high acid gas concentration, the measured temperature rise was over 40°C in the high temperature zone (temperature bulge).

These thermal effects in reactive absorption systems can be mathematically described using the concepts presented in Section 2.6 along with the energy balance around the tray or section of packing. For a countercurrent packed contactor, assuming constant heat capacities, and vapor and liquid flow rates through the column, the following equations describe the energy balances:

At the vapor side,

$$\frac{C_p^v G}{S p \pi^2 f} \left(\frac{dT^v}{dz} \right) = q^v = h^v (T^v - T^i) \quad (2.69)$$

At the liquid side,

$$\frac{Cp^L L}{Sp\pi^2 f} \left(\frac{dT^L}{dz} \right) = q^L = h^L (T^i - T^L) \quad (2.70)$$

Considering the condition of continuity of the energy flux across the vapor-liquid interface (Equations 2.60), the conductive heat flux and convective enthalpy transfer are related by:

$$q^L = q^v + \sum_{k=1}^n (\bar{H}_k^v - \bar{H}_k^L) N_k \quad (2.71)$$

Substituting Equation 2.71 into Equation 2.70 and assuming that most of the resistance to the heat transfer is at the vapor side ($T^L \approx T^i$ and $h^L \rightarrow \infty$), the following set of equations is obtained:

$$\frac{Cp^v G}{Sp\pi^2 f} \left(\frac{dT^v}{dz} \right) = q^v = h^v (T^v - T^L) \quad (2.72)$$

$$\frac{Cp^L L}{Sp\pi^2 f} \left(\frac{dT^L}{dz} \right) = q^L = h^v (T^v - T^L) + \sum_{k=1}^n (\bar{H}_k^v - \bar{H}_k^L) N_k$$

The set of differential equations 2.72 relate the temperature variations through the column with the conductive heat transfer and convective enthalpy transfer. Since the convective enthalpy transfer is coupled with the calculations of the interfacial fluxes of the different components, Equations 2.72 has to be solved simultaneously with the mass balances at the liquid and vapor sides and the condition of continuity of fluxes through the interface.

In order to illustrate a qualitative prediction by Equations 2.72, a linear profile for the fluxes was assumed ($N_k = a + bz$) where z is the position along the column, and the flux of the liquid solvent (water) was allowed to change sign at some point along the column (as it was observed in the rigorous calculations

presented in Chapter 6). The enthalpy change of the diffusing species resembles those for acid gases and water. The dimensions of the column are the same as the packed column described in Chapter 6 for the base case. Figure 2.2 depicts these qualitative temperature profiles.

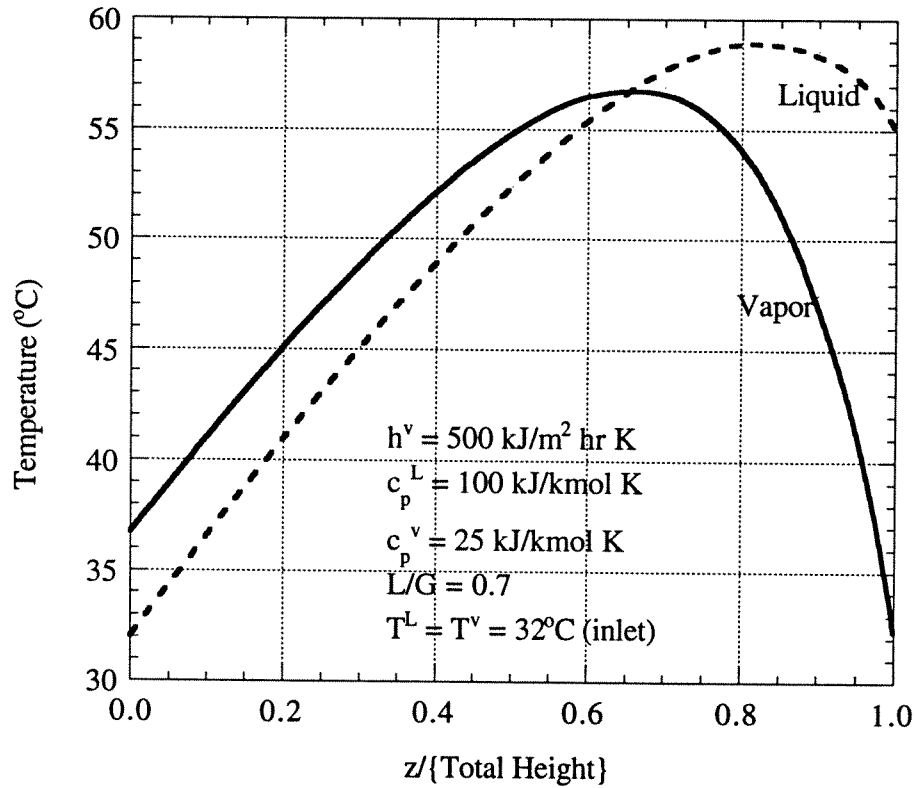


Figure 2.2. Qualitative representation of the temperature profiles predicted by Equations 2.72 assuming linear profiles ($N_k = a + bz$) for the interfacial fluxes. $N_{\text{gas}} = 0.028 + 0.035z'$ (kmol/m² hr) and $N_{\text{water}} = 0.04 - 0.08z'$ (kmol/m² hr).

The temperature profiles represented in Figure 2.2 are qualitatively similar to those calculated rigorously and presented in Chapter 6. In Chapter 6 a more detailed description of these thermal effects will be given with emphasis on the contribution of each heat transfer mechanism along the column.

2.8 NOMENCLATURE

[A]: Concentration of species A (kmol/m³).

C_p: Heat capacity (Kj/kmol K).

D: Fickian Diffusion coefficient (m²/sec).

Đ: Maxwell-Stefan Diffusion coefficient (m²/sec).

D_{i,eff}: Effective Diffusion coefficient of component i in pseudobinary approach (m²/sec).

E: Enhancement factor.

f: Fraction of interfacial area to total area [-].

G: Vapor flow rate (kmol/sec).

h: Heat transfer coefficient (Kj/m² hr K).

H: Column height (m).

\bar{H}_i : Partial molar enthalpy of component i (Kj/kmol).

J_i: Diffusive flux of component i (kmol/m² sec).

k*: Low flux mass transfer coefficient (m/sec).

k₁: Forward reaction rate constant for a first-order reaction (1/sec).

k₂: Forward reaction rate constant for a second-order reaction (m³/kmol sec).

k_{2,p}: Forward reaction rate constant for a second-order reaction that involves a primary or secondary amine (m³/kmol sec).

k_{2,t}: Forward reaction rate constant for a second-order reaction that involves a tertiary amine (m³/kmol sec).

k_{2,r}: Reverse reaction rate constant for a second-order reaction (m³/kmol sec).

k_{L,i}^o: Physical mass transfer coefficient of species i in the liquid phase (m/sec).

K: Equilibrium constant of a chemical reaction [-].

L: Liquid flow rate (kmol/sec).
 N_i : Molar Flux of species i (kmol/m² sec).
 q: Conductive heat flux (Kj/m² hr)
 r: Radius of the column (m).
 R: Rate of reaction (kmol/m³ sec) or gas constant (Joules/kmol K).
 s: Parameter in Danckwerts model. Defined in Equation 11 (1/sec).
 Sp: Specific area of the packing (m²/m³).
 t: Time (sec).
 T: Temperature (K).
 u_i : Velocity of transfer of component i (m/sec).
 x: Spatial coordinate (m).
 x_i : Mole fraction of component i [-].
 z: Position along the column (m).
 z' : Dimensionless position along the column (z/H).

Greek Symbols:

$[\beta]$: Bootstrap matrix [-].
 γ_i : Activity coefficient of component i in solution [-].
 Γ : Thermodynamic factor for binary systems [-].
 $[\Gamma]$: Matrix of thermodynamic factors [-].
 δ : Film thickness (m).
 δ_{ij} : Kronecker delta, 1 if i = j, 0 if i \neq j [-].
 η : Dimensionless spatial coordinate (x/ δ).
 κ_{ij} : Maxwell-Stefan mass transfer coefficients for the pair i-j (m/sec).
 μ_i : Chemical potential of component i (Joules/kmol).
 Ξ : Correction factor for high fluxes in binary mass transfer [-].
 $[\Xi]$: Matrix of high flux correction factor [-].

θ : Contact time (sec).

Superscripts:

*: At equilibrium.

$[\bar{A}]$: Time-mean concentration of species A (kmol/m³).

L: For the liquid.

$[\bar{N}]$: Time-mean interfacial flux (kmol/ m² sec).

v: For the vapor.

Subscripts:

A: Evaluated for component A.

i: At the vapor-liquid interface or related to species i.

o: Evaluated at the liquid bulk.

2.9 REFERENCES

- Astarita, G., Savage, D. W., Bisio, A., "*Gas Treating with Chemical Solvents*," Wiley: New York, 1983.
- Bird, R. B., Stewart, W. E., Lightfoot, E. N., "*Transport Phenomena*," Wiley:
- Blauwhoff, P.M.M., Versteeg, G.F., van Swaaij, W.P.M., "A Study of the Reaction Between CO₂ and Alkanolamines in Aqueous Solutions," *Chem. Engng. Sci.* **1984**, 39, 207. New York, 1960.
- Critchfield, J. E., "CO₂ Absorption/Desorption in Methyldiethanolamine Solutions Promoted with Monoethanolamine and Diethanolamine: Mass Transfer and Reaction Kinetics". Ph.D. Dissertation, The University of Texas at Austin, 1988.
- Critchfield, J. E., Rochelle, G. T., "CO₂ Absorption into Aqueous MDEA and MDEA/MEA Solutions," Presented at the AIChE National Meeting, Houston, Texas, March 1987.
- Danckwerts, P. V., *Gas Liquid Reactions*. McGraw-Hill Inc., New York, 1970.
- Danckwerts, P. V., "The Reaction of CO₂ with Ethanolamines," *Chem. Eng. Sci.* **1979**, 34, 443.

- DeCoursey, W. J., Thring, R. W., "Effects of Unequal Diffusivities on Enhancement Factors for Reversible and Irreversible Reaction," *Chem. Engng. Sci.* **1989**, 44, 1715.
- DeCoursey, W. J., "A Simpler Approximation for Enhancement of Mass Transfer by Second-Order Reversible Reaction," *ICHEME. Symp. Ser.* **1992**, 128, B269.
- Donaldson, T. L., Nguyen, Y. N., "Carbon Dioxide Reaction Kinetics and Transport in Aqueous Amine Membranes," *Ind. Eng. Chem. Fundam.* **1980**, 19, 260.
- Frank, M. J. W., Kuipers, J. A. M., Versteeg, G. F., Van Swaaij, W. P. M., "Modelling of Simultaneous Mass and Heat Transfer with Chemical Reaction Using the Maxwell-Stefan Theory-I. Model Development and Isothermal Study," *Chem. Engng. Sci.* **1995**, 50, 1645.
- Glasscock, D. A., "Modelling and Experimental Study of Carbon Dioxide Absorption into Aqueous Alkanolamines". Ph.D Dissertation, The University of Texas at Austin, 1990.
- Glasscock, D. A., Rochelle, G. T., "Numerical Solution of Theories for Gas Absorption with Chemical Reaction," *AIChE Journal* . **1989**, 35, 1271.
- Hagewiesche, D. P., Ashour, S. S., Al-Ghawas, H. A., Sandall, O. C., "Absorption of Carbon Dioxide into Aqueous Blends of Monoethanolamine and N-Methyldiethanolamine," *Chem. Engng. Sci.* **1995**, 50, 1071.
- Krishna, R., "A Film Model Analysis of Non-Equimolar Distillation of Multicomponent Mixtures," *Chem. Engng. Sci.* **1977**, 32, 1197.
- Krishna, R., Wesselingh, J. A., "The Maxwell-Stefan Approach to Mass Transfer," *Chem. Engng. Sci.* **1997**, 52, 861.
- Krishnamurthy, R., Taylor, R., "Absorber Simulation and Design Using a Nonequilibrium Stage Model," *Can. J. Chem. Eng.* **1986**, 64, 96.
- Raal, J. D., Khurana, M. K., "Gas Absorption with Large Heat Effects in Packed Columns," *Can. J. Chem. Eng.* August **1973**, 51, 162.
- Rinker, E. B., Ashour, S. S., Sandall, O. C., "Kinetics and Modeling of Carbon Dioxide Absorption into Aqueous Solutions of N-methyldiethanolamine," *Chem. Eng. Sci.* **1995**, 50, 755.
- Taylor, R., Krishna, R., *Multicomponent Mass Transfer*. Wiley, New York, 1993.

- Valerio, S., Vanni, M., "Interfacial Mass Transfer and Chemical Reaction in Non-Ideal Multicomponent Systems," *Chem. Engng. Sci.* **1994**, 49, 3297.
- Vanni, M., Baldi, G., "Mass Transfer and Chemical Reaction with Multicomponent Diffusion," *Chem. Engng. Sci.* **1991**, 46, 2465.
- Versteeg, G. F., Kuipers, J. A. M., van Beckum, F. P. H., van Swaaij, W. P. M., "Mass Transfer with Complex Reversible Chemical Reactions-II. Parallel Reversible Chemical Reactions," *Chem. Engng. Sci.* **1990**, 45, 183.
- Zarzycki, R., Chacuk, A., *Absorption, Fundamentals and Applications*. Pergamon Press. Oxford, Great Britain, 1993.

Chapter 3

Packed and Trayed Column Modeling

3.1. INTRODUCTION

It is beyond the scope of this dissertation to explore the hydrodynamics of packed and trayed columns thoroughly. However, some review of the previous work in this area is needed to place the material in Chapter 6 in its proper context. In this chapter the theory of the hydrodynamics of trayed and packed columns is reviewed. Specifically, the different flow regimes that can be encountered in these contactors, as well as the mass transfer characteristics, are analyzed. This theory is a significant part of the sub-models needed for the successful implementation of the rate-based model for reactive absorption that is presented in Chapter 6.

3.2. TRAYED COLUMN HYDRODYNAMICS

From the hydrodynamic point of view, trays can operate under five main hydrodynamic or flow regimes. These regimes may occur on a given tray under different conditions of vapor and liquid flow rates. Lockett (1986), Kister (1992) and Zarzycki et al. (1993) give an excellent description of these flow regimes.

a) *Bubbling Regime*: Exists only at very low gas rates and its main feature is that bubbles rise in swarms through a fairly quiescent liquid which has a very clear surface.

b) *Foam Regime*: Foams tends to result when bubble coalescence is hindered. This regime is more common in aqueous systems and especially at low vapor velocities in columns of small diameter, where the wall provides foam stabilization.

c) *Froth Regime*: This regime is bounded by the bubbling regime at low gas velocities and by the spray regime at high gas velocities. Gas passes through the liquid as jets and bubbles of ill-defined and rapidly changing shape. The froth regime is the most common in distillation practice.

d) *Spray Regime*: While in the three previous flow regimes vapor is distributed in continuous liquid, in the spray regime the liquid on the tray is almost completely dispersed in the form of drops of various sizes. The bulk of the liquid is present as drops that reside at high elevations above the tray. This regime is favoured by high gas momentum and low liquid depths and frequently occurs in industrial vacuum fractionation.

e) *Emulsion Regime*: Occurs at high liquid loading and relatively small gas flow. Due to a high liquid velocity, the gas jets flowing out from the holes in the plate do not flow vertically upwards but are inclined at some angle towards the liquid flow direction. The dispersed gas forms an emulsion with the liquid which flows through the weir to the downcomer where the gas is separated from the liquid phase. This regime is favoured by a high horizontal liquid momentum compared with the vertical gas momentum. In industrial practice, the emulsion regime occurs in high pressure and high liquid rate operations.

Authors like Zarzycki et al. (1993) suggest that the analysis of tray hydrodynamics can be done by considering only the existence of three regimes:

spray, froth and emulsion. Specifically for sieve trays, Lockett (1981) and Zuiderweg et al. (1984) discuss the hydrodynamic conditions for the transition from froth regime to spray and emulsion regimes, respectively. Lockett (1981) used the jet penetration model and a force balance during the bridging of the gas jet by the liquid in order to develop an equation that describes the hydrodynamic condition of the tray during the froth-spray transition. Lockett found that this theoretically derived equation did not compare with experimental data very well; therefore, an empirical correlation was proposed. He found that the transition from froth to spray regime can be achieved when the following condition is satisfied:

$$CF > 0.36 \frac{h_{cl}\phi_b}{d_h} \quad (3.1)$$

where h_{cl} is the clear liquid height (defined below), ϕ_b is ratio of the hole area (A_h) to the bubbling (or active) area (A_b), d_h is the hole diameter and CF (m/s) is the capacity factor defined as:

$$CF = u_{gb} \left(\frac{\rho_g}{\rho_l} \right)^{0.5} \quad (3.2)$$

where u_{gb} (m/s) is the gas velocity based on the gas bubbling area and ρ_g and ρ_l are the vapor and liquid densities, respectively. In Equation 3.1 the constant 0.36 has units of m/s.

With respect to the transition from froth to the emulsion regime, Zuiderweg et al. (1984) considered that it happens when the horizontal momentum flux of the liquid exceeds the vertical momentum flux of the vapor

emerging from the holes in the sieve tray. Combining this consideration with experimental observations, they found that the transition is achieved when:

$$FP > 3h_{cl}b_b \quad (3.3)$$

where b_b is the weir length per bubbling area (m/m²) and FP is the flow parameter defined by:

$$FP = \frac{LMw_L}{GMw_g} \left(\frac{\rho_g}{\rho_l} \right)^{0.5} = \frac{u_{lb}}{u_{gb}} \left(\frac{\rho_l}{\rho_g} \right)^{0.5} \quad (3.4)$$

where L and G are the liquid and vapor molar velocity based on the active area, and u_{lb} is the liquid velocity based on the active area. FP represent a ratio of the kinetics energy of the liquid to that of the vapor.

In the equations presented above, the clear liquid height, h_{cl} , is defined as (Lockett, 1986) the volume of liquid in the dispersion per unit bubbling area, i.e., the liquid depth to which the dispersion would collapse if the gas and liquid flows were instantaneously cut off and weeping could be prevented. The clear liquid height is used to determine the liquid holdup on the tray which in turns is an important variable in reactive processes where chemical reactions take place in the liquid phase. Besides its use in mass balance calculations, the liquid holdup is generally an important variable used to correlate mass transfer coefficients in trayed columns.

The average liquid fraction, α , in the gas/liquid dispersion on the tray is related to the dispersion height h_f by:

$$\alpha = \frac{h_{cl}}{h_f} \quad (3.5)$$

The clear liquid height can be calculated using a purely empirical correlation found by Hofhuis and Zuiderweg (1979) for both spray and emulsion regimes:

$$h_{cl} = 0.6h_w^{0.5}p^{0.25}\left(\frac{FP}{b_b}\right)^{0.25} \quad (3.6)$$

where h_w is the weir height and p is the pitch of the holes on the sieve tray. This correlation is valid in the following range:

$$0.025 \text{ m} < h_w < 0.1 \text{ m} \quad \text{and} \quad 0.007 \text{ m} < d_h < 0.01 \text{ m}$$

Lockett (1986) notes that the validity of Equation 3.6 in the spray regime is questionable since the experimental evidence suggests that h_{cl} is almost independent of the weir height.

Hofhuis (1980) found a correlation for the average liquid fraction, α , in the two phase mixture on the tray. It is as follows:

$$\frac{1}{\alpha} - 1 = C \left(\frac{u_{gb}}{(gh_{cl})^{0.5}} \left(\frac{\rho_g}{\rho_l} \right)^{0.5} \right)^n \quad (3.7)$$

for the spray regime: $C = 265$ and $n = 1.7$.

for the froth and emulsion regimes: $C = 40$ and $n = 0.80$.

From the equations presented above the total liquid holdup on the tray can be calculated using the following relation:

$$\{\text{Liquid holdup}\}(\text{m}^3) = \alpha h_f A_b = h_{cl} A_b \quad (3.8)$$

where A_b is the bubbling area.

Dhulesia (1984) reported an empirical relationship for the clear liquid height in valve trays for froth and mixed flow (froth-spray) regimes,

$$h_{cl} = 0.42h_w^{2/3}\Psi^{1/3} \quad (3.9)$$

with Ψ being a flow ratio group defined by:

$$\Psi = \frac{q/b \left(\frac{\rho_l}{\rho_g} \right)^{0.5}}{u_{gb}} \quad (3.10)$$

where q is the liquid flow rate (m^3/sec) and b is the exit weir length (m).

3.2.1 Mass Transfer Characteristics

Mass transfer coefficients and interfacial areas in gas-liquid contactors are usually estimated from empirical correlations that are developed using chemical or physical methods. These correlations generally express the number of mass transfer units or mass transfer coefficients in terms of the vapor and liquid loads, and transport and physical properties of the system.

The AIChE Bubble-Tray Design Manual (1958) presents a comprehensive calculation procedure for the mass transfer coefficients at the vapor and liquid sides in bubble-cap trays. The following expressions were developed for the vapor and liquid film mass transfer coefficients, respectively:

$$k_g a = \frac{(0.776 + 4.567h_w - 0.2377F + 104.85Q_L)}{P_{\text{tot}} (Sc_g)^{0.5}} G \quad (3.11)$$

$$k_L a = \sqrt{4.127E + 8 D_i^L} (0.213F + 0.15) \left(\frac{Lt_L}{c_{\text{tot}}} \right) \quad (3.12)$$

where a is the interfacial area based on column active area. The liquid residence time, t_L , is calculated by:

$$t_L = \frac{h_{cl} Z_L}{Q_L} \quad (3.13)$$

and the clear liquid height, h_{cl} , (called liquid hold-up by some authors) is calculated from:

$$h_{cl} \text{ (m)} = 0.04191 + 0.19h_w + 2.4545Q_L - 0.0135F \quad (3.14)$$

Equation 3.11 was developed from experimentally measured values of point efficiencies for two systems: the absorption of ammonia from air with water and the distillation of acetone-benzene. Equations 3.12 and 3.14 were obtained from experimental measurements of point efficiencies for the desorption of oxygen from oxygen-rich water with air and the distillation of n-pentane-p-xylene.

Other researchers have published correlations and procedures for estimating mass transfer coefficients in different types of trays. Among them, the work of Chan and Fair (1984) and Miyahara et al. (1990) on sieve trays, and Scheffe and Weiland (1987) on valve trays are worthy of mention. However, there is a tendency to place more emphasis in developing models for gas-film mass transfer coefficients because mass transfer processes in distillation are generally gas-phase controlled. In gas absorption processes, and especially reactive absorption, the mass transfer resistance can be distributed between the vapor and the liquid or completely in the liquid phase. Therefore, good estimates of both resistances are needed.

In the process of choosing the appropriate model for liquid and vapor film mass transfer coefficients, the models mentioned above were compared. In the present work it was found that especially for high vapor and liquid rates Scheffe and Weiland (1987) overestimate the mass transfer coefficient at the liquid side compared with the predictions of Chan and Fair (1984) and Miyahara et al. (1990) for sieve trays, and the AIChE model for bubble-cap trays. The predictions of the vapor-side mass transfer coefficient by Scheffe and Weiland are, for most

conditions, in good agreement with the predictions of other researchers on sieve and bubble-cap trays. This comparison is based on the hypothesis that trayed columns, under the same operating conditions, have similar mass transfer regardless of the type of tray (valve, sieve or bubble-cap). In this work the AIChE model for bubble trays (Equation 3.11 through 3.14) was chosen for estimating the mass transfer coefficients as representative of the general behaviour of trays.

The evaluation and prediction of interfacial area on trays has been a challenge for chemical engineering research for many years (Fair, 1985; Fair, 1997). Significant progress has been made in fulfilling this challenge, but still prediction of interfacial area on trays from first principles is almost impossible to accomplish. This complexity involved in the prediction of interfacial area is accompanied with the fact that, in general, volumetric mass transfer coefficients ($k_L a$, $k_g a$) are correlated from experimental data, but not much emphasis is placed on evaluating the interfacial area itself. This is due in part because efficiencies can be calculated from volumetric mass transfer coefficients.

When modelling reactive absorption, however, both interfacial area and mass transfer coefficients are needed separately in order to represent in the governing equations the effect of the chemical reactions on the interfacial mass transfer. The research results presented by AIChE (1958) on bubble-trays do not include interfacial area measurements.

Scheffe and Weiland (1987) and Miyahara et al. (1991) present empirical correlations for evaluating interfacial areas on valve and sieve trays, respectively. Also, Zuiderweg (1982) reports two expressions for estimating interfacial areas

on sieve trays for spray and mixed/emulsion flow regimes showing that in the range of vacuum to high pressure distillation the interfacial area per unit of active area can vary from 40 to 250 m²/m².

Miyahara et al. (1991) measured the gas-liquid interfacial area and liquid-film volumetric mass transfer coefficient using a chemical method: oxidation of aqueous sodium sulfite with oxygen using cobalt sulfate as a catalyst. This reaction is liquid-film controlled. These researchers correlated data for interfacial area, including data reported by Zuiderweg (1982), in terms of the Weber number (We):

$$a = 548We^{0.5} ; 10^{-3} < We < 10^{-2} \text{ (froth regime)} \quad (3.15)$$

$$a = 63We^{0.2} ; 2 \times 10^{-3} < We < 2 \text{ (partially developed spray/mixed froth regime)} \quad (3.16)$$

Scheffe et al. (1987) measured the interfacial area on valve trays using also a chemical method: absorption of CO₂ into sodium hydroxide. The experimental measurements were correlated using the Reynolds number of the gas and liquid phase and the weir height:

$$a = 0.270Re_G^{0.375}Re_L^{0.247}h_w^{0.515} \quad (3.17)$$

These researchers did not distinguish between the different flow regimes on the tray, and developed general correlations for the whole range of vapor and liquid loads studied.

Figure 3.1 shows a comparison between the interfacial areas predicted by Equations 3.15 and 3.16 with those predicted by Equation 3.17 for low and high liquid and vapor loads. It can be seen that there is good agreement between their predictions. It seems that the accuracy at which interfacial areas can be measured

do not allow to distinguish possible differences between interfacial areas on different type of trays. In this work the correlation 3.17 of Scheffe et al. (1987) was chosen for estimating interfacial areas on bubble cap trays.

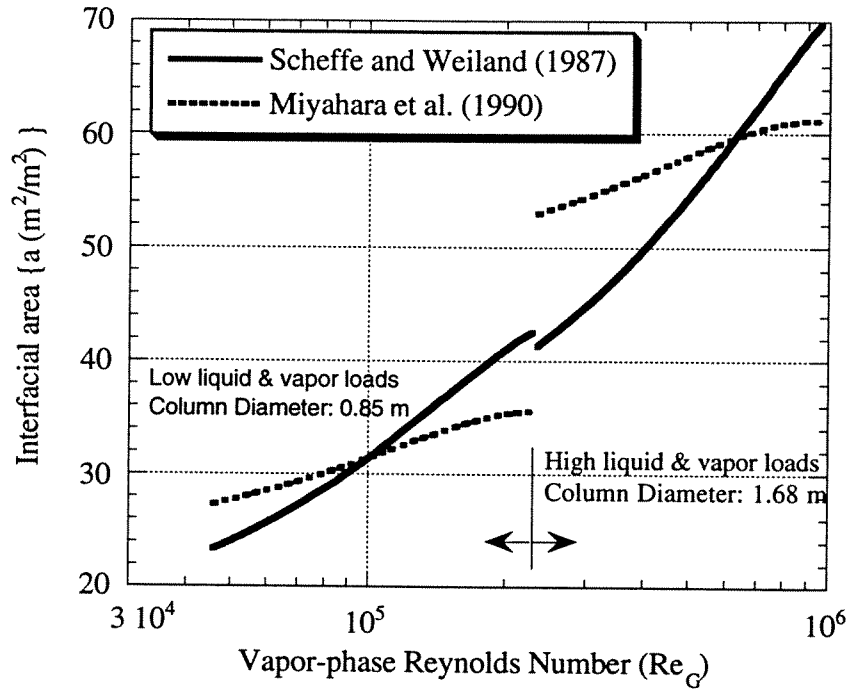


Figure 3.1. Interfacial areas on trays predicted by Scheffe and Weiland (1987) for valve trays and Miyahara et al. (1990) on sieve trays.

3.2.2 Flooding Condition

Flooding occurs when there is excessive accumulation of liquid inside a column. This accumulation of liquid is generally caused by different mechanisms. The reader is referred to Lockett (1981) and Kister (1992) for an in-depth review of flooding mechanisms.

The concept of flooding is important because generally columns are sized such that there is a certain approach to flooding that permits appropriate

operation. The flood point serves as the upper bound for vapor capacity considerations. In the present work, the correlation developed by Fair (1985) was used to assure that the reactive absorption trayed columns modelled had an appropriate approach to flooding. This correlation has been widely used in industry for flooding predictions. The vapor velocity based on the tray net area at flooding is calculated from:

$$u_{N,flood} \text{ (ft/sec)} = C_n \left(\frac{\sigma}{20} \right)^{0.2} \sqrt{\frac{\rho_L - \rho_v}{\rho_v}} \quad (3.18)$$

where the surface tension, σ , is in dyne/cm and the C-factor at flooding, C_n , is determined grafically for a given tray spacing and value of the flow parameter defined by Equation 3.4. The recommended approach to flooding for design purposes is 80 to 85% (Kister, 1992). This safety margin allows for inaccuracies in data and correlations, and also since a significant decrease in efficiency occurs just before the flood point, this practice avoids the problem region.

3.3. PACKED COLUMN HYDRODYNAMICS

Modeling of the fluid dynamics in this type of contacting device is generally based on the assumption that the force over the liquid of density ρ_l exerted by gravity is in equilibrium with the shear forces at any point in a given coaxial layer of thickness s within the liquid film and that the frictional force exerted by the vapor of density ρ_v acts at the surface of the film (Billet, 1995). This force balance leads to the following equation that relates the mean local velocity $u_{l,av}$ of the liquid descending countercurrently to an ascending stream of vapor flowing at a mean velocity $u_{v,av}$ within the bed of packing:

$$u_{l,av} = \frac{s_o}{\mu_l} \left(\frac{1}{3} g s_o \rho_l - \frac{1}{4} \xi u_{vav}^2 \rho_v \right) \quad (3.19)$$

where s_o is the total thickness of the liquid film, μ_l is the viscosity of the liquid and ξ is the resistance factor. The resistance factor is introduced to account for variables like transition from laminar to turbulent flow, the geometry of the packing, and the formation of oblique channels due to the packing texture.

A very important variable used in the modeling and analysis of packed beds is the liquid holdup, h_L . It is defined as the volume of liquid that exists in the form of a film on the surface of the packing or is present in voids, dead spots, and phase boundaries in the bed of packing during the period in which the liquid phase descends at a constant rate onto the surface of the bed. Equation 3.19 can be used to develop a relation for the liquid holdup in the column under operating conditions.

The following relationship exists between the mean liquid velocity $u_{l,av}$ and the liquid volumetric flowrate, u_l , which is commonly used in column design problems:

$$u_{l,av} = \frac{u_l}{h_L} \quad (3.20)$$

The liquid volumetric flowrate, u_l , is given per unit cross section of column and the liquid holdup, h_L , in Equation 3.20 is expressed in terms of volume of liquid per volume of packed column (e.g. m^3/m^3). A similar relationship between the mean vapor velocity, $u_{v,av}$, and the vapor volumetric flowrate, u_v , exists,

$$u_{v,av} = \frac{u_v}{\epsilon - h_L} \quad (3.21)$$

where ϵ is the void fraction of the bed.

If the packing is uniformly wetted, the theoretical relation between the total film thickness, s_o , and the liquid holdup is as follows:

$$h_L = s_o a \quad (3.22)$$

where a is the ratio of the surface area of the packing to the volume of the bed. This parameter only depends on the geometry of the packing. At the liquid loads commonly encountered in practice the surface of the packing is not uniformly wetted. In this case, the thickness s_o of the descending liquid film can be described in terms of the liquid holdup h_L and the *hydraulic* area a_h of the packing surface:

$$s_o = \frac{h_L}{a_h} \quad (3.23)$$

Substituting the expressions for $u_{l,av}$, $u_{v,av}$ and s_o given by Equations 3.20, 3.21 and 3.23 into Equation 3.19, the following equation for the liquid holdup is obtained (Billet, 1995):

$$h_L = \left(\frac{u_l \mu_l a^2}{\frac{1}{3} \rho_l g - \frac{1}{4} \xi_l \frac{a_h \rho_v u_v^2}{h_L (\epsilon - h_L)^2}} \right)^{1/3} \left(\frac{a_h}{a} \right)^{2/3} \quad (3.24)$$

This equation applies for the entire loading range and it allows for all the main parameters that affect the liquid holdup up to the flood point in a two-phase countercurrent column: the phase densities ρ_l and ρ_v , the phase loads u_l and u_v , the liquid viscosity μ_l , the resistance factor ξ_l , and the acceleration of gravity g .

Extensive experimental studies reported by Billet (1995), aimed at analyzing the hydrodynamics of a great variety of packings, led to the following expression for the resistance factor:

$$\xi = \frac{g}{C^2 \left(\left(\frac{\mu_l}{\mu_v} \right)^m \Psi \right)^n} \quad (3.25)$$

where C is a constant that depends only of the type of packing, μ_l / μ_v is the viscosity ratio for the two phases, the exponents m and n are independent of the type of packing and Ψ is the flow parameter given by:

$$\Psi = \frac{L}{G} \left(\frac{\rho_v}{\rho_l} \right)^{1/2} \quad (3.26)$$

where L and G are the mass liquid and vapor flow rates, respectively. Experimental studies have shown that the value of the parameter n in Equation 3.25 is constant in the flow regime where the continuous phase is the gas and the disperse phase is the liquid, but this constant changes to a different value after the phase inversion, that is, when the liquid becomes the continuous phase and the vapor the disperse phase. This phase inversion occurs when the flow parameter is equal to 0.4.

3.3.1. Loading and Flooding Conditions

The loading point in two-phase countercurrent flow is reached whenever the gas velocity is such that the local liquid velocity becomes zero at the surface of the film (gas-liquid interface) and the liquid commences to hold up in the column.

The liquid holdup at the loading point, $h_{L,S}$, is given by the following expression (Billet, 1995 and Billet et al. 1995):

$$h_{L,S} = \left(\frac{12 u_l^2 a}{g} \right)^{1/3} \left(\frac{u_l \rho_l}{a \mu_l} \right)^{-1/3} \left(\frac{a_h}{a} \right)^{2/3} = 12^{1/3} Fr_L^{1/3} Re_L^{-1/3} (a_h/a)^{2/3} \quad (3.27)$$

where Re_L and Fr_L are the Reynolds and Froude numbers of the liquid phase.

The ratio of the hydraulic to total surface area of the packing has been correlated to an empirical function and it was found that this ratio depends on the liquid Reynolds number and the Froude number. The following relations were obtained from fluid dynamics studies in a variety of packings:

$$\left(\frac{a_h}{a} \right) = C_h Re_L^{0.15} Fr_L^{0.1} ; \text{ for } Re_L < 5 \quad (3.28)$$

$$\left(\frac{a_h}{a} \right) = 0.85 C_h Re_L^{0.25} Fr_L^{0.1} ; \text{ for } Re_L > 5 \quad (3.29)$$

The packing constant to allow for liquid holdup, C_h , depends only on the geometry of the packing and is tabulated for the most commonly used packings.

Numerous studies (Mackowiak, 1990; Billet and Schultes, 1995; Billet, 1995) have shown that for vapor loads, u_v , lower than the vapor load at the loading point, $u_{v,S}$, (i.e., in the range of $u_v < u_{v,S}$) the liquid holdup is a function of the liquid load and that the vapor load exerts hardly any effect. For this reason in the analysis of hydrodynamics of packed columns it is important to know the vapor velocity at the loading point. Using the condition that at the loading point the liquid velocity at the gas-liquid interface is zero, Billet (1995) obtained the following relation:

$$u_{v,S} = \left(\frac{g}{\xi_S} \right)^{1/2} \left(\frac{\varepsilon}{a^{1/6}} - a^{1/2} \left(\frac{12\mu_l u_l}{g\rho_l} \right)^{1/3} \right) \left(\frac{12\mu_l u_l}{g\rho_l} \right)^{1/6} (\rho_l/\rho_v)^{1/2} \quad (3.30)$$

As it was mentioned above, the parameter ξ_S accounts for the shape of the flow channels and for the transition from laminar flow in the liquid phase, the general expression to calculate ξ_S is given by Equation 3.25 and the exponent n has to be determined empirically. It was found that there are two different ranges, depending of the value of the flow parameter:

$$\xi_S = \frac{g}{C_s^2 \left(\frac{L}{G} \left(\frac{\rho_v}{\rho_l} \right)^{1/2} \left(\frac{\mu_l}{\mu_v} \right)^{0.4} \right)^{2n}} \quad (3.31)$$

where,

$$n = -0.326 \quad \text{for} \quad \frac{L}{G} \left(\frac{\rho_v}{\rho_l} \right)^{1/2} < 0.4$$

$$n = -0.723 \quad \text{for} \quad \frac{L}{G} \left(\frac{\rho_v}{\rho_l} \right)^{1/2} > 0.4$$

The load point constant, C_s , is specific for the packing and is tabulated for the most commonly used packing.

Above the loading point, the shear stress in the countercurrent gas stream arrests the downward flow of the liquid film, with the result that the liquid holdup rapidly increases. Figure 3.2 depicts the qualitative relationship between the liquid holdup and the phase loads in a packed column. From this figure it can be seen that at the flooding point the derivative of the liquid holdup with respect to the vapor load tends to infinity. Another boundary condition (not seen in Figure 3.2) is that the derivative of the liquid holdup with respect to the liquid load, at

constant vapor load, tends to infinity as well. Applying these conditions to Equation 3.24, the following relations are derived at the flooding point:

for the vapor load, $u_{v,fl}$,

$$u_{v,fl} = \left(\frac{2g \rho_l}{\xi_{fl} a \rho_v} \right)^{1/2} (\epsilon - h_{L,fl})^{3/2} h_{L,fl}^{1/2} \frac{1}{\epsilon^{1/2}} \quad (3.32)$$

for the liquid load, $u_{l,fl}$,

$$u_{l,fl} = \frac{g \rho_l}{3a^2 \mu_l} \left(1 - \frac{3}{2\epsilon} (\epsilon - h_{L,fl}) \right) h_{L,fl}^3 \quad (3.33)$$

and for the liquid holdup, $h_{L,fl}$,

$$h_{L,fl}^3 (3h_{L,fl} - \epsilon) = \frac{6\rho_v \mu_l}{g \rho_l^2} a^2 \epsilon \frac{L}{G} u_{v,fl} \quad (3.34)$$

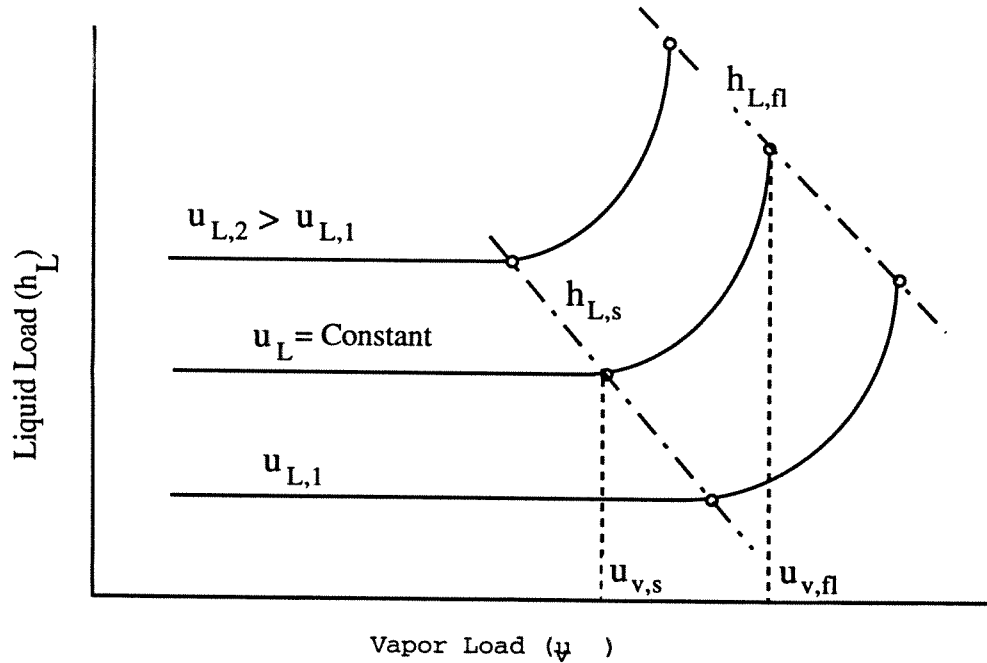


Figure 3.2. Qualitative relationship between the liquid holdup and the phase loads in a packed column.

The resistance factor, ξ_{fl} , needed for calculating the vapor load at the flood point, $u_{v,fl}$, can be calculated from a relation similar to the one used for calculating the resistance factor at the loading point. This equation is as follows:

$$\xi_{fl} = \frac{g}{C_{fl}^2 \left(\frac{L}{G} \left(\frac{\rho_v}{\rho_l} \right)^{1/2} \left(\frac{\mu_l}{\mu_v} \right)^{0.2} \right)^{2n}} \quad (3.35)$$

where the parameter n was determined empirically and, depending of the flow regime, it is given by the following relations:

$$n = -0.194 \text{ for } \frac{L}{G} \left(\frac{\rho_v}{\rho_l} \right)^{1/2} < 0.4 \quad (3.36)$$

$$n = -0.708 \text{ for } \frac{L}{G} \left(\frac{\rho_v}{\rho_l} \right)^{1/2} > 0.4 \quad (3.37)$$

Similarly to C_s , C_{fl} is a constant that depends on the shape and texture of the packing and must be determined empirically. Values thus obtained in numerous loading tests are tabulated.

The liquid holdup at the flood point, $h_{L,fl}$, must be determined by iteration from Equation 3.34. The only values of physical significance are those in the range: $\epsilon/3 < h_{L,fl} < \epsilon$.

Besides the model presented above for analyzing the hydrodynamics of packed columns at flooding, there are other models. Mackrowiak (1990) developed a model for estimating the vapor velocity and the liquid holdup at the flooding point. Mackrowiak represented the flooding in the column as a suspended bed of droplets.

It is important to mention that a comparison between the theoretical expressions presented above for the vapor load at the loading point with respect to the vapor load at the flood point leads to the conclusion that the loading point can be anticipated at about 70% of the flood point. This theoretical prediction is in good agreement with the results of numerous loading tests (Billet, 1995).

In this dissertation, Equations 3.32 through 3.34 were used to estimate the conditions at flooding and then assure a proper selection of the vapor and liquid loads when modeling the reactive absorption packed columns described in Chapter 6.

3.3.2. Mass Transfer Characteristics

Bravo and Fair (1982) concluded that the correlation developed by Onda et al. (1968) constitutes a good source for predicting the liquid and vapor film mass transfer coefficients in packed columns. The reliability of the Onda correlation is based on the wide range of packing types and sizes as well as test systems used for its development. The work conducted by Onda et al. (1968) led to the following correlations:

For the liquid-film mass transfer coefficient,

$$k_{L,i} \left(\frac{\rho_l}{\mu_l g} \right)^{1/3} = 0.0051 \left(\frac{L}{a_w \mu_l} \right)^{2/3} \left(\frac{\mu_l}{\rho_l D_{i,L}} \right)^{-1/2} (aD_p)^{0.4} \quad (3.38)$$

For the gas-film mass transfer coefficient,

$$k_{g,i} \left(\frac{RT}{aD_{i,g}} \right) = 5.23 \left(\frac{G}{a\mu_g} \right)^{0.7} \left(\frac{\mu_g}{\rho_g D_{i,g}} \right)^{1/3} (aD_p)^{-2.0} \quad (3.39)$$

Onda and coworkers used the concept of wetted area of the packing instead of interfacial area. It can be noted that the Reynolds number of the liquid was defined using the wetted area of the packing in Equation 3.38. Moreover, the gas-liquid interfacial area was assumed to be equal to the wetted area of the packing and it was predicted by a correlation developed by these researchers,

$$\frac{a_w}{a} = 1 - \exp \left\{ -1.45 \left(\frac{\sigma_c}{\sigma} \right)^{0.75} \left(\frac{L}{a\mu_l} \right)^{0.1} \left(\frac{L^2 a}{\rho_l^2 g} \right)^{-0.05} \left(\frac{L^2}{\rho_l \sigma a} \right)^{0.2} \right\} \quad (3.40)$$

$$\text{or } \frac{a_w}{a} = 1 - \exp \left\{ -1.45 \left(\frac{\sigma_c}{\sigma} \right)^{0.75} \text{Re}_L^{0.1} \text{Fr}_L^{-0.05} \text{We}^{0.2} \right\}$$

In this correlation σ_c is the critical surface tension which is equal to 61 dynes/cm for ceramic packing, 33 dynes/cm for polyethylene packing, and 75 dynes/cm for steel packing.

In this dissertation Equation 3.40 was used to estimate the interfacial area for mass transfer in packed reactive absorption columns. It was assumed that the wetted area was equal to the interfacial area. Bravo and Fair (1982) developed an improved correlation, specifically for distillation systems, for estimating the effective area for mass transfer in random packing. These researchers recognized that the effective area for mass transfer in packed columns is composed not only by the wetted area over the packing, but also by the area provided by suspended and falling droplets, film falling on the wall of the column and gas bubbles. These additional contributions to the interfacial area were not considered in this work.

3.4. COMPARISON BETWEEN TRAYS AND PACKING PERFORMANCE

Not much has been published on the comparison between the performance of trays and packings in mass transfer applications. The lack of information is especially important when comparing efficiencies for mass transfer. It has been well documented (Kister, 1992; Kurtz et al. 1991) that, for distillation systems and for atmospheric or vacuum columns, simply substituting structure packing for trays can increase the capacity by as much as 50% with an improvement in the separation efficiency as well. This improvement in the performance has been attributed to the much lower pressure drop that occurs in structured and random packing compared with that in trays.

Bravo (1998) indicates that the “rule of thumb” that is used in industry is that, for applications under 50 psig, replacing trays with packing is reflected in an increase of capacity of 20% keeping the same average efficiency, or the efficiency can be increased by 20% keeping the same capacity.

Kurtz et al. (1991) indicated that for high-pressure towers, the low-pressure-drop advantage of packing generally is not important. Moreover, experimental data and models (Lockett, 1986) show that for trays, the efficiency generally increases with increasing pressure. For packing, experimental data indicates that efficiency increases slightly with increasing pressure at moderate pressure, but it begins to decrease as pressure and temperature approach their critical values. This decrease in efficiency is believed to be related to gas back mixing in the column as the pressure and vapor density are increased. Back

mixing destroys the advantage of countercurrent contacting and therefore decreases the efficiency.

Kurts and coworkers concluded that the use of packing to improve the performance of trayed columns has not been nearly as successful for high-pressure applications as for vacuum applications. It is generally noticed that trays tend to perform better at high pressure while packing performs better under vacuum. This is consistent with the results reported by Fair (1970) which indicate that for different test systems, the efficiency of valve trays is greater than that for 1 and 2 inch Pall rings above atmospheric pressure under distillation conditions.

Figure 3.3 represents a sample calculation of the mass transfer kinetics and interfacial areas for mass transfer predicted for a tray and a section of packing using the models described above. That is, for a tray, Equations 3.11, 3.12 and 3.17 were used for the calculation of $k_g a$, $k_L a$ and interfacial area, respectively. Equations 3.38 through 3.40 were used for the calculations on the section of packing. In order to compare the predictions of the interfacial area on the same basis, the interfacial area per volume of active (or bubbling) area given by Equation 3.17 had to be transformed to the m^2 per m^3 of dispersion (froth). This conversion was done estimating the height of the dispersion on the tray using a correlation given by Lockett (1986). In this way, the interfacial area of the packing per packed volume is compared with the interfacial area on the tray per volume of dispersion.

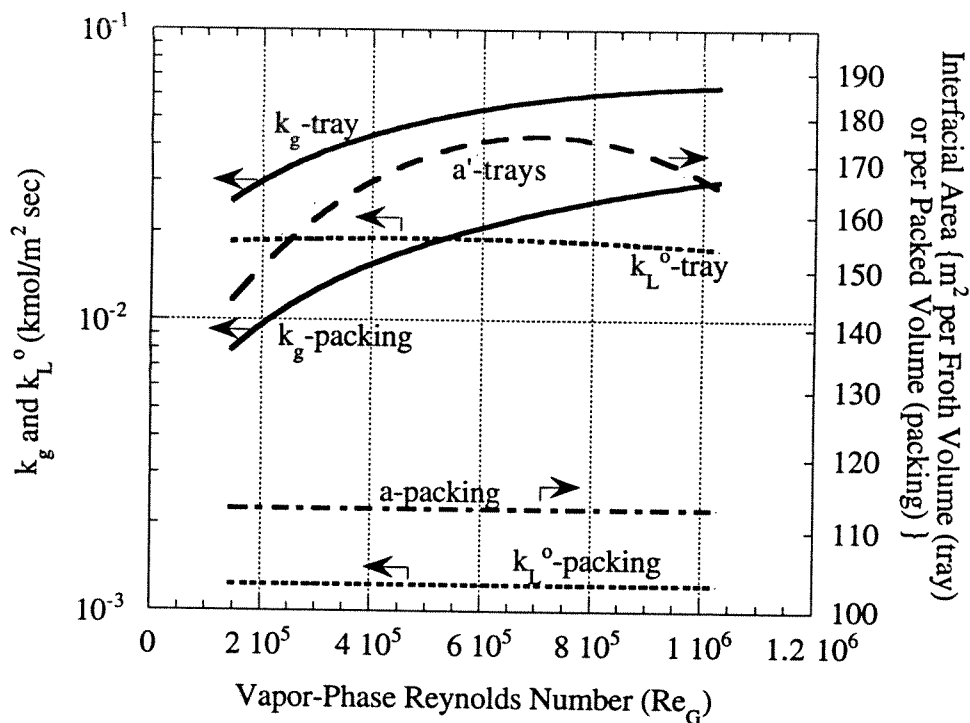


Figure 3.3. Sample calculation of mass transfer coefficients and interfacial area on a tray and packing segment. $0.77 < L/G$ (mole/mole) < 5.4 . Superficial liquid velocity: $10.6 \text{ kg/m}^2 \text{ sec}$. Weir height: 0.0508 m . Column diameter: 1.68 m . $P_{\text{tot}} = 20 \text{ atm}$. $1.5''$ Pall rings.

Figure 3.3 indicates that under the conditions of the calculations, the liquid and gas-film mass transfer coefficients are larger on the tray. The liquid-film mass transfer coefficient is over one order of magnitude larger while the gas-film mass transfer coefficient is from 2 to 3 times larger in the trayed column. It is important to note that the model used for packed columns does not have any dependency of vapor load on k_L^o . That used for trayed columns has a term dependent on the vapor load (through the F factor). However, Figure 3.3

indicates that while k_L° is a weak function of the vapor rate, $k_L^\circ a'$ varies more strongly with vapor rate in the trayed column.

The predicted interfacial area for the trayed column is from 40 to 70% larger than that for the packed column on the basis of froth volume and packed volume. For smaller packing sizes (i.e., larger surface area per unit packed volume), the packing tend to give better interfacial area than the tray which will tend to improve the performace of the packing over the tray.

It can not be concluded from Figure 3.3 that, in general, trays will perform better than packing. Important variables like total pressure of the column and packing size play a crucial role in evaluating the relative advantage of one contactor over the other. Darton et al. (1987) estimated that, for an absorber at 1.3 bar, the liquid-film mass transfer coefficient can be between 3 and 5 times larger on a tray with respect to that for a 51mm Pall ring packing. The gas-film mass transfer coefficient was estimated to be around 2.5 times larger on the tray. These researchers estimated, however, that the mass transfer efficiency of structured packing is higher than that for a random Pall ring packing of a comparable capacity. This was attributed to the somewhat higher gas-film mass transfer coefficient of the structured packing and lower specific area of the random packing.

Kister et al. (1993) compared the actual "as measured" capacity and efficiency of sieve and common valve trays at 24 inch tray spacing with a state-of-the-art 2-2.5 inch random packing and with a state-of-the-art structured packing of 67 ft²/ft³ specic area, all optimally designed. In this comparison only experimental data measured under research conditions with excellent liquid and

vapor distribution were used. The pressure range in this comparison was from 5 to 400 psia. These researchers concluded that:

a) At flow parameters (FP in Equation 3.4) between 0.02 and 0.1 the trays and the random packing have about the same efficiency, but the efficiency of the structured packing is about 50% higher than that for either trays and random packing.

b) At flow parameters between 0.1 to 0.3 again the trays and the random packing have about the same efficiency while the structured packing has between 20 and 50% higher capacity.

When applying the findings of Kister et al. (1993) to conditions encountered in practical applications (far from research conditions), the effect of maldistribution and non-optimum design of trays and packings have to be considered. It is known that liquid and vapor maldistribution is far more detrimental to packing efficiency than to tray efficiency.

This issue of comparing the efficiency for mass transfer between packings and trays is important in this work as trayed and packed reactive absorption columns are modeled and analyzed in Chapter 6.

3.5 NOMENCLATURE

A_b : Bubbling area (m^2).

A_h : Hole area (m^2).

a: Interfacial area based on column active area (m^2/m^2) or ratio of the surface area of the packing to the volume of the bed (m^2/m^3).

- a' : Interfacial area per volume of dispersion on a tray. Same as a for a packed segment (m^2/m^3).
- a_w : Wetted area of the packing per volume of the bed (m^2/m^3).
- b : Exit weir length (m).
- C : Packing constant [-].
- CF : Capacity factor for a trayed column. Defined by Equation 3.2 (m/s).
- c_{tot} : Total molar concentration of the liquid (kmole/m^3).
- D_i^g : Diffusivity of component i in the gas phase (m^2/sec).
- D_i^L : Diffusivity of component i in the liquid phase (m^2/sec).
- D_p : Nominal size of packing (m).
- d : Characteristic length used to define Re_G and Re_L in Equation (3.17). $d=1\text{m}$.
- d_h : Hole diameter in a sieve tray (m).
- F : F factor = $u_{gb}\sqrt{\rho_g}$ ($\text{kg}^{0.5}/\text{sec m}^{0.5}$)
- FP : Flow parameter. Defined by Equation 3.4 [-].
- Fr_L : Froude number of the liquid for a packed column = $\frac{u_L^2 a}{g}$.
- g : Acceleration of gravity (m^2/sec).
- G : Gas molar velocity based on active tray area ($\text{kmole}/\text{m}^2 \text{ sec}$) or superficial mass velocity of the vapor in packed columns ($\text{kg}/\text{m}^2 \text{ sec}$).
- h_{cl} : Clear liquid height (m).
- h_L : Volume of liquid per volume of packed column (liquid holdup) (m^3/m^3).
- h_w : Weir height (m).
- k_g : Gas-film mass transfer coefficient ($\text{kmole}/\text{m}^2 \text{ sec atm}$).

- k_L^o : Liquid-film physical mass transfer coefficient (m/sec).
- L : Liquid molar velocity based on active tray area (kmole/m² sec) or superficial mass velocity of the liquid in packed columns (kg/m² sec).
- Mw: Molecular weight.
- P_{tot} : Total pressure in the column (atm).
- p : Pitch of the holes on a sieve tray [-].
- Q_L : Liquid flow per average path width (m³/sec m).
- q : Liquid flow rate (m³/sec).
- Re_G : Vapor-phase Reynolds number = $\frac{GMw_g d}{\mu_g}$.
- Re_L : Liquid-phase Reynolds number. For a trayed column = $\frac{LMw_L d}{\mu_L}$. For a packed column = $\frac{u_L \rho_L}{a \mu_L}$.
- Sc_g : Schmidt number for the gas phase = $\mu_g / (\rho_g D_1^g)$.
- s_o : Thickness of the liquid film flowing within a bed of packing (m).
- t_L : Liquid residence time (sec).
- u_{gb} : Gas velocity based on active area (m/s).
- u_L : Liquid volumetric flow rate per unit cross section of packed column (m³/m² sec).
- $u_{l,av}$: Mean velocity of the liquid descending within a packing bed (m/sec).
- u_{lb} : Liquid velocity based on active area (m/s).
- $u_{N,flood}$: Vapor velocity at flooding (ft/sec).

u_v : Vapor volumetric flow rate per unit cross section of packed column ($\text{m}^3/\text{m}^2 \text{ sec}$).

$u_{v,av}$: Mean velocity of the vapor ascending within a packing bed (m/sec).

We: Weber number. For trays $= \frac{h_{cl} \rho_g u_{gb} \rho_l u_{lb}}{\sigma}$. For packing $= \frac{L^2}{\rho_l \sigma a}$ [-].

Z_L : Liquid flow path length on a tray (m).

Greek Letters:

α : Average liquid fraction in the gas/liquid dispersion on a tray [-].

ε : Void fraction of the packed bed [-].

ϕ_b : Ratio of the hole area to bubbling area [-].

μ_g : Viscosity of the vapor (kg/m sec).

μ_L : Viscosity of the liquid (kg/m sec).

ρ_g : Density of the vapor (kg/m^3).

ρ_l : Density of the liquid (kg/m^3).

σ : Surface tension (dyne/cm in Equation 3.18, N/m elsewhere).

σ_c : Surface tension (N/m).

ξ : Resistance factor for liquid flow in packings. Defined in Equation 3.19 [-].

ψ : Flow ratio group for trayed columns defined by Equation (3.10) (m). Flow parameter for packed columns defined in Equation 3.26 [-].

Subscripts:

- fl: At flooding.
- g: Evaluated for the gas phase.
- L: Evaluated for the liquid phase.
- s: At the loading point.

3.6 REFERENCES

- American Institute of Chemical Engineers. *Bubble-Tray Design Manual*. New York, 1958.
- Billet, R. *Packed Towers in Processing and Environmental Technology*. VCH Verlagsgesellschaft: Weinheim 1995.
- Billet, R., Schultes, M. "Fluid Dynamics and Mass Transfer in the Total Capacity Range of Packed Columns up to the flood Point," *Chem. Eng. Technol.*, **1995**, 18, 371.
- Bravo, J. L., Shell Oil Company. Private Communication. 1998.
- Bravo, J. L., Fair, J. R., "Generalized Correlation for Mass Transfer in Packed Distillation Columns," *Ind. Eng. Chem. Process Des. Dev.*, **1982**, 21, 162.
- Chan, H., Fair, J. R., "Prediction of Point Efficiencies in Sieve Trays. 1. Binary Systems," *Ind. Eng. Chem. Process Des. Dev.*, **1984**, 23, 814.
- Darton, R. C., Hoek, P. J., Spaninks, J. A. M., Suenson, M. M., Wijn, E. F., "The Effect of Equipment on Selectivity in Amine Treating," I.Chem. E. Symposium Series, **1987**, No.104, A323.
- Dhulesia, H., "Clear Liquid Height on Sieve and Valve Trays," *Chem. Eng. Res. Des.*, **1984**, 62, 321.
- Fair, J. R., "Comparing Trays and Packing," *Chem. Eng. Progress*, **1970**, 66, 45.
- Fair, J. R. "Stagewise Mass Transfer Processes". In "Scaleup of Chemical Processes". Bisio, A., Kabel, R.L. (Ed.), Wiley: New York, 1985.
- Fair, J. R. The University of Texas at Austin. Private Communication, 1997.
- Hofhuis, P.A.M., Thesis (T.U. Delft), 1980. Cited by Zarzycki, R. and Chacuk, A. (1993).

- Hofhuis, P.A.M., Zuiderweg, F. J., "Sieve Trays: Dispersion Density and Flow Regimes," *Inst. Chem. Engrs. Symp. Series.*, **1979**, No. 56, 2.2/1.
- Kister, H. Z., *Distillation Design*, McGraw-Hill Inc., New York, 1992.
- Kister, H. Z., Larson, K. F., Yanagi, T., "Capacity and Efficiency: How Trays and Packings Compare," Presented at the AIChE Spring National Meeting, Houston, Texas, March 31, 1993. Paper 24c.
- Kurtz, D. P., McNulty, K. J., Morgan, R. D., "Stretch the Capacity of High-Pressure Distillation Columns," *Chem. Eng. Progress*, February **1991**, 43.
- Lockett, M.J., "The Froth to Spray Transition on Sieve Trays," *Trans. Inst. Chem. Engrs.*, **1981**, 59, 26.
- Lockett, M. J., *Distillation Tray Fundamentals*, Cambridge University Press, Cambridge, 1986.
- Mackowiak, J., "Determination of Flooding Gas Velocity and Liquid Hold-up at Flooding in Packed Columns for Gas/Liquid Systems," *Chem. Eng. Technol.*, **1990**, 13, 184.
- Miyahara, T., Asoda, M., Takahashi, T., "Gas-liquid Intrefacial Area and Liquid-phase Mass Transfer Coefficient in Sieve-Plate Columns Having Large Free Areas with Downcomers," *J. Chem. Eng. Japan*, **1990**, 23, 760.
- Onda, K., Takeuchi, H., Okumoto, Y., "Mass Transfer Coefficients Between Gas and Liquid Phases in Packed Columns," *J. Chem. Eng. Japan*, **1968**, 1, 56.
- Scheffe, R. D., Weiland, R. H., "Mass Transfer Characteristics of Valve Trays," *Ind. Eng. Chem. Res.*, **1987**, 26, 228.
- Zarzycki, R., Chacuk, A., *Absorption, Fundamentals and Applications*. Pergamon Press. Oxford, Great Britain, 1993.
- Zuiderweg, F. J., "Sieve Trays, A View on the State of the Art," *Chem. Eng. Sci.*, **1982**, 37, 1441.
- Zuiderweg, F. J., Hofhuis, P.A.M., Kuzniar, J., "Flow Regimes on Sieve Trays: The Significance of the Emulsion Flow Regime," *Chem. Eng. Res. Des.*, **1984**, 62, 39.

Chapter 4

Reactive Absorption with Reversible Chemical Reactions: Experimental Methods and Contactor Characterization

4.1. INTRODUCTION

In order to study the fundamentals of gas-liquid chemical reactions, a great variety of reactors or gas-liquid contactors have been used and characterized. Danckwerts (1970) described the application of different reactors first developed in the fifties and sixties and that still are being extensively used. The stirred cell, wetted sphere, laminar jet and wetted-wall column are among the reactors most commonly used in the research of gas-liquid reactions. An important feature of these reactors is that the gas-liquid interfacial area is well defined and known.

The reactors mentioned above have different mass transfer properties which can be exploited to simulate a particular contacting device used in industry. For instance, a typical wetted-wall column gives gas-liquid contact times of the order of 0.5 sec, which is suitable for simulating a packed reactive absorption column. On the other hand, a laminar jet apparatus provides contact times of the order of thousandths of a second which resembles the contact time on trays.

In order to explore the chemical kinetics of gas-liquid reactions, different experimental methods have been developed. The rapid mixing method, for instance, consists of driving the reacting solution into a mixing chamber, from which the mixed solution flows along an observation tube. The temperature or a physical property (e.g., conductivity) of the flowing solution is measured along

the tube at different points. From the temperature rise or the change of the physical property, the extent of the reaction is calculated. Pinsent et al. (1956) determined the kinetics of the reaction between CO_2 and hydroxide ions using this technique measuring the temperature rise. More recently, Hikita et al. (1977) and Alper (1990) used the rapid mixing method in kinetic studies.

Chemical absorption tends to be a method more extensively used than the rapid mixing methods. In a reactor, rates of mass transfer of the reacting gas through the gas-liquid interface are measured, and the rates are interpreted using a mass transfer model. This model accounts for the effect of the chemical reactions on the interfacial mass transfer and chemical kinetics can be extracted. Measurements of the rates of chemical absorption-desorption for a variety of gas-liquid reactions have been conducted using stirred cells (Versteeg et al., 1989; Glasscock, 1990), wetted spheres (Rinker et al. 1995), laminar liquid jets (Hagewiesche et al., 1995) and wetted-wall columns (Mshewa, 1995).

Depending on the mass transfer regime, the mass transfer rates can be significantly affected by both diffusion limitations of reactants and/or reaction products through the liquid boundary layer and approach to equilibrium. This can become a potential disadvantage of the chemical absorption method because under those conditions the chemical kinetics no longer control the mass transfer process. Misleading results can be obtained if it is assumed that only the chemical reactions determine the interfacial mass transfer rates. However, this potential disadvantage can be exploited if a thorough model is used to interpret the rate data. Chemical kinetics, diffusion kinetics and thermodynamic

equilibrium information can be obtained by choosing the appropriate conditions at which the mass transfer rates are measured.

Equation 4.1 is the governing relation that can be used to describe the interfacial mass transfer across a gas-liquid interface. Different limiting conditions can be identified and exploited during the experimental design.

$$J = K_G(P_b - P^*) = \frac{P_b - P^*}{\frac{1}{k_g} + \frac{H}{E k_L^o}} \quad (4.1)$$

1. When the gas-film resistance is unimportant (i.e., $k_g \rightarrow \infty$), the mass transfer is completely liquid-film controlled and Equation 4.1 becomes:

$$J = \frac{E k_L^o}{H}(P_b - P^*) \approx \frac{E k_L^o}{H}(P_i - P^*) \quad (4.2)$$

Under this condition different regimes can be encountered:

1.1. The enhancement of the interfacial flux, E , is mostly determined by reaction kinetics and more specifically by the forward reaction rate. In this case, measurements of mass transfer rates in the reactor and the use of a suitable thermodynamic model to determine P^* , lead to the experimental measurement of E which in turn is directly related to the reaction kinetics.

1.2. The enhancement of the interfacial flux is controlled by the rate of diffusion of reactants and reaction products across the liquid boundary layer (reaction zone). In this case, the experimental measurements of E can be used to determine the diffusion coefficients of the reactants (except the diffusing gas) and reaction products. This regime is generally accompanied by a significant effect of the reverse reaction rate on the mass transfer.

1.3. The mass transfer driving force is significantly affected by the equilibrium partial pressure of the diffusing gas, i.e, P_i is sufficiently close to P^* . This situation can be used in systems with unknown thermodynamics to extract vapor-liquid equilibrium data from rate measurements.

2. At the other extreme, when the gas-film resistance controls the mass transfer, Equation 4.1 becomes,

$$J = k_g(P_b - P^*) \approx k_g(P_b - P_i) \quad (4.3)$$

This situation usually occurs when the enhancement of the mass transfer rate is significantly large due to a very fast reaction. This regime can be used to determine the gas-film mass transfer coefficient of the diffusing gas in the contactor, which is usually done by choosing experimental conditions such that $P_b \gg P^*$ and $J = k_g P_b$.

In practice the most likely situation that occurs is an intermediate regime between the extremes described above. In this intermediate regime, both the liquid and gas-film resistance play a role, the enhancement of the interfacial mass transfer is determined by reaction kinetics (chemical reversibility being important as well) and diffusion limitations, and the effect of the equilibrium partial pressure in determining the mass transfer driving force is significant. From these considerations it is important to note that a thorough mass transfer model is essential in interpreting the rate data measured in a gas-liquid reactor.

In this chapter a detailed description is given on the experimental techniques and reactor used for the rate measurements that constitute the experimental part of this work. The procedures followed for characterizing the

gas and liquid-film mass transfer resistance in the contactor are described as well. A discussion is also presented about the importance of Marangoni instabilities on the interfacial mass transfer.

4.2. RATE MEASUREMENTS IN THE WETTED-WALL COLUMN

Rates of mass transfer of CO₂ in chemical solvents were studied in the laboratory wetted-wall column reactor depicted in Figure 4.1. This contactor was designed, constructed and used by Mshewa (1995), but modifications were made in order to improve the accuracy of the results. A rotameter was added to measure the solution flow rate. Typical liquid rates were from 1.2 to 2.7 cm³/s.

The column was constructed from a stainless steel tube of 1.26 cm outside diameter. It has an exposed length of 9.1 cm and the interfacial area for mass transfer is 38.52 cm², which includes the surface of the column and the top section. The column is enclosed in a thick walled glass tube of 2.54 cm outside diameter which forms the reaction chamber where the gas countercurrently contacts the chemical solvent. The reaction chamber is enclosed in a heat bath constructed from a 10.16 cm outside diameter thick walled glass tube.

Figure 4.2 represents the overall flow diagram of the experimental set up. The chemical solvent is contained in a 400 cm³ stainless steel reservoir that is placed in a heating bath of paraffin oil to keep the solution at the temperature of the experiment.

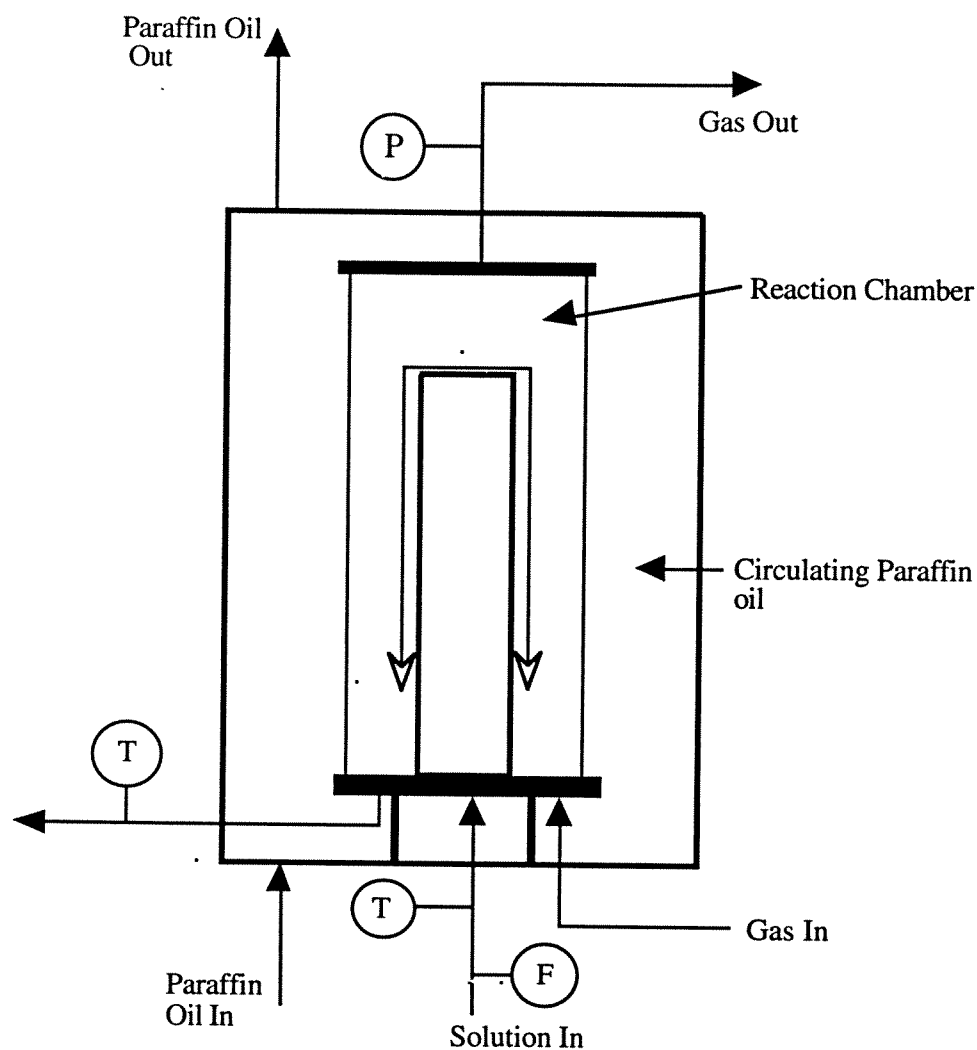


Figure 4.1. Detailed diagram of the wetted-wall column contactor.

The gas stream fed to the contactor is either a mixture of N_2 and CO_2 or pure CO_2 depending on the particular experiment. This gas stream is saturated with water upstream of the contactor in order to avoid mass transfer of water from the chemical solvent to the gas stream in the reactor which would decrease the interfacial temperature. This water saturator is a stainless steel reservoir similar

to the chemical solvent reservoir and is placed in a heat bath with a temperature close to the temperature of the experiment. In this way the gas stream bubbles through the water before entering the reaction chamber.

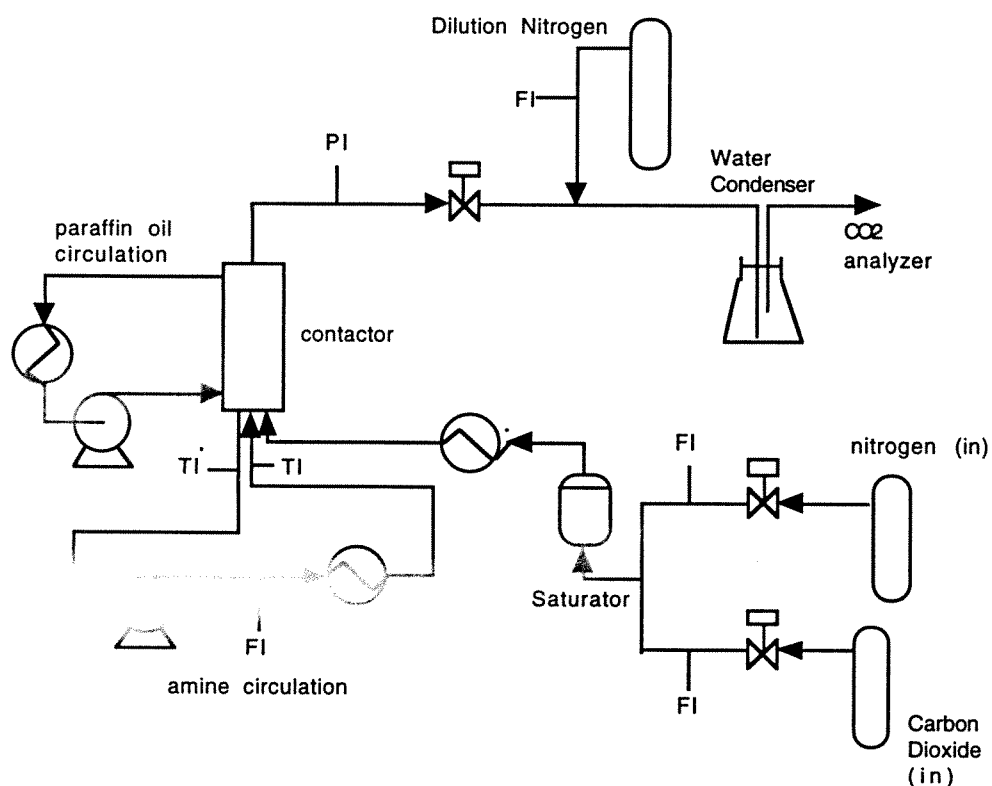


Figure 4.2. Flow Diagram of the Experimental Set up.

Infrared gas phase analyzers, HORIBA model PIR-2000, measured the concentration of CO_2 in the gas phase out of the reactor. Two analyzers were used in series connected to the outlet line of the reactor. One of these analyzer operate in the range of 0-1% and the other at 0-25% CO_2 . This configuration gives more flexibility to the experimental set up and also improves the accuracy of the CO_2 analysis. The infrared analyzers were calibrated using a varying

concentration of CO₂, in a CO₂-N₂ gas mixture, and recording the analyzer output on a strip-chart. The gas flow rate of carbon dioxide and nitrogen to the analyzer was controlled using mass flow controllers. Due to design specifications, the total gas flow rate fed to the infrared analyzer at atmospheric pressure had to be always less than 2 l/min.

The gas flow rate of N₂ and CO₂ was regulated by Brooks mass flow controllers. These flow controllers were calibrated using a soap film meter. Depending on the conditions of the experiments, a stream of dilution nitrogen downstream the reactor was needed to match the CO₂ concentration range of the CO₂ analyzer and to dilute any water vapor that could leave the reactor. The reactor was operated at a total pressure from 1 to 8 atmospheres and with CO₂ partial pressure from 0.005 to 8 atm. The total pressure in the reactor was measured by a pressure gauge located at the outlet gas line at the top of the reactor. The chemical solvent is circulated by a Cole-Parmer micropump with ten speeds. The liquid flow rate is controlled in order to maintain a smooth liquid film on the wetted-wall column. The liquid level at the bottom of the reactor is maintained at approximately the same point where the gas is fed. J-type thermocouples were installed in the solution inlet and outlet lines to the reactor for temperature measurement. The average temperature is reported.

Downstream of the dilution point a condenser removes water from the gas phase leaving the reactor to protect the CO₂ analyzer. This condenser was a 125 cm³ erlenmeyer flask in a 2000 cm³ beaker filled with ice.

Measurements of both CO₂ absorption and desorption were made with a continuously changing solution loading. Every ten to fifteen minutes the output

of the analyzers, total pressure and temperatures were recorded and a liquid sample was obtained to determine the CO₂ loading.

The amount of total CO₂ (free plus chemically combined) in the liquid phase was determined using a total carbon analyzer, model 525 from Oceanography International Corporation. A small amount of liquid sample (from 50 to 150 μ l) is injected into the solution of 30 wt% phosphoric acid to evolve the total CO₂. The CO₂ is carried by a nitrogen stream which bubbles through the acid solution to an infrared analyzer HORIBA model PIR-2000 with a range of 0-0.25% CO₂ in volume basis. The calibration of this analyzer is performed using a standard solution of sodium carbonate of approximately 7 mM concentration. Samples of the standard solution from 10 to 200 μ l are injected and the output of the analyzer is recorded on a strip chart as peaks of different heights. The CO₂ loading of a liquid sample from the reactor is calculated as the ratio of the total moles of CO₂ to the total moles of chemical solvent present in the sample.

The chemical solvents used for the gas-liquid reaction kinetic studies and reactor characterization were commercial grade methyldiethanoamine (MDEA), β,β' -hydroxyaminoethyl ether (or diglycolamine, DGA) and monoethanolamine (MEA).

4.3. COLUMN CHARACTERIZATION

From the discussion given in Section 4.1, it may be inferred that the characterization of the gas and liquid-film mass transfer kinetics (i.e., knowledge of k_g and k_L) is crucial to interpret the experimental rate data in terms of chemical and diffusion kinetics or thermodynamics of the system under study. The wetted-

wall column described in Section 4.2 was characterized by measuring the liquid and gas-film mass transfer coefficients under a wide range of conditions. The following sections described in detail the procedure used.

4.3.1. Liquid-Film Mass Transfer Coefficients

Mshewa (1995) measured rates of desorption of CO₂ from water and aqueous ethylene glycol solutions in order to determine the physical mass transfer coefficient. In this work, additional measurements of CO₂ desorption from water were performed in order to extend the experimental data obtained by Mshewa (1995).

When CO₂ is desorbed (or absorbed) from a liquid flowing down the wetted-wall column, the following equation describes the mass balance at the liquid side,

$$V_L \frac{d[\text{CO}_2]_o^L}{dt} = k_{L,\text{CO}_2}^o a ([\text{CO}_2]_i^L - [\text{CO}_2]_o^L) = \frac{k_{L,\text{CO}_2}^o a}{H_{\text{CO}_2}} (P_{\text{CO}_2,i} - P_{\text{CO}_2}^*) \quad (4.4)$$

where V_L is the volume of liquid circulating through the system, a is the interfacial area for mass transfer in the wetted-wall column, and $P_{\text{CO}_2}^*$ is the partial pressure of CO₂ in equilibrium with the liquid bulk. Assuming that desorption of CO₂ from the liquid is completely liquid film-controlled, the partial pressure of CO₂ at the interface approaches that at the vapor bulk, i.e. $P_{\text{CO}_2,i} \approx P_{\text{CO}_2,o}$. Also, considering that the molar concentration of CO₂ in the vapor is related to its partial pressure by,

$$[\text{CO}_2]_o^g = \frac{P_{\text{CO}_2,o}}{RT} \quad (4.5)$$

Equation 4.4 becomes,

$$V_L \frac{d[\text{CO}_2]_o^L}{dt} = \frac{k_{L,\text{CO}_2}^o a}{H_{\text{CO}_2}} (RT[\text{CO}_2]_o^g - H_{\text{CO}_2}[\text{CO}_2]_o^L) \quad (4.6)$$

The molar concentrations of CO_2 at the vapor and liquid bulk can be related by the mass balance at the vapor side,

$$k_{L,\text{CO}_2}^o ([\text{CO}_2]_i^L - [\text{CO}_2]_o^L) = G([\text{CO}_2]^{g,\text{in}} - [\text{CO}_2]^{g,\text{out}}) \quad (4.7)$$

where G is the vapor volumetric flow rate in the reactor and the superscript g,in and g,out indicate the concentrations at the inlet and outlet of the reactor, respectively. In the experiments performed, CO_2 was desorbed using a gas stream of pure nitrogen; therefore, $[\text{CO}_2]^{g,\text{in}} = 0$. When it is assumed that the main contribution to the driving force at the vapor side is given by the outlet CO_2 concentration (i.e., in Equation 4.6 $[\text{CO}_2]_o^g \approx [\text{CO}_2]_o^{g,\text{out}}$) and when Equation 4.7 is solved for $[\text{CO}_2]_o^L$ and substituted in Equation 4.6, the following is obtained,

$$\frac{d[\text{CO}_2]^{g,\text{out}}}{dt} = - \frac{G}{V_L \left\{ \frac{G}{k_{L,\text{CO}_2}^o a} + \frac{RT}{H_{\text{CO}_2}} \right\}} [\text{CO}_2]^{g,\text{out}} \quad (4.8)$$

This equation can be easily integrated from the start of the desorption ($t = 0$) to a given time t giving,

$$\ln \left\{ \frac{[\text{CO}_2]^{g,\text{out}}(t)}{[\text{CO}_2]^{g,\text{out}}(t=0)} \right\} = - \frac{G}{V_L \left\{ \frac{G}{k_{L,\text{CO}_2}^o a} + \frac{RT}{H_{\text{CO}_2}} \right\}} t \quad (4.9)$$

Equation 4.9 indicates that the physical mass transfer coefficient of CO_2 in the reactor can be determined by measuring the outlet vapor concentration of CO_2 and determining the slope of the plot of $\ln\{[\text{CO}_2]^{g,\text{out}}\}$ vs time. Desorption experiments were performed by first introducing pure CO_2 to the wetted wall

column for approximately three hours, then pure nitrogen is used to desorb the CO_2 and the outlet CO_2 gas concentration is recorded. The Henry's constant of CO_2 in water was taken from experimental data reported by Versteeg et al. (1988). Figure 4.3 represents the typical experimental results for a desorption experiment.

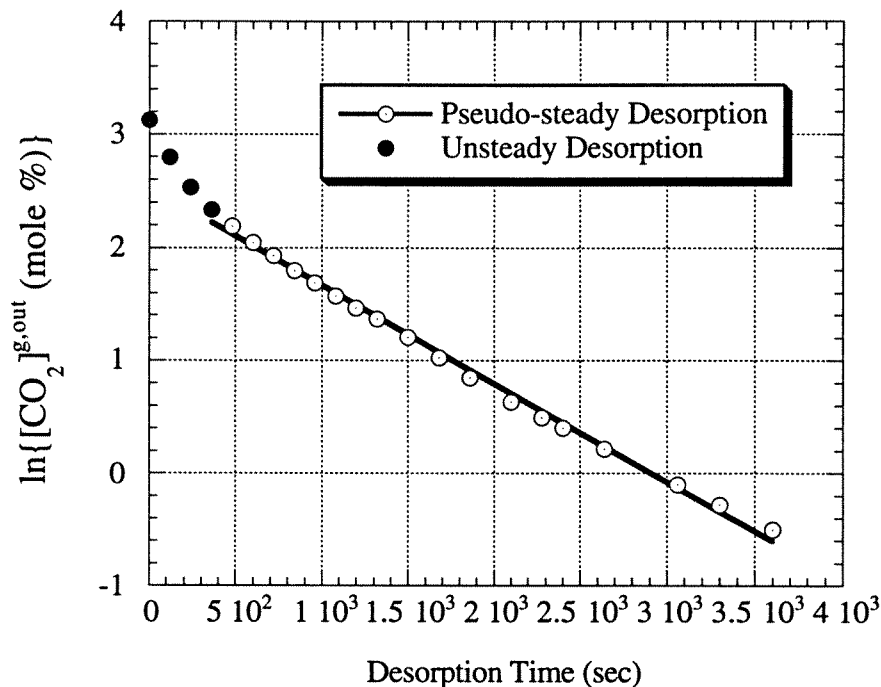


Figure 4.3. Desorption of CO_2 from water in the wetted wall column. Temperature: 50°C . Total pressure: 100 psig; $k_{\text{L},\text{CO}_2}^\circ$ determined: $9.63\text{E-}5$ m/sec.

The physical mass transfer coefficients for CO_2 in the wetted-wall column measured experimentally were analyzed using a fundamental model developed by Pigford (1941). This model is based on the solution of the equation of continuity for diffusion into a falling liquid film where convective transport is considered in the direction of the flow while diffusive transport is considered in the direction perpendicular to the liquid-gas interface. In the development of this model it is assumed that there is a parabolic velocity profile in the liquid phase and that the

concentration of the diffusing species in the liquid-gas interface is uniform. For the diffusing gas A, this model leads to the following expression:

$$\Theta = \frac{[A]_i^L - [A]_o^{L,out}}{[A]_i^L - [A]_o^{L,in}} = 0.7857\exp(-5.121\eta) + 0.1001\exp(-39.21\eta) + 0.036\exp(-105.6\eta) + 0.0181\exp(-204.7\eta) \quad ; \quad \text{for } \eta > 0.01 \quad (4.10)$$

$$\Theta = \frac{[A]_i^L - [A]_o^{L,out}}{[A]_i^L - [A]_o^{L,in}} = 1 - 3\sqrt{\frac{\eta}{\pi}} \quad ; \quad \text{for } \eta < 0.01 \quad (4.11)$$

where $\eta = D_A \tau / \delta^2$ and the time of exposure of the liquid surface, τ , is h/u_{surf}

The film thickness, δ , and the velocity at the surface of the liquid, u_{surf} , are estimated using expressions presented by Bird et al. (1960) based on the momentum balance for a falling film:

$$\delta = \sqrt[3]{\frac{3\mu_L Q_L}{\rho_L g P}} \quad (4.12)$$

$$u_{surf} = \frac{\rho_L g \delta^2}{2\mu_L} \quad (4.13)$$

Once the parameter Θ is known, the mass transfer coefficient for species A based on the logarithmic mean of concentration difference ($k_{L,A(M)}^\circ$) can be estimated using the following expression (Hobler, 1966):

$$k_{L,A(M)}^\circ = -(Q_L/a) \ln \Theta \quad (4.14)$$

where a is the surface area for mass transfer in the wetted wall column.

The mass transfer coefficient for species A based on the logarithmic mean of concentration difference, $k_{L,A(M)}^\circ$, is defined as follows,

$$N_A = k_{L,A(M)}^o \frac{([A]_i^L - [A]_o^{L,in}) - ([A]_i^L - [A]_o^{L,out})}{\ln \left\{ \frac{[A]_i^L - [A]_o^{L,in}}{[A]_i^L - [A]_o^{L,out}} \right\}} = -k_{L,A(M)}^o \frac{([A]_o^{L,out} - [A]_o^{L,in})}{\ln \Theta} \quad (4.15)$$

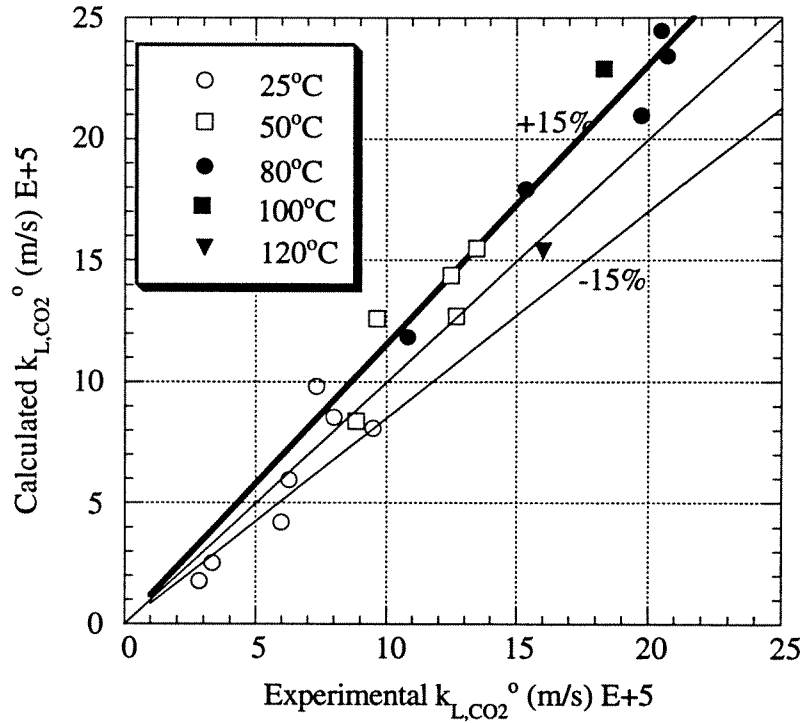


Figure 4.4. Comparison between experimentally measured and calculated physical mass transfer coefficients of CO_2 in the wetted-wall column. Measurements of desorption from water and ethylene glycol solutions.

Another mass transfer coefficient, $k_{L,A}^o$, can be defined using the mass transfer driving force at the inlet of the reactor. $k_{L,A}^o$ can be used to represent the mass transfer coefficient in the reactor because when $\Theta \ll 1$, most of the mass transfer takes place at the inlet of the reactor and, on the other hand, when Θ approaches unity, $k_{L,A}^o$ and $k_{L,A(M)}^o$ are identical (see below). Choosing $k_{L,A(M)}^o$ as the average mass transfer coefficient in the reactor is not appropriate because it does not represent the mass transfer process as $\Theta \rightarrow 0$. $k_{L,A}^o$ is then defined as,

$$N_A = k_{L,A}^o ([A]_i^L - [A]_o^{L,in}) \quad (4.16)$$

Equations 4.15 and 4.16 can be combined leading to the relationship:

$$k_{L,A}^o = -k_{L,A(M)}^o \frac{(1 - \Theta)}{\ln \Theta} = (Q_L/a)(1-\Theta) \quad (4.17)$$

The mass transfer coefficients of CO₂ measured experimentally were compared with those predicted by the model described above. Figure 4.4 shows that the difference between the measured and calculated values is less than 15% for most measurements. The value of the parameter Θ varied from 0.1 to 0.9 and the range of the liquid flow rate was from 0.7 to 5.1 cm³/sec. Table 4.1 shows the conditions and results of the experimental measurements.

Table 4.1. Experimental data for k_{L,CO_2}^o and theoretical calculations.

Run	μ_L (cP)	Temp. (°C)	liq. flow (cm ³ /s)	k_L^o (exp.) E+5 {m/s}	k_L^o (calc.) E+5 {m/s}	Θ
Mshewa-1	4.490	25	1.58	5.97	4.206	0.897
Mshewa-2	8.549	25	0.85	3.32	2.54	0.885
Mshewa-3	13.365	25	0.72	2.82	1.77	0.906
Mshewa-4	0.908	25	1.62	9.47	8.09	0.808
Mshewa-5	0.559	50	2.18	12.67	12.71	0.775
Mshewa-6	0.378	75	2.54	15.35	17.92	0.728
Mshewa-7	0.352	80	0.67	10.80	11.86	0.318
Mshewa-8	0.231	120	0.67	16.00	15.42	0.114
1	0.908	25	0.67	6.28	5.95	0.656
2	0.908	25	1.90	8.00	8.53	0.827
3	0.908	25	2.98	7.34	9.81	0.873
4	0.559	50	2.15	9.63	12.61	0.774
5	0.559	50	3.15	12.49	14.38	0.824
6	0.559	50	4.06	13.45	15.50	0.853
7	0.559	50	0.66	8.85	8.37	0.512
8	0.363	80	4.51	20.72	23.40	0.800
9	0.363	80	3.27	19.74	20.96	0.753
10	0.363	80	5.13	20.50	24.46	0.816
11	0.300	100	2.60	18.30	22.90	0.661

The experimental measurements represented as “Mshewa-#” were performed by Mshewa (1995). In the runs Mshewa-1 through Mshewa-3 aqueous ethylene glycol solutions of 50, 80 and 95wt%, respectively, were used.

4.3.2. Gas-Film Mass Transfer Coefficients

The mass transfer resistance at the gas side in the reactor was estimated from measurements of the rate of absorption of CO₂ in monoethanolamine (MEA) solutions. The reasons for this selection are two-fold. Firstly, the kinetics of reaction of CO₂ with MEA are well known and secondly, the fact that the reaction between CO₂ and MEA is fairly fast makes the contribution of the gas side resistance important. These rate measurements were performed using 2M MEA solutions, with low concentrations of CO₂ in the vapor fed to the reactor, and for most experiments the total pressure in the reactor was 100 psig.

In modeling the gas-film mass transfer coefficient of CO₂, Equation 4.1 can be used to relate the interfacial flux of CO₂ with the resistances to the mass transfer:

$$N_{\text{CO}_2} = \frac{P_{\text{CO}_2,b} - P_{\text{CO}_2}^*}{\frac{1}{k_{g,\text{CO}_2}} + \frac{H_{\text{CO}_2}}{E_{\text{CO}_2} k_{L,\text{CO}_2}^o}} \quad (4.18)$$

When low partial pressures of CO₂ are used it is likely that no significant depletion of reactants or accumulation of products at the gas-liquid interface occurs. Also, the reaction between CO₂ and MEA is first order with respect to CO₂ and first order with respect to MEA (Blauwhoff et al. 1984). Under these conditions, the following approximation can be made (Danckwerts, 1970; Critchfield, 1988):

$$E_{\text{CO}_2} k_{\text{L,CO}_2}^{\circ} \approx \sqrt{(k_2[\text{MEA}]D_{\text{CO}_2})} \quad (4.19)$$

where k_2 is the second order rate constant for the reaction of CO_2 with MEA, $[\text{MEA}]$ is the concentration of MEA in the solution and D_{CO_2} is the diffusivity of CO_2 in the liquid phase.

The rates of reactive absorption of CO_2 were measured at conditions such that the equilibrium partial pressure of CO_2 , $P_{\text{CO}_2}^*$, exerts a negligible effect on the mass transfer driving force. This was accomplished by using always fresh unloaded MEA solutions for every series of experiments. In this way, $P_{\text{CO}_2}^* \ll P_{\text{CO}_2}$. This condition can be further verified considering that at 50°C and for 2M MEA, $P_{\text{CO}_2}^*$ is almost zero for CO_2 loadings (moles of total CO_2 per moles of total MEA) lower than 0.4 (Martin et al. 1978). At 100°C , $P_{\text{CO}_2}^* \approx 0.01$ atm. for a CO_2 loading of around 0.15. These equilibrium partial pressures are significantly lower than the partial pressures of CO_2 at the vapor bulk in the reactor. Moreover, the maximum CO_2 loading obtained during the rate measurements was estimated to be about 0.05.

Combining Equations 4.18 and 4.19 and considering that $P_{\text{CO}_2}^* \ll P_{\text{CO}_2}$, the following equation is obtained:

$$N_{\text{CO}_2} = \frac{P_{\text{CO}_2,b}}{\frac{1}{k_{g,\text{CO}_2}} + \frac{H_{\text{CO}_2}}{\sqrt{k_2[\text{MEA}]D_{\text{CO}_2}}}} \quad (4.20)$$

Since the values of k_2 , D_{CO_2} and H_{CO_2} can be obtained from the literature and the flux of CO_2 is measured experimentally, Equation 4.20 can be used to extract the gas-film mass transfer coefficient, provided that the gas-side resistance is the major part of the total resistance to the mass transfer.

The Henry's law constant for CO₂ in the MEA solutions was estimated using the data of Browning (1993) for solubility of N₂O and the N₂O-CO₂ analogy. Browning only reports solubilities at 25°C. The calculated Henry's law constant for CO₂ in a 2M MEA solution at 25°C was 32.87 m³atm/kmol. Due to the lack of data, the Henry's law constant of CO₂ in MEA solutions at higher temperatures was estimated assuming that the rate of change of this property with temperature is the same as that for a diethanolamine (DEA) solution. The following approximate relation was obtained:

$$H_{\text{CO}_2} (\text{m}^3\text{atm/kmol}) = 7.389\text{E}+3 \exp\{-1614.5/T(\text{K})\} \quad (4.21)$$

The second order rate constant for the MEA-CO₂ reaction used for the k_g calculations was that reported by Blauwhoff et al. (1984), who analyzed kinetic data reported by different researchers:

$$\log_{10} k_2 (\text{m}^3/\text{kmol s}) = 10.99 - 2152/T(\text{K}) \quad (4.22)$$

The diffusion coefficient of CO₂ in MEA solutions was estimated using the Stokes-Einstein relation and diffusivities of CO₂ in water due to the lack of data for diffusivity of N₂O in this system. The relation used was as follows:

$$D_{\text{CO}_2}\mu_L^{0.6} = D_{\text{CO}_2}^o\mu_L^{o0.6} \quad (4.23)$$

Viscosities of MEA solutions were estimated using the correlation regressed by Glasscock (1990) from available experimental data.

Hobler (1966) presents a treatments of the gas-side mass transfer resistance that applies to the laminar flow regime in wetted-wall columns. In this regime it is possible to get an analytical relation between the gas-side mass

transfer coefficient and the parameters that describe the hydrodynamics of the column. Hobler reports the following expressions:

$$Sh = 0.5 Re Sc \frac{d}{h} ; \quad Re Sc \frac{d}{h} < 4.5 \quad (\text{for long columns}) \quad (4.24)$$

$$Sh = 1.62 Re^{1/3} Sc^{1/3} (d/h)^{1/3} ; \quad Re Sc \frac{d}{h} > 13 \quad (\text{for short columns}) \quad (4.25)$$

In the definition of the Reynolds number, d is the hydraulic diameter of the annulus through which the gas flows (outer diameter minus inner diameter of the annulus) estimated to be 0.44 cm, and the transversal section of this annulus (S) is estimated to be 1.30 cm².

Even though Equations 4.24 and 4.25 do not depend on the viscosity of the gas phase because the Schmidt and Reynolds numbers have the same power, the viscosity of the gas phase as a function of temperature was estimated from data reported by Reid et al. (1988).

To obtain the expression that best correlate the experimental data, it was assumed a general relationship equivalent to those reported by Hobler (1966):

$$Sh = C Re^{\alpha} Sc^{\alpha} (d/h)^{\alpha} \quad (4.26)$$

then, the constants C and α were determined.

Table 4.2 presents the experimental rate data used to calculate and correlate the gas-film mass transfer coefficient in the reactor. Figure 4.5 depicts the experimental and correlated values of the mass transfer coefficient as a function of the gas flow rate through the reactor. It is important to mention that these experiments were performed at different liquid flow rates, but no significant dependence of the rate of absorption on the liquid flow rate was observed. This

result is expected since the reaction of CO₂ with MEA is fast enough, that the liquid flow rate does not affect the rate of absorption of CO₂.

Table 4.2. Experimental conditions and results in the measurement of k_g in the reactor.

Run	Temp (°C)	Gas flow $\frac{\text{cm}^3}{\text{s}}$	k_g E+5 $\frac{\text{kmol}}{\text{atm m}^2 \text{s}}$	Re	Sc	Sh	Mean log P _{CO2} (atm)	Flux CO ₂ $\frac{\text{kmol}}{\text{m}^2 \text{s}}$ E+6
MEA-1	25	0.91	2.14	16.27	0.965	1.167	0.145	2.624
MEA-2	25	2.00	3.41	35.53	0.965	1.862	0.183	4.836
MEA-3	25	2.20	3.48	39.41	0.965	1.899	0.208	5.579
MEA-4	25	2.21	3.44	39.52	0.965	1.876	0.066	1.755
MEA-5	25	3.07	4.14	54.90	0.965	2.256	0.226	6.906
MEA-6	25	3.09	4.39	55.26	0.965	2.394	0.070	2.245
MEA-7	25	3.12	4.70	57.22	0.965	2.565	0.200	6.716
MEA-8	25	1.55	2.76	27.72	0.965	1.505	0.172	3.842
MEA-9	25	1.52	2.44	27.18	0.965	1.331	0.112	2.259
MEA-10	25	2.74	4.27	48.99	0.965	2.329	0.1928	6.031
MEA-11	25	2.70	4.02	48.28	0.965	2.192	0.122	3.653
MEA-12	25	1.20	2.07	21.46	0.965	1.129	0.107	1.873
MEA-13	25	1.75	2.84	31.29	0.965	1.549	0.113	2.580
MEA-14	25	2.45	3.79	43.81	0.965	2.067	0.119	3.405
MEA-15	25	1.79	2.90	32.01	0.965	1.581	0.040	0.929
MEA-16	25	3.54	5.34	63.30	0.965	2.914	0.044	1.630
MEA-17	25	2.66	4.12	47.57	0.965	2.249	0.0424	1.293
MEA-18	60	3.00	3.64	42.96	0.974	1.801	0.0412	1.315
MEA-19	60	2.01	2.50	28.78	0.974	1.238	0.0396	0.908
MEA-20	60	3.49	4.29	50.00	0.974	2.126	0.04156	1.543
MEA-21	90	3.26	3.44	39.16	0.997	1.596	0.0412	1.315
MEA-22	90	2.20	2.48	26.28	0.997	1.148	0.0392	0.918
MEA-23	90	3.80	3.92	45.61	0.997	1.816	0.0422	1.516
MEA-24	25	0.26	0.58	4.47	0.931	0.295	0.117	0.642
MEA-25	25	0.50	1.08	8.66	0.931	0.553	0.119	1.170
MEA-26	60	0.56	0.88	8.11	0.940	0.427	0.130	1.109
MEA-27	60	5.26	5.74	43.96	0.943	1.569	0.072	3.422
MEA-28	60	8.79	8.04	43.96	0.943	1.346	0.047	2.874
MEA-29	40	21.76	38.50	44.0	0.948	2.458	0.00385	0.473
MEA-30	60	23.15	24.50	42.39	0.954	1.518	0.00379	0.494

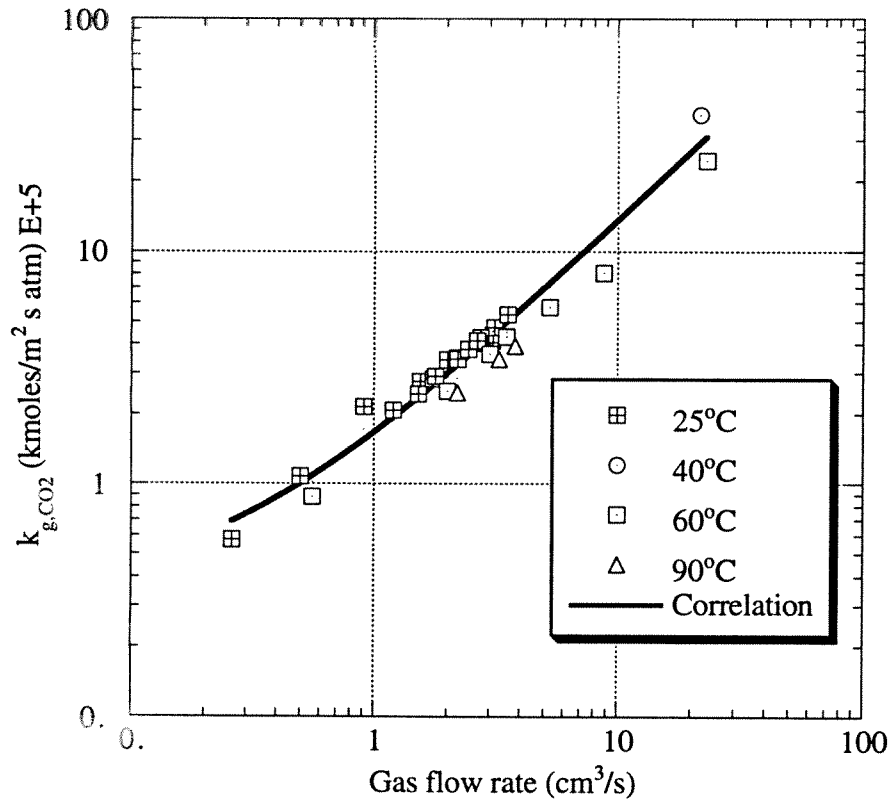


Figure 4.5. Experimental data and correlation of the gas-film mass transfer coefficient in the wetted-wall column.

The correlation represented in Figure 4.5 is as follows,

$$Sh = 1.096 \{ReSc(d/h)\}^{0.80} \quad \text{for } d = \{\text{outer diameter}\} - \{\text{inner diameter}\} \quad (4.27)$$

These measurements of the gas-film mass transfer coefficient were performed under conditions such that the contribution of the gas-side resistance to mass transfer was in the range of 70 to 95% of the total resistance.

4.3.3. Marangoni Effects

The simultaneous mass transfer and chemical reactions that take place in the zone adjacent to the gas-liquid interface can be responsible for local variations

in temperature and/or composition. These temperature and composition variations can cause local variations in surface tension or density, which in turn can initiate, under appropriate conditions, convective movement. The convective flow driven by surface tension gradient is called *Marangoni flow* or *Marangoni instability*. There is a motivation in analyzing the potential formation of these convective flow patterns because if they are intensive enough, they could lead to a significant increase of the interfacial mass transfer rates.

Brian et al. (1971), Fujinawa et al. (1978) and Imaishi et al. (1982) studied the effect of convective flow driven by surface tension gradient upon the gas-liquid interfacial mass transfer rate in non-reactive systems. Even though their conclusions will not be of direct use to analyze our system, they are of qualitative significance. These researchers produced the interfacial tension gradients by desorption of surface-active solutes from aqueous solutions in different types of gas-liquid contactors, including wetted-wall columns. It was found that the liquid-side mass transfer coefficient was enhanced by as much as 3.6-fold by cellular convection when the Marangoni number (Ma) was increased above its critical value (Ma_{cr}). These researchers used the following form of the Marangoni number:

$$Ma = \frac{\sigma_i - \sigma_o}{\mu_L k_L^o} \quad (4.27)$$

This definition of the Marangoni number indicates that the significance of the Marangoni flow is an inverse function of both, the fluid viscosity (“damping” effect) and the mass transfer coefficient in the liquid phase. Spekuljak (1987) indicates that the linear velocity of the liquid proportionally reduces the effect of

the Marangoni flow. This is attributed to the fact that significant velocities produce strong distortion in the convective cells or destroy them entirely.

It is difficult to develop a criterion, based on first principles, to determine if convective flow driven by surface tension or density gradient will affect the interfacial mass transfer. This difficulty is due to the complexity in modeling these local instabilities. Most of the attempts in modeling surface-tension driven convective flow are based on a linearized approach (e.g. Warmuzinski, et al. 1991). Physically, this means that its applicability must be limited to low velocities of circulation within the cells and to small perturbations of concentration, and hence to the moment of inception of the phenomenon.

Experimental observations of previous researchers support the hypothesis that the rate measurements performed in the wetted-wall reactor described in Section 4.2 are not affected by Marangoni flow or interfacial turbulence created by cellular convection. Among those contributions, the following can be cited:

a) Thomas et al. (1969) performed optical measurements of the interfacial turbulence that occurs when CO_2 is chemically absorbed into monoethanolamine (MEA) solutions of different concentrations. These researchers used a diffusion cell where pure CO_2 contacted the MEA solutions in a stagnant pool. For all the cases studied (MEA concentration up to 7M) it was found that a minimum time of 4.5 seconds elapses before turbulence occurs. These authors suggest that the interfacial turbulence accompanying reactive absorption processes may be due not only to surface tension gradients but also to buoyancy forces.

These researchers concluded that since the time it takes for the disturbances to appear was always more than 4 seconds, it is not likely that

interfacial turbulence driven by Marangoni effect will affect the mass transfer rates in contactors like wetted-wall columns or laminar jets where the gas-liquid contact time is much less than 4 seconds. The gas-liquid contact time in the wetted-wall column used in this dissertation was less than one second under most experimental conditions. The results of the experiments of Thomas and coworkers also indicate that, in non-stagnant contactors, Marangoni instabilities are more likely to occur at contact times even larger than 4 sec. due to the “damping” effects of the linear velocity of the liquid and liquid-phase mass transfer coefficient.

b) Linek et al. (1976) studied the enhancement of absorption rates caused by density driven convection at the gas-liquid interface. In spite of the fact that these researchers studied a density driven convection, their conclusions can throw a light upon the general characteristics of the hydrodynamics of interfacial turbulence driven by surface tension gradients or buoyancy forces.

In this work a mechanically agitated gas-liquid contactor was used. It was found that for a gas-liquid reactive system, when the liquid-side physical mass transfer coefficient (k_L^o) of a nonreactive tracer was above $1.3E-5$ m/s, cellular motion does not reach steady state, or does not occur at all. This effect was explained considering the formation of eddies of high energy that disturb the cellular motion. For lower values of k_L^o (lower liquid flow rate or lower agitation) the eddies, having low energy, are not able to disturb the cellular motion; making this motion more stable and increasing the mass transfer enhancement. It was found that the mass transfer enhancement due to cellular convection decreased rapidly with increasing k_L^o for k_L^o values larger than $1.3E-5$ m/s. The values of

k_L° for the diffusing gas (CO_2) in the wetted-wall column described in Section 4.2 are almost always at less three times larger than $1.3\text{E-}5$ m/s under the conditions at which the rate measurements are performed.

4.4. CONCLUSIONS

The wetted-wall column reactor was characterized in terms of the mass transfer resistances at the vapor and liquid film. A fundamental model developed originally by Pigford (1941) was implemented to predict the liquid-film mass transfer coefficient. This model was validated using rate data of desorption of CO_2 from aqueous ethylene glycol and water. Using experimental measurements of rates of reactive absorption for the fast-reacting system CO_2 -MEA, a semi-empirical model was developed to predict the gas-film mass transfer coefficient. This model is based on the analytical solution of the mass transfer problem for laminar flow in a tube presented by Hobler (1966). These two models predict the mass transfer kinetics at the vapor and liquid side.

Based on results of previous researchers, it was shown that there is sufficient evidence that indicates that the effects on mass transfer of convective flow driven by surface tension gradients or buoyancy forces are not present in the wetted-wall column reactor studied.

The characterization and analysis of the wetted-wall column reactor conducted in this chapter are of significant importance for the study of the gas-liquid reactions presented on Chapter 5.

4.5 NOMENCLATURE

- [CO₂]: Concentration of CO₂ at the liquid or vapor phase (kmol/m³).
- [A]: Concentration of species A at the liquid or vapor phase (kmol/m³).
- a: Interfacial area of the wetted-wall column (m²).
- d: Hydraulic diameter of the annulus (m).
- D: Diffusion coefficient (m²/sec).
- G: Gas volumetric flow rate through the wetted-wall column (m³/sec).
- h: Length of the wetted-wall column (m).
- H: Henry's constant (atm m³/kmol).
- J: Diffusive flux (kmol/m² sec).
- k₂: Second-order rate constant for the reaction of CO₂ with MEA (m³/kmol sec)
- k_g: Mass transfer coefficient in the gas phase (kmol/m² sec atm).
- k_L: Physical mass transfer coefficient in the liquid phase (m/sec).
- k_{L,A(M)}^o: Physical mass transfer coefficient for component A in the liquid phase based on the logarithmic mean driving force (m/sec).
- N: Molar flux (kmol/m² sec).
- P: Partial pressure (atm) or wetted perimeter of the wetted-wall column (m).
- Q_L: Liquid flow rate (m³/sec).
- R: Gas constant (atm m³/kmol K)
- Re: Reynolds number for the gas phase = $\frac{(Q_g/S)d\rho_g}{\mu_g}$
- S: Transversal section of the annulus for gas flow in the wetted-wall column (m²).

Sc: Schmidt number for the gas phase = $\frac{\mu_g}{\rho_g D_{\text{CO2(g)}}}$

Sh: Sherwood number for the gas phase = $\frac{k_{g\text{CO2}} RTd}{D_{\text{CO2(g)}}}$

t: Time (sec).

T: Temperature (K).

u_{surf} : Velocity at the surface of the liquid (m/sec).

V_L : Volume of liquid circulating through the experimental apparatus (m^3).

Greek Letters:

δ : Thickness of the liquid film flowing down the wetted-wall column (m).

η : Parameter in Pigford mass transfer model. Defined in Equations 4.10 and 4.11. [-].

μ : Viscosity (kg/m sec or cP).

Θ : Dimensionless concentration change. Defined in Equation 4.10 and 4.11. [-].

ρ : Density (kg/m^3).

σ : Surface tension (N/m).

τ : Time of exposure of the liquid surface (sec).

Superscripts:

*: At equilibrium.

g: For the gas phase.

in: Inlet of the wetted-wall column.

- L: For the liquid phase.
- o: Property evaluated for pure water.
- out: Outlet of the wetted-wall column.

Subscripts:

- CO₂: For CO₂.
- i: At the vapor-liquid interface or for component i.
- o: At the liquid or vapor bulk.

4.6. REFERENCES

- Alper, E., "Kinetics of Reactions of Carbon Dioxide with Diglycolamine and Morpholine," *Chem. Engng. J.*, **1990**, 44, 107.
- Bird, R. B., Stewart, W. E., Lightfoot, E. N., *Transport Phenomena*, Wiley, 1960.
- Blauwhoff, P.M.M., Versteeg, G.F., van Swaaij, W.P.M., "A Study of the Reaction Between CO₂ and Alkanolamines in Aqueous Solutions," *Chem. Engng. Sci.* **1984**, 39, 207.
- Brian, P., Vivian, J., Mayr, S., "Cellular Convection in Desorbing Surface Tension-Lowering Solutes from Water," *Ind. Eng. Chem. Fund.* **1971**, 10, 75.
- Browning, G. J., "Physical Solubility of Carbon Dioxide in Aqueous Alkanolamines Via Nitrous Oxide Analogy," Thesis, Department of Chemical Engineering, The University of Newcastle, Australia, 1993.
- Critchfield, J. E., "CO₂ Absorption/Desorption in Methyldiethanolamine Solutions Promoted with Monoethanolamine and Diethanolamine: Mass Transfer and Reaction Kinetics." Ph.D. Dissertation, The University of Texas at Austin, 1988.
- Danckwerts, P. V., *Gas Liquid Reactions*. McGraw-Hill Inc., New York, 1970.
- Glasscock, D. A., "Modelling and Experimental Study of Carbon Dioxide Absorption into Aqueous Alkanolamines." Ph.D Dissertation, The University of Texas at Austin, 1990.

- Fujinawa, K., Hozawa, M., Imaishi, N., "Effects of Desorption and Absorption of Surface Tension-Lowering Solutes on Liquid-Phase Mass Transfer Coefficients at a Turbulent Gas-Liquid Interface," *J. Chem. Eng. Japan*. **1978**, 11, 107.
- Hagewiesche, D. P., Ashour, S. S., AL-Ghawas, H. A., Sandall, O. C., "Absorption of Carbon Dioxide into Aqueous Blends of Monoethanolamine and N-Methyldiethanolamine," *Chem. Eng. Sci.* **1995**, 50, 1071.
- Hikita, H., Asai, S., Ishikawa, H., Honda, M., "The Kinetics of Reactions of Carbon Dioxide with Monoisopropanolamine, Diglycolamine and Ethylenediamine by a Rapid Mixing Method," *Chem. Engng. J.* **1977**, 14, 27.
- Hobler, T., *Mass Transfer and Absorbers*, Pergamon Press, Oxford, 1966.
- Imaishi, N., Suzuki, Y., Hozawa, M., Fujinawa, K., "Interfacial Turbulence in Gas-Liquid Mass Transfer," *Int. Chem. Eng.* **1982**, 22, 659.
- Linek, V., Hrma, P., "Enhancement of Absorption Caused by Density Driven Convection at Gas-Liquid Interface Induced by Absorption with Chemical Reaction," *Chem. Eng. Sci.* **1976**, 31, 97.
- Martin, J. L., Otto, F. D., Mather, A. E., "Solubility of Hydrogen Sulfide and Carbon Dioxide in a Diglycolamine Solution," *J. Chem. Eng. Data*, **1978**, 23, 163.
- Mshewa, M., "Carbon Dioxide Desorption/Absorption with Aqueous Mixtures of Methyldiethanolamine and Diethanolamine at 40 to 120°C." Ph.D Dissertation, The University of Texas at Austin, 1995.
- Pigford, R., L., "Counter-Diffusion in a Wetted Wall Column," Doctoral Dissertation, The University of Illinois, Urbana, Illinois, 1941.
- Pinsent, B. R. W., Pearson, L., Roughton, F. J. W., "The Kinetics of Combination of Carbon Dioxide with Hydroxide Ions," *Trans. Faraday Soc.* **1956**, 52, 1512.
- Reid, R. C., Prausnitz, J. M., Poling, B. E., *The Properties of Gases and Liquids*, McGraw-Hill Inc., Singapore, 1988.
- Rinker, E. B., Ashour, S. S., Sandall, O. C., "Kinetics and Modeling of Carbon Dioxide Absorption into Aqueous Solutions of N-methyldiethanolamine," *Chem. Eng. Sci.* **1995**, 50, 755.

- Spekuljak, Z., "A Criterion to Determine the Occurrence of the Marangoni effect in a Thin Liquid Film," *Chem. Engng. Sci.* **1987**, 42, 163.
- Thomas, W. J, Nicholl, E., "Interfacial Turbulence Accompanying Absorption with Reaction," *Trans. Instn. Chem. Engrs.* **1969**, 47, p. T325.
- Versteeg, G. F., Kuipers, J. A. M., van Beckum, F. P. H., van Swaaij, W. P. M., "Mass Transfer with Complex Reversible Chemical Reactions-I. Single Reversible Chemical Reaction," *Chem. Engng. Sci.* **1989**, 44, 2295.
- Versteeg, G. F., van Swaaij, W. P. M., "Solubility and Diffusivity of Acid Gases (CO_2 , N_2O) in Aqueous Alkanolamine Solutions," *J. Chem. Eng. Data*, **1988**, 33, 29.
- Warmuzinski, K., Tanczyk, M., "Marangoni Instability During Absorption of Carbon Dioxide into Aqueous Solutions of Monoethanolamine," *Chem. Eng. Process*, **1991**, 30, 113.

Chapter 5

Reactive Absorption with Reversible Chemical Reactions: Model Development and Validation

5.1 INTRODUCTION

Acid gases such as CO_2 and H_2S can be removed from gaseous streams using reactive absorption with a basic alkanolamine solution. A desorption step follows where the reactions are reversed by increasing the temperature and/or decreasing the pressure. In this application the chemical reactions that take place in the liquid phase are generally multiple, parallel (and/or consecutive) and reversible.

The mechanism of the gas-liquid reactions, and especially the study of the mass transfer enhancement due to these reactions has been the focus of attention of a great number of researchers. van Swaaij and Versteeg (1992) gives an overview of the different contributions in this area. Glasscock (1990) modeled rigorously reactive absorption where multiple parallel reactions take place. DeCoursey and Thring (1989) developed an approximate analytical solution of the governing diffusion-reaction equations for a second-order reversible gas-liquid reaction using surface renewal theory and where each species was allowed to have a different diffusion coefficient. This approach of DeCoursey and Thring was based on an earlier work by DeCoursey (1982) who solved the surface renewal model for a reversible second-order reaction by changing the instantaneous concentrations of the different species to time mean concentrations

taking the “s-multiplied” Laplace transform using the Danckwerts (1970) surface renewal theory. The results of the work by DeCoursey and Thring (1989) were evaluated by Winkelman et al. (1992) who solved numerically the governing equations. They found that the approximate solution had a mean deviation between 3.1 and 14% with respect to the numerical solution. Carey et al. (1991) and Glasscock and Rochelle (1993) successfully used a modified form of the approximate solution obtained by DeCoursey (1982) to predict interfacial mass transfer rates of CO₂ when it is chemically absorbed into mixtures of alkanolamines.

Versteeg et al. (1989) used an improved numerical technique to solve rigorously the governing equations showing that reversibility has a pronounced effect on the enhancement of the interfacial mass transfer when reactions with finite rates take place in the liquid phase. They also found that for a second-order reversible reaction, diffusion limitation of the liquid phase reactant starts to happen at lower Hatta-numbers with decreasing equilibrium constants, which could lead to a condition where the pseudo-first order reaction kinetics is no longer valid.

An important issue when modeling mass transfer accompanied with gas-liquid reactions is the treatment of the diffusion of the ionic species frequently formed when the absorbing gas reacts with the chemical solvent. Glasscock (1990) implemented the Nernst-Planck equations to handle the diffusion-reaction of the ionic species and assure overall electroneutrality in the liquid phase. Littel et al. (1991) performed different numerical simulations to study the effect of the diffusion of the ionic species on the absorption rates. The electrostatic potential

gradient, which couples the diffusion of the ionic species, was calculated with the aid of the Nernst-Einstein equation. Comparing the predictions of the more rigorous model with those of a model where the coupling of the diffusion of ions was not taken into account (neglecting the effect of the electrostatic potential gradient and achieving electroneutrality by assuming equal diffusivities for all ionic species in the liquid), these researchers concluded that the deviations between the predictions of the two models were negligible under the conditions usually found in practical applications. Therefore, it seems that not much improvement in the accuracy of the predictions of the interfacial mass transfer rates will be achieved by accounting for phenomena such as ionic diffusion coupling.

In the present work the problem of mass transfer accompanied by parallel reversible gas-liquid chemical reactions was studied. Specifically, the reactive absorption of CO_2 into aqueous solutions of methyldiethanolamine (MDEA), diglycolamine (DGA) and blends of these reactive solvents was studied from the experimental and theoretical points of view. One of the unique characteristics of this work is that a wetted-wall column was used to measure rates of mass transfer of CO_2 under a wide range of CO_2 mass transfer driving force and over the temperature range of 25 to 100°C (temperatures higher than most previous work). Also, the CO_2 loading in the liquid phase was varied. For most experiments 50 wt% MDEA/DGA aqueous solvent was used, including the limiting cases of 50 wt% MDEA and 50 wt% DGA. A mathematical model was developed to interpret and analyze the experimental data. The effects of the reaction kinetics, diffusivities of liquid-phase reactants and reaction products and thermodynamic

interaction parameters on the interfacial mass transfer rates of CO_2 were explored. The mass transfer model is based on the surface renewal theory and accounts for the thermodynamic non-ideality of the liquid phase by the use of the electrolyte NRTL model. This model has been applied with rigorous non-linear parameter estimation in order to obtain parameter values and their confidence intervals.

5.2 REACTIVE SYSTEM STUDIED

When reacting with CO_2 , sterically unhindered primary and secondary alkanolamines form stable carbamate ions. On the other hand, since tertiary alkanolamine molecules do not have the N-H bonds, their reaction with CO_2 produces only bicarbonate and carbonate ions. The chemical behavior of H_2S is the same with primary, secondary or tertiary alkanolamines. When H_2S reacts with alkanolamines there is only a proton transfer and therefore the chemical reaction is essentially instantaneous with respect to mass transfer. Consequently, tertiary alkanolamines are effective solvents for the selective removal of H_2S from gas streams containing CO_2 and H_2S .

The chemical reactions of CO_2 with sterically unhindered primary and secondary alkanolamines present in aqueous solutions increase the CO_2 interfacial reaction rate many times with respect to the mass transfer rate in the absence of the chemical reactions and under the same driving force. However, due to the high heat of reaction associated with carbamate formation, a significant regeneration energy is needed. A tertiary alkanolamine, on the other hand, enhances the interfacial mass transfer rates to a lesser extent, but since the heat of reaction associated with the bicarbonate and carbonate formation are much lower,

the energy required for regeneration is also lower. Chakravarty et al. (1985) suggested the use of mixtures of unhindered primary or secondary alkanolamines with tertiary alkanolamines to take advantage of the features of each molecule. Using this type of mixture the bulk removal of CO₂ can be accomplished and at the same time the regeneration energy costs are reduced.

These ideas constitute a motivation for studying the reactions between methyldiethanolamine (MDEA, a tertiary alkanolamine) and diglycolamine (a primary alkanolamine) with CO₂. As it will be discussed below, many studies have been performed to explore the kinetics of the reaction of aqueous MDEA and CO₂ and the mechanism of this reaction is well understood.

The use of diglycolamine (DGA) for acid gas removal was patented by Blohm and Riesenfeld (1955). DGA is β,β' -hydroxyaminoethyl ether and has the same molecular weight as diethanolamine (DEA). However, it has the reactivity of primary amines with a much lower vapor pressure than other solvents such as monoethanolamine (MEA). Therefore, DGA can be used in more concentrated solutions than other solvents with the same reactivity with the potential decrease in the solvent flow rate.

5.3 MODEL DEVELOPMENT

The model developed in order to analyze and interpret the experimental data is based on the Danckwerts model for mass transfer and the use of the concept of time-mean concentrations (Danckwerts, 1970; DeCoursey, 1992). Using this approach the system of differential equations that describes the process of mass transfer with chemical reactions can be solved analytically, in

approximate form, without neglecting the unsteady term in the mass transfer equations. Since in this system CO_2 reacts in multiple reversible chemical reactions, the description that follows constitutes an extension of the approach presented by DeCoursey and Thring (1989) and DeCoursey (1992).

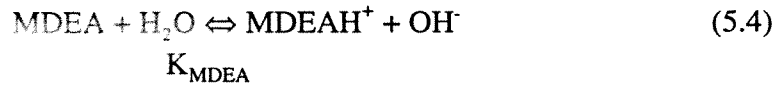
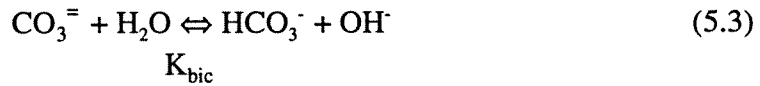
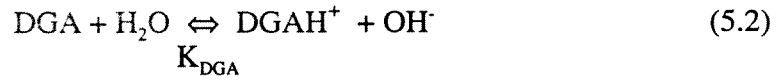
The Henry's equilibrium and chemical reactions that take place when CO_2 is absorbed in aqueous solutions of DGA and (or) MDEA are described below:

Solubility of CO_2



$$H_{\text{CO}_2} = \frac{P_{\text{CO}_2,i}}{[\text{CO}_{2,aq}]_i}$$

Equilibrium Reactions



Since reactions 5.2 through 5.5 involve only a proton transfer, it was assumed that equilibrium for those reactions hold in the entire liquid boundary layer, even at the vapor-liquid interface. The effect of the non-idealities in the liquid phase is accounted for by using the electrolyte-nonrandom two-liquid (NRTL) model (Austgen, 1989). This model was used to calculate the activity coefficient of each species at the temperature and CO_2 loading of the bulk liquid.

Then it was assumed that at the gas-liquid interface the activity coefficients of the species are the same as those in the bulk liquid. In this way equilibrium constants based on concentrations could be defined for the solution of the mass transfer model. The equilibrium constants defined in terms of concentrations are as follows:

$$\begin{aligned} K_{\text{DGA}} &= \frac{[\text{DGAH}^+][\text{OH}^-]}{[\text{DGA}]} & K_{\text{bic}} &= \frac{[\text{HCO}_3^-][\text{OH}^-]}{[\text{CO}_3^{2-}]} \\ K_{\text{MDEA}} &= \frac{[\text{MDEAH}^+][\text{OH}^-]}{[\text{MDEA}]} & K_w &= [\text{OH}^-][\text{H}_3\text{O}^+] \end{aligned} \quad (5.6)$$

The same method was used to define concentration-based equilibrium constants for reversible reactions with finite reaction rates.

Austgen (1989) applied the electrolyte NRTL model to the systems CO_2 -DGA- H_2O and CO_2 -MDEA- H_2O and regressed model parameters using available experimental data. However, due to the lack of experimental data for the system CO_2 -DGA-MDEA- H_2O , thermodynamic interaction parameters between the two reactive solvents could not be found. The chemical equilibrium for reactions 5.2 through 5.5 described using the electrolyte NRTL model was coupled with the transfer equations described below.

Kinetic Reactions

Hikita et al. (1977) and Alper (1990) studied the kinetics for the CO_2 -DGA reaction using a stopped flow method. Littel (1991) studied that reaction using a stirred cell reactor. Hikita et al. (1977) and Alper (1990) reported kinetic data from 5 to 40°C and from 5 to 25°C, respectively. Littel (1991) measured the rate constant at 25 and 45 °C. His experimental data indicated that a first order

reaction with respect to CO_2 and first order with respect to DGA was the most likely mechanism. When reversibility is included in this mechanism the following expression results:

$$\begin{aligned} \text{CO}_2 + \text{H}_2\text{O} + \text{DGA} &\rightleftharpoons \text{DGACOO}^- + \text{H}_3\text{O}^+ \\ &\quad k_{2p}; K_{\text{DGA},K} \end{aligned} \quad (5.7)$$

$$R_{\text{CO}_2}^{(\text{DGA})} = k_{2p}[\text{CO}_2][\text{RR}'\text{NH}] - (k_{2p}/K_{\text{DGA},K})[\text{RR}'\text{NCOO}^-][\text{H}_3\text{O}^+]$$

Pinsent et al. (1956) found that the reaction between CO_2 and hydroxide ions is second order (first order with respect to CO_2 and first order with respect to OH^-):

$$\begin{aligned} \text{CO}_2 + \text{OH}^- &\rightleftharpoons \text{HCO}_3^- \\ &\quad k_{\text{OH}}; K_{\text{OH}} \end{aligned} \quad (5.8)$$

$$R_{\text{CO}_2}^{(\text{OH})} = k_{\text{OH}}[\text{CO}_2][\text{OH}^-] - (k_{\text{OH}}/K_{\text{OH}})[\text{HCO}_3^-]$$

Different researchers (Critchfield 1988, Versteeg et al. 1990, Glasscock, 1990; Rinker et al. 1995, among others) have also found that the reaction between CO_2 and MDEA is also first order with respect to CO_2 and first order with respect to MDEA:

$$\begin{aligned} \text{CO}_2 + \text{H}_2\text{O} + \text{MDEA} &\rightleftharpoons \text{MDEAH}^+ + \text{HCO}_3^- \\ &\quad k_{2t}; K_{\text{MDEA},K} \end{aligned} \quad (5.9)$$

$$R_{\text{CO}_2}^{(\text{MDEA})} = k_{2t}[\text{CO}_2][\text{R}_3\text{N}] - (k_{2t}/K_{\text{MDEA},K})[\text{R}_3\text{NH}^+][\text{HCO}_3^-]$$

Considering these reaction kinetics and the reversibility of these rate controlled reactions, the following expression represents the rate of reaction of CO_2 :

$$R_{\text{CO}_2} = R_{\text{CO}_2}^{(\text{DGA})} + R_{\text{CO}_2}^{(\text{OH})} + R_{\text{CO}_2}^{(\text{MDEA})} \quad (5.10)$$

or we can write:

$$R_{\text{CO}_2} = (k_{2p}[\text{DGA}] + k_{\text{OH}}[\text{OH}^-] + k_{2t}[\text{MDEA}])([\text{CO}_2] - [\text{CO}_2]_{\text{eq}}) \quad (5.11)$$

where $[\text{CO}_2]_{\text{eq}}$ is the concentration of CO_2 that would be at chemical equilibrium, that is the concentration of CO_2 that gives $R_{\text{CO}_2} = 0$.

The following are the main assumptions of the mass transfer model developed:

- 1) The diffusion coefficients of reactants (except the diffusing gas) and products are the same, and therefore the electrostatic potential gradient which couples the diffusion of ionic species is neglected. That is, differentiation is established only between the diffusivity of CO_2 and the composite diffusivity of the rest of the species. This assumption is justified considering that different researchers (e.g., Littel et al., 1991) have shown that the introduction of the electrostatic potential gradient in the modeling of mass transfer with parallel and consecutive chemical reactions is only responsible for minor changes in absorption rate predictions.
- 2) A concentration profile of CO_2 is assumed (DeCoursey, 1992). The concentration gradient of CO_2 given by Equation 5.12 below is correct in value and slope for a general reversible second-order chemical reaction at the interface and liquid bulk, but deviates from the true profile in between. For a pseudo-first order reaction it is exactly correct:

$$[\overline{\text{CO}_2}] - [\text{CO}_2]_o = ([\text{CO}_2]_i - [\text{CO}_2]_o) \exp(-xE k_{L,\text{CO}_2}^o / D_{\text{CO}_2}) \quad (5.12)$$

where E is the enhancement factor for the mass transfer of CO_2 , and k_{L,CO_2}^o and D_{CO_2} are related through the parameter s in Danckwerts model that expresses the fraction of surface area replaced per unit time, i.e., $k_{L,\text{CO}_2}^o = \sqrt{s D_{\text{CO}_2}}$. Equation 5.12 is introduced because an approximate concentration gradient for CO_2 is needed to find analytical solutions of the diffusion-reaction equations that govern the mass transfer process in this system.

5.3.1 Mass Balance of Molecular CO₂

Using the diffusion-reaction equation that governs the mass transfer rate of CO₂ and the concept of the time-mean concentrations, an analytical expression for the enhancement of the interfacial mass transfer (E) can be obtained. Applying the “s-multiplied” Laplace transform to the diffusion-reaction equation of CO₂, the following expression results:

$$D_{\text{CO}_2} \frac{d^2[\overline{\text{CO}_2}]}{dx^2} - s([\overline{\text{CO}_2}] - [\text{CO}_2]_o) - \overline{R}_{\text{CO}_2} = 0 \quad (5.13)$$

Making the approximation that at any point of the reaction zone the reaction rate can also be expressed in terms of time-mean concentrations, Equation 5.11 can be written as:

$$\overline{R}_{\text{CO}_2} = \left(k_{2p}[\overline{\text{DGA}}] + k_{\text{OH}}[\overline{\text{OH}^-}] + k_{2t}[\overline{\text{MDEA}}] \right) ([\overline{\text{CO}_2}] - [\overline{\text{CO}_2}]_{\text{eq}}) \quad (5.14)$$

where it is assumed also that the equilibrium can be expressed in terms of time-mean concentrations as well.

Substituting Equations 5.12 and 5.14 into Equation 5.13 at the gas-liquid interface ($x=0$) and solving for the enhancement factor, the following relation is obtained:

$$E = \sqrt{1 + \frac{D_{\text{CO}_2} \left(k_{2p}[\overline{\text{RR}'\text{NH}}]_i + k_{\text{OH}}[\overline{\text{OH}^-}]_i + k_{2t}[\overline{\text{R}_3\text{N}}]_i \right)}{k_{\text{L},\text{CO}_2}^2}} (1 - \theta) \quad (5.15.a)$$

where,

$$\theta = \frac{[\overline{\text{CO}_2}]_{\text{e},i} - [\text{CO}_2]_o}{[\overline{\text{CO}_2}]_i - [\text{CO}_2]_o} \quad (5.15.b)$$

and where $[\overline{\text{CO}_2}]_{\text{eq},i}$ is the concentration of CO_2 that would be at chemical equilibrium at the interface, i.e., the CO_2 concentration at the interface that gives $\overline{R}_{\text{CO}_2} = 0$:

$$[\overline{\text{CO}_2}]_{\text{eq},i} = \frac{\frac{k_{2p}}{K_{\text{DGA},K}} [\overline{\text{DGACOO}^-}]_i [\overline{\text{H}_3\text{O}^+}]_i + \frac{k_{\text{OH}}}{K_{\text{OH}}} [\overline{\text{HCO}_3^-}]_i + \frac{k_{2t}}{K_{\text{MDEA},K}} [\overline{\text{MDEAH}^+}]_i [\overline{\text{HCO}_3^-}]_i}{\left(k_{2p} [\overline{\text{DGA}}]_i + k_{\text{OH}} [\overline{\text{OH}^-}]_i + k_{2t} [\overline{\text{MDEA}}]_i \right)} \quad (5.15.c)$$

It is important to note that Equation 5.15.a constitutes a well documented model for the enhancement factor, however it is significantly different from the intuitive approximation used by Glasscock et al. (1993) where the enhancement factor varies as $E \sim 1-\theta$ instead of $E \sim \sqrt{1-\theta}$ as indicated by Equation 5.15.a. In this dissertation these two approaches were compared for a general second order reversible reaction and for most conditions the difference between the predicted enhancement factors was less than 5%. In Section C.5 of Appendix C details of this comparison are presented.

Equations 5.15 can then be used to calculate the enhancement of the interfacial mass transfer rates of CO_2 which are given by:

$$\overline{N}_{\text{CO}_2} = -D_{\text{CO}_2} \left[\frac{d}{dx} ([\overline{\text{CO}_2}] - [\text{CO}_2]_0) \right]_{x=0} = Ek_{L,\text{CO}_2}^0 ([\text{CO}_2]_i - [\text{CO}_2]_0) \quad (5.16)$$

5.3.2 Total CO_2 Diffusion-Reaction

Considering the reaction scheme presented above (Equations 5.2 through 5.5 and 5.7 through 5.9), when the diffusion-reaction equations for free CO_2 and

reacted CO_2 are combined and assuming that the diffusivities of bicarbonate, carbonate and carbamate are all equal, the following expression is obtained:

$$\frac{\partial[\text{CO}_2]}{\partial t} + \frac{\partial\{[\text{CO}_2]_{\text{R}}\}}{\partial t} = D_{\text{CO}_2} \frac{\partial^2[\text{CO}_2]}{\partial x^2} + D_{\text{pr}} \frac{\partial^2\{[\text{CO}_2]_{\text{R}}\}}{\partial x^2} \quad (5.17)$$

where D_{pr} is the diffusivity of the products and reactants and the concentration of reacted CO_2 , $[\text{CO}_2]_{\text{R}}$, is given by $[\text{CO}_2]_{\text{R}} = [\text{HCO}_3^-] + [\text{CO}_3^{2-}] + [\text{RR}'\text{NCOO}^-]$. In order to solve Equation 5.17 let us define the following variable:

$$[\text{CO}_2]_{\text{T}} = [\text{CO}_2] + [\text{CO}_2]_{\text{R}}$$

On rearrangement, Equation 5.17 becomes:

$$\frac{\partial^2[\text{CO}_2]_{\text{T}}}{\partial x^2} - \frac{1}{D_{\text{pr}}} \frac{\partial[\text{CO}_2]_{\text{T}}}{\partial t} - \frac{(D_{\text{pr}} - D_{\text{CO}_2})}{D_{\text{pr}}} \frac{\partial^2[\text{CO}_2]}{\partial x^2} = 0 \quad (5.18)$$

Taking the “s-multiplied” Laplace transform, Equation 5.18 can be written in terms of time-mean concentrations:

$$\frac{d^2[\overline{\text{CO}_2}]_{\text{T}}}{dx^2} - \frac{s}{D_{\text{pr}}} ([\overline{\text{CO}_2}]_{\text{T}} - [\text{CO}_2]_{\text{T},0}) - \frac{(D_{\text{pr}} - D_{\text{CO}_2})}{D_{\text{pr}}} \frac{d^2[\overline{\text{CO}_2}]}{dx^2} = 0 \quad (5.19)$$

where the following initial condition was used:

$$\text{at } t=0 \text{ and } x>0; [\text{CO}_2]_{\text{T}} = [\text{CO}_2]_{\text{T},0} = [\text{CO}_2]_0 + [\text{CO}_2]_{\text{R},0}$$

In order to solve Equation 5.19 an approximation is needed for the second derivative of $[\text{CO}_2]$. Substituting Equation 5.12 into Equation 5.19, the following equation is obtained:

$$\begin{aligned} \frac{d^2[\overline{\text{CO}_2}]_{\text{T}}}{dx^2} - \frac{s}{D_{\text{pr}}} [\overline{\text{CO}_2}]_{\text{T}} = & - \frac{s}{D_{\text{pr}}} [\text{CO}_2]_{\text{T},0} + \\ & \frac{(D_{\text{pr}} - D_{\text{CO}_2})}{D_{\text{pr}}} E^2 \left(\frac{k_{\text{L},\text{CO}_2}^0}{D_{\text{CO}_2}} \right)^2 ([\text{CO}_2]_{\text{i}} - [\text{CO}_2]_0) \exp(-xE k_{\text{L},\text{CO}_2}^0 / D_{\text{CO}_2}) \end{aligned} \quad (5.20)$$

Since the *sum* of the concentration gradients of $\text{CO}_3^{=}$ and HCO_3^- is zero at the vapor-liquid interface, the boundary conditions for Equation 5.20 are:

$$\begin{aligned} \text{at } x=\infty ; [\overline{\text{CO}_2}]_T &= [\text{CO}_2]_T = [\text{CO}_2]_{T,o} = [\text{CO}_2]_o + [\text{CO}_2]_{R,o} \\ \text{at } x=0 ; \frac{d[\overline{\text{CO}_2}]_T}{dx} &= \frac{d[\overline{\text{CO}_2}]}{dx} = -E \left(\frac{k_{L,\text{CO}_2}^o}{D_{\text{CO}_2}} \right) ([\text{CO}_2]_i - [\text{CO}_2]_o) \end{aligned} \quad (5.21)$$

The solution of the boundary value problem described by Equations 5.20 and 5.21 is:

$$\Delta[\overline{\text{CO}_2}]_T = [\overline{\text{CO}_2}]_{T,i} - [\overline{\text{CO}_2}]_{T,o} = \{ \bar{N}_{\text{CO}_2} / k_{L,\text{CO}_2}^o \} \frac{(E + \sqrt{r_{pr}})}{E\sqrt{r_{pr}} + 1} ; r_{pr} = D_{pr}/D_{\text{CO}_2} \quad (5.22)$$

where \bar{N}_{CO_2} is the interfacial flux of CO_2 .

5.3.3 Mass Balance for the Reactive Solvents

Using an approach similar to the one described above, the mass balances for the chemical solvents can also be solved. Combining the diffusion-reaction equations for DGA, DGAH^+ and DGACOO^- , and assuming that the diffusion coefficients of these species are the same, the combined mass balance is given by:

$$\frac{\partial \{ [\text{DGA}] + [\text{DGAH}^+] + [\text{DGACOO}^-] \}}{\partial t} = D_{pr} \frac{\partial^2 \{ [\text{DGA}] + [\text{DGAH}^+] + [\text{DGACOO}^-] \}}{\partial x^2} \quad (5.23)$$

The boundary condition at the vapor-liquid interface needed to solve Equation 5.23 also requires the knowledge of the concentration gradients of $\text{RR}'\text{NH}_2^+$ and $\text{RR}'\text{NH}$ that are involved not only in a rate-controlled reactions but also in equilibrium reactions through the boundary layer (reactions 5.2 and 5.7). A mass balance over a small layer Δx adjacent to the gas-liquid interface gives as a result that the *sum* of the concentration gradients of DGAH^+ and DGA is zero at

the vapor-liquid interface. Since DGACOO^- is only involved in a rate controlled reaction its non-volatility implies that the concentration gradient at the gas-liquid interface is zero.

Defining $[\text{DGA}]_T = [\text{DGA}] + [\text{DGAH}^+] + [\text{DGACOO}^-]$, Equation 5.23 can then be solved taking the “s-multiplied” Laplace transform and using the following initial and boundary conditions:

$$\text{at } t = 0 \text{ and } x > 0; \quad [\text{DGA}]_T = [\text{DGA}]_{T,0}$$

$$\text{at } t > 0 \text{ and } x = \infty; \quad [\overline{\text{DGA}}]_T = [\text{DGA}]_{T,0}$$

$$\text{and at } t > 0 \text{ and } x = 0; \quad \frac{d[\overline{\text{DGA}}]_T}{dx} = 0$$

The condition of no concentration gradient (zero flux) at the gas-liquid interface for all non-volatile and ionic species is considered in the boundary condition at $x=0$. Equation 5.23 is then solved giving:

$$\Delta[\overline{\text{DGA}}]_T = [\overline{\text{DGA}}]_{T,i} - [\text{DGA}]_{T,0} = 0 \quad (5.24)$$

Similarly, the diffusion-reaction equations can be solved for the species MDEA and MDEAH^+ giving the following relationship:

$$\Delta[\overline{\text{MDEA}}]_T = 0; \quad [\overline{\text{MDEA}}]_T = [\overline{\text{MDEA}}] + [\overline{\text{MDEAH}^+}] \quad (5.25)$$

5.3.4 Charge Flux

The condition of zero charge flux or dynamic electroneutrality through the mass transfer zone when the diffusion coefficients of all the ions are equal can be expressed as follows:

$$\Delta[\overline{\text{DGAH}^+}] + \Delta[\overline{\text{MDEAH}^+}] = \Delta[\overline{\text{DGACOO}^-}] + \Delta[\overline{\text{HCO}_3^-}] + \Delta[\overline{\text{OH}^-}] + 2\Delta[\overline{\text{CO}_3^{2-}}] \quad (5.26)$$

where the concentration of hydronium ions has been neglected.

5.3.5 Mass Balance of Carbamate

The combined differential mass balance for CO₂ and carbamate is given by:

$$D_{CO_2} \frac{\partial^2 [CO_2]}{\partial x^2} - \frac{\partial [CO_2]}{\partial t} + D_{pr} \frac{\partial^2 [DGACOO^-]}{\partial x^2} - \frac{\partial [DGACOO^-]}{\partial t} - (R_{CO_2}^{(OH)} + R_{CO_2}^{(MDEA)}) = 0 \quad (5.27)$$

This equation can be rearranged to the following form:

$$\frac{\partial^2 \{[CO_2] + [DGACOO^-]\}}{\partial x^2} - \frac{1}{D_{pr}} \frac{\partial \{[CO_2] + [DGACOO^-]\}}{\partial t} - \left(1 - \frac{1}{r_{pr}}\right) \frac{\partial^2 [CO_2]}{\partial x^2} - \frac{1}{D_{pr}} (R_{CO_2}^{(OH)} + R_{CO_2}^{(MDEA)}) = 0 \quad (5.28)$$

Applying the s-multiplied Laplace transform using the initial condition that at $t = 0$ and $x > 0$, $\bar{Q} = Q_o$, Equation 5.28 can be solved analytically assuming a constant time-mean $\bar{R}_{CO_2}^{(OH)}$ and $\bar{R}_{CO_2}^{(MDEA)}$ through the reaction zone. Also using Equation 5.12 to determine the functionality of the gradient of the CO₂ concentration and defining the variable $Q = [CO_2] + [DGACOO^-]$, the following equation results.

$$\frac{d^2 \bar{Q}}{dx^2} - \frac{s}{D_{pr}} \{ \bar{Q} - Q_o \} - \left(1 - \frac{1}{r_{pr}}\right) E^2 \left(\frac{k_{L,CO_2}^o}{D_{CO_2}} \right)^2 ([CO_2]_i - [CO_2]_o) \exp(-xE k_{L,CO_2}^o / D_{CO_2}) - \frac{1}{D_{pr}} (\bar{R}_{CO_2}^{(OH)} + \bar{R}_{CO_2}^{(MDEA)}) = 0 \quad (5.28.a)$$

Equation 5.28.a can be solved using the following boundary conditions:

$$\text{at } t > 0 \text{ and } x = \infty; \quad \bar{Q} = Q_o \text{ (finite)} \quad (5.28.b)$$

$$\text{and at } t > 0 \text{ and } x = 0; \quad \frac{d\bar{Q}}{dx} = \frac{d[CO_2]}{dx} = -E \left(\frac{k_{L,CO_2}^o}{D_{CO_2}} \right) ([CO_2]_i - [CO_2]_o) \quad (5.28.c)$$

giving:

$$\bar{Q} - Q_o = C_1 \exp(-xE k_{L,pr}^o / D_{pr}) + C_2 \exp(xE k_{L,pr}^o / D_{pr}) - \frac{1}{s} (\bar{R}_{CO_2}^{(OH)} + \bar{R}_{CO_2}^{(MDEA)}) +$$

$$+ E^2 \left(\frac{r_{pr} - 1}{r_{pr} E^2 - 1} \right) ([CO_2]_i - [CO_2]_o) \exp(-xE k_{L,CO_2}^o / D_{CO_2}) \quad (5.28.d)$$

Using the boundary conditions 5.28.b and 5.28.c and evaluating the solution and average reaction rates $\bar{R}_{CO_2}^{(OH)}$ and $\bar{R}_{CO_2}^{(MDEA)}$ at the vapor-liquid interface, the following relationship is obtained:

$$\Delta[\overline{CO_2}] + \Delta[\overline{RR'NCOO^-}] = E(\Delta[\overline{CO_2}]) \left(\frac{E + \sqrt{r_{pr}}}{1 + E\sqrt{r_{pr}}} \right) - \frac{D_{CO_2}}{k_{L,CO_2}^o} \left(\bar{R}_{CO_2}^{(OH)} + \bar{R}_{CO_2}^{(MDEA)} \right)_i \quad (5.29)$$

For the limiting situation where r_{pr} approaches unity, Equation 5.29 becomes:

$$\Delta[\overline{RR'NCOO^-}] = (E - 1)\Delta[\overline{CO_2}] - \frac{D_{CO_2}}{k_{L,CO_2}^o} \left(\bar{R}_{CO_2}^{(OH)} + \bar{R}_{CO_2}^{(MDEA)} \right)_i \quad (5.30)$$

which establishes that the flux of carbamate through the reaction zone is equal to the flux of CO_2 “used” by all the chemical reactions ($E-1$ term) minus the flux of CO_2 “used” by the CO_2 -OH⁻ and CO_2 -MDEA reactions.

In Appendix C a discussion is given and example calculations shown on the use of the approximation represented by Equation 5.29. Since the interfacial reaction rate is always larger than the average reaction rate through the reaction zone, it is likely that Equation 5.29 would overestimate the importance of the rate of the slower reaction and the profile given by Equation 5.28.d would be farther from the true profile the closer to the liquid bulk. The approximation involved in Equation 5.29 is probably the most important deficiency in the present mass transfer model. In Section C.3 of Appendix C it is shown that Equation 5.29 resembles the more intuitive MCFLUX (Glasscock et al. 1993) approximation.

5.3.6 Mass Transfer Resistance at the Vapor Phase

In order to account for the finite gas-side mass transfer resistance in the wetted-wall column, the following flux equation was incorporated to the model:

$$\bar{N}_{\text{CO}_2} = k_g (P_{\text{CO}_2(\text{b})} - P_{\text{CO}_2(\text{i})}) = Ek_{\text{L},\text{CO}_2}^0 \left(\frac{P_{\text{CO}_2(\text{i})} - P_{\text{CO}_2}^*}{H_{\text{CO}_2}} \right) \quad (5.31)$$

$$\text{where, } [\text{CO}_2]_{\text{i}} = \frac{P_{\text{CO}_2(\text{i})}}{H_{\text{CO}_2}} \text{ and } [\text{CO}_2]_{\text{o}} = \frac{P_{\text{CO}_2}^*}{H_{\text{CO}_2}}$$

where $P_{\text{CO}_2(\text{b})}$ is the partial pressure of CO_2 at the vapor bulk, $P_{\text{CO}_2}^*$ is the partial pressure of CO_2 in equilibrium with the bulk liquid and H_{CO_2} is the solubility of CO_2 in the solution estimated from the CO_2 - N_2O analogy. The CO_2 - N_2O analogy will be discussed below.

5.3.7 Numerical Solution

The model described above is based on a set of 11 linear and non-linear algebraic equations (Equations 5.6, 5.16, 5.22, 5.24, 5.25, 5.26, 5.29 and 5.31) that can be solved to obtain the interfacial concentrations of all the species and the interfacial flux of CO_2 . The concentration of the species at the liquid bulk are given by the electrolyte NRTL thermodynamic model (Austgen, 1989) since chemical equilibrium is assumed. The Newton-continuation algorithm (Hanna and Sandall, 1995) was used to solve the system of linear and non-linear equations because an algorithm based on the ordinary Newton method was tried, but robustness in convergence was not achieved.

The Newton-continuation method is based on the introduction of the continuation parameter λ to the system of linear and non-linear equations to be solved. When the system of equations to be solved is represented as $\mathbf{f}[\mathbf{x}] = 0$,

where \mathbf{f} and \mathbf{x} are the vectors of equations and independent variables; the continuation parameter λ can be introduced transforming the equations to the following form $\mathbf{f}[\mathbf{x}(\lambda)] = (1-\lambda) \mathbf{f}[\mathbf{x}_0]$. This form of expressing the system of equations indicates that for $\lambda=0$, $\mathbf{f}[\mathbf{x}(\lambda=0)] = \mathbf{f}[\mathbf{x}_0]$ where \mathbf{x}_0 is the vector of initial guesses (or starting points) and for $\lambda=1$, $\mathbf{f}[\mathbf{x}(\lambda=1)] = 0$. Therefore, the value of the vector \mathbf{x} when $\lambda=1$ constitutes the desired solution.

Once the continuation parameter λ is introduced, the resulting transformed systems of equations can be differentiated with respect to λ leading to:

$$\sum_{j=1}^n \frac{\partial f_i}{\partial x_j} \frac{dx_j}{d\lambda} = -\lambda f[\mathbf{x}_0]$$

In this way the original system of algebraic equations is transformed to a system of differential equations where λ is the independent variable of integration and where the initial condition is $\mathbf{x} = \mathbf{x}_0$ (starting point) for $\lambda=0$. Upon integration, the solution \mathbf{x}^* for the system $\mathbf{f}[\mathbf{x}] = 0$ is found when the solution of the differential equations is evaluated for $\lambda=1$. In the present work a variable step algorithm for the integration was used (Hanna and Sandal, 1995).

5.4 RESULTS AND DISCUSSION

5.4.1 Approach

The mass transfer rates of CO_2 measured in the wetted-wall column reactor were interpreted using the model described above. The vapor and liquid-film physical mass transfer coefficients in the reactor were calculated using the models described in Chapter 4, and the transport and thermo-physical properties of the liquid and vapor were calculated using the models and correlations presented in

Appendix B. The model was coupled to a Generalized REGression package, GREG, (Caracotsios, 1986) to estimate parameter values and confidence intervals. Depending on the controlling mechanism, reaction rate constants, diffusion coefficients of reactants and products, or thermodynamic interaction parameters were extracted from the experimental measurements.

5.4.2 Reactive Absorption into Aqueous Solutions of MDEA

The conditions under which the interfacial rates of mass transfer of CO₂ into aqueous solutions of MDEA were measured are described in Table 5.1.

Table 5.1. Experimental Conditions for the Rate Measurements. System MDEA-water- CO₂

MDEA Concentration (wt%)	35 and 50
Temperature (°C)	25 - 100
CO ₂ Loading (moles CO ₂ /moles MDEA)	0.03 - 0.37
P _{CO2} (atm)	0.7 - 7.4

The second order rate constant for the reaction between CO₂ and MDEA was regressed as a function of temperature:

$$k_{2t} = k_{2t(T=313K)} \exp \left\{ -\frac{E_a}{R} \left(\frac{1}{T} - \frac{1}{313K} \right) \right\} \quad (5.32)$$

When the experimental data obtained at all the temperatures were regressed simultaneously, the following parameters were obtained:

$$k_{2t(T=313K)} = 6.28 \pm 1.62 \text{ m}^3/\text{kmol s}$$

$$E_a = 11.68 \pm 1.47 \text{ kcal/mol.}$$

The value of E_a compares favorably with that published by other researchers: 9.1 kcal/mol (Rinker et al., 1995), 11.5 kcal/mol (Rangwala et al., 1992), 13.7 kcal/mol (Critchfield, 1988), and 10.2 kcal/mol (Versteeg and van

Swaaij, 1988b). Figure 5.1 shows a comparison between the rate constants found in this work and those reported by previous researchers.

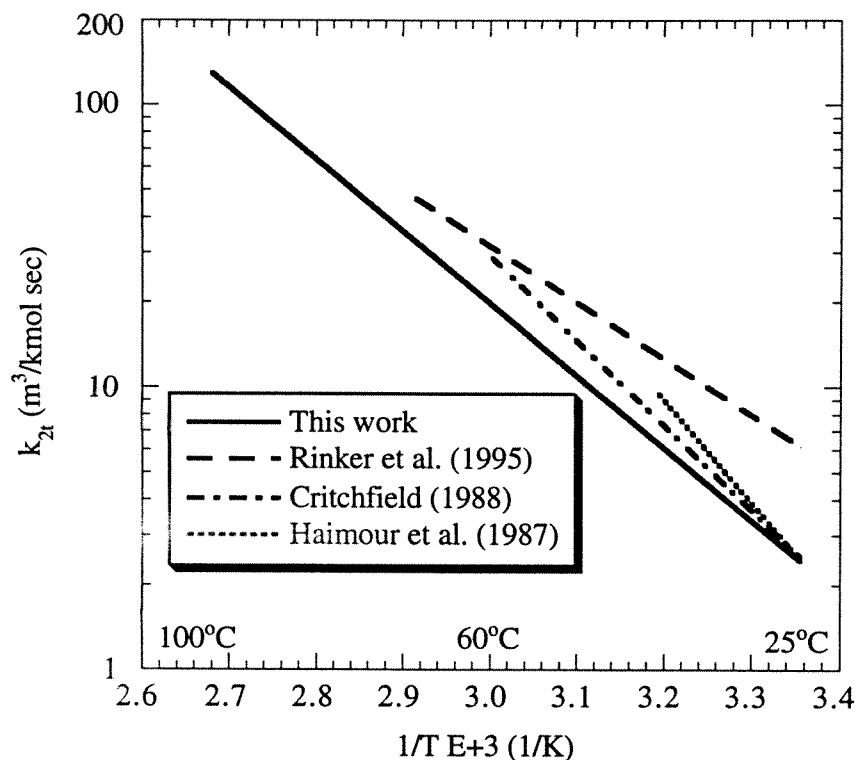


Figure 5.1. Second-order rate constant for the reaction between CO₂ and MDEA.

From Equations 5.15 it can be seen that when θ approaches zero there is no effect of the reversibility of the chemical reactions on the mass transfer rates and the mass transfer enhancement is entirely controlled by the forward reaction rate. On the other hand when θ approaches unity the enhancement of the mass transfer rate no longer depends upon the forward rate constant and other phenomena like equilibrium approach and diffusion limitations of reactants and products through the reaction zone control the mass transfer enhancement.

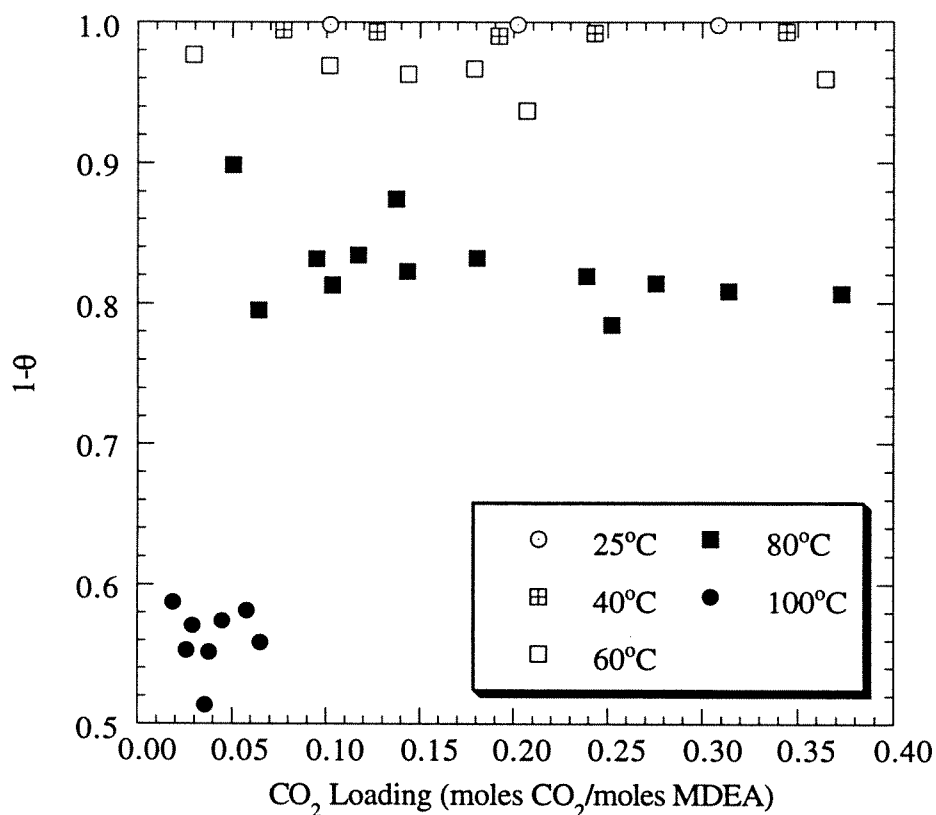


Figure 5.2. Effect of the reversibility of the reaction between CO_2 and MDEA on the enhancement of the mass transfer. Experimental data for 35 and 50 wt% MDEA at 0.7 to 7.4 atm CO_2 in the wetted-wall column.

Figure 5.2 depicts the parameter θ as a function of the total amount of CO_2 in the liquid phase (CO_2 loading) for five series of experimental data. This plot shows that in our data sets the effect of the reversibility of the chemical reaction increases with temperature. This effect can be explained considering that as the forward reaction rate increases with temperature, the concentration of reaction products increases in the reaction zone; this accumulation of product in the reaction zone tends to make the contribution of the reverse reaction more important.

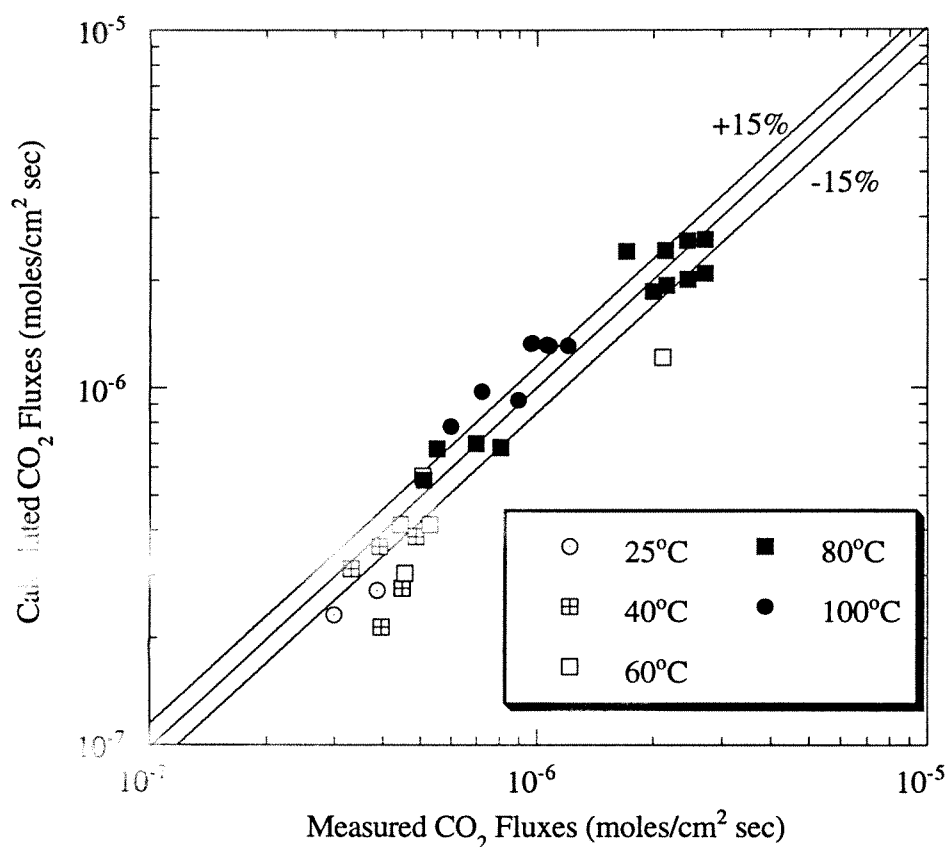


Figure 5.3. Comparison between the calculated and measured interfacial fluxes of CO_2 for the system MDEA-water- CO_2 .

An important implication of the previous discussion is that our ability to extract reaction rate constants from experimental measurements of rates of mass transfer in reactive absorption systems decreases with increasing temperature.

Figure 5.3 presents a comparison of the measured interfacial fluxes of CO_2 in the wetted-wall column and those calculated by the mass transfer model. For most experiments the measured flux is within 15% of the calculated flux.

5.4.3 Reactive Absorption into Aqueous Solutions of DGA

Table 5.2 gives the conditions of the experimental results on the mass transfer of CO₂ in aqueous solutions of DGA.

Table 5.2. Experimental Conditions for the Rate Measurements. System DGA-water- CO₂

DGA Concentration (wt%)	25 and 50
Temperature (°C)	25 - 60
CO ₂ Loading (moles CO ₂ /moles MDEA)	0.015 - 0.48
P _{CO2} (atm)	4E-3 - 0.22

Since the reaction rate between CO₂ and DGA is much faster than that between CO₂ and MDEA, the contribution of the gas-side resistance becomes more important. For this reason the interfacial mass transfer rates of CO₂ in aqueous DGA solutions were measured near atmospheric pressure in order to increase the vapor flow rate and decrease the contribution of the gas-side resistance. Also lower CO₂ partial pressures were used to achieve lower CO₂ loading and avoid significant deviations from the kinetic controlled regime and pseudo-first order mechanism. Since the total pressure in the contactor was always close to atmospheric pressure, the rate measurements could not be performed at temperature higher than 60°C.

For this system the second order rate constant for the reaction between CO₂ and DGA (Equation 5.7) was extracted from the experimental measurements of the interfacial mass transfer rates of CO₂:

$$k_{2p} \left(\frac{\text{m}^3}{\text{kmol s}} \right) = (5.08 \pm 1.51)E + 3 \exp \left\{ -(7.95 \pm 1.94)E + 3 \left(\frac{1}{T} - \frac{1}{298 \text{ K}} \right) \right\} \quad (5.33)$$

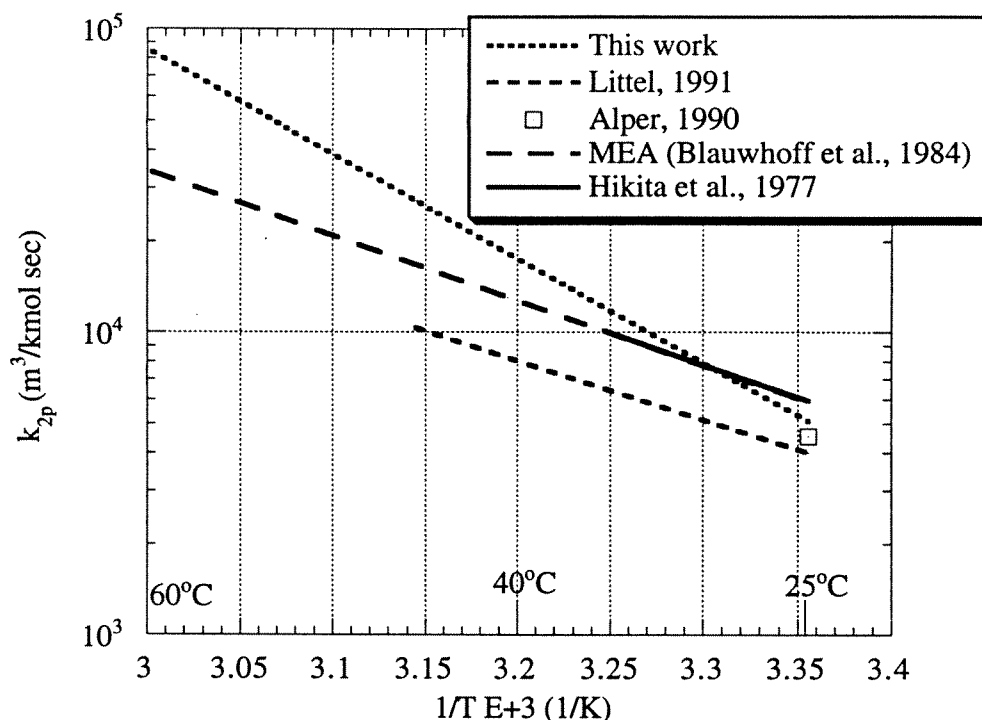


Figure 5.4. Second-order rate constant for the reaction between CO_2 and DGA.

Figure 5.4 compares the second order rate constant for the reaction between CO_2 and DGA with literature values for DGA and MEA. At temperatures below 40°C there is good agreement between the rate constants for the DGA reaction found in this work and those reported by other researchers. Also at lower temperature the kinetics for the reaction between CO_2 and DGA found in this work are similar to the kinetics for the reaction between CO_2 and MEA reported by Blauwhoff et al. (1984). Due to the limited amount of experimental data at higher temperature, the confidence interval of the rate constant increases with temperature and a larger activation energy was obtained. The contribution of the gas-side resistance was between 20 and 40% for most experimental points.

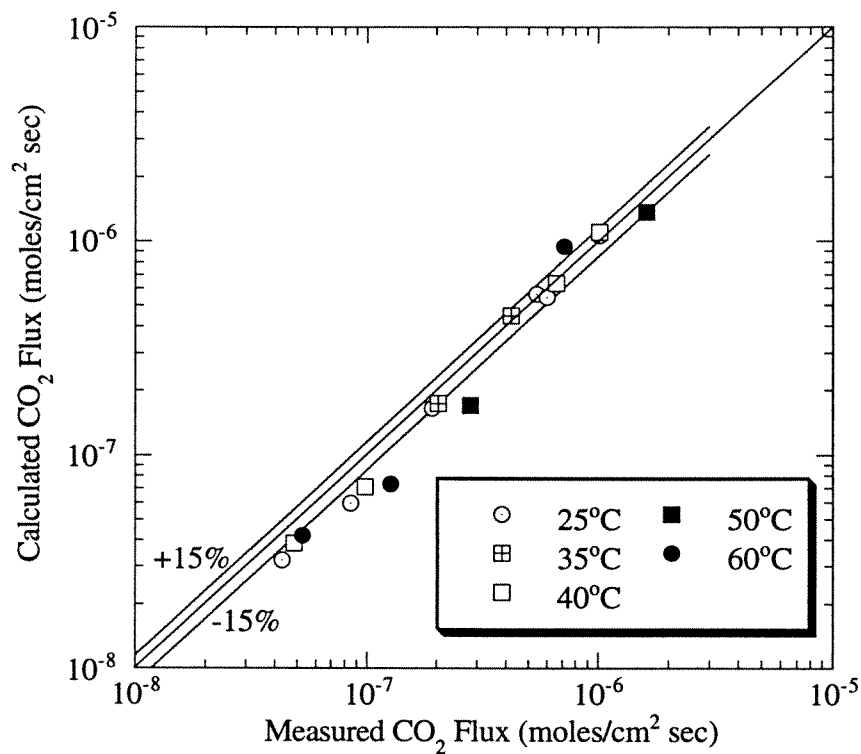


Figure 5.5. Comparison between the experimental and measured interfacial fluxes of CO_2 for the system DGA-water- CO_2 .

The values of the parameter $1-\theta$ for the reaction between DGA and CO_2 varied from 0.95 and 1. Therefore, reaction reversibility was a negligible factor in the analysis of the data. The temperatures at which this reaction was studied were relatively low and therefore the accumulation of the reaction products in the reaction zone was not enough to make the reverse reaction rate significant.

Figure 5.5 shows a comparison between the calculated and measured fluxes of CO_2 for the DGA system. For most points the model predicts the experimental measurements within 15%.

5.4.4 Reactive Absorption into Aqueous Solutions of Mixtures of MDEA and DGA

Table 5.3 describes the experimental conditions chosen to study the reactive system CO₂-water-DGA-MDEA. Two mixtures of these reactive solvents were studied, 5wt% DGA/45wt% MDEA and 15wt%DGA/35wt% MDEA, and for each temperature the experimental data were analyzed in terms of the importance of reaction kinetics, diffusion phenomena and thermodynamic interactions for describing the interfacial mass transfer rates of CO₂.

Table 5.3. Experimental Conditions for the Rate Measurements. System DGA-MDEA-water- CO₂

DGA / MDEA Concentrations	5 wt%DGA/45wt%MDEA ; 15wt%DGA/35wt% MDEA
Temperature (°C)	40 - 100
CO ₂ loading (mol CO ₂ /mol amine)	0.08 - 0.55
P _{CO2} (atm)	0.3 - 8

Figures 5.6 and 5.7 show the typical effects of the reaction rate constants, diffusion coefficients of reactants and reaction products and a thermodynamic interaction parameter on the interfacial mass transfer rates of CO₂ for different temperatures.

The thermodynamic interaction parameter $\tau(\text{water, DGACOO}^-\text{-MDEAH}^+)$ describes the non-ideality of the interaction for water and the DGA carbamate-protonated MDEA pair (DGACOO⁻-MDEAH⁺). Due to the lack of VLE data for the system CO₂-water-DGA-MDEA, this interaction parameter is unknown. Austgen (1989) assumed that for this system $\tau(\text{water, DGACOO}^-\text{-MDEAH}^+)$ was

equal to the equivalent for the system CO_2 -water-MEA-MDEA, that is $\tau(\text{water}, \text{MEACOO}^- \text{-MDEAH}^+)$.

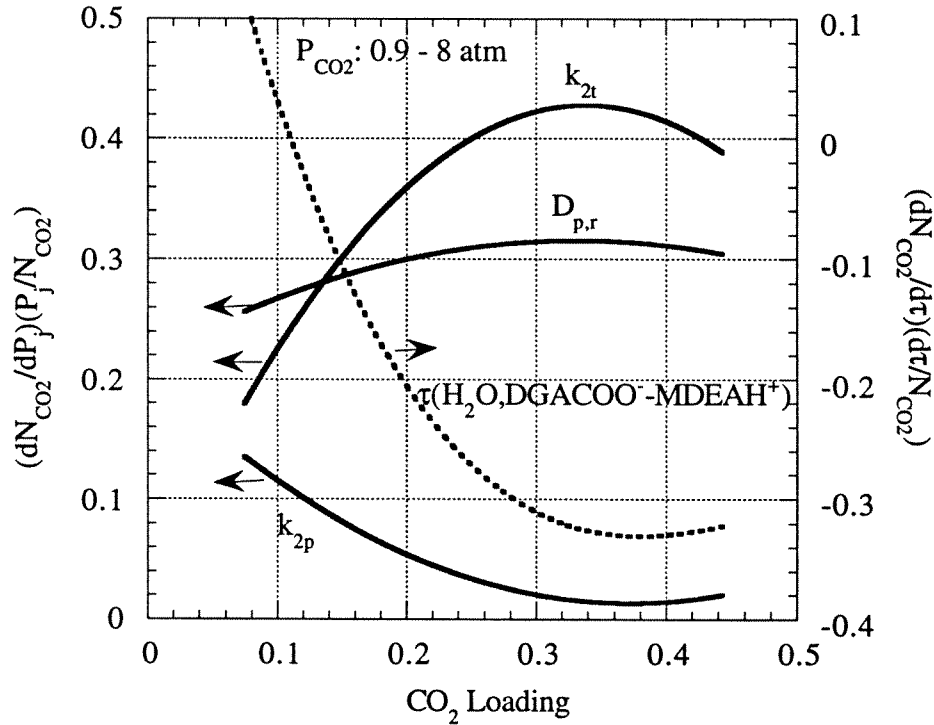


Figure 5.6. Sensitivity of calculated CO_2 flux (N_{CO_2}) to values (P_j) of the rate constants, diffusion coefficients of reactants and products, and thermodynamic interaction parameters. 5wt% DGA/45wt% MDEA, 40°C.

Figure 5.6 shows that at 40°C the calculated flux is more sensitive to $D_{p,r}$, the product-reactant diffusion coefficient, than to the CO_2 -DGA reaction rate constant (k_{2p}), suggesting that the diffusion of reactants and products starts to play a role on the CO_2 flux. At higher CO_2 loading the calculated flux is more sensitive to the second order rate constant for the CO_2 -MDEA reaction (k_{2t}) than to $D_{p,r}$; at lower loading their effects are similar. At lower CO_2 loading the calculated flux is

relatively insensitive to $\tau(\text{water, DGACOO}^-\text{-MDEAH}^+)$, but its effect is larger as loading increases.

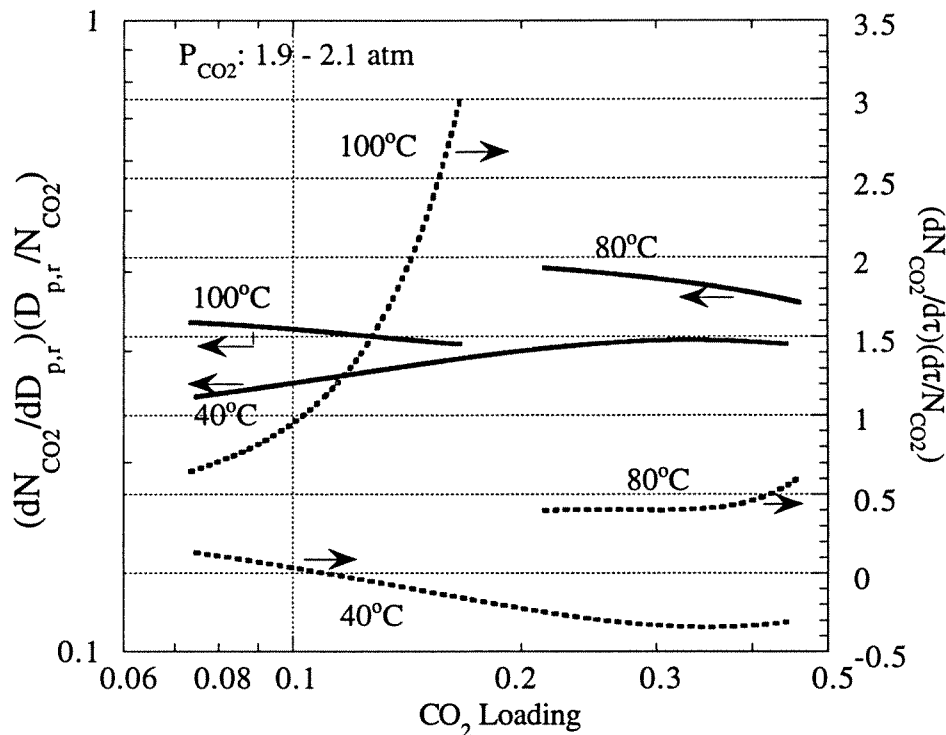


Figure 5.7. Sensitivity of calculated CO_2 flux (N_{CO_2}) to values of the diffusion coefficients of reactants and products ($D_{p,r}$), and thermodynamic interaction parameter $\tau(\text{water, DGACOO}^-\text{-MDEAH}^+)$. 5wt% DGA/45wt% MDEA.

Figure 5.7 represents the effect of $\tau(\text{water, DGACOO}^-\text{-MDEAH}^+)$ and $D_{p,r}$ on the calculated flux of CO_2 for temperatures from 40 to 100°C. At temperatures above 60°C the effect of the reaction rate constants ($k_{2,p}$ and $k_{2,i}$) on the CO_2 flux is almost negligible. The effect of both $\tau(\text{water, DGACOO}^-\text{-MDEAH}^+)$ and $D_{p,r}$ increases with temperature for most conditions studied. These two parameters seem to have an equally important effect at 40 and 80°C, but at 100°C the effect of $\tau(\text{water, DGACOO}^-\text{-MDEAH}^+)$ overshadows that of $D_{p,r}$. The sensitivity to

$\tau(\text{water, DGACOO}^-\text{-MDEAH}^+)$ increases with CO_2 loading due to the accumulation of reaction products in the mass transfer zone.

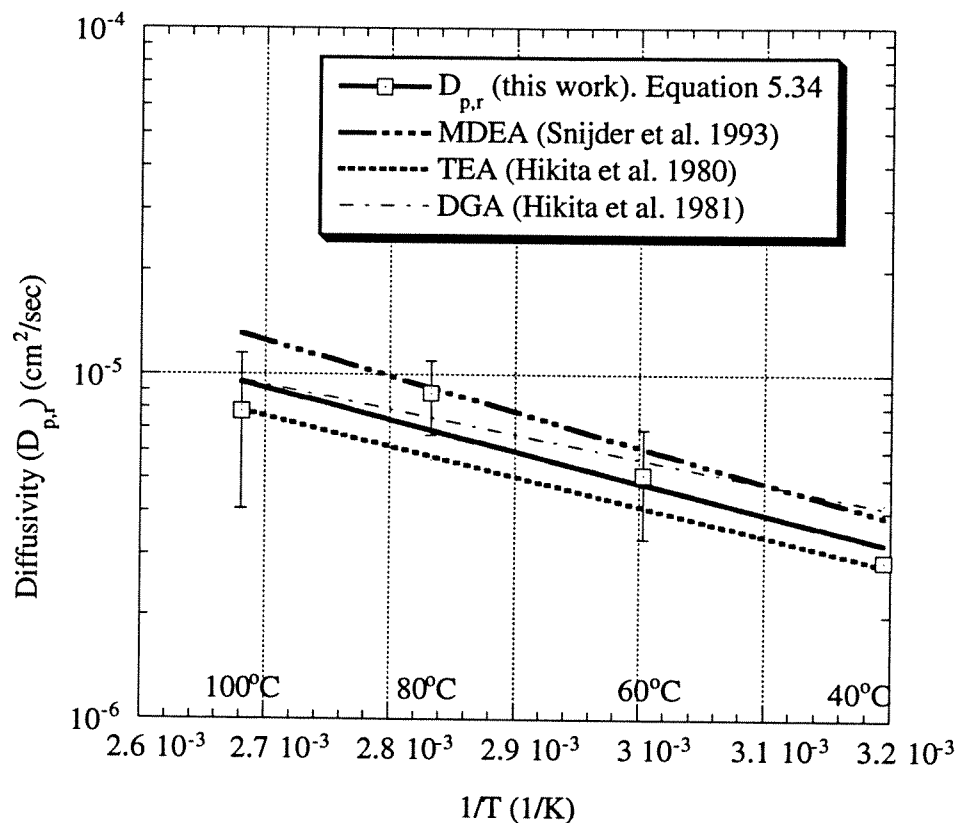


Figure 5.8. Diffusivities of reactants and products obtained from the measured interfacial mass transfer rates of CO_2 for the system DGA-MDEA-water- CO_2 .

Due to their importance, the parameters $D_{p,r}$ and $\tau(\text{water, MDEAH}^+\text{-DGACOO}^-)$ were regressed from the experimental data. $D_{p,r}$ could not be regressed with statistical significance at 40°C , perhaps because the effect of the reaction kinetics is still important. Figure 5.8 gives the regressed values of $D_{p,r}$ and Figure 5.9 gives the values of $\tau(\text{water, MDEAH}^+\text{-DGACOO}^-)$ obtained in the

same regression. These regressions were done for each temperature instead of for all temperatures simultaneously.

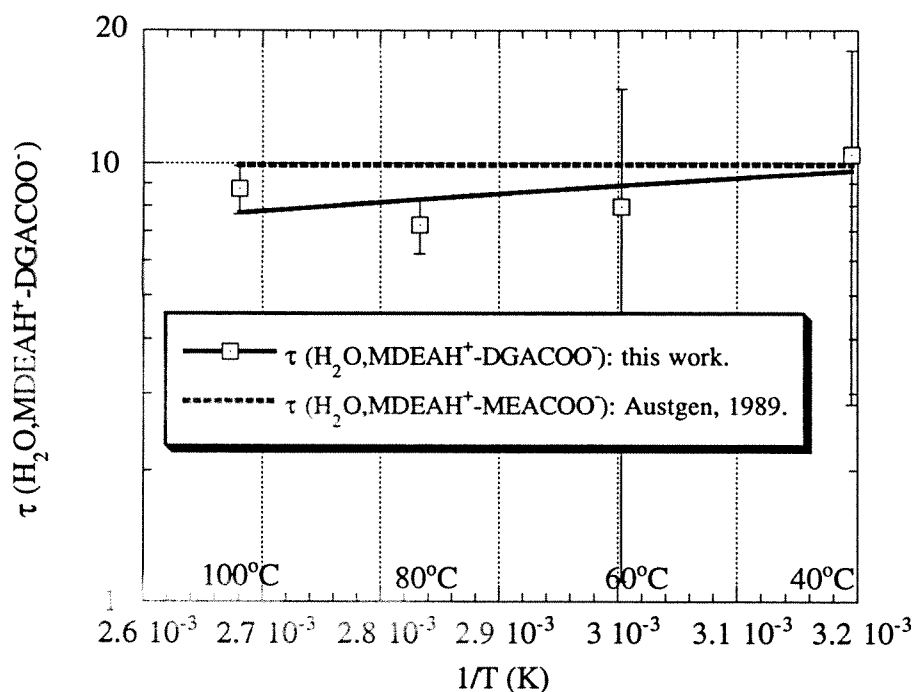


Figure 5.9. Parameter τ (water, DGACOO⁻-MDEAH⁺) of the electrolyte NRTL model obtained from the experimental CO₂ fluxes for the system DGA-MDEA-water-CO₂.

The regressed values of the diffusion coefficients of the reactants and reaction products are close to the diffusion coefficient of MDEA measured at 25 to 75°C (Snijder et al. 1993) and that of DGA. The diffusivity of DGA presented in Figure 5.8 represents an extrapolation of the measurements performed by Hikita et al. (1981) at 25°C. We correlated these data with varying DGA concentration as a function of viscosity and applied a modified Stokes-Einstein equation to extrapolate in temperature.

The regressed values of $D_{p,r}$ shown in Figure 5.8 were correlated using a form of the Stokes-Einstein expression giving:

$$D_{p,r} \text{ (cm}^2\text{/sec)} = \frac{2.845\text{E-}8}{\mu_l \text{ (cP)}^{0.5752}} T \text{ (K)} \quad (5.34)$$

Figure 5.9 shows that the values of $\tau(\text{water, DGACOO}^-\text{-MDEAH}^+)$ calculated for all the temperatures are relatively close to $\tau(\text{water, MEACOO}^-\text{-MDEAH}^+)$ regressed by Austgen (1989) from experimental VLE data. Austgen (1989) could not determine the temperature dependence of $\tau(\text{water, MEACOO}^-\text{-MDEAH}^+)$ with statistical significance.

The following equation correlates the values of $\tau(\text{water, DGACOO}^-\text{-MDEAH}^+)$ with temperature:

$$\tau(\text{water, DGACOO}^-\text{-MDEAH}^+) = -2.06 + \frac{3640.6}{T \text{ (K)}} \quad (5.35)$$

Table 5.4 presents the regressed values, confidence intervals and covariance obtained during the regression of $D_{p,r}$ and $\tau(\text{water, DGACOO}^-\text{-MDEAH}^+)$.

Table 5.4. Results of the regression of $D_{p,r}$ and $\tau(\text{water, DGACOO}^-\text{-MDEAH}^+)$ for the system DGA-MDEA- $\text{H}_2\text{O-CO}_2$.

Temp.(°C)	$D_{p,r}$ (cm ² /s)E+6	$\tau(\text{water, DGACOO}^-\text{-MDEAH}^+)$	Covariance
40	2.89*	10.45 ± 7.64	—
60	5.14 ± 1.80	7.94 ± 6.83	-0.67
80	8.84 ± 2.12	7.23 ± 1.03	-0.74
100	7.80 ± 3.72	8.77 ± 1.11	-0.78

* Not regressed.

The confidence intervals of the regressed $\tau(\text{water, DGACOO}^-\text{-MDEAH}^+)$ decrease with temperature because the mass transfer rate of CO_2 is more significantly controlled by this variable as temperature increases. The confidence interval of $D_{p,r}$ increased at 100°C because the thermodynamic interactions

reflected in $\tau(\text{water, DGACOO}^-\text{-MDEAH}^+)$ are even more important than the diffusion of reactants and products in describing the CO_2 flux.

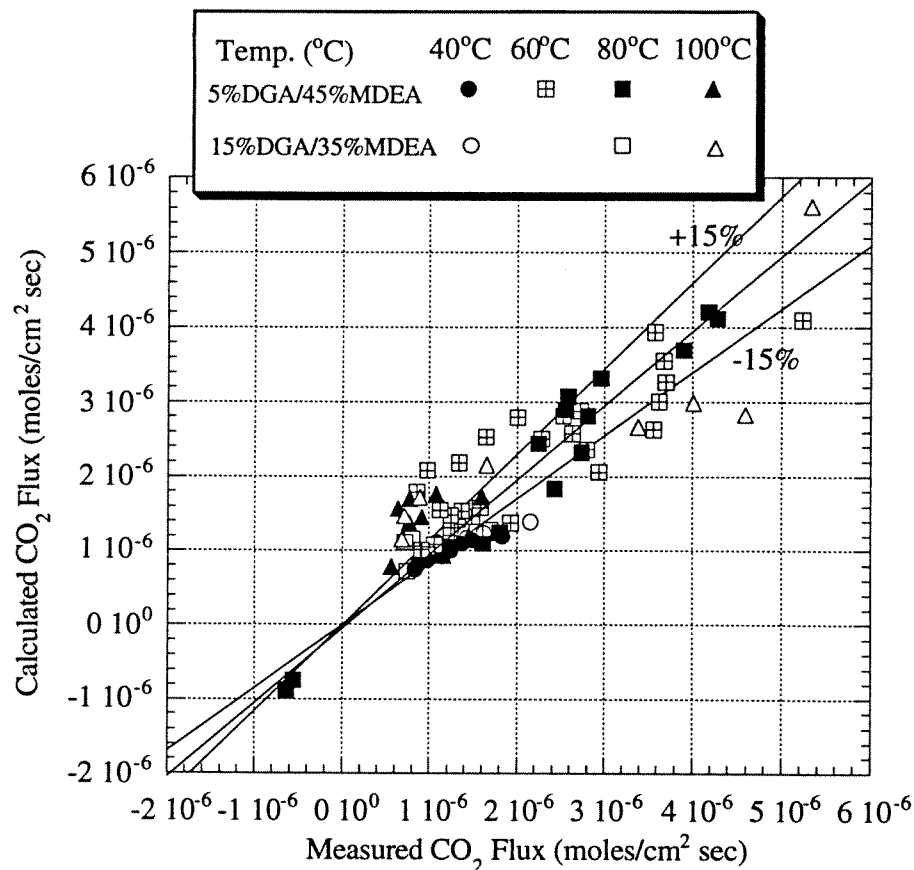


Figure 5.10. Comparison between the measured and calculated fluxes of CO_2 for the system DGA-MDEA-water- CO_2 .

Figure 5.10 compares the model predictions with the measured interfacial mass transfer rates of CO_2 for the system DGA-MDEA-water- CO_2 . The reaction rate constants used were those found when studying each single reactive solvent, that is, MDEA-water- CO_2 and DGA-water- CO_2 . This figure indicates that for most experimental points there is a relatively small deviation between the

measured and predicted interfacial fluxes of CO₂ over a wide range of mass transfer driving forces and temperatures.

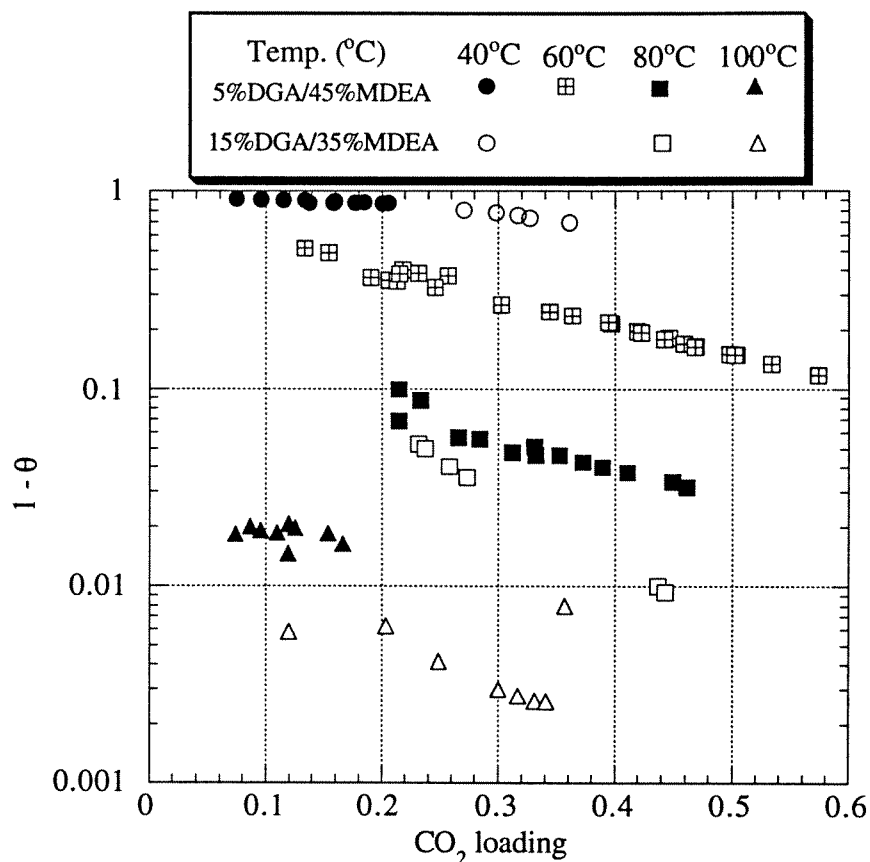


Figure 5.11. Effect of the reversibility of the chemical reactions for the system DGA-MDEA-water-CO₂. 50 wt% total reactive solvent.

Figure 5.11 shows the effect of the reversibility of the chemical reactions on the flux of CO₂. As in the single-solvent systems, the reversibility of the chemical reactions is more important at greater temperature and loading. However, for the blended system, DGA-MDEA-water-CO₂, reversibility is important at temperature as low as 60°C with relatively high CO₂ loading. At 80 and 100°C the effect of reversibility becomes dominant even at low CO₂ loading.

A second effect that can be analyzed from Figure 5.11 is the role of the diffusion limitations of the reactants in the liquid phase. From Equations 5.15 it can be seen that when the parameter $1-\theta$ deviates from unity, the enhancement factor deviates from the limiting situation where $E = Ha$, the larger this deviation the more important the diffusion and/or equilibrium limitations. Consequently, the significant deviations from unity of the parameter $1-\theta$ seen in Figure 5.11 also reflect the importance of the diffusion process described above coupled with the reversibility of the chemical reactions in the boundary layer.

5.4.5. Effect of Individual Reactions on the Mass Transfer Enhancement and Equilibrium Approach

Figure 5.11 depicts the overall approach to equilibrium at the gas-liquid interface calculated using the mass transfer model; however, this figure does not distinguish between the importance of each individual reaction to the overall equilibrium approach. Figure 5.12 shows the equilibrium approach for the DGA-CO₂ and MDEA-CO₂ reactions individually, as well as the overall interfacial equilibrium. The close approach of the values of θ_{DGA} to θ and the considerable difference between θ_{MDEA} and θ indicates that the chemical equilibrium at the interface is mostly governed by the DGA reaction, that is, the concentration of CO₂ that would be in equilibrium at the interface approaches significantly that determined for the DGA-CO₂ reaction. This is due to the fact that the DGA-CO₂ reaction approaches a fast reversible reaction under most conditions, while the MDEA-CO₂ reaction is much slower.

The considerable approach to equilibrium for the DGA-CO₂ reaction at higher temperatures ($\theta_{DGA} \approx \theta \rightarrow 1$) leads to the hypothesis that reactive

absorption of CO_2 into blends of DGA and MDEA can be modelled as well by considering the DGA- CO_2 reaction as an infinitely fast reversible reaction throughout the reaction zone while the MDEA- CO_2 reaction is kept as rate-controlled.

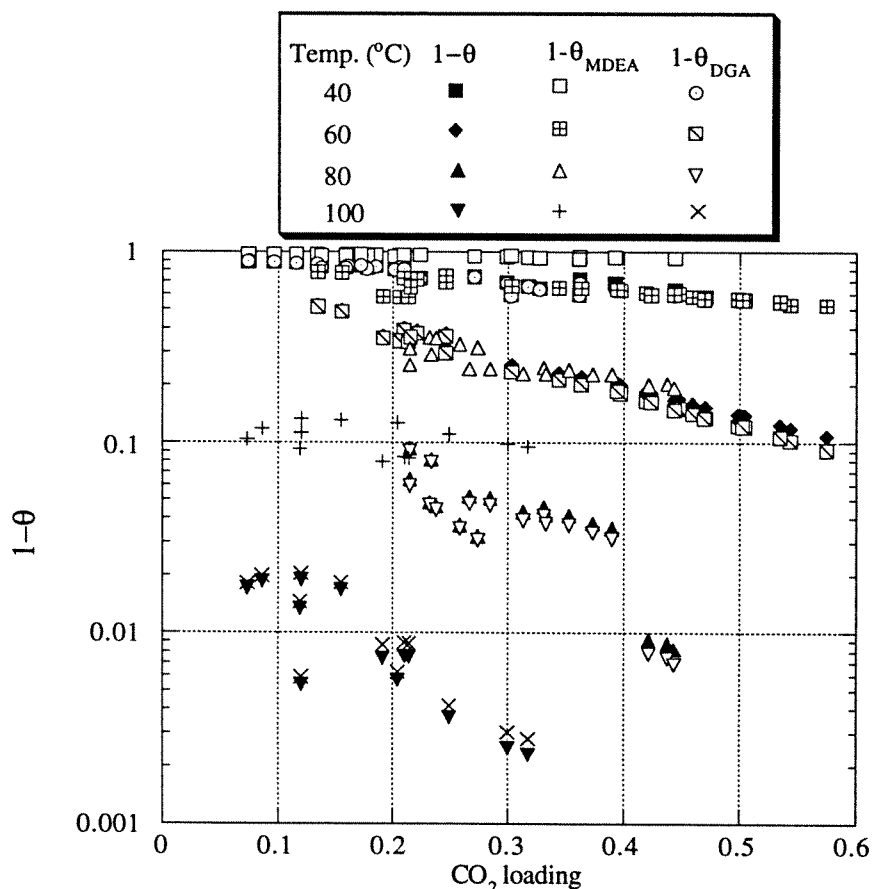


Figure 5.12. Individual approach to interfacial equilibrium for the DGA- CO_2 and MDEA- CO_2 reaction and comparison with the overall interfacial equilibrium. 50 wt% total reactive solvent, both 5wt%DGA-45wt%MDEA and 15wt%DGA-35wt%MDEA.

In order to test the hypothesis of chemical equilibrium for the DGA- CO_2 reaction, Equation 5.7 was considered as a reversible instantaneous reaction.

Combining this equation with the other ionic equilibria (Equations 5.4 and 5.5) and with the MDEA-CO₂ reaction (Equation 5.9), the following reaction is obtained:



The rate of this reaction is equal to the rate of the MDEA-CO₂ reaction. Therefore, the carbamate balance can be written considering Equation 5.36 and the condition of chemical equilibrium for reaction 5.7 throughout the boundary layer. That is,

$$D_p \frac{\partial^2 [\text{DGACOO}^-]}{\partial x^2} - \frac{\partial [\text{DGACOO}^-]}{\partial t} = R_{\text{CO}_2}^{(\text{MDEA})} = k_{2t} [\text{R}_3\text{N}] \{ [\text{CO}_2] - [\text{CO}_2]_{\text{eq,MDEA}} \} \quad (5.37)$$

where $[\text{CO}_2]_{\text{eq,MDEA}}$ is the concentration of CO₂ in equilibrium with bicarbonate,

$$[\text{CO}_2]_{\text{eq,MDEA}} = \frac{[\text{MDEAH}^+][\text{HCO}_3^-]}{K_{\text{MDEA,K}}[\text{MDEA}]} \quad (5.38)$$

Since CO₂ is in equilibrium throughout the reaction zone with DGA and DGACOO⁻, the following reaction results from combining the equilibrium reactions given by Equations 5.4, 5.5 and 5.7:



Therefore, the CO₂ concentration can be expressed as:

$$[\text{CO}_2] = \frac{[\text{DGACOO}^-][\text{MDEAH}^+]}{K_{\text{DM}}[\text{DGA}][\text{MDEA}]} \quad (5.40)$$

Substituting Equations 5.40 and 5.38 into $R_{\text{CO}_2}^{(\text{MDEA})}$, the following expression is obtained:

$$R_{\text{CO}_2}^{(\text{MDEA})} = k_{2t}[\text{MDEAH}^+] \left(\frac{[\text{DGACOO}^-]}{K_{\text{DM}}[\text{DGA}]} - \frac{[\text{HCO}_3^-]}{K_{\text{MDEA,K}}} \right) \quad (5.41)$$

When Equation 5.41 is substituted into Equation 5.37 and the concentration of all the components is evaluated at the interface (except DGACOO^-), an analytical solution can be found for the gradient of carbamate. Using the interfacial concentrations for MDEAH^+ , DGA and HCO_3^- in Equation 5.41 is not likely to introduce a significant error because the gradient of these species through the boundary layer obtained from the analysis described in Section 5.4.4 is not too large. It will be shown below that only for the conditions studied for the lower temperature data (40 and 60°C) the gradient of DGA is significant.

When the DGA-CO_2 reaction is considered as an equilibrium reaction, the gradient of DGACOO^- is not zero at the interface. However, from the total DGA balance the flux of *total* DGA is zero, that is,

$$\frac{d\{[\text{DGA}]+[\text{DGAH}^+]+[\text{DGACOO}^-]\}}{dx} = 0 \text{ at } x = 0 \quad (5.42)$$

The concentrations of DGAH^+ and DGACOO^- are related to the concentration of DGA through the following equilibria:

$$[\text{DGAH}^+] = \frac{K_{\text{DGA}}[\text{DGA}]}{[\text{OH}^-]} \quad (5.43)$$

$$[\text{DGACOO}^-] = \frac{K_{\text{DGA,K}}[\text{DGA}][\text{CO}_2]}{[\text{H}_3\text{O}^+]} \quad (5.44)$$

Substituting Equations 5.44 and 5.43 into Equations 5.42, and using the concentration gradient for CO_2 at the interface given by the definition of the enhancement factor (Equation 5.21), the following expression is obtained for the gradient of carbamate at the interface in terms of time-mean concentrations:

$$\left(\frac{d[\overline{\text{DGACOO}^-}]}{dx} \right)_{x=0} = K_{\text{DM}} \left(\frac{[\overline{\text{MDEA}}]}{[\overline{\text{MDEAH}^+}]} \right) E \left(\frac{k_{\text{L,CO}_2}^0}{D_{\text{CO}_2}} \right) [\overline{\text{DGA}}]_i \Delta[\overline{\text{CO}_2}] \left\{ \frac{[\overline{\text{DGACOO}^-}]}{[\overline{\text{DGA}}]_{\text{T,i}}} - 1 \right\} \quad (5.45)$$

Taking the s-multiplied Laplace transform of Equation 5.37 and using Equation 5.45 as the boundary condition at the interface, an analytical expression for the carbamate concentration profile is obtained. The details of this solution are given in Appendix C. Due to the assumptions mentioned above, it is likely that this profile provides an accurate representation close to the interface and deviates from the true profile closer to the liquid bulk.

When the solution of Equation 5.37 is used as the carbamate balance for predicting the interfacial mass transfer rates of CO_2 instead of Equation 5.29, the results shown in Figure 5.13 are obtained. This figure depicts the ratio of the fluxes predicted by the model described in Section 5.3 to those obtained assuming that the DGA- CO_2 reaction is instantaneous. Besides using the solution of Equation 5.37, the forward rate constant for the DGA- CO_2 reaction was set to an arbitrarily large value such that a close approach to equilibrium for that reaction is achieved at the interface. The approach to equilibrium is given by the close approach of θ_{DGA} to unity.

Figure 5.13 shows that at 80 and 100°C the fluxes predicted assuming that the DGA- CO_2 reaction is instantaneous are only within 10% of those predicted when the reaction is considered as rate-controlled. This result proves the hypothesis of the DGA- CO_2 reaction being instantaneous at high temperatures from the values of the parameter θ described above. The comparison shown on

Figure 5.13 also proves that the mass transfer model developed on Section 5.3 is reliable even for the limiting situation where equilibrium is approached.

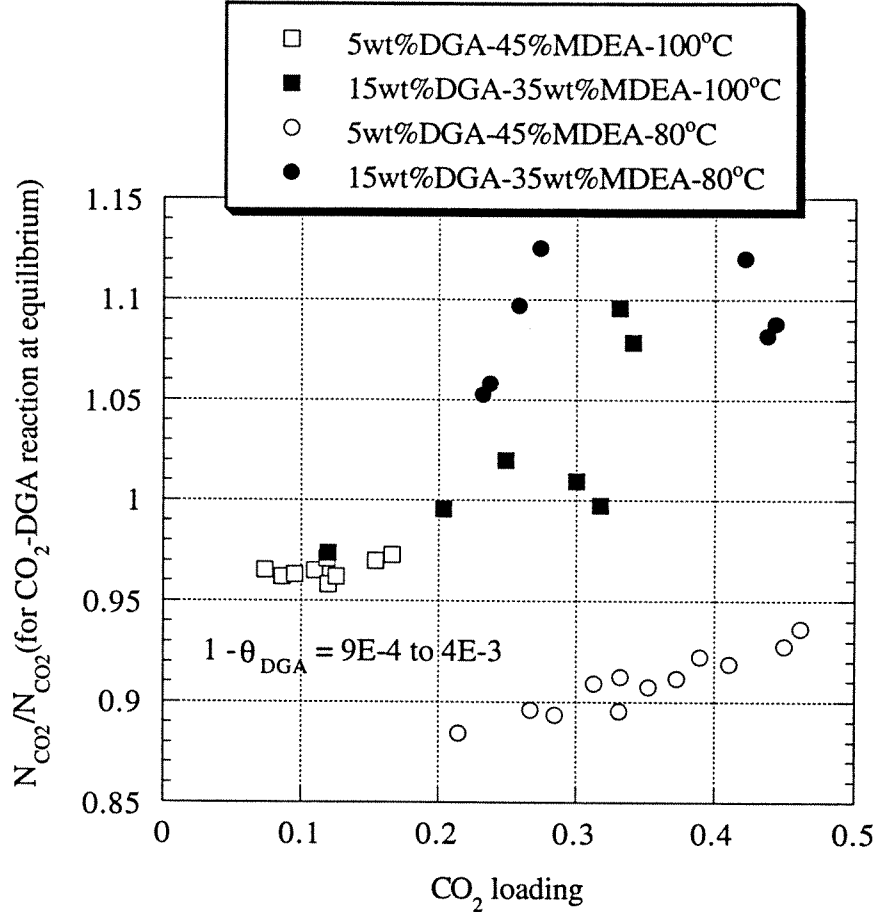


Figure 5.13. Comparison between the interfacial mass transfer rates of CO_2 predicted considering the DGA- CO_2 reaction as instantaneous and as rate-controlled.

It is important to analyze further the effect of the interaction between the DGA- CO_2 and the MDEA- CO_2 reactions on the interfacial mass transfer rate of CO_2 . The carbamate reversion to free DGA through the formation of bicarbonate (Equation 5.36) defines this interaction. By setting the rate constant for the MDEA- CO_2 reaction to zero the effect of this interaction can be studied. Figure

5.14 represents the ratio of the CO_2 fluxes calculated by the model described in Section 5.3 to those calculated when k_{2t} is set to zero.

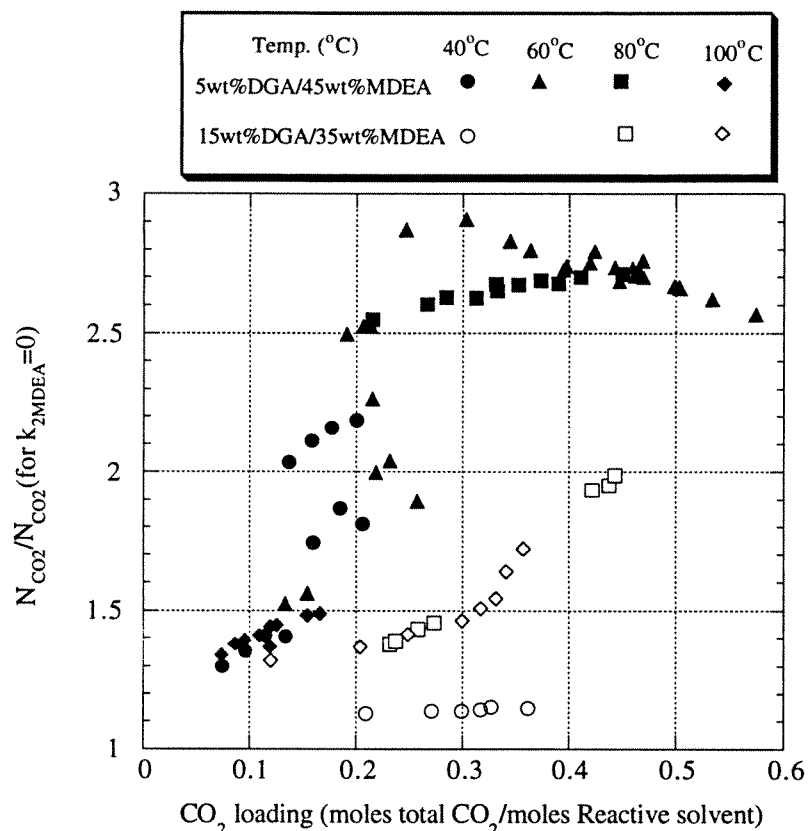


Figure 5.14. Effect of the DGA regeneration by the MDEA- CO_2 reaction on the interfacial mass transfer rate of CO_2 .

Figure 5.14 indicates that the CO_2 -MDEA reaction tends to affect more the interfacial fluxes of CO_2 at higher temperatures. At higher temperatures the equilibrium limitations and the effect of the diffusion of reactants and products control the CO_2 flux. When the path for regeneration of DGA through Equation 5.36 is eliminated there is more accumulation of carbamate at the interface which tends to increase the equilibrium limitation (θ closer to unity) and therefore reduce the mass transfer rate of CO_2 . At 40°C there is no significant effect of the

accumulation of products at the interface and the decrease of the CO_2 flux when k_{2i} is set to zero is mainly due to a decrease in the forward pseudo-first order reaction rate.

Figure 5.14 also shows that the importance of the MDEA reaction is due not only to its direct effect on the mass transfer enhancement (through the forward reaction rate), but also due to its more subtle effect on the regeneration of free DGA which in turn affects the accumulation of products on the reaction zone.

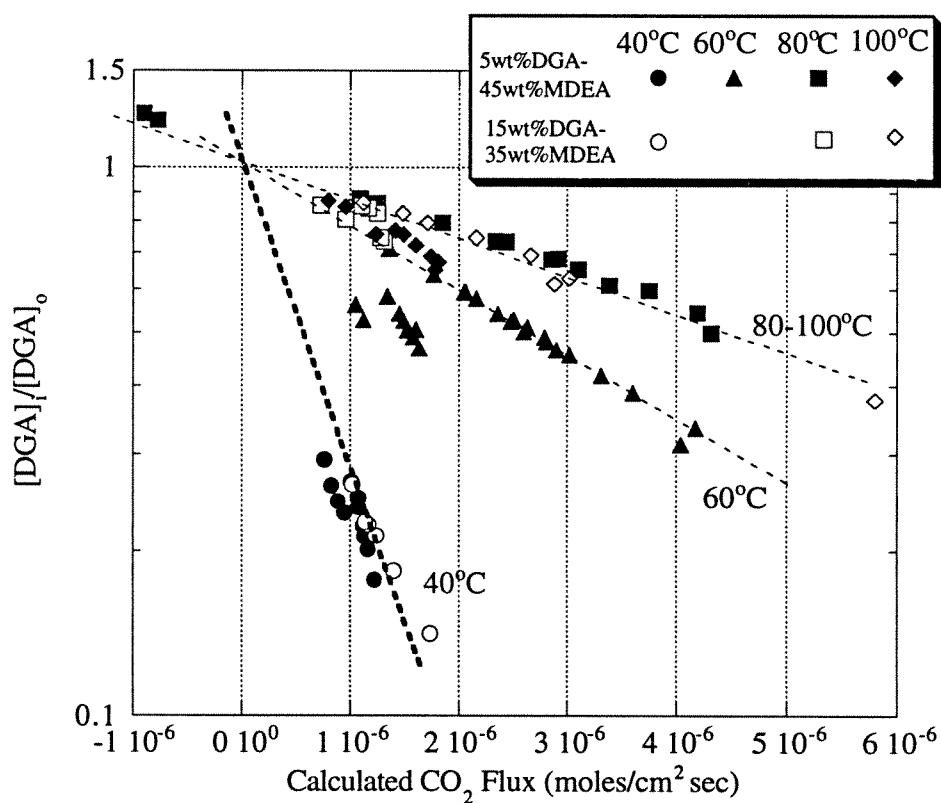


Figure 5.15. Difference between the interfacial and liquid bulk concentration for the fast reactant, DGA.

5.4.6. Diffusion of Reactants and Products

Figure 5.15 depicts the ratio between the interfacial and liquid bulk concentration for the fast reactant, DGA, as calculated by the mass transfer model described in Section 5.3. This figure indicates that under the conditions studied the depletion of the fast reactant is more significant at lower temperature. The diffusion limitation for the fast reactant is more important at 40 and 60°C, while at 80 and 100°C the faster diffusion tends to decrease the concentration difference through the reaction zone. This indicates that the condition of pseudo-first order reaction kinetics is not valid even at low temperature since not all the liquid-bulk reactant is available for reaction.

It is important to note that even if equilibrium at the interface is not approached in any significant extent ($\theta \rightarrow 0$), the condition for pseudo-first order kinetics may not be satisfied because of diffusion limitations. This addresses two different issues observed in the present analysis: diffusion limitations of the fast reactant tend to be important at low temperature, but equilibrium is not limiting in any significant extent (see Figure 5.11); the converse is true at high temperature.

Figure 16 represents the contribution of the fluxes of the reaction products to the interfacial flux of CO₂ as predicted by the mass transfer model. At low CO₂ loading and low temperature the contribution of the flux of bicarbonate and DGA carbamate tend to be equally important. As loading increases the interfacial flux of CO₂ is given mostly by the flux of bicarbonate and the fraction of the total CO₂ flux given by the DGA carbamate flux decreases. This can be explained considering that as loading increases free DGA tends to react faster than MDEA

does, and therefore the DGA reaction tends to be quickly limited by its equilibrium. Consequently, the CO_2 mass transfer enhancement is mostly controlled by the MDEA reaction or, in other words, the CO_2 flux is mostly given by the bicarbonate flux.

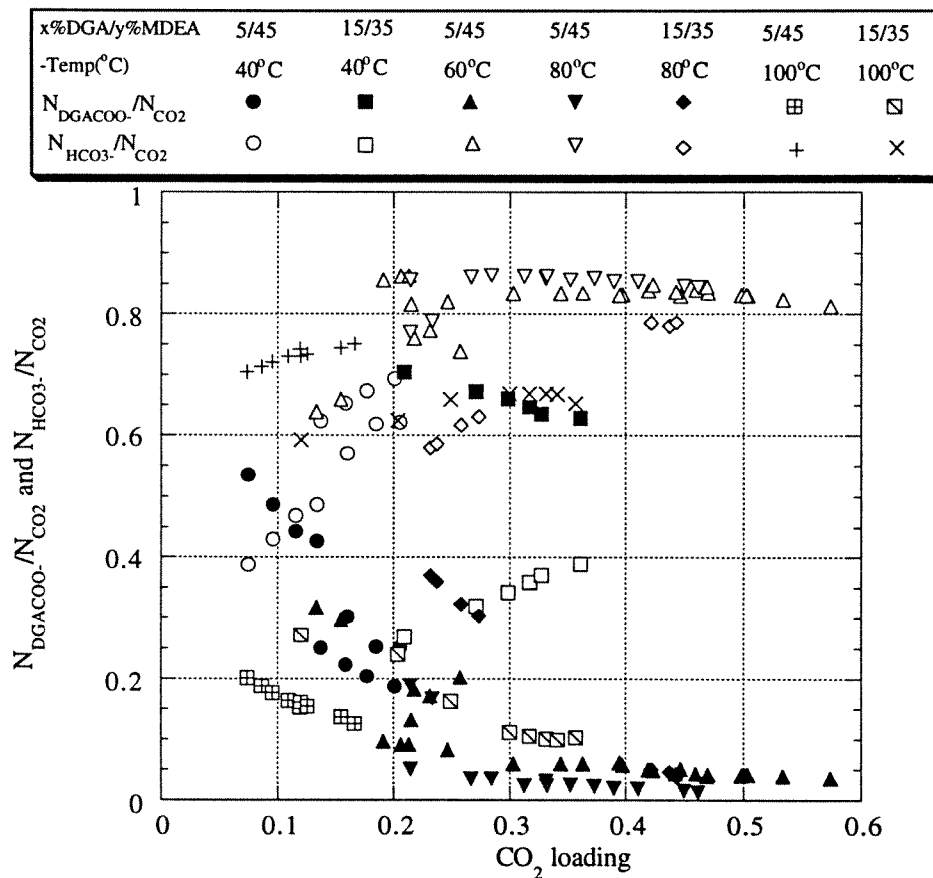


Figure 5.16. Contribution of the fluxes of the reaction products to the interfacial CO_2 flux.

Figure 5.16 also indicates that the advantage of using DGA for mass transfer enhancement in a mixture of DGA and MDEA is achieved mainly at low temperature and low loading, that is, under the conditions encountered near the top of reactive absorption columns. At high loading and high temperature

(conditions encountered in the stripper), mostly the MDEA reaction controls the mass transfer enhancement. This effect is beneficial in practical applications because the advantage of the faster reactant to increase the mass transfer enhancement is exploited in the absorber while the advantage of the slower reactant with a lower heat of absorption-reaction (and therefore, heat of desorption of CO₂) is exploited in the stripper.

5.4.7. Calculated Mass Transfer Enhancement: Contribution of the DGA Reaction

It is difficult to quantify the contribution of the DGA reaction to the interfacial mass transfer enhancement from the experimental data because of the range of mass transfer coefficients, k_L° , that were used for the rate measurements. In order to quantify the contribution of the DGA reaction under consistent basis, a series of calculations were performed using the mass transfer model developed in Section 5.3. The CO₂ enhancement factors were calculated using a physical mass transfer coefficient typical of a packed column, $k_{L,CO_2}^\circ = 4.E-3$ cm/sec, and the gas-side mass transfer coefficient was set to an arbitrarily large value such that the gas-side resistance was vanishingly small. These mass transfer calculations were performed for the different reactive solvents for two cases of mass transfer driving force: one where an equilibrium “pinch” is approached ($P_{CO_2} = 1.05P_{CO_2}^*$) and the other for a larger mass transfer driving force ($P_{CO_2} = 3.0P_{CO_2}^*$).

Figure 5.17 compares the calculated enhancement factors for absorption of CO₂ into 50wt% MDEA with those for the DGA-MDEA blends. At low CO₂ loading, replacing 5 wt% MDEA with 5 wt% DGA in the 50 wt% MDEA

solution, the mass transfer enhancement increases by over 15 times at 40°C, around 10 times at 80°C, and about 5 times at 100°C.

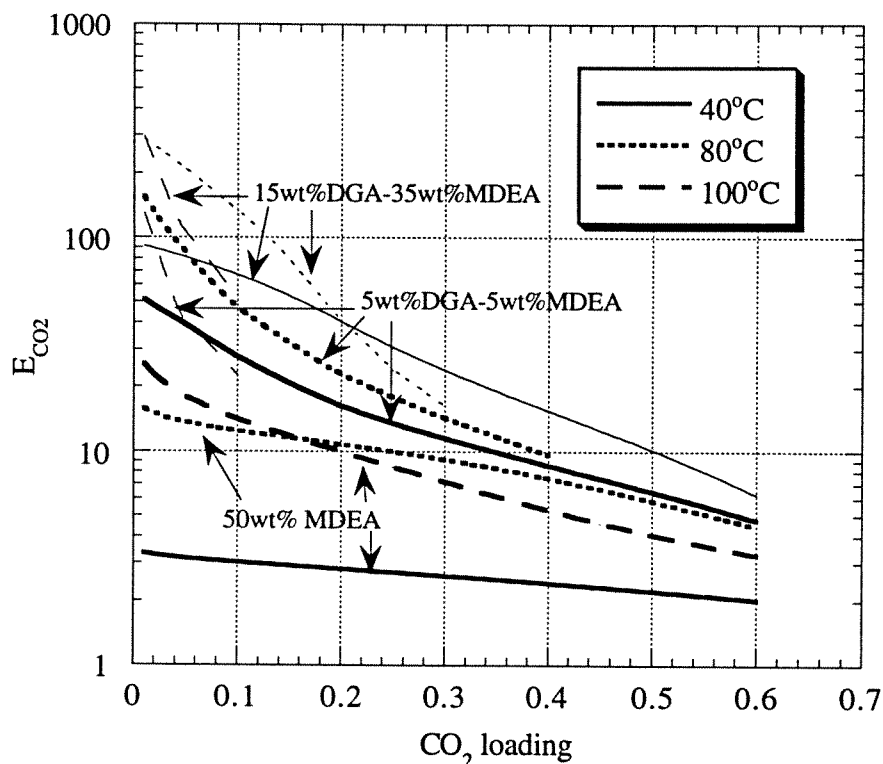


Figure 5.17. Calculated enhancement factors for CO_2 under low mass transfer driving force ($P_{\text{CO}_2} = 1.05P_{\text{CO}_2}^*$) for reactive absorption of CO_2 into aqueous MDEA and blends of MDEA and DGA. $k_{\text{L},\text{CO}_2}^0 = 4.E-3 \text{ cm/sec}$.

Figure 5.17 reiterates what was concluded from Figure 5.16, i.e., the increasing mass transfer enhancement due to the presence of the faster reactant, DGA, is mostly achieved at low CO_2 loading because free DGA is quickly depleted with increasing loading. Figure 5.16 also indicates that due to the increasing equilibrium limitation as temperature increases, the enhancement factors at 80°C can be larger than those at 100°C in the region of higher CO_2 loading (for 50wt% MDEA) or even in the low loading region (for the DGA-

MDEA blends). Figure 5.18 depicts the equilibrium limitation as indicated by the parameter $1-\theta$ in the enhancement factor model.

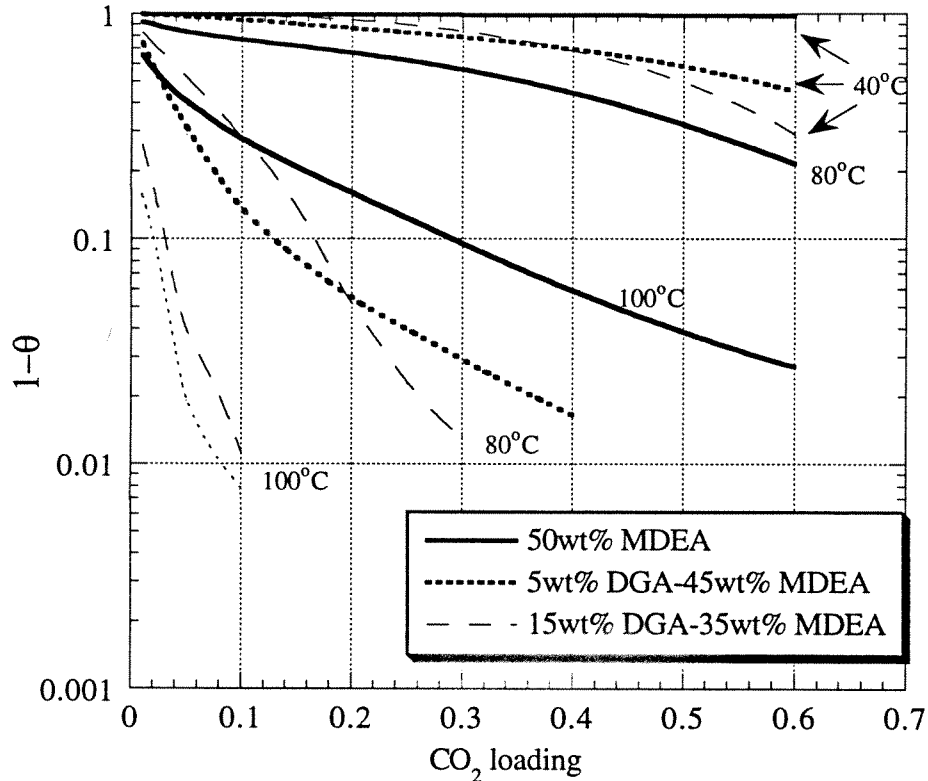


Figure 5.18. Approach to equilibrium at the interface under low mass transfer driving force ($P_{\text{CO}_2} = 1.05P_{\text{CO}_2}^*$) for reactive absorption of CO_2 into aqueous MDEA and blends of MDEA and DGA. $k_{\text{L,CO}_2}^0 = 4. \text{E-}3 \text{ cm/sec}$.

Figure 5.18 shows that at 80 and 100°C the parameter $1-\theta$ quickly approaches zero as loading increases. This effect is much stronger at 100°C. This indicates that the equilibrium approach, rather than the reaction rate, controls the interfacial mass transfer rate. This effect is responsible for the relative difference between the enhancement factors at low and high temperature as seen in Figure 5.17. As shown in Section 5.4.5, the equilibrium approach in this system is

mostly controlled by the CO_2 -DGA reaction, while the CO_2 -MDEA reaction has a minor effect on the equilibrium approach, but a significant effect on the mass transfer enhancement in the region of high loading.

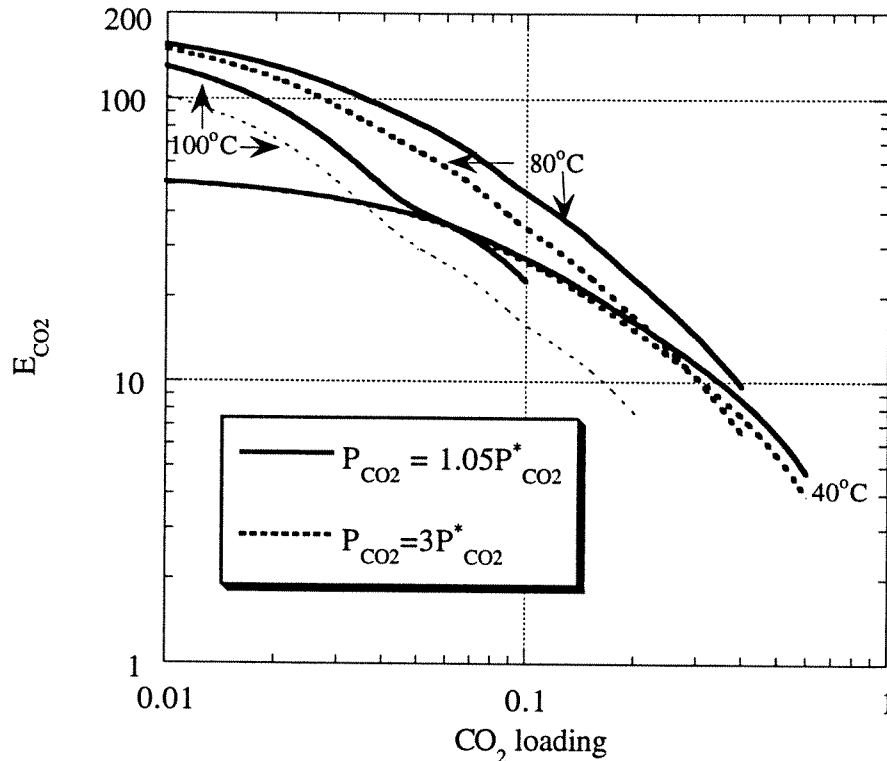


Figure 5.19. Effect of mass transfer driving force on the mass transfer enhancement for reactive absorption of CO_2 into a aqueous mixture of 5 wt% DGA and 45 wt% MDEA. $k_{L,\text{CO}_2}^0 = 4.E-3 \text{ cm/sec}$.

Figure 5.19 depicts the effect of the mass transfer driving force on the mass transfer enhancement for the system 5wt% DGA-45wt% MDEA. This figure indicates that the mass transfer enhancement decreases with increasing driving force, however the higher mass transfer driving force overshadows the decrease of the enhancement factor and the net effect is still higher interfacial fluxes. The decrease of the mass transfer enhancement with increasing driving

force is due to the accumulation of reaction products and therefore increasing importance of the equilibrium approach at the interface, this effect can be seen in Figure 5.20 reflected on the parameter $1-\theta$ of the enhancement factor model.

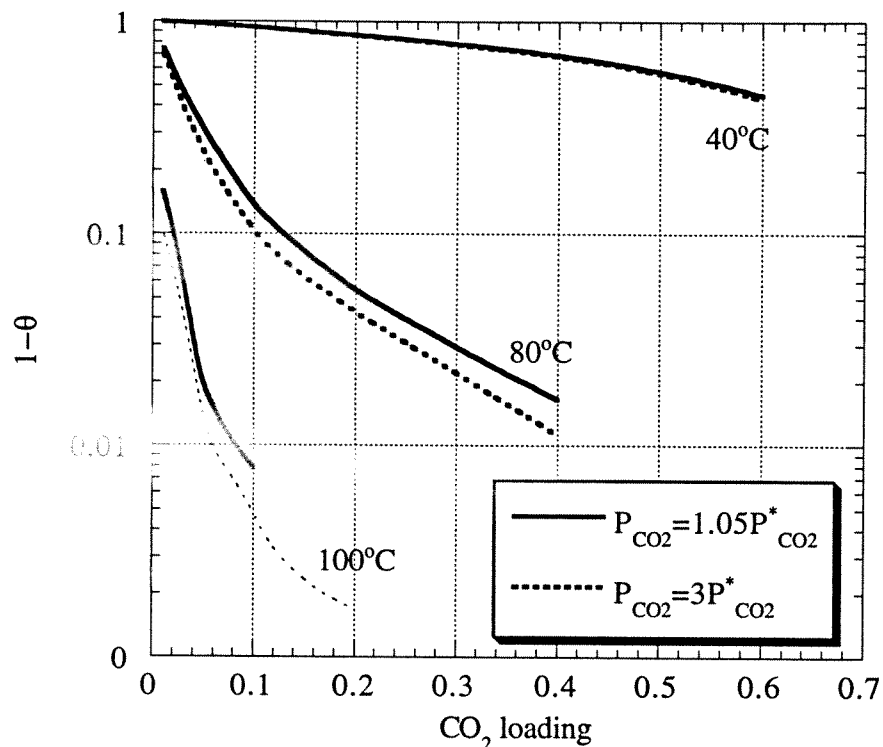


Figure 5.20. Effect of mass transfer driving force on the approach to equilibrium at the interface. System: 5 wt% DGA and 45 wt% MDEA. $k_{L,CO_2}^0 = 4.E-3$ cm/sec.

In this section the non-equilibrium effects on the mass transfer of the presence of the faster reactant, DGA, are addressed. In Appendix D equilibrium calculations are reported showing the effect of DGA on the vapor-liquid equilibria which in turn affects the mass transfer rates.

5.5 CONCLUSIONS

The rates of reactive absorption of CO_2 into aqueous alkanolamine solutions can be calculated using a mathematical model developed in this study. This mass transfer model accounts for the effects of the reversibility of the chemical reactions, diffusion of reactants and products through the reaction zone and the thermodynamic non-ideality of the liquid phase. The concept of the time-mean concentrations in the framework of the surface renewal theory developed by Danckwerts (1970) and DeCoursey (1982, 1992) was used.

Interfacial rates of mass transfer of CO_2 into different aqueous solutions of DGA, MDEA and blends of these two reactive solvents were measured and interpreted using the mass transfer model. It was shown that the reversibility of the chemical reactions, the diffusion of reactants and products and the thermodynamic interaction between water and cation-anion pairs, specifically (water, DGACOO^- - MDEAH^+), play a crucial role in describing the enhancement of the interfacial mass transfer. The effects of the reversibility on the mass transfer enhancement can be significant even at low CO_2 loading.

The diffusion of the reactants (other than the absorbing gas) and of the reaction products in the mass transfer zone is an effect often overlooked while interpreting experimental rates of reactive absorption. In this work it was shown that for reactive absorption systems appropriately accounting for the interaction between diffusion of reactants and products and the reversibility of the chemical reactions is crucial in interpreting and predicting the mass transfer kinetics.

Reaction rate constants, diffusion coefficients of reactants and products and electrolyte interaction parameters were extracted from the experimentally measured interfacial mass transfer rates depending on the controlling mechanism.

5.6 NOMENCLATURE

- a: Interfacial area for mass transfer (m^2).
- [A]: Concentration of species A (kmol/m^3).
- d: Hydraulic diameter of the annulus (m).
- D: Diffusion coefficient (m^2/sec or cm^2/sec).
- E: Enhancement factor.
- E_a : Activation energy (kcal/mol).
- h: Length of the column (m).
- H_i : Henry's constant for species i ($\text{atm cm}^3/\text{moles}$).
- k_{2p} : Forward reaction rate constant for CO_2 -DGA reaction ($\text{m}^3/\text{kmol sec}$).
- k_{2t} : Forward reaction rate constant for CO_2 -MDEA reaction ($\text{m}^3/\text{kmol sec}$).
- $k_{g,i}$: Mass transfer coefficient of species i in the gas-phase ($\text{kmol}/\text{m}^2 \text{ sec atm}$).
- $k_{l,i}$: Physical mass transfer coefficient of species i in the liquid phase (m/sec).
- k_{OH} : Forward reaction rate constant for CO_2 - OH^- reaction ($\text{m}^3/\text{kmol sec}$).
- K: Concentration-based equilibrium constants for reactions 2 through 7.
- N_i : Flux of species i ($\text{kmol}/\text{m}^2 \text{ sec}$).
- P: Total or partial Pressure (atm) or wetted perimeter of the column (m).
- Q: Flow rate (m^3/sec).
- r_{pr} : Ratio of the diffusion coefficient of the reaction products to that of CO_2 .
- R: Gas constant ($\text{kcal}/\text{mole K}$).
- $R^{(i)}$: Rate of reaction i ($\text{kmol}/\text{m}^3 \text{ sec}$).
- s: Parameter in Danckwerts model ($1/\text{sec}$).
- S: Transversal section of the column (m^2).
- t: Time (sec).

T: Temperature (K).
x: Spatial coordinate in the liquid boundary layer (m).

Greek Symbols:

δ : Film thickness (m).
 μ : Viscosity (kg/m sec or cP).
 θ : Parameter in enhancement factor model (defined in Equation 35).
 ρ : Density (kg/m³).
 τ : Electrolyte interaction parameter.

Superscripts:

$[\bar{A}]$: Time-mean concentration of species A.
 \bar{R} : Time-mean reaction rate (kmol/ m³ sec).
 $^{\circ}$: Property evaluated in pure water.

Subscripts:

CO₂: Evaluated for CO₂.
e,i: In equilibrium at the interface.
g: Gas phase.
i: At the vapor-liquid interface or related to species i.
l: Liquid phase.
o: Evaluated at the liquid bulk.
pr: Evaluated for reaction products and reactant (except CO₂).
R: For reacted CO₂.
T: Total.

5.7 REFERENCES

Al-Ghawas, H. A., Hagewiesche, D. P., Ruiz-Ibanez, G., Sandall, O. C.,
"Physicochemical Properties Important for Carbon Dioxide Absorption in
Aqueous Methyldiethanolamine," *J. Chem. Eng. Data*, **1989**, 34, 385.

- Alper, E., "Kinetics of Reactions of Carbon Dioxide with Diglycolamine and Morpholine," *Chem. Engng. J.* **1990**, 44, 107.
- Austgen, D. M., "A Model of Vapor-Liquid Equilibria for Acid gas-Alkanolamine-water Systems". Ph.D. Dissertation, The University of Texas at Austin, 1989.
- Bird, R. B., Stewart, W. E., Lightfoot, E. N., *Transport Phenomena*, Wiley, New York, 1960.
- Blauwhoff, P.M.M., Versteeg, G.F., van Swaaij, W.P.M., "A Study of the Reaction Between CO₂ and Alkanolamines in Aqueous Solutions," *Chem. Engng. Sci.* **1984**, 39, 207.
- Blohm, C. L., Riesenfeld, F. C., U.S. Patent 2712978, July 12, 1955.
- Caracotsios, M., "Model Parametric Sensitivity Analysis and Nonlinear Parameter Estimation. Theory and Applications," Doctoral Dissertation, The University of Wisconsin - Madison, 1986.
- Carey, T. R., Hermes, J. E., Rochelle, G. T., "A Model of Acid Gas Absorption/Stripping Using Methyldiethanolamine with Added Acid," *Gas Separation and Purification*, **1991**, 5, 95.
- Chakravarty, T., Phukan, U. K., Weiland, R., H., "Reactions of Acid Gases with Mixtures of Amines," *Chem. Engng. Prog.* **1985**, 81, 32.
- Critchfield, J. E., "CO₂ Absorption/Desorption in Methyldiethanolamine Systems Promoted with Monoethanolamine and Diethanolamine: Mass Transfer and Reaction Kinetics". Ph.D. Dissertation, The University of Texas at Austin, 1988.
- Danckwerts, P. V., *Gas Liquid Reactions*. McGraw-Hill Inc., New York, 1970.
- DeCoursey, W. J., "Enhancement Factors for Gas Absorption with Reversible Reaction," *Chem. Engng. Sci.* **1982**, 37, 1483.
- DeCoursey, W. J., "A Simpler Approximation for Enhancement of Mass Transfer by Second-Order Reversible Reaction," *ICHEME. Symp. Ser.* **1992**, 128, B269.
- DeCoursey, W. J., Thring, R. W., "Effects of Unequal Diffusivities on Enhancement Factors for Reversible and Irreversible Reaction," *Chem. Engng. Sci.* **1989**, 44, 1715.

- Glasscock, D. A., "Modelling and Experimental Study of Carbon Dioxide Absorption into Aqueous Alkanolamines". Ph.D Dissertation, The University of Texas at Austin, 1990.
- Glasscock, D. A., Rochelle, G. T., "Approximate Simulation of CO₂ and H₂S Absorption into Aqueous Alkanolamines," *AIChE Journal*. **1993**, 39, 1389.
- Hagewiesche, D. P., Ashour, S. S., Sandall, O. C., "Solubility and Diffusivity of Nitrous Oxide in Ternary Mixtures of Water, Monoethanolamine, and N-Methyldiethanolamine and Solution Densities and Viscosities," *J. Chem. Eng. Data*, **1995**, 40, 627.
- Hanna, O., Sandall O., *Computational Methods in Chemical Engineering*. Prentice Hall. New Jersey, 1995.
- Hikita, H., Asai, S., Ishikawa, H., Honda, M., "The Kinetics of Reactions of Carbon Dioxide with Monoisopropanolamine, Diglycolamine and Ethylenediamine by a Rapid Mixing Method," *Chem. Engng. J.* **1977**, 14, 27.
- Hikita, H., Ishikawa, H., Murakami, T., Ishii, T., "Densities, Viscosities and Amine Diffusivities of Aqueous MIPA, DIPA, DGA and EDA Solutions," *Journal Chem. Eng. Japan*, **1981**, 14, 5.
- Hobler, T., *Mass Transfer and Absorbers*, Pergamon Press, Oxford, 1966.
- Jefferson Chemical Company. Technical Service Information, 1970.
- Licht, S.E., Weiland, R. H., "Density and Physical Solubility of CO₂ in Partially Loaded Solutions of MEA, DEA and MDEA," Presented at the AIChE National Meeting **1989**, Paper No. 57f, Houston, Texas.
- Littel, R. J., "Selective Carbonyl Sulfide Removal in Acid Gas Treating Processes," Doctoral Dissertation. Twente University of Technology. The Netherlands, 1991.
- Littel, R. J., Filmer, B., Versteeg, G. F., Van Swaaij, W. P. M., "Modeling of Simultaneous Absorption of H₂S and CO₂ in Alkanolamine Solutions: The Influence of Parallel and Consecutive Reversible Reactions and the Coupled Diffusion of Ionic Species," *Chem. Engng. Sci.* **1991**, 46, 2313.
- Mshewa, M., "Carbon Dioxide Desorption/Absorption with Aqueous Mixtures of Methyldiethanolamine and Diethanolamine at 40 to 120°C". Ph.D Dissertation, The University of Texas at Austin, 1995.

- Pigford, R., L., "Counter-Diffusion in a Wetted Wall Column," Doctoral Dissertation, The University of Illinois, Urbana, Illinois, 1941.
- Pinsent, B. R. W., Pearson, L., Roughton, F. J. W., "The Kinetics of Combination of Carbon Dioxide with Hydroxide Ions," *Trans. Faraday Soc.* **1956**, 52, 1512
- Rangwala, H. A., Morell, B. R., Mather, A. E. Otto, F. D., "Absorption of CO₂ into Aqueous Tertiary Amine/MEA Solutions," *Can. J. Chem. Engng.* **1992**, 70, 482.
- Rinker, E. B., Ashour, S. S., Sandall, O. C., "Kinetics and Modeling of Carbon Dioxide Absorption into Aqueous Solutions of N-methyldiethanolamine," *Chem. Eng. Sci.* **1995**, 50, 755.
- Rinker, E.B., Oelschlager, D.W., Colussi, A.T., Henry, K.R., Sandall, O.C., "Viscosity, Density, and Surface Tension of Binary Mixtures of Water and N-Methyldiethanolamine and Water and Diethanolamine and Tertiary Mixtures of These Amines with Water over the Temperature Range 20-100°C," *J. Chem. Eng. Data.* **1994**, 39, 392.
- Sandall, O. C., Rinker, E. B., Ashour, S., "Acid Gas Treating by Aqueous Alkanolamines," Annual Report for the Gas Research Institute, **1993**.
- Snijder, E. D., te Riele, M. J. M., Versteeg, G. F., van Swaaij, W.P.M., "Diffusion Coefficients of Several Aqueous Alkanolamine Solutions," *J. Chem. Eng. Data.* **1993**, 38, 475.
- Tamimi, A., Rinker, E. B., Sandall, O.C., "Diffusion Coefficients for Hydrogen Sulfide, Carbon Dioxide, and Nitrous Oxide in Water over the Temperature Range 293-368K," *J. Chem. Eng. Data.* **1994a**, 39, 330.
- Tamimi, A., Rinker, E. B., Sandall, O.C., "Diffusivity of Nitrous Oxide in Aqueous Solutions of N-methyldiethanolamine and Diethanolamine from 298 to 368 K," *J. Chem. Eng. Data.* **1994b**, 39, 396.
- van Swaaij, W. P. W., Versteeg, G. F., "Mass Transfer Accompanied with Complex Reversible Chemical Reactions in Gas-Liquid Systems: An Overview," *Chem. Engng. Sci.* **1992**, 47, 3181.
- Versteeg, G. F., van Swaaij, W. P. M., "Solubility and Diffusivity of Acid Gases (CO₂, N₂O) in Aqueous Alkanolamine Solutions". *J. Chem. Eng. Data.* **1988a**, 33, 29.

- Versteeg, G. F., van Swaaij, W. P. M., "On the Kinetics Between CO₂ and Alkanolamines both in Aqueous and non-Aqueous Solutions-II. Tertiary Amines," *Chem. Engng. Sci.* **1988b**, 43, 587.
- Versteeg, G. F., Kuipers, J. A. M., van Beckum, F. P. H., van Swaaij, W. P. M., "Mass Transfer with Complex Reversible Chemical Reactions-I. Single Reversible Chemical Reaction," *Chem. Engng. Sci.* **1989**, 44, 2295.
- Versteeg, G. F., Kuipers, J. A. M., van Beckum, F. P. H., van Swaaij, W. P. M., "Mass Transfer with Complex Reversible Chemical Reactions-II. Parallel Reversible Chemical Reactions," *Chem. Engng. Sci.* **1990**, 45, 183.
- Winkelman, J.G.M., Brodsky, S. J., Beenackers, A.A.C.M, "Effect of Unequal Diffusivities on Enhancement Factors for Reversible Reactions: Numerical Solutions and Comparison with DeCoursey's Method," *Chem. Engng. Sci.* **1992**, 47, 485.

Chapter 6

Rate-Based Modeling of Reactive Absorption Columns

6.1 INTRODUCTION

Many researchers (Krishnamurthy and Taylor, 1986; Sivasubramanian, 1985; Seader, 1989; Darton, 1992; Taylor and Krishna, 1993; Krishna and Wesselingh 1997) have recognized the importance of using a fundamental rate-based approach for modeling the heat and mass transfer processes present in separation systems. However, the use of the fundamentals of rate-based modeling in reactive separation processes, like reactive absorption or reactive distillation, is a relatively recent development (Darton, 1992). In this chapter the effort aimed at developing a better understanding of the rate processes present in reactive absorption systems is described in detail.

Methyldiethanolamine (MDEA) is a tertiary amine used extensively in industry for the selective absorption of H_2S from natural gas, refinery gases, and gases from coal gasification (Astarita et al., 1983). The reaction rates of H_2S with MDEA are effectively instantaneous with respect to the mass transfer rates. On the contrary, the reaction rates of CO_2 with MDEA are finite and slow with respect to the mass transfer rate of CO_2 (Astarita et al., 1983). This difference in reaction rates leads to the kinetic selectivity for H_2S .

DeCoursey and coworkers (1982, 1989, 1992) have studied the effect of reversibility of the chemical reactions and unequal diffusivities on the enhancement of mass transfer due to a second-order gas-liquid chemical reaction.

Glasscock and Rochelle (1993) used a modified form of the expression developed by DeCoursey (1982) for the enhancement factor in order to model the enhancement of the mass transfer of CO_2 when it is chemically absorbed in aqueous alkanolamine solutions.

Tomcej et al. (1987) implemented an efficiency model based on the solution of the differential mass balance on a tray of a given contactor. A modified vapor Murphree efficiency is calculated in terms of the hydrodynamics of the tray and approximate enhancement factors for the gas-liquid reactions. In the application to the removal of CO_2 using alkanolamines as the chemical solvent, a pseudo-first order model was used for estimating the enhancement factor and the reversibility of the chemical reaction is neglected. For reactive absorption of CO_2 and H_2S into aqueous MDEA in bubble-cap trays, enhancement factors from 1 to 3 for CO_2 and from 100 to 2000 for H_2S are reported.

Sivasubramanian (1985), Taylor and Weiland (1987), and Carey et al. (1991) integrated the interfacial transport processes into the mass and energy balance at a given segment or tray of the column for the simultaneous absorption of CO_2 and H_2S into aqueous alkanolamines. Sivasubramanian (1985) assumed that the enhancement factor for the mass transfer of CO_2 into aqueous methyldiethanolamine was equal to unity, while Carey et al. (1991) calculated the enhancement factor using a modification of the model developed by DeCoursey (1982). The non-equilibrium model reported by Taylor and Weiland (1987) is based on the work by Sivasubramanian (1985). Due to the interaction with the absorption of CO_2 , Sivasubramanian determined the existence of an optimum number of trays for the selective removal of H_2S using aqueous diethanolamine.

Carey et al. (1991) modeled the integrated absorber-stripper system analyzing the effect of different operating variables. The vapor-liquid equilibria were represented by an empirical expression that was fitted to experimental data and the use of activity coefficients was avoided.

In the present work, RATEFRAC[®], the rate-based distillation module of Aspen Plus[®], was used for modeling the mass and heat transfer processes involved in the reactive absorption of CO₂ and H₂S into aqueous solutions of methyldiethanolamine. The system conditions studied for the base case were those typical for the selective removal of H₂S from fuel gas produced by coal gasification. RATEFRAC[®] uses the Generalized Maxwell-Stefan (GMS) approach to multicomponent mass transfer and has the integration capability needed to model the mass and heat transfer processes throughout the contactor. RATEFRAC[®] is supplied with the appropriate models for estimating gas and liquid film mass and heat transfer coefficients and interfacial area. Inside the routine that supplies mass transfer coefficients, a mass transfer model is solved to calculate the enhancement factors and therefore account for the effect of the chemical reactions on the interfacial mass transfer. RATEFRAC[®] also uses enthalpy models to account for the important heat effects.

Among the distinguishing features in this work, the Maxwell-Stefan approach to mass transfer is combined with the enhancement factor theory (based on pseudo-binary mass transfer) to model both kinetic and equilibrium controlled reactions. Frank et al. (1995a,b) showed that these two theories were consistent for first and second order irreversible reactions. Also, reaction kinetics was

combined with a rigorous thermodynamic description based on the electrolyte NRTL model.

A detailed analysis of the interactions between the heat effects and the approach to equilibrium for H₂S has demonstrated the existence of “pinches” at the temperature bulge. The existence of an optimum packing height for the removal of H₂S due to the “pinch” was also identified. The controlling mechanisms for the mass transfer of CO₂ and H₂S were compared in packed and trayed columns where reactive absorption takes place.

6.2. MASS TRANSFER MODEL

6.2.1 Reactive System

When CO₂ and H₂S react with MDEA or other tertiary amines in an aqueous solution, the following Henry’s equilibria and equilibrium reactions occur:

Solubility of CO₂ and H₂S

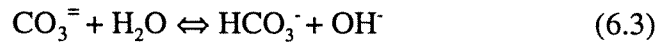


$$H_{\text{CO}_2} = \frac{P_{\text{CO}_2,i}}{[\text{CO}_{2,aq}]_i}$$



$$H_{\text{H}_2\text{S}} = \frac{P_{\text{H}_2\text{S},i}}{[\text{H}_2\text{S}_{aq}]_i}$$

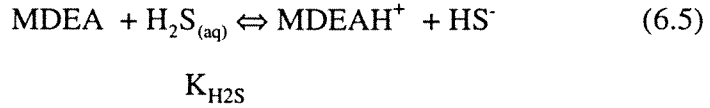
Equilibrium Reactions



K_{bic}



K_{MDEA}



Since reactions 6.3 through 6.5 involve only a proton transfer, they were assumed to be at equilibrium in the entire liquid boundary layer, even at the vapor liquid interface. Both theoretical and experimental studies have been performed to study the thermodynamics of the system $\text{CO}_2\text{-H}_2\text{S-MDEA-H}_2\text{O}$. Austgen (1989) and Posey (1996) applied the electrolyte-nonrandom two-liquid (NRTL) model to this system and regressed model parameters using available experimental data. The chemical equilibrium for reactions 6.3 through 6.5 described using the electrolyte NRTL model (Austgen, 1989) was coupled with the transfer equations described below.

Two parallel reactions are included with reversible kinetics:



$$R_{\text{MDEA}} = k_{2t}[\text{CO}_2][\text{MDEA}] - \left(\frac{k_{2t}}{K_{2t}} \right) [\text{MDEAH}^+][\text{HCO}_3^-] \quad (6.7)$$

$$k_{2t} (\text{m}^3/\text{kmol s}) = 2.576 \times 10^9 \exp \left\{ -\frac{6024}{T} \right\}; \quad (6.8)$$

The reaction rate constants for the CO_2 reaction with MDEA given by Equation 6.8 were obtained from the analysis of the experimental rate data measured from 25 to 100°C in the bench-scale wetted-wall column reactor described in Chapter 5. The reaction rate constants given by Equation 6.8 are not exactly the same as those given by Equation 5.32 because this rate modeling work was concluded before the analysis of the experimental data was completed. The

activation energy and rates predicted by Equation 6.8 are about 2% and 30% larger, respectively, than those given by Equation 5.32.

Pinsent et al. (1956) measured the rate of reaction of CO₂ with hydroxide ions from 0 to 40 °C. They determined that the reaction is second order,



$$R_{\text{OH}} = k_{\text{OH}}[\text{CO}_2][\text{OH}^-] - \left(\frac{k_{\text{OH}}}{K_{\text{OH}}} \right) [\text{HCO}_3^-] \quad (6.10)$$

$$k_{\text{OH}} (\text{m}^3/\text{kmol s}) = 4.315 \times 10^{13} \exp \left\{ -\frac{6666}{T} \right\} \quad (6.11)$$

In order to account for the effect of the non-idealities of the liquid phase on the reaction kinetics, the electrolyte NRTL model (Austgen, 1989) was used to calculate the activity coefficient of each species at the temperature and CO₂ loading of the bulk liquid. Then it was assumed that at the gas-liquid interface the activity coefficients of the species are the same as those in the bulk liquid. In this way equilibrium constants based on concentrations, K_{2t} and K_{OH} , and constants for reactions 6.1 through 6.5, could be defined for the solution of the mass transfer model.

6.2.2 Mass Transfer at the Liquid Boundary Layer: Point Modeling

Mass transfer in the liquid film is modeled by an approximate solution of the diffusion-reaction equations that describe the mass balance of the different species. Fick's law was used to represent the fluxes assuming pseudo-binary diffusion. The ionic equilibria are coupled with the approximate solution of the diffusion-reaction equations. Details about this model are given in Chapter 5 and Appendix C. For the system chosen, the following are the governing equations:

Total CO₂ Mass Balance:

$$\{[\overline{\text{CO}_2}]_i - [\text{CO}_2]_o\} + \{[\overline{\text{HCO}_3^-}]_i - [\text{HCO}_3^-]_o\} + \{[\overline{\text{CO}_3^{2-}}]_i - [\text{CO}_3^{2-}]_o\} = \frac{\overline{N}_{\text{CO}_2}}{k_{\text{L,CO}_2}^\circ} \frac{(E_{\text{CO}_2} + \sqrt{r_{\text{Prod}}})}{(E_{\text{CO}_2} \sqrt{r_{\text{Prod}}} + 1)} \quad (6.12)$$

where $[\overline{A}]_i$ represents the time-mean interfacial concentration of species A, r_{Prod} is the ratio of the diffusivity of the reaction products to that of CO₂ ($=D_{\text{Prod}}/D_{\text{CO}_2}$) and E_{CO_2} is the enhancement factor of CO₂ defined by the flux relationship:

$$\overline{N}_{\text{CO}_2} = E_{\text{CO}_2} k_{\text{L,CO}_2, \text{eff}}^\circ ([\text{CO}_2]_i - [\text{CO}_2]_o) = E_{\text{CO}_2} k_{\text{L,CO}_2, \text{eff}}^\circ \left(\frac{P_{\text{CO}_2, i} - P_{\text{CO}_2}^*}{H_{\text{CO}_2}} \right) \quad (6.13)$$

Total Balance of the Liquid Reactant:

Since the flux of total MDEA (MDEA plus MDEAH⁺) through the reaction zone must be zero and because these species are assumed to have equal diffusion coefficients, the MDEA balance is:

$$([\overline{\text{MDEA}}]_i - [\text{MDEA}]_o) + ([\overline{\text{MDEAH}^+}]_i - [\text{MDEAH}^+]_o) = 0 \quad (6.14)$$

Flux of CO₂ at the Vapor-Liquid Interface

Applying the method of DeCoursey (1992), the following expression for the enhancement factor for CO₂ is obtained (See Section 5.3.1 in Chapter 5):

$$E_{\text{CO}_2} = \sqrt{1 + \frac{D_{\text{CO}_2} \{k_{21} [\text{MDEA}]_i + k_{\text{OH}} [\text{OH}^-]_i\}}{k_{\text{L,CO}_2, \text{eff}}^{\circ 2}}} (1 - \theta) \quad (6.15)$$

where the parameter θ is a measure of the approach to chemical equilibrium at the interface:

$$\theta = \frac{[\overline{\text{CO}_2}]_{e, i} - [\text{CO}_2]_o}{[\text{CO}_2]_i - [\text{CO}_2]_o} \quad (6.16)$$

$[\overline{\text{CO}_2}]_{e,i}$ is the interfacial concentration of CO_2 if chemical equilibrium would hold at the interface. Considering the MDEA hydrolysis (reaction 6.4), it can be shown that the equilibrium condition for reactions 6.6 and 6.9 is the same,

$$[\overline{\text{CO}_2}]_{e,i} = \frac{[\overline{\text{MDEAH}^+}]_i [\overline{\text{HCO}_3^-}]_i}{K_{2t} [\overline{\text{MDEA}}]_i} = \frac{[\overline{\text{HCO}_3^-}]_i}{K_{\text{OH}} [\overline{\text{OH}^-}]_i} \quad (6.17)$$

For the limiting condition where there is no diffusion limitation of the liquid-phase reactants, the effect of the $\text{CO}_2\text{-OH}^-$ reaction is negligible, the effect of reversibility is unimportant, and the rate of reaction is significantly faster than the diffusion rate of CO_2 , the pseudo-first order regime is approached where the enhancement factor is given by:

$$E_{\text{CO}_2} = \frac{\sqrt{D_{\text{CO}_2} k_{2t} [\overline{\text{MDEA}}]}}{k_{\text{L,CO}_2,\text{eff}}^0} \quad (6.18)$$

Flux of H_2S at the Vapor-Liquid Interface

Chang and Rochelle (1982) validated that the enhancement factor with surface renewal theory for a reversible instantaneous reaction such as reaction 6.5 could be approximated by:

$$E_{\text{H}_2\text{S}}^\infty = 1 + \sqrt{\frac{D_{\text{HS}^-}}{D_{\text{H}_2\text{S}}}} \left(\frac{[\overline{\text{HS}^-}]_i - [\text{HS}^-]_o}{[\text{H}_2\text{S}]_i - [\text{H}_2\text{S}]_o} \right) \quad (6.19)$$

where the concentration of bisulfide at the interface $[\overline{\text{HS}^-}]_i$ is calculated from the approximate solution of the diffusion-reaction equation for HS^- and H_2S coupled with the equilibrium condition throughout the liquid boundary layer (Astarita et al., 1980):

$$[\overline{\text{HS}^-}]_i = [\text{HS}^-]_o + \frac{\bar{\xi}}{\sqrt{D_{\text{HS}^-}/D_{\text{H}_2\text{S}}}} \quad (6.20)$$

where $\bar{\xi}$ is a parameter equivalent to the extent of the reaction in the absence of diffusion phenomena. Using Equation 6.20, equivalent relations for MDEA and MDEAH⁺, and the condition of chemical equilibrium, the following relationship is obtained:

$$\psi = \frac{[\overline{\text{H}_2\text{S}}]_i}{[\text{H}_2\text{S}]_o} = \frac{\left(1 + \frac{\bar{\xi}}{\sqrt{r_{pr}} [\text{MDEAH}^+]_o}\right) \left(1 + \frac{\bar{\xi}}{\sqrt{r_{pr}} [\text{HS}^-]_o}\right)}{\left(1 - \frac{\bar{\xi}}{\sqrt{r_{pr}} [\text{MDEA}]_o}\right)} \quad (6.21)$$

The variable r_{pr} is the ratio of the diffusion coefficient for bisulfide to that for H₂S. In Equation 6.21 it was assumed that the diffusivity of MDEA, MDEAH⁺ and HS⁻ are equal to the diffusivity of the reaction products. Also, in Equations 6.19 through 6.21 the diffusivity ratios were replaced by their square roots because Chang and Rochelle (1982) found that using the square roots of the ratios improves the agreement between the predictions of film and surface renewal theory. Equations 6.19 through 6.21 were originally developed using film theory. Comparing Equations 6.20 and 6.19, it can be seen that the enhancement factor for H₂S can be expressed as:

$$E_{\text{H}_2\text{S}}^\infty = 1 + \left(\frac{\bar{\xi}}{[\overline{\text{H}_2\text{S}}]_i - [\text{H}_2\text{S}]_o} \right) \quad (6.22)$$

Once the enhancement factor for H₂S is calculated, the interfacial flux of H₂S is given by:

$$\bar{N}_{\text{H}_2\text{S}} = E_{\text{H}_2\text{S}}^\infty k_{\text{L,H}_2\text{S,eff}}^\circ ([\text{H}_2\text{S}]_i - [\text{H}_2\text{S}]_o) \quad (6.23)$$

Charge Flux Balance

The net charge flux should be zero through the boundary layer, giving:

$$\begin{aligned} \left([\overline{\text{MDEAH}^+}]_i - [\text{MDEAH}^+]_o \right) &= \left([\overline{\text{HCO}_3^-}]_i - [\text{HCO}_3^-]_o \right) + \left([\overline{\text{HS}^-}]_i - [\text{HS}^-]_o \right) + \\ & \left([\overline{\text{OH}^-}]_i - [\text{OH}^-]_o \right) + 2 \left([\overline{\text{CO}_3^{=}}]_i - [\text{CO}_3^{=}]_o \right) \end{aligned} \quad (6.24)$$

where the diffusivities of all the reaction products were assumed to be equal and the concentration of hydronium ions was neglected. Littel et al. (1991) showed that neglecting the effect of the electrostatic potential gradient on the diffusion of the ionic species has minor effects on the prediction of the interfacial mass transfer rates.

Gas-film Resistance

In this model, the gas-film resistance to mass transfer is accounted for by allowing RATEFRAC[®] to solve the Generalized Maxwell-Stefan (GMS) equations at the vapor side. For a multicomponent system the GMS equations can be expressed as (Taylor et al., 1993; Krishna et al., 1997),

$$-\frac{y_i}{RT} \nabla_{T,p} \mu_i = \sum_{j=1}^n \frac{y_j N_i - y_i N_j}{c_{\text{tot}} \mathfrak{D}_{i,j}} = \sum_{j=1}^n \frac{y_j J_i - y_i J_j}{c_{\text{tot}} \mathfrak{D}_{i,j}}; \quad i = 1, 2, \dots, n \quad (6.25)$$

where $\mathfrak{D}_{i,j}$ are the binary Maxwell-Stefan diffusion coefficients. Equations 6.25 can be written in matrix form where the driving force is expressed as the mole fraction difference and a correction for the thermodynamic non-ideality. Usually, when applying these equations, mass transfer coefficients instead of diffusivities are used to avoid the estimation of a film thickness.

6.3 PHYSICAL AND TRANSPORT PROPERTIES

The diffusivity of CO_2 in the liquid phase based on the N_2O analogy (Haimour and Sandall, 1984) was introduced by multiplying the binary mass transfer coefficients of CO_2 by the square root of the ratio of the effective diffusion coefficient for CO_2 to that originally calculated by Aspen Plus[®]. In the models used, the mass transfer coefficients in the liquid phase vary as the square root of the diffusivity.

A ratio of the Henry's constant for CO_2 estimated originally by Aspen Plus[®] to that estimated from the N_2O analogy was calculated. Since the CO_2 interfacial mass transfer flux is given by Equation 13, when we multiply the physical mass transfer coefficient of CO_2 by this ratio of Henry's constants we are using the Henry's constant from the N_2O analogy to calculate the mass transfer driving force for CO_2 . This correction assumes that the speciation of the liquid phase is not significantly affected when the Henry's constant estimated from the N_2O analogy is used.

The model uses diffusivities of CO_2 and N_2O in water and aqueous methyldiethanolamine reported by Versteeg et al. (1988). Solubilities of CO_2 and N_2O in water and of N_2O in aqueous solutions of methyldiethanolamine have been reported by Versteeg and van Swaaij (1988) and Sandall et al. (1993), respectively. The combined correction to account for the diffusivity and Henry's constant estimated from the N_2O analogy is usually minor, less than 5%.

In this work it was assumed that the diffusion coefficients of all the reaction products and reactants (except CO_2 and H_2S) were equal to the diffusion

coefficient of MDEA. The correlation obtained by Snijder et al. (1993) for the diffusivity of MDEA was implemented in RATEFRAC[®] in the routine that solves the point model.

The effect of the CO₂ loading on the viscosity of the liquid solvent was accounted for by using a correlation determined by Glasscock (1990) from available experimental data.

Appendix B describes these models, correlations and data used for predicting the transport and thermophysical properties.

6.4 CONFIGURATIONS OF CONTACTORS STUDIED AND FEED COMPOSITION

Table 1 shows the characteristics of the packed and trayed contactors that were used as the base cases for the modeling study. The composition, flow rate and conditions of the reactive solvent and vapor streams fed to the contactors are described in Table 2. The composition of the vapor stream is typical of the fuel gas produced by coal gasification.

Table 6.1. Characteristics of the packed and trayed columns

	Packed Column	Trayed Column
Column Diameter (m)	1.68	1.68
Packing height (m)	8.0	–
Number of trays or segments	15	6
Type of Contactor	Pall rings 0.0381 m	Bubble-Cap
Surface tension of packing (dyne/cm)	75.0	–
Void fraction of the packing	0.95	–
Tray Spacing (m)	–	0.61
Exit weir height (m)	–	0.0508

The liquid holdup per non-equilibrium segment for the packed columns was estimated using the theory presented by Billet (1995). The liquid holdup per tray was approximated by using the correlation found by Dhulesia (1984) for valve trays. The flow configuration used for the non-equilibrium segments was well-mixed liquid and linear profiles in the vapor for both packed and trayed columns.

The estimated approach to flooding at the conditions of Tables 6.2 was 80.6% (Billet, 1995) for the packed column and 86.8% (Fair, 1985) for the trayed column.

Table 6.2. Composition of the reactive solvent and feed vapor stream, L/G = 0.823 mole/mole.

	Reactive Solvent	Feed vapor
MDEA	50 wt %	—
H ₂ S	{(mol H ₂ S total)*/mol MDEA}: 0.005	mole fraction: 0.006
CO ₂	{(mol CO ₂ total)*/mol MDEA}: 0.005	mole fraction: 0.15
H ₂ O	Balance	saturated
CH ₄	—	mole fraction: 0.8405
Flow Rate (kmol/hr)	2700	3280
Temperature (°C)	32	32
Pressure (atm)	20	20

*Total H₂S is defined as the sum of the physically absorbed and chemically combined H₂S. Similar applies for CO₂.

6.5 MODELING APPROACH

RATEFRAC[®], the rate-based distillation module of Aspen Plus[®], was used to integrate the point model for describing the performance of the whole contactor. Several FORTRAN routines were developed and linked to RATEFRAC[®] as shown in Figure 6.1.

Mass transfer coefficients: This routine was used to calculate the physical mass transfer coefficients in the vapor and liquid phases. For packed columns, the correlations developed by Onda et al. (1968) and validated by Bravo and Fair (1982) were used for predicting liquid and gas side mass transfer coefficients. For trayed columns, the AIChE (1958) method for bubble-cap trays was used for predicting mass transfer coefficients as representative of mass transfer kinetics on trays. These models and correlations are described in detail in Chapter 3.

The point model described above (Equations 6.12 through 6.17 and 6.19 through 6.24, and the equilibrium relations 6.1 through 6.5) was also solved in this routine to compute the enhancement factors for the transferring species (CO_2 and H_2S). RATEFRAC[®] was then supplied with *reactive* mass transfer coefficients for CO_2 and H_2S equal to the product of the corresponding enhancement factor and the *physical* mass transfer coefficient. That is, instead of the physical binary mass transfer coefficients for CO_2 ($k_{L,(\text{CO}_2,j)}^\circ$) and H_2S ($k_{L,(\text{H}_2\text{S},j)}^\circ$), RATEFRAC[®] was supplied with $E_{\text{CO}_2} k_{L,(\text{CO}_2,j)}^\circ$ and $E_{\text{H}_2\text{S}}^\infty k_{L,(\text{H}_2\text{S},j)}^\circ$, where the subscript j is the index for all the species in the liquid phase.

RATEFRAC[®] uses binary mass transfer coefficients to perform the matrix calculations needed to solve the Maxwell-Stefan equations while the pseudo-binary model uses the same binary mass transfer coefficients to estimate effective mass transfer coefficients and calculate the enhancement factors. In this work the effective mass transfer coefficient of species i , $k_{L,i,\text{eff}}^\circ$, is calculated following the procedure suggested by Taylor et al. (1993) and Frank et al. (1995a), which for the system MDEA- H_2O - H_2S - CO_2 reduces to the following expression:

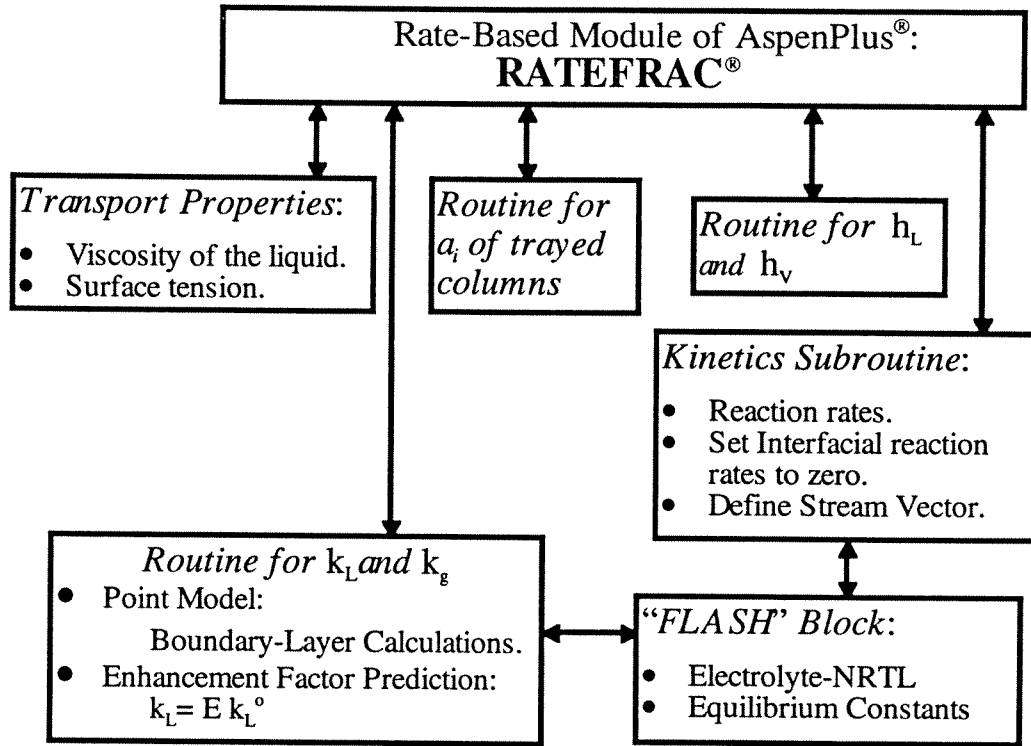


Figure 6.1. Approach used for modeling reactive absorption with RATEFRAC®.

$$\frac{1}{k_{L,i,\text{eff}}^o} = \frac{1 - x_{\text{MDEA}}}{k_{L,(i,\text{H}_2\text{O})}^o} + \frac{x_{\text{MDEA}}}{k_{L,(i,\text{MDEA})}^o} \quad (6.26)$$

where $k_{L,(i,j)}^o$ is the binary mass transfer coefficient of the pair i-j and x_{MDEA} is the *total* concentration of MDEA (free plus chemically combined) in the liquid bulk. The effective mass transfer coefficients calculated using Equation 6.26 are then used in Equations 6.13 or 6.23 to calculate the interfacial mass transfer rates.

Consequently, in this work it is assumed that the enhancement factors calculated using $k_{L,i,\text{eff}}^o$ from Equation 6.26 can be applied to the physical interfacial mass transfer rates estimated from the Maxwell-Stefan approach. Frank et al. (1995a) found that in case of absorption with irreversible chemical

reaction the mass transfer rate could be formulated as the product of the mass flux for physical absorption, calculated using the Maxwell-Stefan approach, and the enhancement factor, where this enhancement factor possesses the same functional dependency with respect to the Hatta number as is the case when Fick's law is used to describe the mass transfer process. Close agreement was found to exist between this approach and the rigorous solution of the Maxwell-Stefan equations with chemical reactions for conditions of equal or unequal mass transfer coefficients for the different species and for a wide range of reaction rates. The results of Frank and coworkers support our approach.

Since in this work the $k_{L(i,j)}^{\circ}$, rather than the physical fluxes, are affected by the enhancement factor, it is assumed that the physical fluxes calculated from the Maxwell-Stefan approach for species i are directly proportional to $k_{L(i,j)}^{\circ}$. From the theory of multicomponent mass transfer (Taylor and Krishna, 1993; Sections 8.3.1 and 8.3.2), this is true if the concentration of the diffusing gases in the liquid phase is low and when the matrix of correction factors of the mass transfer coefficients is equal to the identity matrix, i.e., if the finite flux mass transfer coefficient matrix is equal to the zero-flux mass transfer coefficient. This assumption was validated performing numerical simulations in one non-equilibrium segment using RATEFRAC® and it was found that when $k_{L(i,j)}^{\circ}$ are affected by a factor of α , the enhancement factor predicted (ratio of the flux of i to the driving force) deviates from α within 2 to 4%.

Heat Transfer Coefficients: The heat transfer coefficients for the liquid and vapor are estimated using the Chilton-Colburn analogy (Bird et al., 1960) between heat and mass transfer:

$$\bar{k}_{i,j}^o (Sc_i)^{2/3} = \frac{h_{mix}}{c_{tot} C_{p_{mix}}} (Pr)^{2/3} \quad (6.27)$$

The unweighted arithmetic average of the binary *physical* mass transfer coefficients, $\bar{k}_{i,j}^o$, is used in Equation 6.27 to estimate the heat transfer coefficient in the vapor and liquid.

Chemical Kinetics: With this routine the kinetics of the rate controlled reactions, Equations 6.6 and 6.9, are supplied to RATEFRAC[®]. These kinetics are based on Equations 6.7 through 6.10. Since the effect of the chemical reactions on the mass transfer is accounted for by the use of enhancement factors, an arbitrarily small value is supplied for the reaction rate (in kmol/hr) at the liquid interface, in this way the chemical reactions (rate and equilibrium controlled) are allowed to occur only at the liquid bulk.

At the liquid bulk, the product of the reaction rates (in kmol/hr m³) and the liquid holdup estimated by the models and correlations mentioned above (Billet 1995; Dhulesia 1984) is supplied to RATEFRAC[®]. In this routine a stream vector based on the liquid bulk compositions is created in order to perform a flash of the liquid and calculate the equilibrium constants of the chemical reactions. In this flash calculation the electrolyte-NRTL model is used with binary parameters obtained by Austgen (1989). This is done in order to account for the non-ideality of the liquid phase when predicting the equilibrium constants.

Interfacial Area: The interfacial area for trayed columns was estimated using the correlation by Scheffe et al. (1987) for valve trays. This correlation was coded in the routine. For packed columns the correlation by Onda et al. (1968)

was used. The uncertainties involved in predicting interfacial areas for mass transfer in these contactors are addressed in Chapter 3.

Transport Properties: Routines for calculating viscosities of the liquid mixture and surface tensions were provided. Viscosity was estimated by the correlation of Glasscock (1990) which includes effects of temperature, MDEA concentration and CO₂ loading. The surface tension was estimated by a correlation obtained from the data reported by Rinker et al. (1994) at 20 to 100°C.

6.6 RESULTS AND DISCUSSION

6.6.1 Modeling of Packed Columns

Interfacial Mass Transfer Rates, Heat Effects and Enhancement of Mass Transfer

Figures 6.2, 6.3, and 6.5 depict the interfacial mass transfer rates, enhancement factors for mass transfer and temperature profiles, respectively, calculated for the packed column described in Table 6.1. This case will be considered as the base case in the discussion that follows. Figures 6.2 and 6.5 show that the CO₂ mass transfer rate follows the trend of the temperature profile. At the conditions studied the enhancement of the mass transfer of CO₂ is given approximately by Equation 6.18.

The parameter $\sqrt{k_{2t} D_{CO_2}} / H_{CO_2}$ (from Equations 6.13 and 6.18), increases a factor of approximately 2.8 from the top segment to segment 12 where the temperature reaches a maximum, then it starts to decrease. Similarly, the CO₂ flux increases by a factor of 2.5 from the top to segment 12. Therefore, the maximum in the CO₂ rate results from a combination of temperature effects on the reaction kinetics, diffusivity and solubility of CO₂.

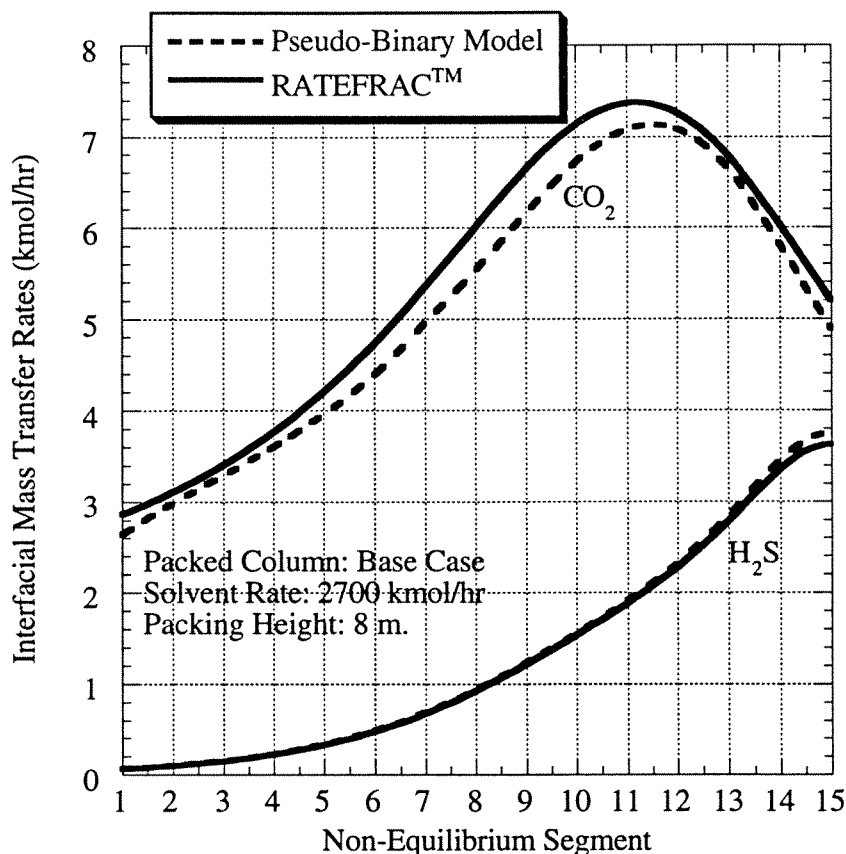


Figure 6.2. Interfacial mass transfer rates for the packed column described in Table 6.1.

The enhancement factor for CO₂ represented in Figure 6.3 is practically constant (4.3 to 5.3) because $k_{L,CO_2,eff}^o$ varies with temperature like $\sqrt{k_{2t}D_{CO_2}}$. Near the bottom of the column, the reactive solvent, MDEA, is depleted somewhat causing a decrease in the pseudo-first order rate constant and a slight decrease in the enhancement factor.

The steady decrease in the H₂S interfacial mass transfer from bottom to top results primarily from a decreasing driving force for mass transfer as the H₂S concentration in the gas decreases over a factor of 200 from the bottom to the top

segment. Figure 6.3 shows that over the same range the H_2S enhancement factor increases a factor of around 7. The concentration gradient of bisulfide through the reaction zone, governed by the solution equilibria, increases around 20 times from the top to the bottom segment, while that for H_2S increases around 140 times. This decreasing ratio between the concentration gradient through the liquid boundary layer of the reaction product, HS^- , with respect to the gradient of H_2S (see Equation 6.19) leads to the decrease of the mass transfer enhancement for H_2S .

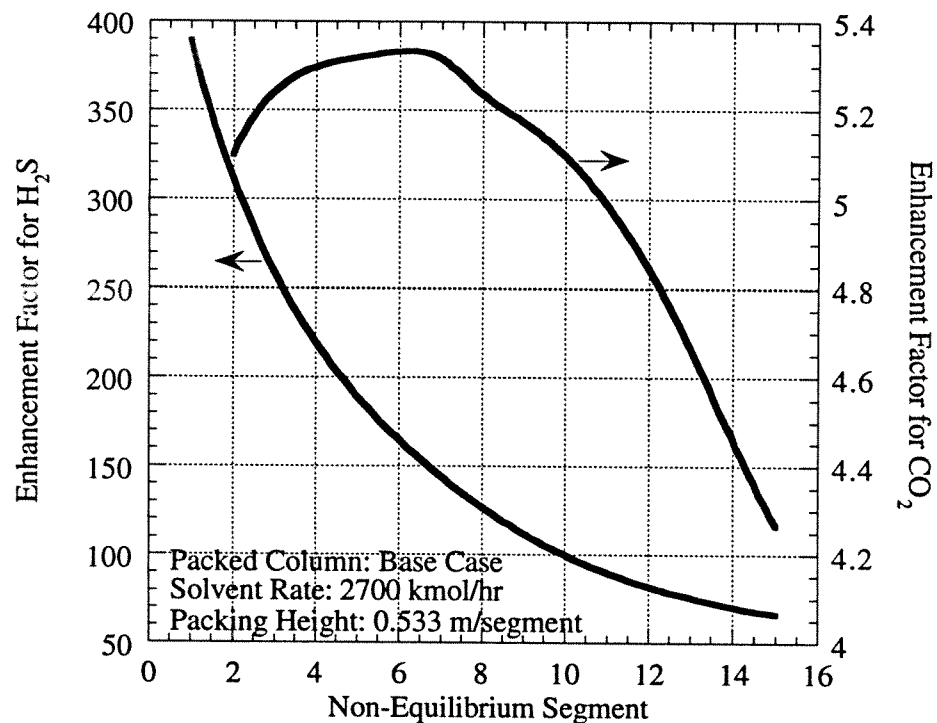


Figure 6.3. Profiles of enhancement factors calculated for the packed column described on Table 6.1. $L/G = 0.823$ moles/moles. Total packing height: 8 m.

The results of the pseudo-binary point model indicate that the interfacial flux of H_2S is almost completely controlled by the diffusion of bisulfide through the reaction zone. That is, the interfacial flux of H_2S can be approximated by

$$\bar{N}_{\text{H}_2\text{S}} \approx k_{\text{L,HS}^-}^{\circ} ([\text{HS}^-]_i - [\text{HS}^-]_o) \quad (6.28)$$

within $\pm 2\%$. Figure 6.4 depicts the concentration gradient of HS^- through the reaction zone and the fluxes of H_2S and HS^- .

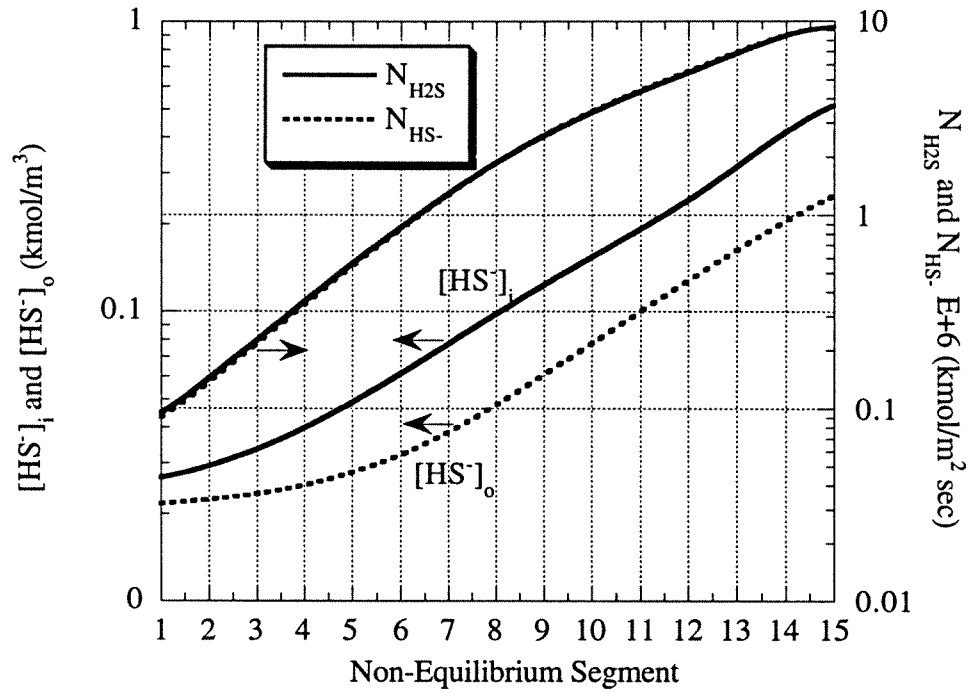


Figure 6.4. Concentration gradient of bisulfide and fluxes of H_2S and bisulfide. Packed column described on Table 6.1. $L/G = 0.823$ mole/mole. Total packing height: 8 m.

For most conditions studied, the maximum difference between the interfacial mass transfer rates predicted by the point model described above

(pseudo-binary model) and those predicted by the Maxwell-Stefan approach to mass transfer coupled with the enhancement factor approach, is on the order of 6% (see Figure 6.2). Consistency between these two approaches is crucial since enhancement factors affect the binary mass transfer coefficients of the Maxwell-Stefan model in order to account for the effect of the chemical reactions.

In Figure 6.5 the bulk liquid and bulk vapor temperature variations are shown. The interfacial temperature is almost the same as the liquid bulk temperature, the largest difference being of the order of tenth of a degree.

The energy balance in a segment of the contactor indicates that the enthalpy change of the liquid is given by the contribution of the purely conductive heat flux and the convective enthalpy transfer due to the different diffusing species. Figure 6.6 quantifies the contribution of each of these heat transfer processes. As the reactive solvent flows down the column the heat released due to the absorption and reaction of CO_2 ($\lambda_{\text{CO}_2} N_{\text{CO}_2}$) and H_2S ($\lambda_{\text{H}_2\text{S}} N_{\text{H}_2\text{S}}$) tends to increase the temperature of the solvent. This process is accompanied by the conductive heat flux from the vapor to the liquid (as hot vapor is flowing up) and the convective enthalpy transfer due to water diffusion ($\lambda_{\text{H}_2\text{O}} N_{\text{H}_2\text{O}}$). Figure 6.6 indicates that under the conditions of our base case the convective enthalpy transfer due to the absorption of the reacting gases accounts for about 50% of the total heat transfer up to segment 8. In this region the conductive heat flux and heat effect of water transfer accounts for about 20 to 50% of the convective enthalpy transfer of the reacting gases.

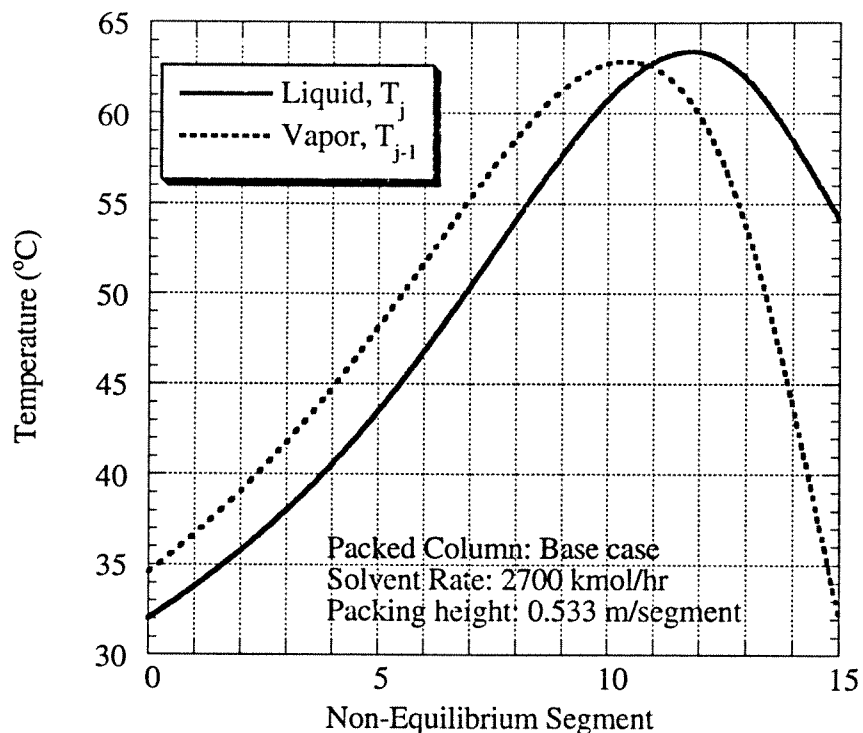


Figure 6.5. Temperature profiles calculated for the packed column described on Table 6.1. Total packing height 8 m. $L/G = 0.823$ moles/moles.

Figure 6.6 shows that from segments 1 to 11 these three heat transfer effects tend all to increase the liquid temperature (heat and enthalpy are transferred to the liquid). This temperature increase favors the vaporization of water and therefore the decrease of the solvent temperature. Temperature peaks at around segment 11 and the temperature crossover occurs. Around segment 11 the contribution of the conductive heat transfer and convective enthalpy transfer of water becomes vanishingly small because of the sign change of the water flux and the temperature crossover. After segment 11 the liquid temperature stays above that of the vapor because the conductive heat transfer is more intense and makes the vapor temperature decrease sharper. From segments 11 to 15 even though the

enthalpy transfer of the reacting gases becomes more significant it is overshadowed by the opposite heat effects of water enthalpy transfer to the vapor and conductive heat transfer making the solvent temperature to decrease.

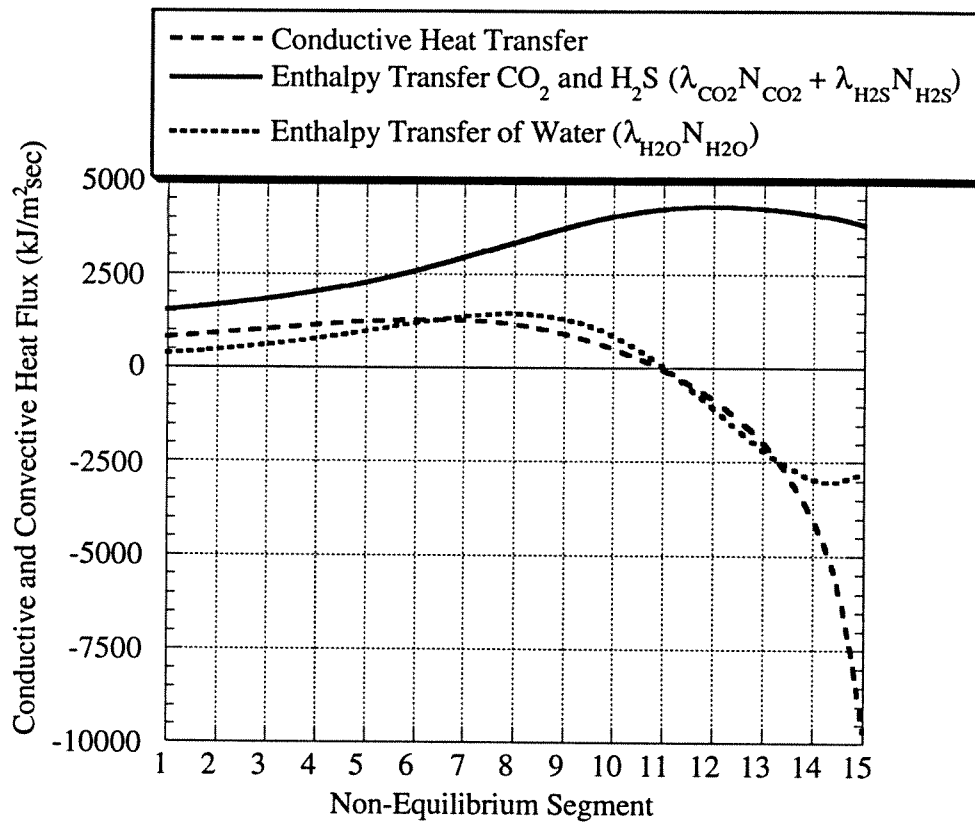


Figure 6.6. Contribution of the different heat effects on the temperature profile. Packed column described on Table 6.1.

An indication of the importance of the mass transfer of water on the heat effects is given by the relative magnitude of the mass transfer rates: the vaporization rate of water at the bottom of the column is over 60% larger than the interfacial mass transfer rate of CO₂ and over two times larger than that for H₂S; however, at the top of the column the condensation rate of water accounts for only 25% of the total mass transfer rate. Heat effects similar to those presented in

Figure 6.5 have been reported for non-reactive systems by Raal et al. (1973) and Krishnamurthy et al. (1986).

Detailed Results on the Point Modeling

Figure 6.7 depicts some of the detailed results of the reaction-diffusion modeling in the liquid film for the packed contactor. The values of the parameter $1-\theta$ (see Equation 6.15) approaching unity indicate that the effect of the reversibility of the rate-controlled reaction (CO_2 -MDEA) is unimportant. Also, the increasing depletion of the liquid-phase reactant (MDEA) towards the bottom of the column reflects the larger interfacial fluxes of CO_2 and H_2S . This figure also shows that the driving force for mass transfer of bicarbonate is fairly constant and finite throughout the contactor. However, the concentration of bicarbonate decreases towards the top of the column due to the decreasing interfacial flux of CO_2 . The diffusion of bicarbonate through the reaction zone accounts for between 70 and 90% of the total CO_2 flux (not shown in Figure 6.7).

Murphree Vapor-Phase Efficiencies

The Murphree vapor-phase efficiency for component i on a segment of packing or on a tray j is defined as follows:

$$E_{i,j}^{\text{MV}} = \frac{y_{i,j} - y_{i,j+1}}{y_{i,j}^* - y_{i,j+1}} \quad (6.29)$$

where $y_{i,j}$ is the vapor bulk composition of component i on segment j and $y_{i,j}^*$ is the mole fraction of component i in a vapor that would be in equilibrium with the bulk liquid on segment j . $y_{i,j}^*$ is determined performing a bubble-point calculation at the temperature and composition of the liquid leaving segment j .

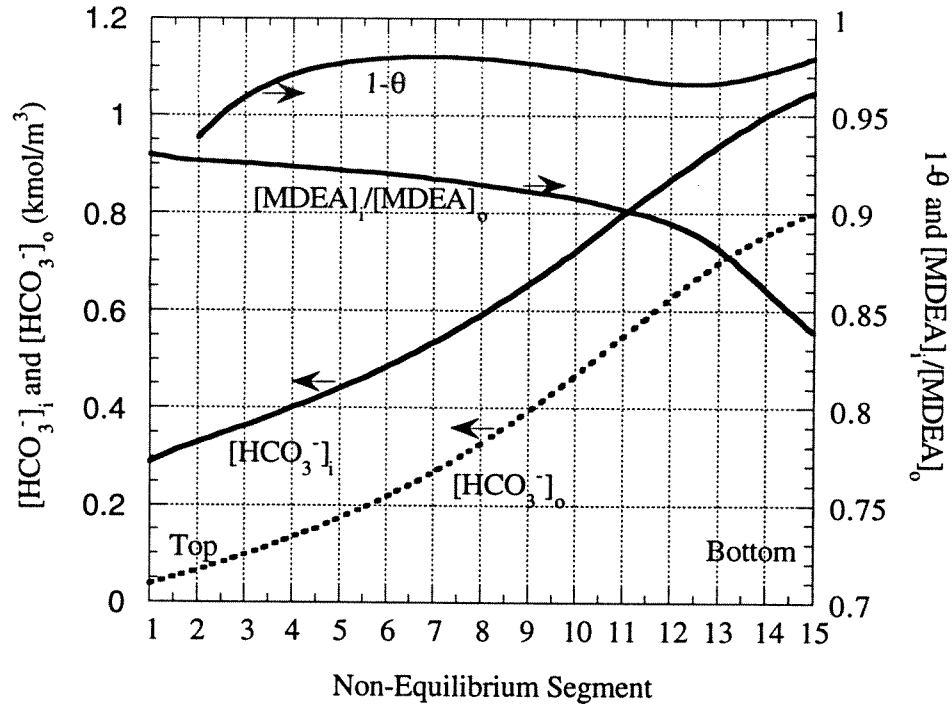


Figure 6.7. Detailed results on the point modeling. Packed column described in Table 6.1.

Since the driving force for mass transfer at the vapor side is the gradient of fugacity (or partial pressure for the ideal case) through the vapor boundary layer, it seems logical to define a modified Murphree vapor-phase efficiency based on partial pressures instead of mole fractions. In this case Equation 6.29 becomes:

$$E_{i,j}^{M-P} = \frac{P_{i,j} - P_{i,j+1}}{P_{i,j}^* - P_{i,j+1}} \quad (6.30)$$

It can be shown that the relationship between the Murphree efficiencies defined by Equations 6.29 and 6.30 is as follows:

$$\frac{E_{i,j}^{M-V}}{E_{i,j}^{M-P}} = \frac{P_{i,j}^* - P_{i,j+1}}{P_{i,j}^* \left(\frac{P_{tot}}{P_{tot}^*} \right) - P_{i,j+1}} \quad (6.31)$$

where P_{tot} is the total pressure in the column and P_{tot}^* is the bubble-point total pressure. If P_{tot} and P_{tot}^* were the same, Equations 6.29 and 6.30 would be identical, but under absorption conditions P_{tot}^* is usually lower than P_{tot} . Equation 6.31 also indicates that a close approach to equilibrium makes the difference between $E^{\text{M-V}}$ and $E^{\text{M-P}}$ larger.

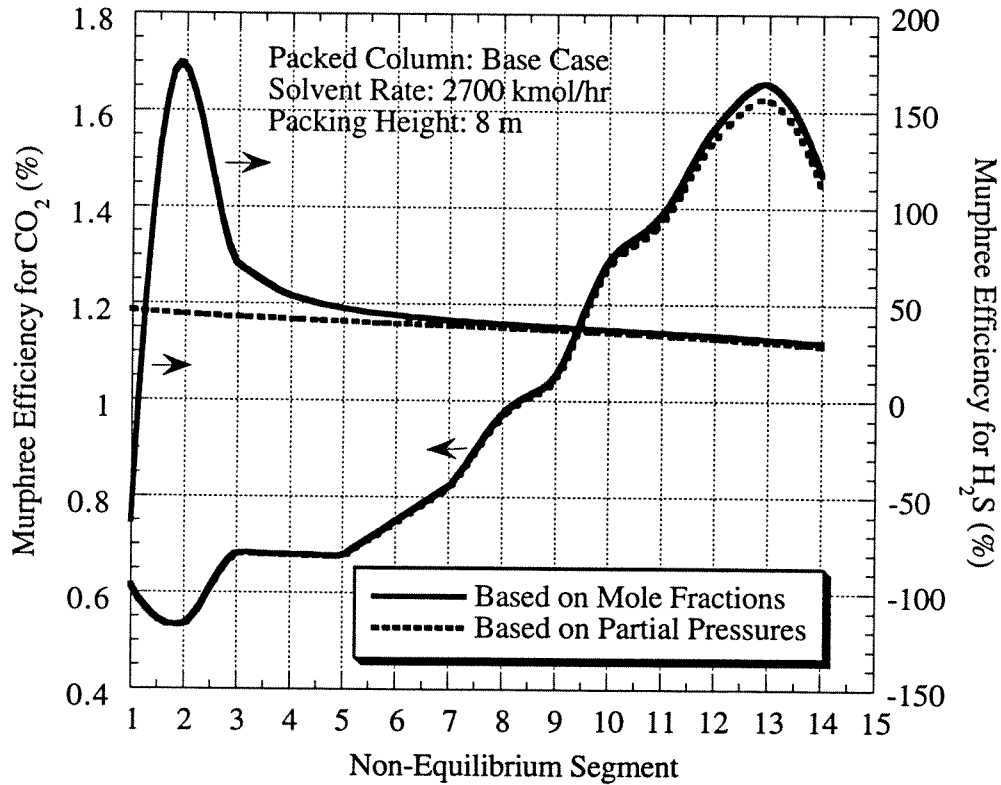


Figure 6.8. Murphree vapor-phase efficiencies for CO_2 and H_2S . Packed column described in Table 6.1.

Figure 6.8 compares the calculated Murphree vapor-phase efficiencies for CO_2 and H_2S using Equations 6.29 and 6.30. The increase in the efficiencies for CO_2 towards the bottom of the absorber corresponds to the greater values of the parameter $\sqrt{k_{21} D_{\text{CO}_2}} / H_{\text{CO}_2}$. Since CO_2 always has a large driving force for mass

transfer, the Murphree efficiencies based on mole fractions and partial pressures are almost identical. With respect to H_2S , the Murphree efficiencies based on partial pressures are better behaved and the difference between the two definitions is due to a closer approach to equilibrium, especially near the top of the column. Due to the lower temperature towards the top of the absorber, P_{tot}^* decreases significantly, increasing even more the difference between $E^{\text{M-V}}$ and $E^{\text{M-P}}$. The efficiencies of H_2S decrease towards the bottom of the absorber because of significantly lower enhancement factors.

Figure 6.8 shows that the Murphree vapor-phase efficiencies are not bounded between 0 and 100%. It has been shown both theoretically and experimentally (Krishna et al., 1977; Taylor and Krishna, 1993; Krishna and Wesselingh, 1997) that for systems where multicomponent mass transfer takes place, the component point Murphree efficiencies are unbounded and could have values ranging between $-\infty$ and $+\infty$. This “odd”, un-binary like behaviour can be rationalized on the basis of the multicomponent mass transfer formulations in the Maxwell-Stefan approach.

Effects of Packing Height and Liquid to Vapor Flow Ratio

Figure 6.9 shows the model predictions of the H_2S concentration in the outlet gas (H_2S leak) as a function of packing height and L/G (moles/moles) for a contactor with 15 non-equilibrium segments. At $L/G = 1.43$ moles/moles, the H_2S leak does not continuously decrease with packing height, but approaches a broad minimum of about 13 ppm at a packing height of 10 meters. Since CO_2 removal increases linearly with packing height, H_2S removal becomes limited by a “pinch”

at the temperature bulge, caused by increased CO_2 loading and CO_2 heat of absorption. The sharp increase in the H_2S leak as the packing height decreases is due to the insufficient mass transfer capability.

With $L/G = 0.823$ moles/moles, model convergence is difficult to achieve at greater packing height because of a larger temperature bulge and an increased tendency for an equilibrium “pinch”.

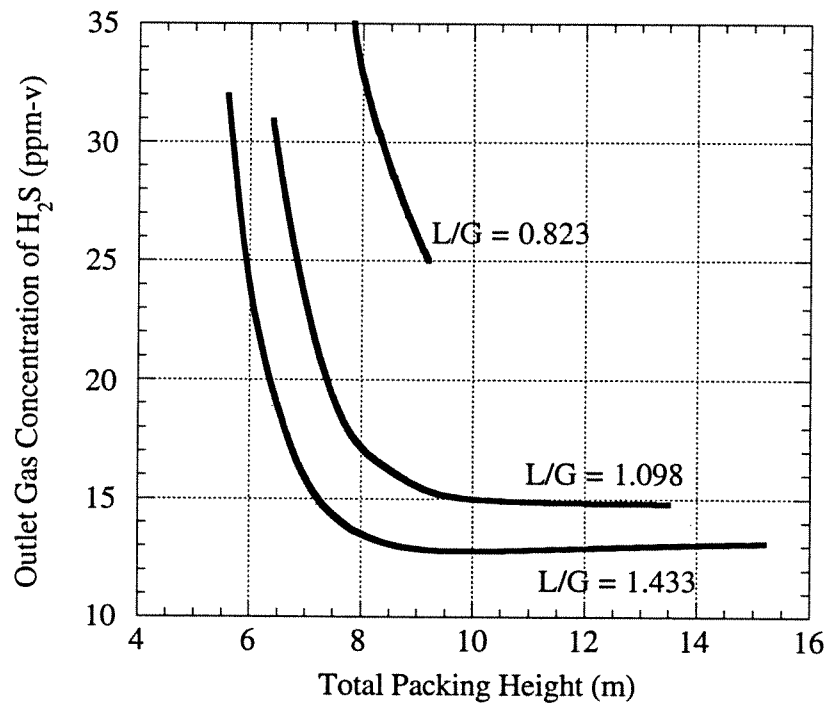


Figure 6.9. H_2S performance of the packed absorber described in Table 6.1. 15 non-equilibrium segments.

Mass Transfer Resistance

The fraction of the liquid film resistance to mass transfer, R_L , can be defined as:

$$R_L = \{\text{Fraction of Liquid - film Resistance}\} = \frac{\frac{H_j}{E_j k_{L,j}^o}}{\frac{1}{K_{G,j}}} = \frac{\frac{H_j}{E_j k_{L,j}^o}}{\frac{P_j^\delta - P_j^*}{\bar{N}_j}} \quad (6.29)$$

Figure 6.10 shows the contribution of the liquid-film resistance to mass transfer of CO₂ and H₂S for the packed column described in Table 6.1. Absorption of CO₂ is almost completely liquid-film controlled throughout the contactor. Because the enhancement factor for the mass transfer of H₂S is much greater, the contribution of liquid-film resistance for absorption of H₂S varies from 24% at the top of the absorber to 65% at the bottom.

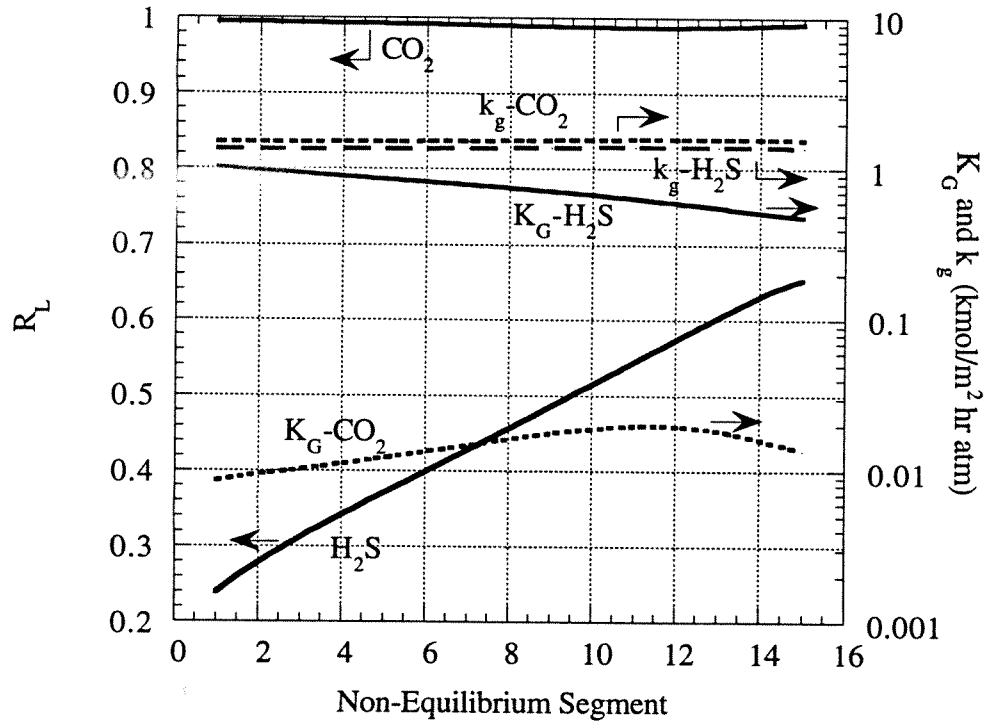


Figure 6.10. Liquid-side mass transfer resistance and gas-side mass transfer coefficients for the packed column described in Table 6.1.

The gas-film (k_g), and overall gas-phase mass transfer coefficient (K_G) are also depicted in Figure 6.10. For CO_2 , K_G is over two orders of magnitude lower than k_g ; while for H_2S , K_G approaches k_g towards the top of the absorber. This behavior reflects the importance of the resistance to the mass transfer in each phase as described above.

For the trayed column described in Table 6.1 the liquid-film resistance to absorption of H_2S is less significant than in the packed column, but follows the same qualitative behaviour, varying from 31% at the bottom to 8% at the top. The physical mass transfer coefficients in the liquid film estimated for the trayed column can be ten times greater than those for the packed column, while the gas side mass transfer coefficients are only about a factor of two larger in the trayed column. As in the packed column, the interfacial mass transfer of CO_2 is still entirely liquid-phase controlled.

“Pinch” Analysis for H_2S Absorption

Unlike simple absorption systems, the determination of a minimum liquid rate for H_2S absorption is complicated by the absorption of CO_2 and by the presence of the temperature bulge.

Figures 6.11 and 6.12 represent the driving force for mass transfer of H_2S in terms of partial pressures ($P_{\text{H}_2\text{S}}$ and $P_{\text{H}_2\text{S}}^*$), showing the “pinch” of H_2S at the temperature bulge and at the top of the column. The equilibrium H_2S partial pressure is given for actual column conditions (variable temperature and CO_2 and H_2S loading). The operating line represents the actual gas phase composition in contact with the respective liquid phase composition.

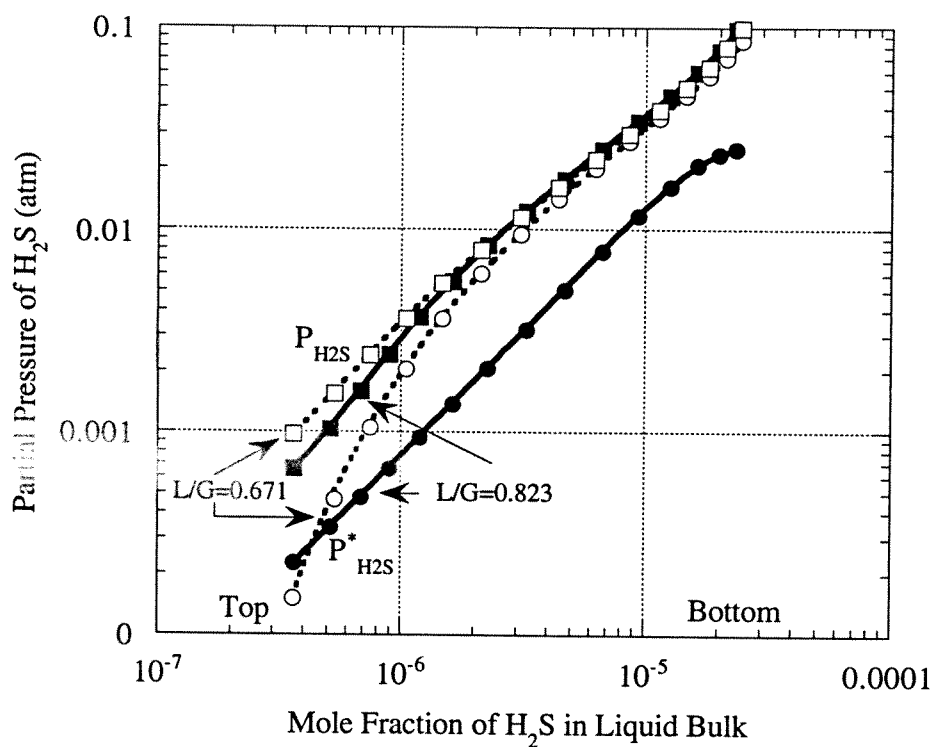


Figure 6.11. H_2S pinch at the temperature bulge. Packed column described in Table 6.1 and conditions of the reactive solvent and vapor feed described in Table 6.2. Packing height 8 m. Squares \square, \blacksquare : operating curves ($P_{\text{H}_2\text{S}}$), circles \circ, \bullet : equilibrium curves ($P_{\text{H}_2\text{S}}^*$).

Figure 6.11 compares the base case ($L/G = 0.823$ moles/moles) to a case with lower L/G (0.671) giving a “pinch” at the temperature bulge. The slope of the operating curve does not appear to change significantly in this representation, but the equilibrium curve for the lower L/G is shifted up, due to the temperature rise, causing a “pinch” near the temperature bulge. For both liquid rates represented in Figure 6.11, the lowest relative driving force for H_2S absorption is not achieved at the bottom segment, but instead at the segments where the temperature bulge occurs.

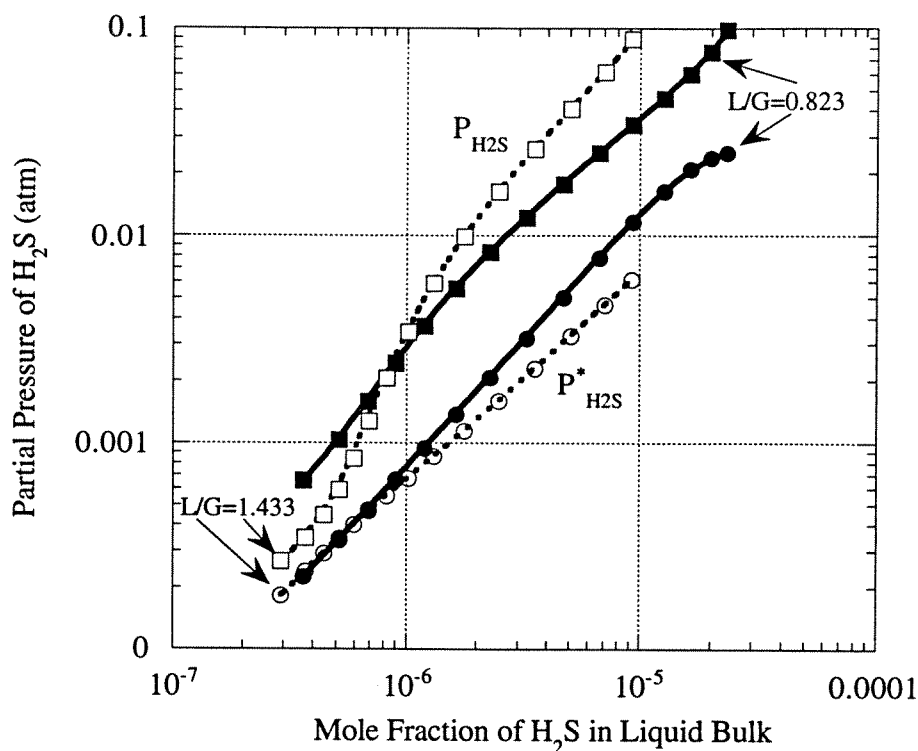


Figure 6.12. H_2S pinch at the top of the absorber. Packed column described in Table 6.1 and conditions of the reactive solvent and vapor feed described in Table 6.2. Packing height: 8 m. Squares \square, \blacksquare : operating curves ($P_{\text{H}_2\text{S}}$), circles \circ, \bullet : equilibrium curves ($P^*_{\text{H}_2\text{S}}$).

Figure 6.12 compares the base case to that with a greater L/G (1.433) giving a lean-end “pinch” at the top of the absorber. The equilibrium curve shifts down because of reduced temperature. The operating line appears to have a greater slope creating a close approach to equilibrium at the top of the absorber.

6.6.2 Comparison Between Trayed and Packed Columns

Table 6.3 compares the performance of the trayed column from Table 6.1 to two different packed columns. Packed column I has 5.75 m of packing to provide 8.6% CO_2 removal, the same as the trayed column. Packed column II has

3.2 m of packing to provide the same total gas-liquid interfacial area as the trayed column. Packed column II is close to the packing height expected if the trays were replaced by an equivalent height of packing. In both cases the concentration of H₂S in the outlet gas is significantly greater with the packed columns, more so with the reduced packing height of Packed column II.

Table 6.3. Comparison between the performance of trayed and packed columns.

	Trayed Column	Packed Column I	Packed Column II
Overall Removal of CO ₂ (%)	8.6	8.6	4.4
Total Dimensionless Interfacial Area: a_i/A_c	323	584	323
Total Height of Packing (m)	—	5.75	3.20
$N_L^{\text{tot}} - \text{CO}_2$	7.57	1.57	0.72
$N_V^{\text{tot}} - \text{H}_2\text{S}$	13.66	11.12	6.13
$y_{\text{H}_2\text{S}}^{\text{out}}$ (ppm-v)	17.5	40.5	543

Table 6.3 presents the total number of mass transfer units for the liquid and vapor phases (N_L^{tot} and N_V^{tot}) for CO₂ and H₂S defined as:

$$N_{L,j}^{\text{tot}} = \sum_{k=1}^{N_a} \frac{k_{L,j}^{o,(k)} a_i^{(k)}}{Q_L} \quad \text{and} \quad N_{V,j}^{\text{tot}} = \sum_{k=1}^{N_a} \frac{k_{g,j}^{(k)} a_i^{(k)}}{Q_V} \quad (6.30)$$

where subscript j represents species j, superscript k indicates the segment or tray number, $a_i^{(k)}$ is the interfacial area for mass transfer in segment or tray k in m² and Q_L and Q_V are the liquid and vapor volumetric flows, respectively.

Figure 6.14 gives the H₂S and CO₂ enhancement factors for the trayed column and Packed column I. Packed column I achieves the same CO₂ removal as the trayed column by having around 80% more interfacial area, even though the number of physical mass transfer units for CO₂, $N_{L,\text{CO}_2}^{\text{tot}}$, is five times less. This

is possible because in the packed column CO_2 absorption occurs with fast reaction in the boundary layer at an enhancement factor of about 5. In the trayed column the enhancement factor is nearly unity.

Since the enhancement factors for H_2S for the trayed column and Packed column I are not very different, the larger number of total physical mass transfer units in the trayed column explains the better performance for H_2S .

For the case where the total interfacial area for mass transfer is constant between the two contactors, the much lower total number of mass transfer units for the liquid and vapor phases for both CO_2 and H_2S explains the poorer performance of the packed column.

For the trayed column, the partial-pressure-based Murphree efficiency per non-equilibrium tray varies from 1.1 to 1.2% for CO_2 while that for H_2S varies between 84 and 90%.

Figures 6.13 and 6.14 compare the main modeling results obtained for the case where the overall CO_2 removal is the same for the trayed and packed columns. Figure 6.13 indicates that the trayed column approaches a tight pinch on the top trays (lean-end pinch), while the packed contactor is characterized by a finite driving force for mass transfer of H_2S throughout the column. The equilibrium curve ($P_{\text{H}_2\text{S}}^* - x$) for the packed column is slightly above the one for the trayed column near the bottom of the column because the liquid temperature is slightly higher for the packed column at the temperature bulge (not shown), which tends to increase the equilibrium partial pressure in that region.

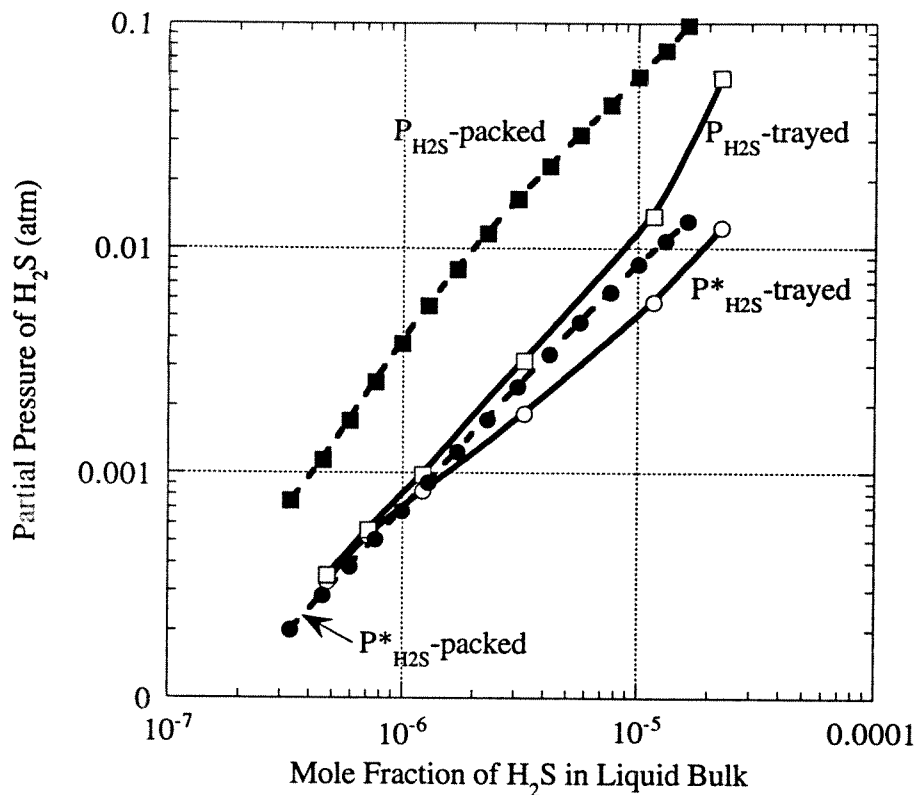


Figure 6.13. Representation of the approach to pinch for H_2S . Trayed and packed columns with same overall removal of CO_2 . The packed and trayed columns are described in Table 6.1. Squares \square, \blacksquare : operating curves (P_{H_2S}), circles \circ, \bullet : equilibrium curves ($P^*_{H_2S}$).

Figure 6.14 compares the predictions of the enhancement factors for CO_2 and H_2S for both contactors. The enhancement factors for H_2S through both contactors are fairly close to each other because the enhancement of the interfacial mass transfer rate of H_2S is defined by the equilibria, which is similar in both situations considering that the temperature profiles are not very different. There is a more significant difference on the enhancement factors for CO_2 in the two contactors.

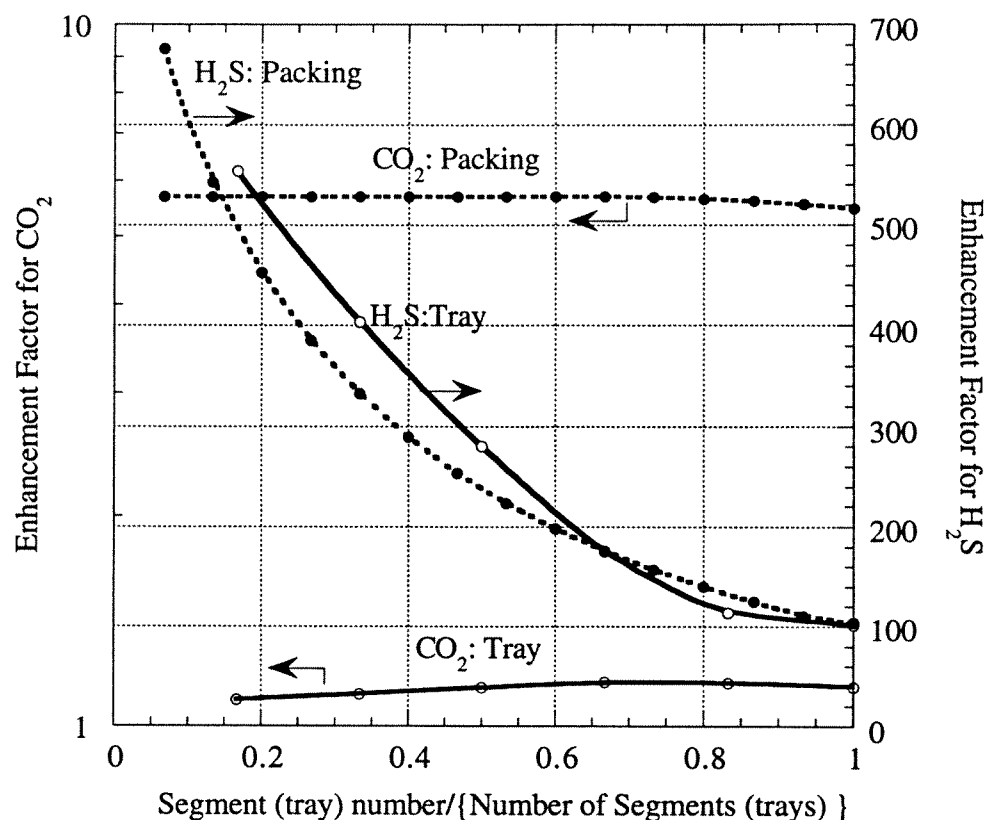


Figure 6.14. Comparison of the enhancement factors for CO₂ and H₂S for trayed and packed columns. Contactors with the same overall removal of CO₂.

Since trayed columns have higher liquid phase mass transfer coefficients than packed columns, the ratio of reaction to diffusion time through the liquid boundary layer is lower than for packed columns which tends to give enhancement factors closer to unity for rate-controlled reactions with moderate reaction rates in trayed columns. Therefore, the enhancement of the interfacial mass transfer of CO₂ with respect to physical absorption is always less than 20% for the trayed column studied, while for the packed column the reactive interfacial flux is between 5 and 6 times larger than the physical flux.

6.7 CONCLUSIONS

In this chapter a general framework has been developed which can be used to model the interfacial heat and mass transport processes that take place during reactive absorption when both rate and equilibrium controlled reactions take place in the liquid phase. This framework has been successfully applied to the selective absorption of H_2S from fuel gas containing CO_2 , representative of product from coal gasification at 20 atm.

In packed columns, CO_2 absorption occurs with fast chemical reaction in the liquid boundary layer. In trayed columns, CO_2 absorption occurs at enhancement factors close to unity, therefore it is primarily controlled by physical absorption without reaction in the boundary layer. Gas film resistance is never significant for CO_2 absorption.

In trayed columns, H_2S absorption is mostly controlled by gas film diffusion. In packed columns about half of the resistance to H_2S absorption is in gas film diffusion and about half is in diffusion of bisulfide in the liquid boundary layer. The extent of liquid film resistance increases a factor of about three from the lean end to the rich end of the absorber. This reflects a typical decrease in the H_2S enhancement factor from 400 to 60.

With a greater height of packing or a reduced liquid rate, the maximum liquid temperature above the bottom of the absorber tends to increase. This maximum temperature can be 15 to 25 °C greater than the temperature at the top segment. At the extreme this condition results in an equilibrium “pinch” at the temperature bulge. The “pinch” at the temperature bulge for H_2S occurs instead of

a rich-end “pinch”. This effect leads to the existence of an optimum packing height for the H₂S removal.

For a given CO₂ removal or a given total interfacial area, trayed columns give better H₂S performance than packed columns, primarily because trays are characterized by a much larger liquid film mass transfer coefficient. Before generalizing this conclusion, a thorough analysis of the accuracy of the submodels and correlations used for estimating the mass transfer coefficients and interfacial area for mass transfer is needed. The Murphree vapor efficiency for CO₂ varies from 0.2 to 1.7% in the packed columns studied. In the trayed column it is about 1.1%. The profile of Murphree efficiencies for CO₂ in the trayed and packed contactors follows closely the temperature profile due to the effect of the temperature on the transport properties and the reaction kinetics. The Murphree efficiency based on partial pressures for H₂S varies from 84 to 90% in the trayed column.

6.8 NOMENCLATURE

- a_i : Interfacial area for mass transfer (m²).
- A_c : Column cross sectional area (m²).
- $[A]$: Concentration of species A (kmol/m³).
- C_p : Heat capacity (J/kmole K).
- c_{tot} : Total concentration (kmol/m³).
- D_i : Fickian diffusion coefficient of species i (m²/sec).
- \mathcal{D}_{ij} : Binary Maxwell-Stefan diffusion coefficient for the pair i-j (m²/sec).
- E_i : Enhancement factor of species i.
- E^{M-P} : Murphree component efficiency based on partial pressure.
- E^{M-V} : Murphree component efficiency based on mole fractions.
- G : Gas flow rate (kmol/hr).

h : Heat transfer coefficient (J/sec K).
 H : Henry's constant (atm m³/kmol).
 J_i : Diffusive flux of species i (kmol/m² sec).
 L : Liquid flow rate (kmol/hr).
 N_i : Molar flux of species i (kmol/m² sec).
 P_i : Partial pressure of species i (atm).
 P_{tot} : Total pressure of species i (atm).
 k_{2t} : Forward reaction rate constant for reaction 6.6 (m³/kmol sec).
 $k_{g,i}$: Mass transfer coefficient of species i in the gas-phase (m/s in Equation 6.30, kmol/m² sec atm elsewhere).
 $k_{L,i}^o$: Physical mass transfer coefficient of species i in the liquid phase (m/sec).
 $k_{L(i,j)}^o$: Binary physical mass transfer coefficient for the pair i - j in liquid phase (m/sec).
 $\bar{k}_{i,j}^o$: Arithmetic average of the binary physical mass transfer coefficient of species i (m/sec).
 k_{OH} : Forward reaction rate constant for reaction 6.9 (m³/kmol sec).
 K_G : Overall gas-side mass transfer coefficient (kmol/m² sec atm).
 K : Concentration-based equilibrium constants.
 Mw : Molecular weight.
 N_i : Molar flux of component i (kmol/m² sec).
 N_{pj} : Number of transfer units of component j in phase p [-].
 N_{st} : Number of non-equilibrium segments or trays [-].
 \bar{N}_i : Time-mean molar flux of component i (kmol/m² sec).
 Pr : Prandtl number = $C_{p_{mix}}\mu_{mix}/(Mw_{mix}\kappa_{mix})$.
 Q : Volumetric flow rate (m³/sec).
 r_{prod} : Ratio of the diffusion coefficient of the reaction products to that of CO₂.
 R_i : Rate of reaction i (kmol/m³ sec).
 R^L : Fraction of liquid-film resistance [-].
 R : Gas constant (J/kmol K).

Sc_i : Schmidt number for component $i = \mu_{\text{mix}}/(\rho_{\text{mix}}D_i)$.

T : Temperature (K).

x : Spatial coordinate in the liquid boundary layer (m).

x_i : Mole fraction of species i .

Greek Symbols:

κ : Thermal conductivity (J/sec K m).

λ_i : Enthalpy of absorption-reaction or vaporization of species i (kJ/kmol).

μ : Viscosity (kg/sec m).

μ_i : Chemical potential of species i (J/kmol).

θ : Parameter in enhancement factor model.

ρ : Density (kg/m³).

∇ : Gradient.

Superscripts:

$*$: At equilibrium.

$[\bar{A}]$: Time-mean concentration of species A .

δ : Evaluated at the vapor bulk.

tot : Total.

∞ : For an equilibrium reaction.

Subscripts:

aq : In aqueous solution.

CO_2 : Evaluated for CO_2 .

eff : Effective.

e,i : In equilibrium at the interface.

g : For the gas phase.

- H₂S: Evaluated for H₂S.
- i: At the vapor-liquid interface or related to species I.
 - j: Evaluated at segment or tray j or for species j.
 - L: For the liquid phase.
 - mix: Mixture.
 - o: Evaluated at the liquid bulk.
 - v: Evaluated at the vapor or gas phase.

6.9 REFERENCES

- American Institute of Chemical Engineers (A.I.Ch.E). "Bubble-Tray Design Manual. Prediction of Fractionation Efficiencies," New York, 1958.
- Astarita, G., Savage, D. W., "Gas Absorption and Desorption with Reversible Instantaneous Chemical Reaction," *Chem. Engng. Sci.* **1980**, 35, 10, 1755
- Astarita, G., Savage, D. W., Bisio, A., *Gas Treating with Chemical Solvents*, Wiley, New York, 1983.
- Austgen, D. M., "A Model of Vapor-Liquid Equilibria for Acid gas-Alkanolamine-water Systems." Ph.D. Dissertation, The University of Texas at Austin, 1989.
- Billet, R. "*Packed Towers in Processing and Environmental Technology*," VCH Verlagsgesellschaft, Weinheim: Federal Republic of Germany, 1995.
- Bird, R. B., Stewart, W. E., Lightfoot, E. N., *Transport Phenomena*, Wiley, New York, 1960.
- Bravo, J. L., Fair, J. R., "Generalized Correlation for Mass Transfer in Packed Distillation Columns," *Ind. Eng. Chem. Process Des. Dev.* **1982**, 21, 162.
- Carey, T. R., Hermes, J. E., Rochelle, G. T., "A Model of Acid Gas Absorption/Stripping Using Methyldiethanolamine with Added Acid," *Gas Separation and Purification*. **1991**, 5, 95.
- Chang, C. S., Rochelle, G. T., "Mass Transfer Enhanced by Equilibrium Reactions," *Ind. Eng. Chem. Fundam.* **1982**, 21, 379.
- Critchfield, J. E., "CO₂ Absorption/Desorption in Methyldiethanolamine Solutions Promoted with Monoethanolamine and Diethanolamine: Mass

- Transfer and Reaction Kinetics.” Ph.D. Dissertation, The University of Texas at Austin, 1988.
- Danckwerts, P. V., *Gas Liquid Reactions*. McGraw-Hill, New York, 1970.
- Darton, R. C., “Distillation and Absorption Technology: Current Market and New Developments,” *Trans. IChemE*. **1992**, 70 (Part A), 435.
- DeCoursey, W. J., “Enhancement Factors for Gas Absorption with Reversible Reaction,” *Chem. Engng. Sci.* **1982**, 37, 1483.
- DeCoursey, W. J., Thring, R. W., “Effects of Unequal Diffusivities on Enhancement Factors for Reversible and Irreversible Reaction,” *Chem. Engng. Sci.* **1989**, 44, 1715.
- DeCoursey, W. J., “A Simpler Approximation for Enhancement of Mass Transfer by Second-Order Reversible Reaction,” *IChemE. Symp. Ser.* **1992**, 128, B269.
- Dhulesia, H., “Clear Liquid Height on Sieve and Valve Trays,” *Chem. Eng. Res. Des.* **1984**, 62.
- Fair, J. R. “Stagewise Mass Transfer Processes.” In *Scaleup of Chemical Processes*. Bisio, A., Kabel, R.L. (Ed.), Wiley: New York, 1985.
- Frank, M. J. W., Kuipers, J. A. M., Versteeg, G. F., Van Swaaij, W. P. M., “Modelling of Simultaneous Mass and Heat Transfer with Chemical Reaction Using the Maxwell-Stefan Theory-I. Model Development and Isothermal Study,” *Chem. Engng. Sci.* **1995a**, 50, 1645.
- Frank, M. J. W., Kuipers, J. A. M., Krishna, R., Van Swaaij, W. P. M., “Modelling of Simultaneous Mass and Heat Transfer with Chemical Reaction Using the Maxwell-Stefan Theory-II. Non-Isothermal Study,” *Chem. Engng. Sci.* **1995b**, 50, 1661.
- Glasscock, D. A., “Modelling and Experimental Study of Carbon Dioxide Absorption into Aqueous Alkanolamines.” Ph.D Dissertation, The University of Texas at Austin, 1990.
- Glasscock, D. A., Rochelle, G. T., “Approximate Simulation of CO₂ and H₂S Absorption into Aqueous Alkanolamines,” *AIChE J.* **1993**, 39, 1389.
- Haimour, N., K., Sandall, O. C., “Absorption of Carbon Dioxide into Aqueous Methyldiethanolamine,” *Chem. Eng. Sci.* **1984**, 39, 1791.
- Krishna, R., Martinez, H. F., Sreedhar, R., Standart, G. L., “Murphree Point Efficiencies in Multicomponent Systems,” *Trans. IChemE*. **1977**, 55, 178.

- Krishna, R., Wesselingh, J. A., "The Maxwell-Stefan Approach to Mass Transfer," *Chem. Engng. Sci.* **1997**, 52, 861.
- Krishnamurthy, R., Taylor, R., "Absorber Simulation and Design Using a Nonequilibrium Stage Model," *Can. J. Chem. Eng.* **1986**, 64, 96.
- Littel, R. J., van Swaaij, W. P. M., Vestee, G. F., "Kinetics of Carbon Dioxide with Tertiary Amines in Aqueous Solutions," *AIChE J.* **1990**, 36, 1633.
- Littel, R. J., Filmer, B., Versteeg, G. F., Van Swaaij, W. P. M., "Modeling of Simultaneous Absorption of H_2S and CO_2 in Alkanolamine Solutions: The Influence of Parallel and Consecutive Reversible Reactions and the Coupled Diffusion of Ionic Species," *Chem. Engng. Sci.* **1991**, 46, 2313.
- Mshewa, M., "Carbon Dioxide Desorption/Absorption with Aqueous Mixtures of Methyldiethanolamine and Diethanolamine at 40 to 120°C." Ph.D. Dissertation, The University of Texas at Austin, 1995.
- Onda, K., Takeuchi, H., Okumoto, Y., "Mass Transfer Coefficients Between Gas and Liquid Phases in Packed Columns," *Journal Chem. Engng. Japan.* **1968**, 1, 56.
- Pinsent, B. R. W., Pearson, L., Roughton, F. J. W., "The Kinetics of Combination of Carbon Dioxide with Hydroxide Ions," *Trans. Faraday Soc.* **1956**, 52, 1512.
- Posey, M. L., "Thermodynamic Model for Acid Gas Loaded Aqueous Amine Solutions." Ph.D. Dissertation, The University of Texas at Austin, 1996.
- Raal, J. D., Khurana, M. K., "Gas Absorption with Large Heat Effects in Packed Columns," *Can. J. Chem. Eng.* **1973**, 51, 162.
- Rinker, E. B., Ashour, S. S., Sandall, O. C., "Kinetics and Modeling of Carbon Dioxide Absorption into Aqueous Solutions of N-methyldiethanolamine," *Chem. Eng. Sci.* **1995**, 50, 755.
- Rinker, E. B., Oelschlager, D. W., Colussi, A. T., Henry, K. R., Sandall, O. C., "Viscosity, Density, and Surface Tension of Binary Mixtures of Water and N-Methyldiethanolamine and Water and Diethanolamine and Tertiary Mixtures of These Amines with Water over the Temperature Range 20-100°C," *J. Chem. Eng. Data.* **1994**, 39, 392.
- Sandall, O. C., Rinker, E. B., Ashour, S., "Acid Gas Treating by Aqueous Alkanolamines," Annual Report for the Gas Research Institute, **1993**.

- Scheffe, R. D., Weiland, R. H., "Mass Transfer Characteristics of Valve Tray," *Ind. Eng. Chem. Res.* **1987**, 26, 228.
- Seader, J. D. "The Rate-based Approach for Modeling Staged Separations," *Chem. Eng. Prog.* **1989**, 85, 41.
- Sivasubramanian, M. S., "The Heat and Mass Transfer Rate Approach for the Simulation and Design of Acid Gas Treating Units". Ph. D. Dissertation, Clarkson University, 1985.
- Snijder, E. D., te Riele, M. J. M., Versteeg, G. F., van Swaaij, W.P.M., "Diffusion Coefficients of Several Aqueous Alkanolamine Solutions," *J. Chem. Eng. Data.* **1993**, 38, 475.
- Taylor, R., Krishna, R., *Multicomponent Mass Transfer*, Wiley, New York, 1993.
- Tomcej, R. A., Otto, F. D., Rangwala, H. A., Morrell, B. R., "Tray Design for Selective Absorption," Presented at the Gas Conditioning Conference. **1987**. Norman, Oklahoma, USA.
- Versteeg, G. F., Kuipers, J. A. M., van Beckum, F. P. H., van Swaaij, W. P. M., "Mass Transfer with Complex Reversible Chemical Reactions-II. Parallel Reversible Chemical Reactions," *Chem. Engng. Sci.* **1990**, 45, 183.
- Versteeg, G. F., van Swaaij, W. P. M., "Solubility and Diffusivity of Acid Gases (CO_2 , N_2O) in Aqueous Alkanolamine Solutions," *J. Chem. Eng. Data.* **1988**, 33, 29.

Chapter 7

Conclusions and Future Directions

Although each chapter in this dissertation provides conclusions for each major section, it is important to summarize the salient accomplishments and give recommendations on future directions.

7.1 CONCLUSIONS

7.1.1 Reaction-Diffusion Modeling and Validation

- A comprehensive reaction-diffusion model was developed to describe the mass transfer processes that take place in the liquid and vapor films during chemical absorption. This model is based on the approximate solution of the diffusion-reaction equations using surface renewal theory. It accounts for thermodynamic non-idealities, effects of diffusion of reactants and reaction products through the liquid boundary layer, and interactions between the chemical reactions.
- For the purpose of validating the reaction-diffusion model, rates of mass transfer of CO₂ were measured in a wetted-wall column reactor using three different reactive systems: aqueous solutions of methyldiethanolamine, diglycolamine and blends of these solvents at temperatures from 25 to 100°C.
- The model was used for a parametric study to determine the mechanisms that control the interfacial mass transfer rate of the diffusing gas under a wide range of conditions.

- For the single solvent systems and using mostly low driving force measurements, the rate constants for the reaction between CO₂ and MDEA, and CO₂ and DGA were obtained by using non-linear parameter estimation. The experimental measurements for the single solvent systems were performed under conditions that approach the pseudo-first order limiting case.

- It was found that temperature and mass transfer driving force has significant effects on the mass transfer mechanisms. At temperatures above 60°C, especially for the mixtures of DGA and MDEA, the effect of the reversibility of the reactions becomes significant which in turn makes the diffusion of reactants (other than the absorbing gas) and reaction products the controlling mechanism. Therefore, at high temperature and high CO₂ loading diffusion and equilibrium approach, instead of reaction kinetics, control the mass transfer enhancement.

- Due to the importance of the equilibrium approach and diffusion of reactants and reaction products for the reactive absorption of CO₂ into mixtures of DGA and MDEA, a non-linear parameter estimation algorithm was implemented to determine the diffusion coefficient of reactants (other than the absorbing gas) and products and a thermodynamic interaction parameter between water and cation-anion pairs, specifically $\tau(\text{water}, \text{DGACOO}^- \text{-MDEAH}^+)$. The functionality of the diffusion coefficient of the reactants and products with temperature resembles the reported experimental values of diffusivity of MDEA and DGA into aqueous solutions measured by other researchers. The values of $\tau(\text{water}, \text{DGACOO}^- \text{-MDEAH}^+)$ obtained were similar to those previously reported

for $\tau(\text{water, MEACOO}^-\text{-MDEAH}^+)$ obtained from vapor-liquid-equilibrium experimental data.

7.1.2. Rate-based Modeling of Reactive Absorption Columns

- The reaction-diffusion model described in Section 7.1.1 was assembled as a part of a rate-based column model for the simulation of reactive absorption columns. Submodels for predicting the mass transfer coefficients for physical absorption, heat transfer coefficients, interfacial areas and to account for the thermodynamic non-ideality of the vapor-liquid system are the other constituents of this rate-based column model.

- This rate-based column model has two distinguishing features. Firstly, the reaction-diffusion part of the model uses the Maxwell-Stefan approach to multicomponent mass transfer to determine the interfacial mass transfer rates for physical absorption, and the enhancement factor theory to account for the effect of the chemical reactions. Secondly, the model is generic and can be used for other reactive absorption systems with minor modifications on the thermodynamics and reaction kinetics. The rate-based model, however, cannot be used when there are considerable uncertainties in the submodels, for instance when the reaction kinetics, physical mass transfer coefficients or thermodynamics of the system are not known with certainty.

- This general framework was used to model the interfacial heat and mass transport processes that take place during reactive absorption when both rate and equilibrium controlled reactions take place in the liquid phase. This

framework was successfully applied to the selective absorption of H_2S from fuel gas containing CO_2 , representative of product from coal gasification at 20 atm.

- In packed columns, CO_2 absorption occurs with fast chemical reaction in the liquid boundary layer. In trayed columns, CO_2 absorption occurs at enhancement factors close to unity, therefore it is primarily controlled by physical absorption without reaction in the boundary layer. The difference in mechanism for CO_2 absorption between the packed and trayed column is due to the difference in the ratio of reaction to diffusion time. Gas film resistance is never significant for CO_2 absorption.

- In trayed columns, H_2S absorption is mostly controlled by gas film diffusion. In packed columns about half of the resistance to H_2S absorption is in gas film diffusion and about half is in diffusion of bisulfide in the liquid boundary layer. The extent of liquid film resistance increases a factor of about three from the lean end to the rich end of the absorber. This reflects a typical decrease in the H_2S enhancement factor from 400 to 60.

- With a greater height of packing or a reduced liquid rate, the maximum liquid temperature above the bottom of the absorber tends to increase. This maximum temperature can be 15 to 25 °C greater than the temperature at the top segment. At the extreme this condition results in an equilibrium “pinch” at the temperature bulge. The “pinch” at the temperature bulge for H_2S occurs instead of a rich-end “pinch”. This effect leads to the existence of an optimum packing height for the H_2S removal.

- The formation of the temperature bulge in reactive absorption columns was analyzed in detail and it was found that it is due to the combined effects of

purely conductive heat flux and the convective enthalpy transfer due to the different diffusing species. The convective enthalpy transfer due to the absorption-reaction of the transferring gases and that due to the vaporization-condensation of water are the constituents of the overall convective enthalpy transfer.

- For a given CO₂ removal or a given total interfacial area, trayed columns give better H₂S performance than packed columns, primarily because trays are characterized by a much larger liquid film mass transfer coefficient. The generalization of this conclusion requires a more detailed analysis of the accuracy of the submodels and correlations used for predicting mass transfer coefficients and interfacial areas for mass transfer. The Murphree vapor efficiency for CO₂ extracted from the rate calculations varies from 0.2 to 1.7% per 0.53 m section in the packed columns studied. In the trayed column it is about 1.1% per tray. The profile of Murphree efficiencies for CO₂ in the trayed and packed contactors follows closely the temperature profile due to the effect of the temperature on the transport properties and the reaction kinetics. The Murphree efficiency based on partial pressures for H₂S varies from 84 to 90% in the trayed column.

7.2. RECOMMENDATIONS ON FUTURE DIRECTIONS

7.2.1 Reaction-Diffusion Studies

The logical next step to the reaction-diffusion studies documented in this dissertation is to extend the reaction-diffusion model to allow different diffusion coefficients for the reactants (different from the diffusing gas) and reaction

products. This model would be useful to differentiate between the importance of the diffusion of reactants and products when the interfacial mass transfer is not controlled by reaction kinetics.

In this work a thermodynamic interaction parameter was determined with reasonable confidence from mass transfer rate data using non-linear parameter estimation. This proves that under the appropriate experimental conditions, rate data can be used to determine not only kinetics but also chemical equilibrium parameters. It is suggested that to improve confidence on the determination of equilibrium parameters, mass transfer rate data measured in gas-liquid reactors and vapor-liquid-equilibrium data be used simultaneously during the non-linear parameter estimation.

In the mass transfer model for reactive absorption with multiple reactions developed in this dissertation, a key assumption was made in the solution of the diffusion-reaction equation for carbamate as a product of the faster reaction. The treatment of this diffusion-reaction equation has implications on the predictions of the distribution of the fluxes of bicarbonate and carbamate through the reaction zone. It is recommended that rigorous modeling be used to elucidate the mechanism of the distribution of these fluxes and therefore explore the implications of the assumption made in this work.

The use of rigorous modeling of the reaction-diffusion problem is also recommended to study the accuracy of the approximate enhancement factor models discussed in this dissertation. In Section C.5 of Appendix C these enhancement factor models are compared with each other, but a comparison with a numerical solution would be required to address the advantages and

disadvantages of these approximations under a wide range of conditions with emphasis on diffusion and equilibrium controlled regimes.

The recent literature on modeling and analysis of reaction-diffusion systems under reactive absorption conditions lacks in-depth studies on the coupling effect between the phenomena of diffusion of reactants (other than the diffusing gases) and reaction products, and the reversibility of the chemical reactions. In the work documented in this dissertation it was shown that an accurate description of these phenomena is crucial for predicting interfacial mass transfer rates when the mass transfer process is not completely controlled by reaction kinetics. A rigorous numerical simulation that specifically addresses this coupling effect between diffusion and equilibrium approach would be an important contribution.

7.2.2 Modeling of Reactive Absorption Columns

The reaction-diffusion model developed and validated in this dissertation can be used to describe the interfacial mass transfer where more than one reactive solvent is present in the liquid phase. This reaction-diffusion model was integrated on a rate-based column model where two gases (CO_2 and H_2S) undergo reactive absorption with one solvent (methyldiethanolamine). The capability of the reaction-diffusion model to describe reactive absorption with multiple reactions should be exploited in the framework of the rate-based column simulation. A suitable system to study would be reactive absorption of CO_2 and/or H_2S into mixtures of DGA and MDEA.

The rate-based column model algorithm described in this dissertation combines the Generalized Maxwell-Stefan approach to multicomponent mass transfer and the enhancement factor concept which is a pseudo-binary theory. The reliability of this approach depends on the consistency between these two theories. As it was described in detail in Chapters 2 and 6, it has been shown recently that these two theories are consistent for first and second order irreversible reactions. To study the consistency between these two approaches for reversible and instantaneous equilibrium reactions is an area where research is needed.

One of the original goals of this dissertation was the development of a short-cut method for designing reactive absorption columns. However, due to the complexity of the transport processes and the close interaction between thermal effects, chemical kinetics, and mass transfer effects; it was soon realized that the development of such a general short-cut method was quite difficult to accomplish. The current form of the rate-based reactive absorption column model in the framework of RATEFRAC[®] requires a stepwise convergence procedure where the column is first converged for a simple case, usually low reactant concentration, and then steps are taken towards the desired condition to be analyzed. Before further developments are attempted to made towards the ultimate goal of developing a short-cut method, the issue of difficulty of convergence needs to be addressed.

When during the course of the present work the performances of trayed and packed columns were compared, it was realized that there is lack of data and models to describe the physical mass transfer coefficients and interfacial area for

mass transfer in industrial contactors under absorption conditions. This leads to important uncertainties on the determination of mass transfer coefficients, especially at the liquid side, which are crucial for absorption modeling. This gap in the physical mass transfer coefficient submodels needs to be filled to increase confidence on the rate-based modeling results and to arrive to a generalized conclusion about the relative advantage of using packed or trayed columns in reactive absorption.

Appendix A

Experimental Rate Measurements of Reactive Absorption of CO₂

In this Appendix P_{CO_2} is the mean log partial pressure of CO₂ between the inlet and outlet of the reactor.

Table A.1. Rate data of reactive absorption of CO₂ into aqueous MDEA solutions. 35wt% MDEA/65wt% water.

Run #	T (°C)	μ_L (cP)	$\frac{N_{CO_2}}{\text{moles}} \frac{\text{cm}^2}{\text{sec}}$	P_{CO_2} (atm)	$\frac{k_{g,CO_2}}{\text{moles}} \frac{\text{cm}^2}{\text{atm sec}}$	k_{L,CO_2}° (cm/sec)	CO ₂ ldg $\frac{\text{moles}}{\text{moles}}$
M-35-65-1	25	4.495	2.741E-7	0.7336	4.034E-6	2.966E-3	0.102
M-35-65-2	25	4.872	3.868E-7	1.5001	4.027E-6	3.271E-3	0.202
M-35-65-3	25	5.307	2.983E-7	1.6796	8.975E-7	3.054E-3	0.309
M-35-65-4	40	2.790	3.949E-7	0.7109	4.056E-6	4.104E-3	0.127
M-35-65-5	40	2.680	3.907E-7	1.1043	4.056E-6	4.644E-3	0.077
M-35-65-6	40	3.064	4.855E-7	1.4813	4.050E-6	4.290E-3	0.243
M-35-65-7	40	3.323	3.302E-7	1.6430	9.007E-7	4.666E-3	0.344
M-35-65-8	60	1.634	4.548E-7	0.6949	4.107E-6	6.497E-3	0.179
M-35-65-9	60	1.448	4.429E-7	0.6970	4.108E-6	6.343E-3	0.029
M-35-65-10	60	1.535	5.055E-7	1.0771	4.103E-6	6.635E-3	0.102
M-35-65-11	60	1.896	2.471E-7	1.7062	9.253E-7	6.167E-3	0.365
M-35-65-12	80	1.109	1.973E-8	0.7536	4.236E-6	8.341E-3	0.199
M-35-65-13	80	0.984	5.084E-7	0.6737	4.195E-6	9.043E-3	0.050
M-35-65-14	80	1.056	5.498E-7	1.0512	4.191E-6	8.869E-3	0.138

Table A.2. Rate data of reactive absorption of CO₂ into aqueous MDEA solutions. 50wt% MDEA/50wt% water.

Run #	T (°C)	μ_L (cP)	$\frac{N_{CO_2}}{\text{moles}} \frac{\text{cm}^2}{\text{sec}}$	P_{CO_2} (atm)	$\frac{k_{g,CO_2}}{\text{moles}} \frac{\text{cm}^2}{\text{atm sec}}$	k_{L,CO_2}° (cm/sec)	CO ₂ ldg $\frac{\text{moles}}{\text{moles}}$
M-50-50-1	40	5.800	4.476E-7	1.8388	7.304E-7	2.669E-3	0.192
M-50-50-2	60	2.858	5.270E-7	1.7084	7.315E-7	4.711E-3	0.144
M-50-50-3	90	1.458	2.960E-8	2.2107	8.172E-7	6.405E-3	0.164
M-50-50-4	60	3.008	2.110E-6	3.690	N/A*	3.504E-3	0.207
M-50-50-5	80	1.945	8.867E-7	3.550	N/A	4.945E-3	0.252
M-50-50-6	95	1.489	5.330E-7	7.378	N/A	6.364E-3	0.319
M-50-50-7	81	1.674	8.062E-7	2.195	6.808E-7	6.277E-3	0.095
M-50-50-8	81	1.717	6.969E-7	2.277	7.236E-7	6.187E-3	0.117
M-50-50-9	96	1.136	1.201E-6	1.647	8.920E-7	7.079E-3	0.019
M-50-50-10	97	1.132	1.061E-6	1.922	8.847E-7	7.109E-3	0.029

*: pure CO₂ fed to the reactor.

Table A.2.(Continued) Rate data of reactive absorption of CO₂ into aqueous MDEA solutions. 50wt% MDEA/50wt% water.

Run #	T (°C)	μ_L (cP)	N_{CO_2} moles cm ² sec	P_{CO_2} (atm)	k_{g,CO_2} moles cm ² atm sec	k_{L,CO_2}^o (cm/sec)	CO ₂ ldg moles moles
M-50-50-1	99	1.104	9.750E-7	2.081	8.773E-7	7.572E-3	0.038
M-50-50-2	99	1.105	8.964E-7	2.199	8.792E-7	7.580E-3	0.045
M-50-50-3	97	1.153	7.220E-7	2.421	8.889E-7	7.381E-3	0.058
M-50-50-4	99	1.129	5.988E-7	2.586	8.875E-7	7.502E-3	0.065
M-50-50-5	98	1.140	5.053E-7	2.718	8.821E-7	7.464E-3	0.074
M-50-50-6	98	1.157	3.917E-7	2.792	9.015E-7	7.080E-3	0.081
M-50-50-7	98	1.105	1.077E-6	1.842	9.098E-7	7.228E-3	0.026
M-50-50-8	100	1.081	9.672E-7	2.101	8.749E-7	7.354E-3	0.036
M-50-50-9	100	1.072	7.856E-7	2.403	8.639E-7	7.406E-3	0.042
M-50-50-11	102	1.051	6.373E-7	2.456	9.165E-7	7.519E-3	0.051
M-50-50-12	99	1.119	5.939E-7	2.513	9.150E-7	7.209E-3	0.056
M-50-50-13	100	1.097	5.376E-7	2.584	9.142E-7	7.146E-3	0.062
M-50-50-14	99	1.118	4.616E-7	2.630	9.292E-7	7.057E-3	0.066
M-50-50-15	100	1.109	2.691E-7	2.765	9.544E-7	7.116E-3	0.078
M-50-50-16	80	1.688	2.707E-6	3.282	N/A	6.097E-3	0.064
M-50-50-17	80	1.734	2.450E-6	3.348	N/A	6.121E-3	0.103
M-50-50-18	80	1.785	2.161E-6	3.483	N/A	6.133E-3	0.144
M-50-50-19	79	1.871	1.999E-6	3.661	N/A	5.964E-3	0.181
M-50-50-20	80	1.931	2.707E-6	5.594	N/A	6.072E-3	0.239
M-50-50-21	80	1.975	2.438E-6	6.000	N/A	6.098E-3	0.276
M-50-50-22	80	2.043	2.137E-6	6.206	N/A	5.988E-3	0.314
M-50-50-23	79	2.195	1.698E-6	7.237	N/A	5.885E-3	0.373
M-50-50-24	101	1.123	-4.854E-7	0.878	6.029E-07	7.285E-3	0.114
M-50-50-25	101	1.106	-3.847E-7	0.807	5.859E-07	7.345E-3	0.104
M-50-50-26	99	1.139	-3.244E-7	0.706	6.193E-07	7.010E-3	0.095
M-50-50-27	109	0.944	-5.661E-7	0.923	6.176E-07	8.504E-3	0.089
M-50-50-28	108	0.948	-5.296E-7	0.844	6.526E-07	8.461E-3	0.078
M-50-50-29	108	0.938	-4.311E-7	0.793	6.280E-07	8.509E-3	0.072
M-50-50-30	106	0.969	-3.257E-7	0.717	6.095E-07	8.312E-3	0.061
M-50-50-31	104	1.011	-2.759E-7	0.680	5.978E-07	7.892E-3	0.051

Table A.3. Rate data of reactive absorption of CO₂ into aqueous diglycolamine solutions. 50wt% DGA/50wt% water.

Run #	T (°C)	μ_L (cP)	$\frac{N_{CO_2}}{\text{moles}} \frac{\text{cm}^2}{\text{sec}}$	P_{CO_2} (atm)	$\frac{k_{g,CO_2}}{\text{moles}} \frac{\text{cm}^2}{\text{atm sec}}$	k_{L,CO_2}^o (cm/sec)	CO ₂ ldg $\frac{\text{moles}}{\text{moles}}$
D-50-50-1	25	7.0	4.293E-8	3.925E-3	3.197E-5	2.396E-3	≈ 0
D-50-50-2	25	7.0	8.481E-8	7.332E-3	3.206E-5	2.311E-3	≈ 0
D-50-50-3	25	7.0	1.010E-6	1.772E-1	3.129E-5	2.598E-3	0.206
D-50-50-4	25	6.0	5.433E-7	8.678E-2	3.155E-5	3.177E-3	0.229
D-50-50-5	40	4.0	4.828E-8	3.709E-3	3.278E-5	3.924E-3	≈ 0
D-50-50-6	40	4.0	9.799E-8	6.843E-3	3.287E-5	3.843E-3	≈ 0
D-50-50-7	40	4.0	1.010E-6	1.736E-1	3.208E-5	4.149E-3	0.331
D-50-50-8	40	4.0	6.612E-7	8.232E-2	3.228E-5	4.040E-3	0.257
D-50-50-9	60	2.2	1.269E-7	5.681E-3	3.526E-5	6.410E-3	≈ 0
D-50-50-10	60	2.2	5.270E-8	3.374E-3	3.518E-5	5.460E-3	≈ 0

Table A.4. Rate data of reactive absorption of CO₂ into aqueous diglycolamine solutions. 25wt% DGA/75wt% water.

Run #	T (°C)	μ_L (cP)	$\frac{N_{CO_2}}{\text{moles}} \frac{\text{cm}^2}{\text{sec}}$	P_{CO_2} (atm)	$\frac{k_{g,CO_2}}{\text{moles}} \frac{\text{cm}^2}{\text{atm sec}}$	k_{L,CO_2}^o (cm/sec)	CO ₂ ldg $\frac{\text{moles}}{\text{moles}}$
D-25-75-1	25	2.2	1.925E-7	2.021E-2	3.240E-5	3.942E-3	0.101
D-25-75-2	25	2.2	6.036E-7	1.186E-1	3.340E-5	4.945E-3	0.386
D-25-75-3	35	1.8	2.039E-7	1.970E-2	3.290E-5	3.274E-3	0.139
D-25-75-4	35	1.8	4.215E-7	1.208E-1	3.402E-5	5.914E-3	0.483
D-25-75-5	50	1.2	2.808E-7	1.715E-2	3.410E-5	3.991E-3	0.159
D-25-75-6	50	1.3	1.612E-6	1.907E-1	1.664E-5	6.256E-3	0.194
D-25-75-7	65	1.2	7.130E-7	2.245E-1	1.751E-5	7.477E-3	0.423

Table A.5. Rate data of reactive absorption of CO₂ into aqueous solutions of DGA and MDEA. 5wt% DGA-45wt% water/50wt% water. Temperature: 40°C.

Run Blend-40-#	μ_L (cP)	$\frac{N_{CO_2}}{\text{moles}} \frac{\text{cm}^2}{\text{sec}}$	P_{CO_2} (atm)	$\frac{k_{g,CO_2}}{\text{moles}} \frac{\text{cm}^2}{\text{atm sec}}$	k_{L,CO_2}^o (cm/sec)	CO ₂ ldg $\frac{\text{moles}}{\text{moles}}$
5-45-1	4.627	1.147E-6	0.888	4.951E-6	3.505E-3	0.075
5-45-2	4.755	9.774E-7	0.937	4.830E-6	3.474E-3	0.096
5-45-3	4.906	8.681E-7	0.969	4.753E-6	3.387E-3	0.115
5-45-5	4.859	8.288E-7	0.939	4.931E-6	3.442E-3	0.134
5-45-6	4.949	1.085E-6	1.843	4.461E-6	3.522E-3	0.160
5-45-7	5.263	1.167E-6	1.937	4.214E-6	3.265E-3	0.185
5-45-8	5.130	1.248E-6	1.925	4.210E-6	3.382E-3	0.206

Table A.5. (Continued) Rate data of reactive absorption of CO₂ into aqueous solutions of DGA and MDEA. 5wt% DGA-45wt% water/50wt% water. Temperature: 40°C.

Run Blend-40-#	μ_L (cP)	N_{CO_2} moles cm ² sec	P_{CO_2} (atm)	k_{g,CO_2} moles cm ² atm sec	k_{L,CO_2}^o (cm/sec)	CO ₂ ldg moles moles
5-45-9	4.799	1.830E-6	1.992	3.856E-6	2.966E-3	0.137
5-45-10	4.889	1.499E-6	2.009	3.944E-6	2.869E-3	0.159
5-45-11	4.990	1.373E-6	2.045	3.920E-6	2.814E-3	0.177
5-45-12	5.086	1.246E-6	2.081	3.897E-6	2.769E-3	0.201
5-45-13	5.570	3.311E-6	6.947	N/A	2.852E-3	0.361
5-45-14	5.774	3.166E-6	7.084	N/A	2.686E-3	0.393
5-45-15	6.148	3.136E-6	7.902	N/A	2.523E-3	0.444

Table A.6. Rate data of reactive absorption of CO₂ into aqueous solutions of DGA and MDEA. 5wt% DGA-45wt% water/50wt% water. Temperature: 60°C.

Run Blend-60-#	μ_L (cP)	N_{CO_2} moles cm ² sec	P_{CO_2} (atm)	k_{g,CO_2} moles cm ² atm sec	k_{L,CO_2}^o (cm/sec)	CO ₂ ldg moles moles
5-45-1	2.772	1.063E-6	0.951	4.711E-6	5.154E-3	0.134
5-45-2	2.848	9.072E-7	0.981	4.681E-6	5.141E-3	0.155
5-45-3	3.021	1.488E-6	1.911	4.166E-6	4.840E-3	0.218
5-45-4	3.142	1.328E-6	1.969	4.103E-6	4.708E-3	0.231
5-45-5	3.059	1.248E-6	1.978	4.114E-6	5.305E-3	0.257
5-45-6	3.032	3.580E-6	5.727	N/A	4.893E-3	0.246
5-45-7	3.127	5.231E-6	7.425	N/A	4.680E-3	0.303
5-45-8	3.299	3.677E-6	7.156	N/A	4.598E-3	0.344
5-45-9	3.367	3.704E-6	6.953	N/A	4.548E-3	0.363
5-45-10	3.480	3.623E-6	7.159	N/A	4.533E-3	0.397
5-45-11	3.633	3.558E-6	7.636	N/A	4.438E-3	0.447
5-45-12	3.842	2.939E-6	7.842	N/A	4.237E-3	0.504
5-45-13	4.097	2.056E-6	7.848	N/A	4.035E-3	0.543
5-45-14	3.971	1.930E-6	8.042	N/A	4.266E-3	0.574
5-45-15	3.526	2.720E-6	6.753	N/A	4.537E-3	0.394
5-45-16	3.623	2.533E-6	7.367	N/A	4.347E-3	0.419
5-45-17	3.839	2.278E-6	7.780	N/A	4.177E-3	0.459
5-45-18	3.718	2.010E-6	8.116	N/A	4.279E-3	0.443
5-45-19	3.779	1.647E-6	8.184	N/A	4.254E-3	0.470
5-45-20	3.840	1.335E-6	8.046	N/A	4.231E-3	0.498

Table A.6. (Continued) Rate data of reactive absorption of CO₂ into aqueous solutions of DGA and MDEA. 5wt% DGA-45wt% water/50wt% water. Temperature: 60°C.

Run Blend-60-#	μ_L (cP)	$\frac{N_{CO_2}}{\text{moles}} \frac{\text{cm}^2}{\text{sec}}$	P_{CO_2} (atm)	$\frac{k_{g,CO_2}}{\text{moles}} \frac{\text{cm}^2}{\text{atm sec}}$	k_{L,CO_2}^o (cm/sec)	$\frac{CO_2 \text{ ldg}}{\text{moles}} \frac{\text{moles}}{\text{moles}}$
5-45-21	3.857	9.780E-7	7.843	N/A	4.219E-3	0.502
5-45-22	3.878	8.539E-7	7.975	N/A	4.242E-3	0.534
5-45-23	2.914	1.583E-6	2.032	3.885E-6	3.374E-3	0.191
5-45-24	2.933	1.373E-6	2.080	3.869E-6	3.371E-3	0.206
5-45-25	2.938	1.246E-6	2.030	4.010E-6	3.372E-3	0.213
5-45-26	2.888	1.118E-6	2.064	3.988E-6	4.147E-3	0.215
5-45-27	3.491	2.631E-6	6.883	N/A	4.231E-3	0.423
5-45-28	3.646	2.796E-6	7.701	N/A	4.127E-3	0.469
5-45-29	3.903	2.048E-6	8.185	N/A	3.426E-3	0.505

Table A.7. Rate data of reactive absorption of CO₂ into aqueous solutions of DGA and MDEA. 5wt% DGA-45wt% water/50wt% water. Temperature: 80°C.

Run Blend-80-#	μ_L (cP)	$\frac{N_{CO_2}}{\text{moles}} \frac{\text{cm}^2}{\text{sec}}$	P_{CO_2} (atm)	$\frac{k_{g,CO_2}}{\text{moles}} \frac{\text{cm}^2}{\text{atm sec}}$	k_{L,CO_2}^o (cm/sec)	$\frac{CO_2 \text{ ldg}}{\text{moles}} \frac{\text{moles}}{\text{moles}}$
5-45-1	1.979	-6.382E-7	0.297	3.482E-6	5.987E-3	0.233
5-45-2	1.841	-5.526E-7	0.281	3.519E-6	6.270E-3	0.215
5-45-3	1.895	2.964E-6	5.977	N/A	6.292E-3	0.285
5-45-4	1.984	2.806E-6	6.390	N/A	6.545E-3	0.331
5-45-5	2.060	2.744E-6	7.004	N/A	6.373E-3	0.373
5-45-6	2.111	2.431E-6	7.479	N/A	6.428E-3	0.410
5-45-7	2.174	1.809E-6	7.819	N/A	6.539E-3	0.450
5-45-8	2.241	1.605E-6	8.033	N/A	6.419E-3	0.461
5-45-9	2.316	8.589E-7	7.703	N/A	6.355E-3	0.468
5-45-10	1.825	4.182E-6	5.510	N/A	6.310E-3	0.215
5-45-11	1.918	4.284E-6	6.807	N/A	6.292E-3	0.267
5-45-12	2.010	3.904E-6	7.628	N/A	6.177E-3	0.313
5-45-13	2.068	2.589E-6	7.089	N/A	6.177E-3	0.332
5-45-14	2.102	2.558E-6	7.293	N/A	6.482E-3	0.352
5-45-15	2.224	2.250E-6	7.849	N/A	6.376E-3	0.389
5-45-16	2.293	1.745E-6	7.914	N/A	6.341E-3	0.440
5-45-17	2.341	1.364E-6	7.912	N/A	6.385E-3	0.470
5-45-18	2.471	1.121E-6	7.991	N/A	6.279E-3	0.506
5-45-19	2.479	6.281E-7	8.062	N/A	6.325E-3	0.502

Table A.8. Rate data of reactive absorption of CO₂ into aqueous solutions of DGA and MDEA. 5wt% DGA-45wt% water/50wt% water. Temperature: 100°C.

Run Blend-100-#	μ_L (cP)	$\frac{N_{CO_2}}{\text{moles}} \frac{\text{cm}^2}{\text{sec}}$	P_{CO_2} (atm)	$\frac{k_{g,CO_2}}{\text{moles}} \frac{\text{cm}^2}{\text{atm sec}}$	k_{L,CO_2}^o (cm/sec)	$\frac{CO_2 \text{ Idg}}{\text{moles}} \frac{\text{moles}}{\text{moles}}$
5-45-1	1.249	1.485E-6	7.454	N/A	7.722E-3	0.191
5-45-2	1.202	1.206E-6	7.608	N/A	8.120E-3	0.210
5-45-3	1.245	6.909E-7	6.957	N/A	7.940E-3	0.214
5-45-4	1.261	5.681E-7	7.152	N/A	7.522E-3	0.242
5-45-5	1.218	4.947E-7	7.271	N/A	7.649E-3	0.221
5-45-6	1.208	3.891E-7	7.389	N/A	7.727E-3	0.234
5-45-7	1.091	1.594E-6	1.912	4.137E-6	7.365E-3	0.074
5-45-8	1.102	1.081E-6	2.017	4.106E-6	7.971E-3	0.086
5-45-9	1.105	7.730E-7	2.075	4.097E-6	7.979E-3	0.096
5-45-10	1.119	6.387E-7	2.110	4.072E-6	8.092E-3	0.110
5-45-11	1.077	1.455E-6	1.972	4.065E-6	7.166E-3	0.119
5-45-12	1.099	1.156E-6	2.046	4.024E-6	8.995E-3	0.154
5-45-13	1.100	9.128E-7	2.051	4.096E-6	8.757E-3	0.120
5-45-14	1.122	7.627E-7	2.075	4.100E-6	8.662E-3	0.126
5-45-15	1.164	5.571E-7	2.120	4.080E-6	8.603E-3	0.166

Table A.9. Rate data of reactive absorption of CO₂ into aqueous solutions of DGA and MDEA. 15wt% DGA-35wt% water/50wt% water. Temperature: 40°C.

Run Blend-40-#	μ_L (cP)	$\frac{N_{CO_2}}{\text{moles}} \frac{\text{cm}^2}{\text{sec}}$	P_{CO_2} (atm)	$\frac{k_{g,CO_2}}{\text{moles}} \frac{\text{cm}^2}{\text{atm sec}}$	k_{L,CO_2}^o (cm/sec)	$\frac{CO_2 \text{ Idg}}{\text{moles}} \frac{\text{moles}}{\text{moles}}$
15-35-1	4.116	4.055E-06	1.342	4.945E-6	3.712E-3	0.074
15-35-2	4.585	3.410E-06	1.465	4.904E-6	3.455E-3	0.171
15-35-3	4.813	2.820E-06	1.589	4.821E-6	3.372E-3	0.209
15-35-4	5.211	2.159E-06	1.705	4.785E-6	3.322E-3	0.271
15-35-5	5.373	1.624E-06	1.939	4.039E-6	3.239E-3	0.299
15-35-6	5.491	1.441E-06	2.000	3.984E-6	3.177E-3	0.317
15-35-7	5.622	1.230E-06	2.048	3.965E-6	3.098E-3	0.327
15-35-8	5.631	1.230E-06	2.047	3.967E-6	3.128E-3	0.361
15-35-9	4.643	5.379E-06	2.656	N/A	3.688E-3	0.223
15-35-10	4.962	5.206E-06	4.016	N/A	3.660E-3	0.303
15-35-11	5.504	5.044E-06	5.313	N/A	3.428E-3	0.377
15-35-12	5.949	4.451E-06	6.132	N/A	3.274E-3	0.419
15-35-13	6.239	4.103E-06	7.085	N/A	3.180E-3	0.479
15-35-14	6.589	3.264E-06	7.902	N/A	3.036E-3	0.531

Table A.10. Rate data of reactive absorption of CO₂ into aqueous solutions of DGA and MDEA. 15wt% DGA-35wt% water/50wt% water. Temperature: 80°C.

Run Blend-80-#	μ_L (cP)	$\frac{N_{CO_2}}{cm^2 sec}$ moles	P_{CO_2} (atm)	$\frac{k_{g,CO_2}}{cm^2 atm sec}$ moles	k_{L,CO_2}^o (cm/sec)	CO ₂ ldg $\frac{moles}{moles}$
15-35-1	1.871	1.701E-06	1.677	5.092E-6	7.145E-3	0.232
15-35-2	1.877	1.371E-06	1.743	5.030E-6	7.214E-3	0.237
15-35-3	1.930	9.859E-07	1.817	4.971E-6	7.054E-3	0.258
15-35-4	1.931	7.398E-07	1.858	4.951E-6	7.091E-3	0.274
15-35-5	1.980	4.859E-07	2.203	3.957E-6	6.838E-3	0.313
15-35-6	2.072	-3.454E-07	0.706	3.550E-6	7.112E-3	0.314
15-35-7	2.123	-3.130E-07	0.701	3.542E-6	7.049E-3	0.313
15-35-8	2.140	8.009E-07	8.088	N/A	6.586E-3	0.437
15-35-9	2.213	7.225E-07	8.305	N/A	6.357E-3	0.443

Table A.11. Rate data of reactive absorption of CO₂ into aqueous solutions of DGA and MDEA. 15wt% DGA-35wt% water/50wt% water. Temperature: 100°C.

Run Blend-100-#	μ_L (cP)	$\frac{N_{CO_2}}{cm^2 sec}$ moles	P_{CO_2} (atm)	$\frac{k_{g,CO_2}}{cm^2 atm sec}$ moles	k_{L,CO_2}^o (cm/sec)	CO ₂ ldg $\frac{moles}{moles}$
15-35-1	1.057	5.337E-6	6.051	N/A	7.970E-3	0.120
15-35-2	1.191	4.592E-6	3.851	N/A	8.288E-3	0.204
15-35-3	1.260	4.008E-6	5.988	N/A	8.238E-3	0.249
15-35-4	1.314	3.382E-6	7.965	N/A	8.306E-3	0.300
15-35-5	1.328	1.660E-6	7.826	N/A	8.295E-3	0.317
15-35-6	1.338	8.857E-7	7.618	N/A	8.295E-3	0.331
15-35-7	1.284	7.125E-7	7.568	N/A	8.563E-3	0.341
15-35-8	1.348	6.834E-7	7.809	N/A	8.440E-3	0.357

Appendix B

Thermo-Physical and Transport Properties

B.1. SYSTEM MDEA-WATER-CO₂

Table B.1 summarizes the correlations and methods used to estimate the physical and transport properties for the system MDEA-water-CO₂.

Table B.1. Correlations and Source of Data for Physical and Transport Properties for the System MDEA-water-CO₂.

Property	Correlation/Data
Viscosity	Glasscock (1990), Rinker et al. (1994), Hagedorn et al. (1995)
Density	Licht and Weiland (1989)
Diffusivity of CO ₂	Al-Ghawas et al. (1989), Versteeg et al. (1988) and N ₂ O Analogy
Diffusivity of MDEA	Snijder et al. (1993)
	Al-Ghawas et al. (1989), Versteeg et al. (1988), Hagedorn et al. (1995), Sandall (1993)

B.1.1 Viscosity of the Solution

Using published experimental data for viscosity of different amine solutions, Glasscock (1990) obtained the following correlation for the viscosity of MDEA solutions:

$$\ln \mu = A + B/T + CT \quad (B.1)$$

where,

$$A = -19.52 - 23.40w_{f_{MDEA}} - 31.24w_{f_{MDEA}}^2 + 36.17w_{f_{MDEA}}^3 \quad (B.2)$$

$$B = 3912 + 4894w_{f_{MDEA}} + 8477w_{f_{MDEA}}^2 - 8358w_{f_{MDEA}}^3 \quad (B.3)$$

$$C = 0.02112 + 0.03339w_{f_{MDEA}} + 0.02780w_{f_{MDEA}}^2 - 0.04202w_{f_{MDEA}}^3 \quad (B.4)$$

wf_{MDEA} is the weight fraction of total MDEA in the solution, T is the temperature in Kelvin and μ is the viscosity in cP. This correlation is considered to be valid in the range of 20 to 50°C and for a MDEA concentration up to 50 wt%.

From 60°C to 100°C Rinker et al. (1994) reports viscosities of 50 wt% MDEA solutions. The following equation correlates that data:

$$\mu(\text{cP}) = 6.0337\text{E-}4 \exp(2780.9/T) ; \quad 333 \text{ K} < T < 373 \text{ K} \quad (\text{B.5})$$

Hagewiesche et al. (1995) report viscosities for 30 and 40 wt% MDEA solutions in the range of 30 to 50 °C. These data were used to compare the predictions of Equation B.1 for estimating viscosities of 35 wt% MDEA solutions. The correlation reported by these researchers is as follows:

$$\ln \mu(\text{kg/m s}) = A + B/T(\text{K}) ; \quad 0.3 < wf_{MDEA} < 0.4 \quad (\text{B.6})$$

$$A = -12.197 - 8.905 wf_{MDEA} \quad (\text{B.7})$$

$$B = 1438.717 + 4218.749 wf_{MDEA} \quad (\text{B.8})$$

The estimates of viscosities of correlations B.1 and B.6 were fairly close.

B.1.2. Density of the Solution

The correlation of Licht and Weiland (1989) was used to estimate the density of the MDEA solutions. This correlation can be also used to estimate the density of blended solutions. This correlation is as follows:

$$\frac{1}{\rho_L(\text{g/cm}^3)} = wf_w V_w^o \exp\{b_w(T - T^o)\} + wf_{MDEA} V_{MDEA}^o \exp\{b_{MDEA}(T - T^o)\} + wf_{Am2} V_{Am2}^o \exp\{b_{Am2}(T - T^o)\} \quad (\text{B.9})$$

where:

T° : 308K

V_i° : specific volume of component i (shown in Table B.2).

b_i : bulk thermal expansivity (1/K) (shown in Table B.2).

Table B.2. Parameters needed for the correlation of Licht and Weiland (1989).

	water	MDEA	DEA	MEA
Specific Volume (V°) (cm^3/g)	1.010	0.918	0.894	0.964
Bulk Thermal Expansivity (b) (1/K)	3.44E-4	5.28E-4	4.87E-4	5.68E-3

B.1.3. Diffusivity of CO_2 in the Solution

The diffusivity of CO_2 in MDEA solutions was estimated using the N_2O - CO_2 analogy and data and correlations for the diffusivity of N_2O in the chemical solvent. According to the N_2O - CO_2 analogy, the diffusion coefficients of N_2O and CO_2 in the aqueous amine solutions and in pure water (represented by the superscript $^{\circ}$) are related by the following expression:

$$\frac{D_{\text{CO}_2}}{D_{\text{CO}_2}^{\circ}} = \frac{D_{\text{N}_2\text{O}}}{D_{\text{N}_2\text{O}}^{\circ}} \quad (\text{B.10})$$

Versteeg et al. (1988) measured the diffusion coefficient of N_2O in aqueous solutions of up to around 35 wt% MDEA and from 20 to 60°C. Al-Ghawas et al. (1989) report measurements of diffusion coefficients of N_2O in aqueous solutions from 10 to 50 wt% MDEA and from 15 to 50°C. These data are represented in Figure B.1.

The correlation represented in Figure B.1 is a modified form of the Stokes-Einstein equation,

$$D_{\text{N}_2\text{O}} (\text{cm}^2/\text{sec}) = 5.533 \times 10^{-8} \frac{T}{\mu_L^{0.545}} \quad (\text{B.11})$$

where the viscosity of the liquid, μ_L , is in cP and the temperature in K.

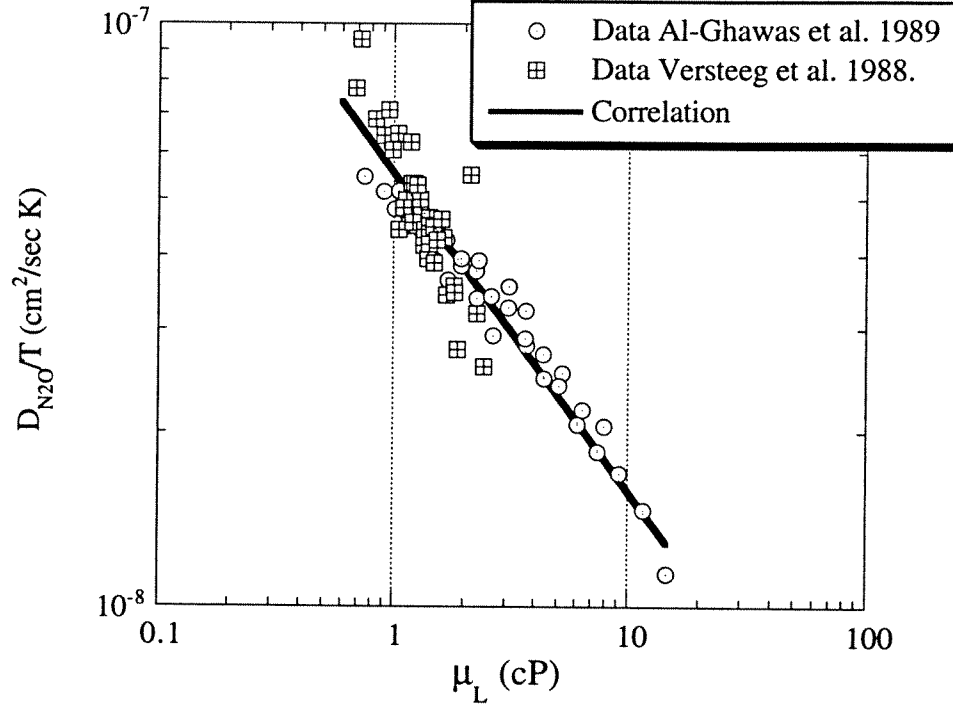


Figure B.1. Diffusivity of N₂O in aqueous MDEA solutions.

The diffusivity of CO₂ and N₂O in pure water was correlated using the data reported by Versteeg et al. (1988) and Tamimi et al. (1994). Figure B.2 represents the data of diffusion coefficients of CO₂ in water reported by these researchers while Figure B.3 depicts that of N₂O in water.

The correlations for the diffusion coefficients of CO₂ in water obtained from Figure B.2 are as follows:

$$D_{\text{CO}_2}^{\circ} (\text{cm}^2/\text{s}) = 0.02397 \exp\{-2122.2/T(\text{K})\}; \text{ Versteeg et al. (1988)} \quad (\text{B.12})$$

$$D_{\text{CO}_2}^{\circ} (\text{cm}^2/\text{s}) = 0.03389 \exp\{-2213.7/T(\text{K})\}; \text{ Tamimi et al. (1994)} \quad (\text{B.13})$$

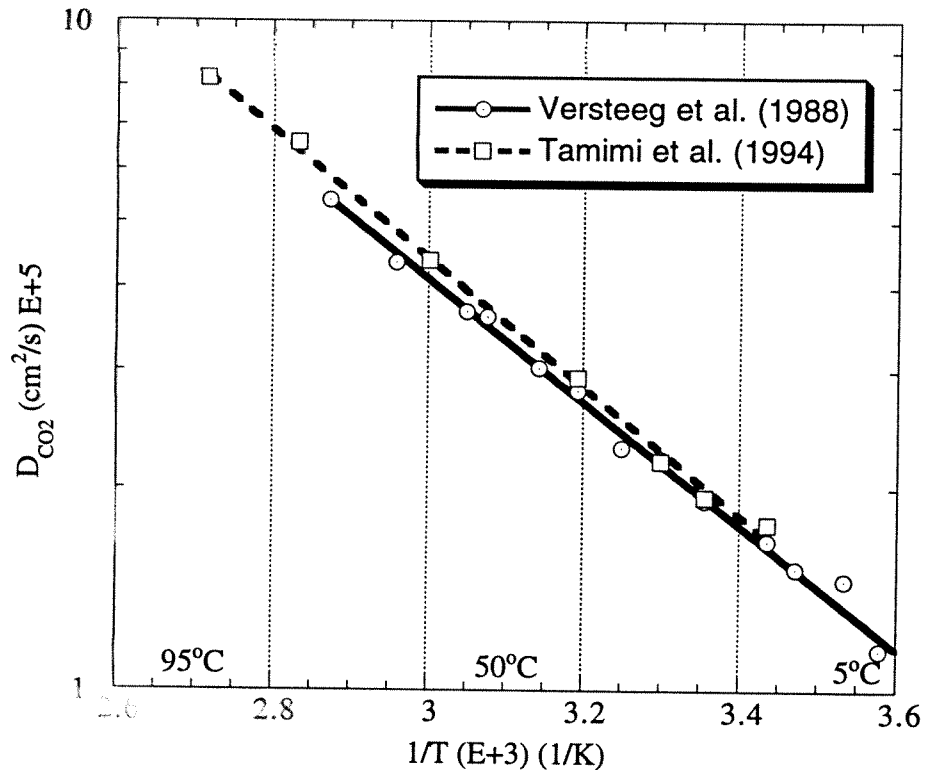


Figure B.2. Diffusion coefficients of CO₂ in pure water.

The correlations for the diffusion coefficients of N₂O in water obtained from Figure B.3 are as follows:

$$D_{N_2O}^o \text{ (cm}^2\text{/s)} = 0.04041 \exp\{-2288.4/T(K)\}; \quad \text{Versteeg et al. (1988)} \quad (B.14)$$

$$D_{N_2O}^o \text{ (cm}^2\text{/s)} = 0.03168 \exp\{-2209.4/T(K)\}; \quad \text{Tamimi et al. (1994)} \quad (B.15)$$

From this development it can be seen that knowing the viscosity of the solution, Equation B.11 can be used to predict the diffusion coefficient of N₂O in the chemical solvent, then the diffusion coefficients of N₂O and CO₂ in water can be estimated from the correlations presented above and the diffusion coefficient

of CO_2 in the chemical solvent can be calculated through the N_2O - CO_2 analogy (Equation B.10).

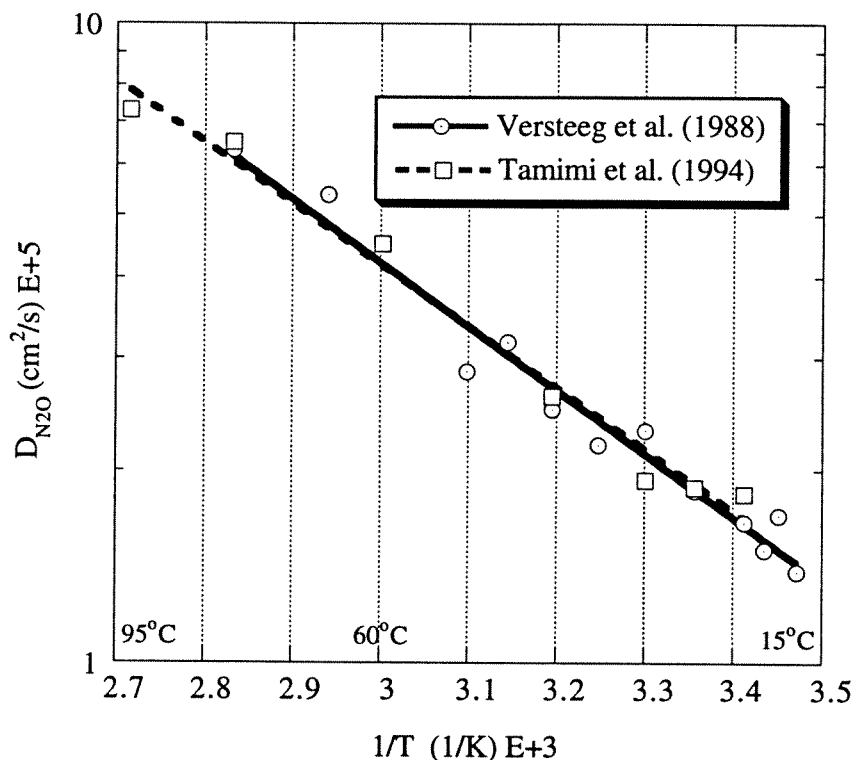


Figure B.3. Diffusion coefficients of N_2O in pure water.

B.1.4. Diffusivity of MDEA in the Solution

Snijder and coworker (1993) measured the diffusion coefficients of MEA, DEA, MDEA and DIPA in the corresponding aqueous alkanolamine solutions using the Taylor dispersion method. This technique is based on the fact that due to a combination of axial laminar convection and radial diffusion, axial dispersion takes place when a solute is introduced in a solvent flowing slowly through a long capillary tube. By solving the mass balance for such a system, the diffusion

coefficient can be related to the measured axial dispersion coefficient. The diffusion coefficients were correlated as a function of temperature and concentration for the alkanolamines mentioned above. Figure B.4 depicts the measured diffusion coefficients of MDEA in MDEA solutions.

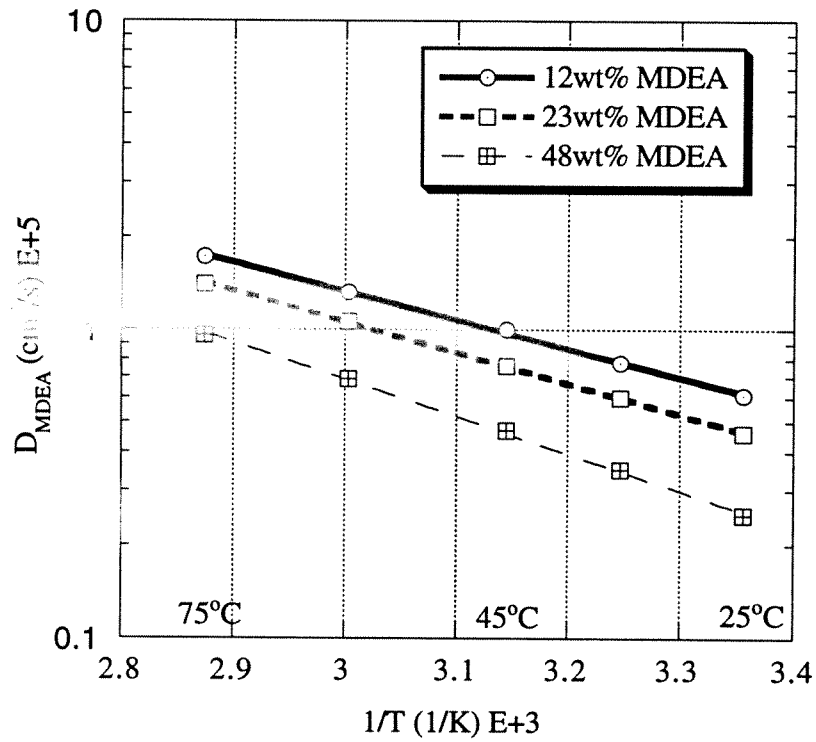


Figure B.4. Diffusion coefficients of MDEA in MDEA solutions measured by Snijder et al. (1993).

The following correlation reported by Snijder and coworkers (1993) fits all data points within 9% accuracy:

$$D_{\text{MDEA}} (\text{cm}^2/\text{s}) = 0.0207 \exp\{-2360.7/T(\text{K}) - 24.727\text{E-}5 C_{\text{MDEA}}\} \quad (\text{B.16})$$

where C_{MDEA} is the concentration of MDEA in the solution in moles/m³. This correlation was developed based on diffusivity data for MDEA solutions up to 48 wt% MDEA and for a range of temperature from 25 to 75°C.

B.1.5. Solubility of CO₂ in the Solution

Similarly to the estimation of the diffusion coefficient of CO₂ in the chemical solvent, the solubility of CO₂ in the chemical solvent is calculated using the CO₂-N₂O analogy, i.e.,

$$\frac{H_{\text{CO}_2}}{H_{\text{CO}_2}^0} = \frac{H_{\text{N}_2\text{O}}}{H_{\text{N}_2\text{O}}^0} \quad (\text{B.17})$$

where H_i and H_i^0 are the Henry's law constant of species i in the chemical solvent and in pure water, respectively. Figure B.5 depicts measurements of the Henry's law constant of N₂O in pure water.

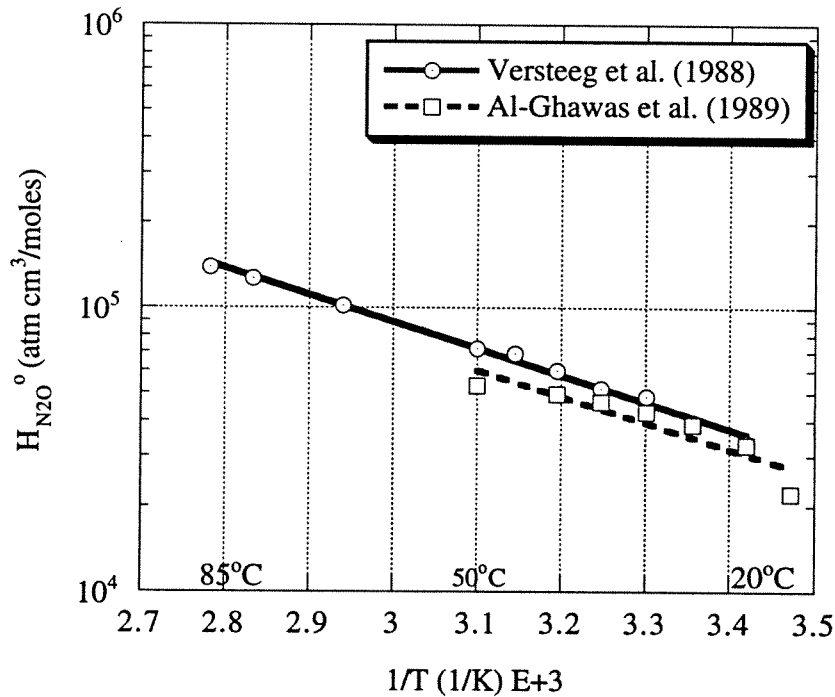


Figure B.5. Henry's Law Constant of N₂O in Pure Water.

The data reported by Versteeg et al. (1988) which cover a wider range of temperature are correlated by the following equation:

$$H_{N_2O}^o \text{ (atm cm}^3\text{/moles)} = 6.2489E+7 \exp\{-2183.6/T(K)\} \quad (B.18)$$

The Henry's law constant data of CO₂ in pure water measured by Versteeg et al. (1988) and those reported by Al-Ghawas et al. (1989), which were taken from the International Critical Tables, are depicted in Figure B.6. The following equation correlates these data,

$$H_{CO_2}^o \text{ (atm cm}^3\text{/moles)} = 1.7107E+7 \exp\{-1886.1/T(K)\} \quad (B.19)$$

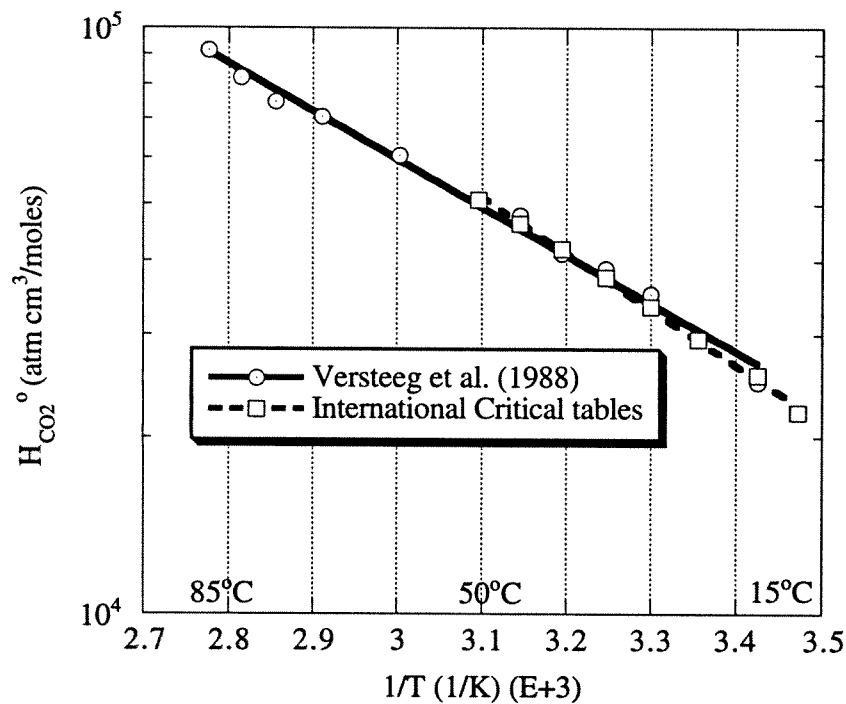


Figure B.6. Henry's law constant of CO₂ in pure water.

Regarding the Henry's law constant of N_2O in MDEA solutions, the data is more scarce. Al-Ghawas et al. (1989) measured this property for aqueous MDEA solutions from 10 to 50 wt% and for temperatures from 15 to 50°C. Sandall et al. (1993) also report Henry's law constants of N_2O in the same range of MDEA concentration and up to 80°C. Figure B.7 shows the data reported by Al-Ghawas and coworkers for different MDEA solutions while Figure B.8 compares the data for 50 wt% MDEA from both sources.

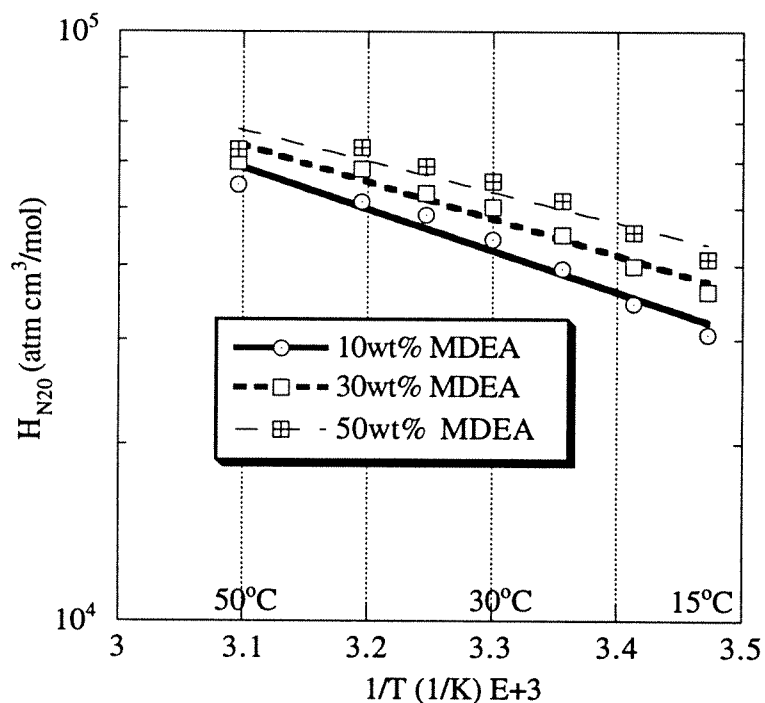


Figure B.7. Henry's law constant of N_2O in different MDEA solutions. Data from Al-Ghawas et al. (1989).

The following equation correlates the data obtained by Sandall et al. (1993) for 50 wt% MDEA:

$$H_{N_2O} \text{ (atm cm}^3\text{/moles)} = 3.2194E+6 \exp\{-1211.8/T(K)\} \quad (B.20)$$

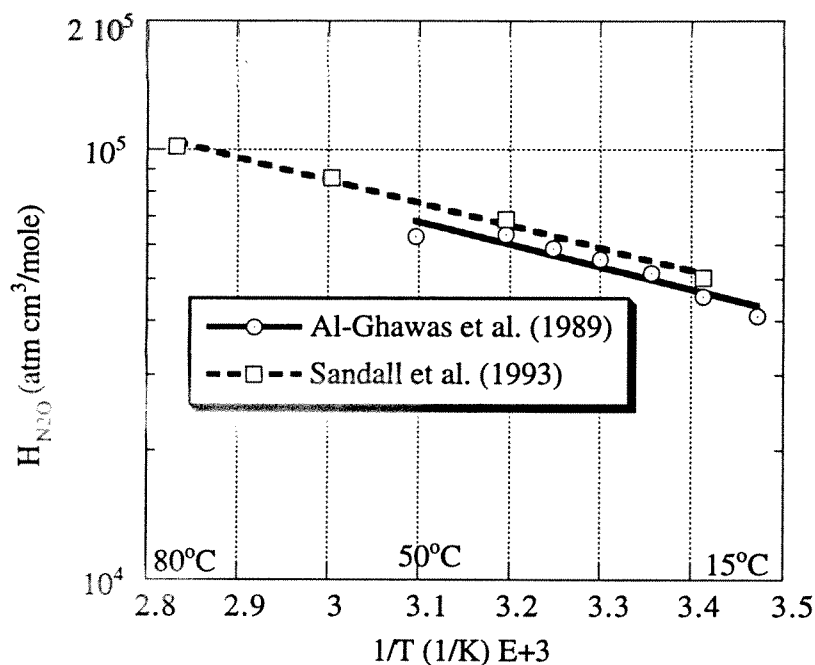


Figure B.8. Henry's law constant of N₂O in 50wt% MDEA.

B.2. SYSTEM DGA-WATER-CO₂

Table B.3 summarizes the correlations and methods used to estimate the physical and transport properties for the system DGA-water-CO₂.

Table B.3. Correlations and Source of Data for Physical and Transport Properties for the System DGA-water-CO₂.

Property	Correlation/Data
Viscosity	Jefferson Chemical Company. Technical Bulletin (1970)
Density	Jefferson Chemical Company. Technical Bulletin (1970)
Diffusivity of CO ₂	Modified Stokes-Einstein Equation
Diffusivity of DGA	Hikita et al. (1981), Snijder et al. (1993)
Solubility of CO ₂	Littel (1991)

B.2.1. Viscosity of DGA Solutions

Figure B.9 represents the data used for viscosity of aqueous DGA solutions.

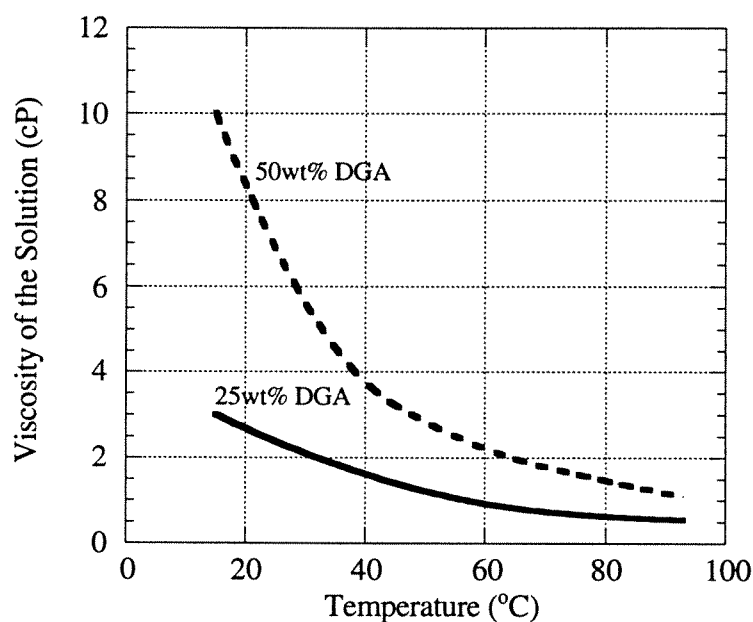


Figure B.9. Viscosity of aqueous DGA solutions. Jefferson Chemical Company. Technical Bulletin (1970).

B.2.2. Density of DGA Solutions

Figure B.10 depicts the data used for density of aqueous DGA solutions.

B.2.3. Diffusivity of CO₂ in the Solution

To the author's knowledge there is no published data on diffusivities of N₂O in aqueous DGA solutions, needed for the estimation of the diffusivity of CO₂ through the N₂O-CO₂ analogy. This transport property was estimated from the diffusion coefficient of CO₂ in water and using the modified Stokes-Einstein relation, that is,

$$D_{\text{CO}_2}^0 \mu^{0.6} = D_{\text{CO}_2} \mu_L^{0.6} \quad (\text{B.21})$$

This equation is equivalent to estimating the diffusion coefficient of N_2O in the aqueous DGA solution using the modified Stokes-Einstein relation and then using the N_2O - CO_2 analogy to get the diffusion coefficient of CO_2 in the solution. Versteeg et al. (1988) determined that a relationship equivalent to Equation B.21 can be used to correlate experimental data of diffusion coefficient of N_2O in aqueous solution of different reactive solvents like MDEA, DEA and DIPA.

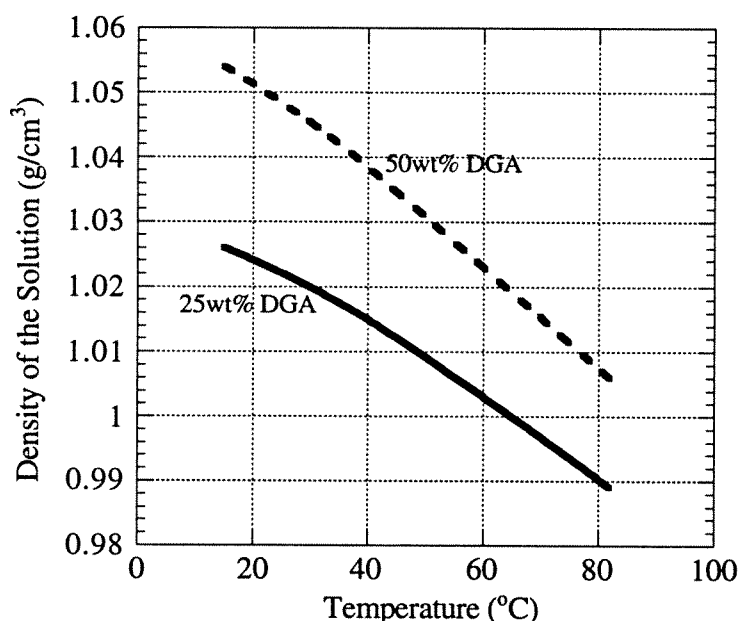


Figure B.10. Density of aqueous solutions of DGA. Jefferson Chemical Company. Technical Bulletin (1970).

B.2.4. Diffusivity of DGA in DGA Solutions

Experimental data for diffusion coefficients of DGA in DGA solutions are scarce. Hikita et al. (1981) measured diffusivities of DGA at 25°C in different aqueous DGA solutions. Since DGA and DEA have the same molecular weight,

diffusion coefficients of these two species can be compared. Figure B.11 compares the experimental measurements of diffusion coefficients of DEA by Snijder et al. (1993) and those of DGA measured by Hikita et al. (1981) at 25°C. From this figure it can be seen that the diffusivities of DEA and DGA are fairly close.

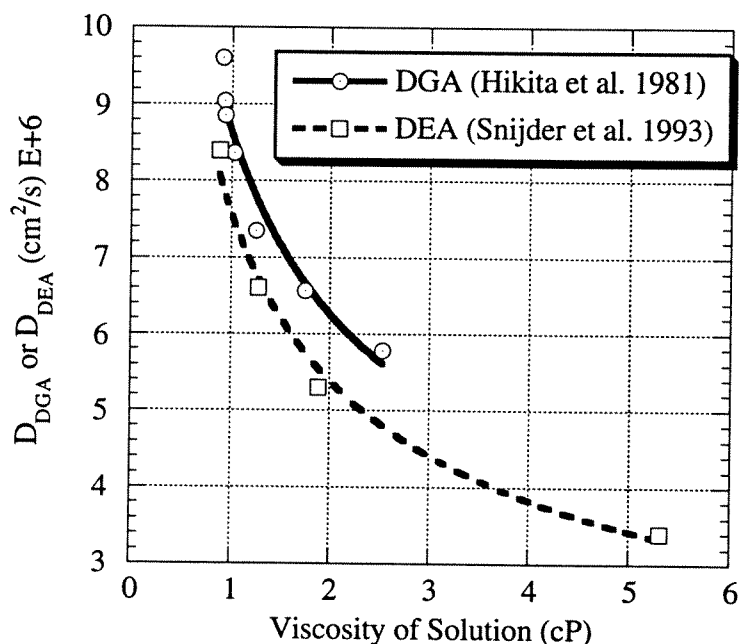


Figure B.11. Diffusion coefficients of DEA and DGA at 25°C.

Since Hikita and coworkers measured the diffusion coefficients of DGA in DGA solutions up to around 30wt% varying in this way the viscosity of the solution, it is possible to correlate those data using a modified Stokes-Einstein equation. Although only data at 25°C are available, the Stokes-Einstein relation indicates that diffusivity varies linearly with absolute temperature. The following equation was obtained from the data reported by Hikita et al. (1981):

$$D_{DGA} \text{ (cm}^2\text{/s)} = 2.868\text{E-}8\mu^{-0.449}T(\text{K}) \quad (\text{B.22})$$

Figure B.12 shows that there is a fairly good agreement between the diffusivities of DEA measured by Snijder et al. (1993) and the predictions of Equation B.22 at temperatures larger than 25°C, corroborating that DEA and DGA have similar diffusivities at a given temperature and viscosity of the solution.

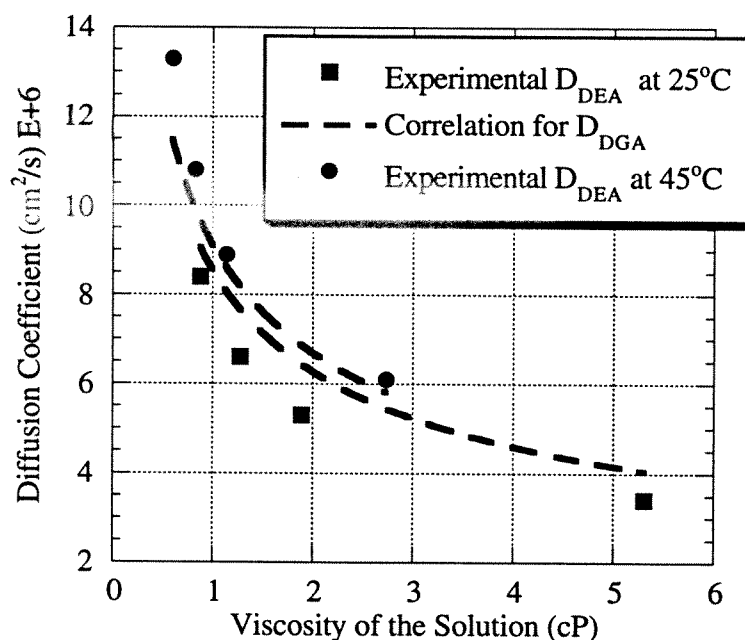


Figure B.12. Comparison between the experimental diffusivities of DEA and the predicted diffusivities of DGA.

B.2.5. Solubility of CO₂ in the Solution

Experimental data of solubility of N₂O in aqueous DGA solutions are very limited as well. Littel (1991) measured solubilities of N₂O in aqueous DGA solutions up to about 35wt% DGA (65wt% only at 25°C) and from 25 to 60°C. Using the Henry's constant of N₂O in DGA solutions from this source and the

$\text{N}_2\text{O-CO}_2$ analogy, the Henry's constant of CO_2 in the solution was estimated. These experimental data are depicted in Figure B.13. This figure indicates that the Henry's constant of CO_2 in the solution is only 5 to 20% larger than that in water and that this difference decreases as temperature increases.

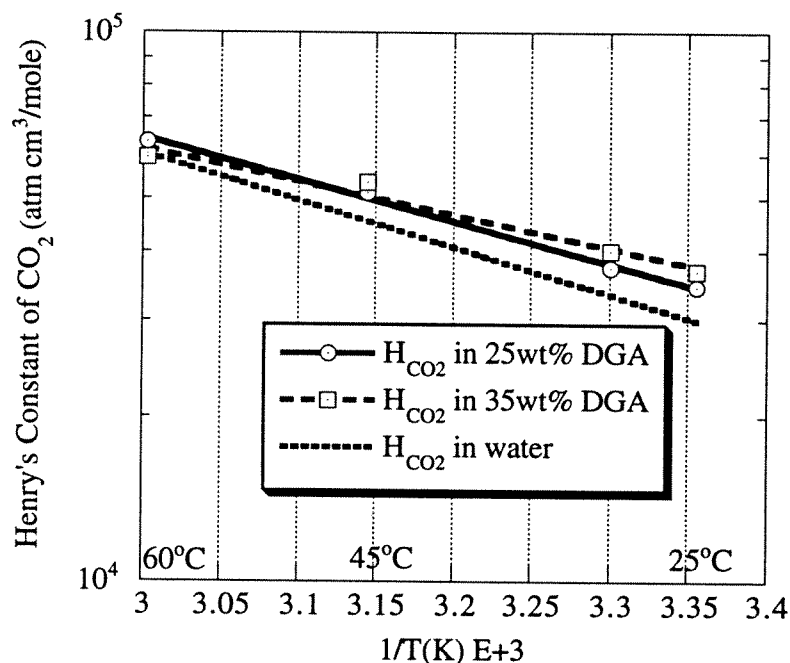


Figure B.13. Henry's constant of CO_2 in aqueous DGA solutions. Calculated using experimental data for $H_{\text{N}_2\text{O}}$ from Littel (1991) and the $\text{N}_2\text{O-CO}_2$ analogy.

B.3. SYSTEM DGA-MDEA-WATER- CO_2

Due to the lack of data for the physical and transport properties for the blended solvent system DGA/MDEA, the properties of a 50wt% MDEA solution were used for the analysis of the rate data obtained for the system 5wt% DGA-45wt% MDEA/50wt% water and 15wt% DGA-35wt% MDEA/50wt% water.

B.4. PROPERTIES FOR THE VAPOR PHASE

B.4.1. Diffusion Coefficient of CO₂

The diffusivity of CO₂ in the gas phase was estimated using the Chapman-Enskog equation derived from the theory describing diffusion in binary gas mixtures at low to moderate pressure. When analyzing the rate data measured in the wetted-wall reactor, the effect of water vapor on the diffusion of CO₂ was neglected. Therefore, only the binary diffusion coefficient of CO₂ in nitrogen was needed. The Chapman-Enskog equation for the binary mixture CO₂-N₂ is as follows (Reid et al., 1988):

$$D_{\text{CO}_2}^E (\text{cm}^2/\text{sec}) = 1.858 \times 10^{-23} \frac{T^{3/2}}{P_{\text{tot}} \sigma_{\text{CO}_2\text{-N}_2}^2 \Omega_D} \left[\frac{1}{M_{\text{CO}_2}} + \frac{1}{M_{\text{N}_2}} \right]^{1/2} \quad (\text{B.23})$$

In Equation B.23, Ω_D is the collision integral for diffusion, it is a function of temperature and depends upon the choice of the intermolecular force law between colliding molecules. $\sigma_{\text{CO}_2\text{-N}_2}$ is a characteristic length which also depends upon the intermolecular force law selected.

The Lennard-Jones 12-6 potential is a commonly used correlation relating the intermolecular energy between two molecules to the distance of separation. This potential is a function of a characteristic energy ϵ and a characteristic length σ . For a binary system with components A and B it can be shown that Ω_D is a function only of kT/ϵ_{AB} . The interaction values of σ_{AB} and ϵ_{AB} can be calculated from σ and ϵ of each species by the following rules (Reid et al., 1988):

$$\sigma_{AB} = \frac{\sigma_A + \sigma_B}{2} \quad \text{and} \quad \epsilon_{AB} = \sqrt{\epsilon_A \epsilon_B} \quad (\text{B.24})$$

The values of σ_i and ϵ_i are tabulated for the 12-6 Lennard-Jones potential for a variety of components. Also, the values of Ω_D are tabulated as a function of kT/ϵ_{AB} (Bird et al., 1960; Reid et al., 1988). For CO_2 and N_2 the following values have been reported:

$$\begin{aligned}\sigma_{\text{N}_2} &= 3.798 \text{ \AA}; & \sigma_{\text{CO}_2} &= 3.941 \text{ \AA} \\ \epsilon_{\text{N}_2}/k &= 71.4 \text{ K}; & \epsilon_{\text{CO}_2}/k &= 195.2 \text{ K}\end{aligned}$$

and the following interaction values are obtained:

$$\sigma_{\text{CO}_2\text{-N}_2} = 3.87 \text{ \AA} \quad \text{and} \quad \epsilon_{\text{CO}_2\text{-N}_2}/k = 118.06 \text{ K}.$$

For the range of temperature of interest in this dissertation $\epsilon_{\text{CO}_2\text{-N}_2}/kT$ varies from 2.52 to 3.16, which gives values of Ω_D from 0.99 to 0.94.

B.4.2. Density of the Gas Phase

The molar density of a gas, ρ^g , can be expressed as follows:

$$P_{\text{tot}} = Z\rho^g RT \quad (\text{B.25})$$

where the compressibility factor Z accounts for the nonideality of the vapor phase. Z depends upon the reduced temperature and pressure of the gas phase. For the experimental conditions used in the wetted-wall column reactor, the situation that could lead to a nonideality of the vapor phase is that where the pressure in the reactor approaches the highest possible, that is around 100 psig (7.8 atm). At this extreme pressure and for temperatures from 25 to 100°C, the departure from ideality of the gas phase is of the order of 2 to 3%. Therefore, the gas phase can be assumed as ideal and the molar density can be calculated as:

$$\rho^g = \frac{P_{\text{tot}}}{RT} \quad (\text{B.26})$$

B.4.2. Viscosity of the Gas Phase

In the model presented in Chapter 4 to describe the gas-film mass transfer coefficient, k_g is independent of the viscosity of the gas. However, in order to estimate the magnitude of the Schmith and Reynolds number of the gas phase in the wetted-wall column reactor, the values of viscosity of CO_2 and N_2 reported by Reid et al. (1988) were used. Table B.4 indicates experimental viscosity data.

Table B.4. Experimental values of viscosity of CO_2 and N_2 (Source: Reid et al. 1988).

Temp. ($^{\circ}\text{C}$)	$\mu_{\text{CO}_2}^g$ (μP)	Temp. ($^{\circ}\text{C}$)	$\mu_{\text{N}_2}^g$ (μP)
20	146.6	20	175.8
37	154.0	50	188.0
127	194.0	71	197.5

The viscosities of CO_2 shown in Table B.4 were used to determine the order of magnitude of the Schmith and Reynolds number of the gas phase. Linear interpolation in temperature was used due to the relatively weak temperature dependence in the temperature range of interest.

B.5. NOMENCLATURE

- b_i : bulk thermal expansivity of species i ($1/\text{K}$). Used in Equation B.9.
 D_i : Fickian diffusion coefficient of species i (cm^2/sec).
 H : Henry's constant ($\text{atm cm}^3/\text{mol}$).
 k : Boltzmann's constant ($1.380\text{E-}16$ erg/(molecule K)).
 M_i : Molecular weight of species i .
 P_{tot} : Total pressure (atm).
 R : Gas constant (82.057 atm $\text{cm}^3/(\text{K mole})$).

T: Temperature (K).

V_i^0 : specific volume of component i (cm^3/g). Used in Equation B.9.

wf: Weight fraction.

Z: Compressibility factor [-].

Greek Symbols:

ϵ_{AB} : Maximum attractive energy between molecules A and B (erg/molecule).

μ : Viscosity (cP or kg/sec m).

ρ : Density (g/cm^3 or mole/ cm^3).

σ_{AB} : Collision diameter between molecules A and B (\AA).

Ω_D : Collision integral for diffusion [-].

Superscripts:

o: Property for pure water or reference temperature in Equation A.9.

Subscripts:

Am2: Property for the second amine in Equation A.9.

CO₂: Evaluated for CO₂.

g: For the gas or vapor phase.

L: For the liquid phase.

N₂: Evaluated for N₂.

N₂O: Evaluated for N₂O.

w: Evaluated for water.

B.5. REFERENCES

- Al-Ghawas, H. A., Hagewiesche, D. P., Ruiz-Ibanez, G., Sandall, O. C., "Physicochemical Properties Important for Carbon Dioxide Absorption in Aqueous Methyldiethanolamine," *J. Chem. Eng. Data*, **1989**, 34, 385.
- Bird, R. B., Stewart, W. E., Lightfoot, E. N., *Transport Phenomena*, Wiley, New York, 1960.
- Glasscock, D. A., "Modelling and Experimental Study of Carbon Dioxide Absorption into Aqueous Alkanolamines." Ph.D Dissertation, The University of Texas at Austin, 1990.
- Hagewiesche, D. P., Ashour, S. S., Sandall, O. C., "Solubility and Diffusivity of Nitrous Oxide in Ternary Mixtures of Water, Monoethanolamine, and N-Methyldiethanolamine and Solution Densities and Viscosities," *J. Chem. Eng. Data*, **1995**, 40, 627.
- Hikita, H., Ishikawa, H., Murakami, T., Ishii, T., "Densities, Viscosities and Amine Diffusivities of Aqueous MIPA, DIPA, DGA and EDA Solutions". *Journal Chem. Eng. Japan.*, **1981**, 14, 411.
- Jefferson Chemical Company. Technical Service Information, 1970.
- Licht, S.E., Weiland, R. H., "Density and Physical Solubility of CO₂ in Partially Loaded Solutions of MEA, DEA and MDEA". Presented at the AIChE National Meeting **1989**, Paper No. 57f, Houston, Texas.
- Littel, R. J., "Selective Carbonyl Sulfide Removal in Acid Gas Treating Processes," Doctoral Dissertation. Twente University of Technology. The Netherlands, 1991.
- Reid, R. C., Prausnitz, J. M., Poling, B. E., *The Properties of Gases and Liquids*, McGraw-Hill, Singapore, 1988.
- Rinker, E. B., Oelschlager, D. W., Colussi, A. T., Henry, K. R., Sandall, O. C., "Viscosity, Density, and Surface Tension of Binary Mixtures of Water and N-Methyldiethanolamine and Water and Diethanolamine and Tertiary Mixtures of These Amines with Water over the Temperature Range 20-100°C," *J. Chem. Eng. Data*, **1994**, 39, 392.
- Sandall, O. C., Rinker, E. B., Ashour, S., "Acid Gas Treating by Aqueous Alkanolamines," Annual Report for the Gas Research Institute, 1993.

- Snijder, E. D., te Riele, M. J. M., Versteeg, G. F., van Swaaij, W.P.M., "Diffusion Coefficients of Several Aqueous Alkanolamine Solutions," *J. Chem. Eng. Data*, **1993**, 38, 475.
- Tamimi, A., Rinker, E. B., Sandall, O.C., "Diffusion Coefficients for Hydrogen Sulfide, Carbon Dioxide, and Nitrous Oxide in Water over the Temperature Range 293-368K," *J. Chem. Eng. Data*, **1994**, 39, 330.
- Versteeg, G. F., van Swaaij, W. P. M., "Solubility and Diffusivity of Acid Gases (CO_2 , N_2O) in Aqueous Alkanolamine Solutions," *J. Chem. Eng. Data*, **1988**, 33, 29.

Appendix C

Solution of Diffusion-Reaction Equations for Reactive Absorption: Parallel Reactions

C.1. APPROXIMATE SOLUTION

One of the purposes of this dissertation is the development of an approximate approach for modeling the mass transfer and chemical reaction processes that take place during reactive absorption. As it was described in Chapter 5, this approach, although approximate, is based on first principles and can be used for the integrated modeling of reactive absorption columns. This Appendix describes the details of the concepts and numerical methods used for the reaction-diffusion modeling.

Let us consider the general problem where gas A is transferred between the vapor and the liquid phase and two second-order reversible parallel reactions take place in the liquid phase:



The differential equation that governs the mass balance with diffusion and reaction in the liquid phase for component J is as follows:

$$D_J \frac{\partial^2 [J]}{\partial x^2} - \frac{\partial [J]}{\partial t} = -\nu_J R_J ; J = A, B, C, D, E, F, G \quad (C.3)$$

where R_J is the rate of reaction of component J. The rate of the chemical reactions C.1 and C.2 can be expressed as,

$$R_1 = k_{21}[A][B] - \frac{k_{21}}{K_1}[C][D] \quad (C.4)$$

$$R_2 = k_{22}[A][E] - \frac{k_{22}}{K_2}[F][G] \quad (C.5)$$

The initial condition for Equations C.3 is

$$\text{at } t = 0 \text{ and } x > 0, [J] = [J]_o, \quad (C.6)$$

where subscript o indicates conditions at the liquid bulk. It is assumed that chemical equilibrium holds at the liquid bulk. The boundary conditions for Equations C.3 are,

$$\text{at } x = \infty, [J] = [J]_o \quad (C.7)$$

and assuming that species other than A are non-volatile (flux at the interface is zero),

$$\text{at } x = 0 \text{ and } t > 0, [A] = [A]_i, \frac{\partial[B]}{\partial x} = \frac{\partial[C]}{\partial x} = \frac{\partial[D]}{\partial x} = \frac{\partial[E]}{\partial x} = \frac{\partial[F]}{\partial x} = \frac{\partial[G]}{\partial x} = 0 \quad (C.8)$$

When the Danckwerts surface renewal model of mass transfer is used to describe the hydrodynamics at the liquid film, the time-mean concentrations of the different species are given by the “s-multiplied” Laplace transform of instantaneous concentrations (Danckwerts, 1970; DeCoursey and Thring, 1989; DeCoursey, 1992):

$$[\bar{J}]_{(x)} = s \int_0^{\infty} [J]_{(x,t)} e^{-st} dt \quad (C.9)$$

where s is the rate of replacement of surface area for Danckwerts model. The mass transfer coefficient and diffusivity of component A are related with s by: $k_{L,A}^o = \sqrt{sD_A}$.

The following development shows how the solution of the diffusion-reaction problem is simplified by the introduction of the concept of time-mean

concentrations. In the description that follows it is assumed that the diffusion coefficients of components other than the diffusing gas are all the same, i.e., $D_B=D_C=D_D=D_E=D_F=D_G (=D_{pr})$.

In order to solve the diffusion-reaction problem described above, an approximate expression for the concentration profile of component A is needed. DeCoursey and Thring (1989) and DeCoursey (1992) proposed the following expression:

$$[\bar{A}] - [A]_o = ([\bar{A}]_i - [A]_o) \exp \left\{ -x E_A \sqrt{\frac{s}{D_A}} \right\} \quad (C.10)$$

This expression is exact for pseudo-first order reactions. For general second-order reactions it is correct in value and slope at the interface and liquid bulk, but deviates from the true profile in between. Equation C.10 can be used to determine the enhancement of the interfacial mass transfer of component A due to the chemical reactions. The diffusion-reaction equation for component A is,

$$D_A \frac{\partial^2 [A]}{\partial x^2} - \frac{\partial [A]}{\partial t} = (R_1 + R_2) \quad (C.11)$$

Applying the s-multiplied Laplace transform to Equation C.11, the following expression is obtained:

$$D_A \frac{d^2 [\bar{A}]}{dx^2} - s \{ [\bar{A}] - [A]_o \} = (\bar{R}_1 + \bar{R}_2) = (k_{21} [\bar{B}] + k_{22} [\bar{E}]) ([\bar{A}] - [\bar{A}]_{eq}) \quad (C.12)$$

where \bar{R} is the time-mean rate of reaction and $[A]_{eq}$ is the equilibrium concentration of species A which in this work is defined as the concentration of A that makes the overall rate equal to zero. When the concentration gradient given by expression C.10 is substituted into Equation C.12 and the resulting expression is evaluated at the vapor-liquid interface ($x=0$),

$$E_A^2 = 1 + \frac{(k_{21}[\bar{B}]_i + k_{22}[\bar{E}]_i) ([\bar{A}]_i - [\bar{A}]_{eq})}{s ([A]_i - [A]_o)} \quad (C.13)$$

Equation C.13 can be written in terms of dimensionless variables,

$$E_A = \sqrt{1 + (\beta_1 Ha_1^2 + \beta_2 Ha_2^2)(1 - \theta)} \quad (C.14)$$

where the following dimensionless variables have been defined:

$$Ha_1^2 = \frac{D_A k_{21} [B]_o}{k_{L,A}^o{}^2}; \quad Ha_2^2 = \frac{D_A k_{22} [E]_o}{k_{L,A}^o{}^2}; \quad \beta_1 = \frac{[\bar{B}]_i}{[B]_o}; \quad \beta_2 = \frac{[\bar{E}]_i}{[E]_o} \quad \text{and} \quad (C.15)$$

$$\theta = \frac{[\bar{A}]_{eq,i} - [A]_o}{[A]_i - [A]_o}$$

The Hatta number (Ha) is a measure of the ratio of the reaction to diffusion times, β quantifies the depletion of the liquid phase reactants at the interface, and θ indicates the approach to equilibrium at the interface.

Reactions C.1 and C.2 indicate that components C and F (or D and G) can be considered as chemically combined forms of component A. Therefore, combining the diffusion-reaction equations for species A, C and F, a relationship for the mass balance of *total* A can be found. Considering that the reaction rates of component A, C and F are $R_A = -(R_1 + R_2)$, $R_C = R_1$, and $R_F = R_2$, when the diffusion-reaction equations for these components are added, the following relationship is obtained

$$D_A \frac{\partial^2 [A]}{\partial x^2} + D_P \frac{\partial^2 \{[C] + [F]\}}{\partial x^2} = \frac{\partial [A]}{\partial t} + \frac{\partial \{[C] + [F]\}}{\partial t} \quad (C.16)$$

Following the procedure described in Chapter 5, Equation C.16 can be solved giving,

$$\frac{[\bar{A}]_{T,i} - [A]_{T,o}}{[A]_i - [A]_o} = \frac{E_A (E_A + \sqrt{r_{pr}})}{E_A \sqrt{r_{pr}} + 1} \quad (C.17)$$

where $[A]_T = [A] + [C] + [F]$, $r_{pr} = D_p/D_A$.

The rest of the relationships needed to determine the interfacial concentrations and the mass transfer enhancement can be obtained by combining the diffusion-reaction equations such that the nonlinearity introduced by the reaction term is eliminated. For example, combining the diffusion-reaction equations for components B and D, the following relation is obtained:

$$D_p \frac{\partial^2 \{[B] + [D]\}}{\partial x^2} - \frac{\partial \{[B] + [D]\}}{\partial t} = 0 \quad (C.18)$$

Applying the s-multiplied Laplace transform to Equation C.18, it becomes,

$$D_p \frac{d^2 [\bar{U}]}{dx^2} - s([\bar{U}] - [U]_o) = 0 \quad (C.19)$$

where $[\bar{U}] = [\bar{B}] + [\bar{D}]$. The solution of Equation C.19 is:

$$[\bar{U}] = C_1 e^{-\sqrt{sD_p}x} + C_2 e^{\sqrt{sD_p}x} + [U]_o \quad (C.20)$$

Since $[\bar{U}]$ is finite as $x \rightarrow \infty$, and considering boundary condition C.8, $C_1 = C_2 = 0$. Therefore, Equation C.20 evaluated at the interface becomes:

$$[\bar{U}]_i - [U]_o = ([\bar{B}]_i - [B]_o) + ([\bar{D}]_i - [D]_o) = 0 \quad (C.21)$$

Because component D can be considered as a chemically combined form of component B, Equation C.21 can be visualized as the mass balance of *total* reactant B which establishes that the flux of B plus the chemically combined B is zero.

Similarly, the diffusion reaction equations for the other components can be combined leading to the following relationships:

$$([\bar{E}]_i - [E]_o) + ([\bar{F}]_i - [F]_o) = 0 \quad (C.22)$$

$$([\bar{C}]_i - [C]_o) + ([\bar{B}]_i - [B]_o) = 0 \quad (C.23)$$

$$([\bar{G}]_i - [G]_o) + ([\bar{E}]_i - [E]_o) = 0 \quad (C.24)$$

Equation C.22 can be visualized as the mass balance of total reactant E, while Equations C.23 and C.24 reflect the stoichiometry of the chemical reactions.

In order to completely define the problem an additional relationship is needed. This additional piece of information can be obtained from the approximate solution of the diffusion-reaction equation for one of the species in the system. For example, for component F:

$$D_F \frac{\partial^2 [F]}{\partial x^2} - \frac{\partial [F]}{\partial t} = -R_2 \quad (C.25)$$

Taking the s-multiplied Laplace transform the following equation is obtained,

$$D_F \frac{d^2 [\bar{F}]}{dx^2} - s\{[\bar{F}] - [F]_o\} = -\bar{R}_2 \quad (C.26)$$

At this point a key assumption has to be made: the time-mean average \bar{R}_2 in Equation C.26 is considered as an average reaction rate through the reaction zone, \bar{R}_2^{av} . With this assumption Equation C.26 can be solved giving:

$$[\bar{F}] - [F]_o = C_1 e^{\sqrt{s/D_F} x} + C_2 e^{-\sqrt{s/D_F} x} + \frac{\bar{R}_2^{av}}{s} \quad (C.27)$$

Since $[\bar{F}]$ is finite as $x \rightarrow \infty$, and considering boundary condition C.8, $C_1 = C_2 = 0$. Therefore, Equation C.27 becomes:

$$[\bar{F}] - [F]_o = \frac{\bar{R}_2^{av}}{s} \quad (C.28)$$

which when evaluated at the gas-liquid interface is:

$$[\bar{F}]_i - [F]_o = \frac{\bar{R}_{2(i)}}{s} = \frac{D_A k_{22} [\bar{E}]_i ([A]_i - [\bar{A}]_{eq,rxn2})}{k_{L,A}^2} \quad (C.29)$$

where $[\bar{A}]_{eq,rxn2}$ is the concentration of A that would be in equilibrium in reaction C.2 at the interface, i.e.,

$$[\bar{A}]_{eq,rxn1} = \frac{[\bar{F}]_i [\bar{G}]_i}{K_2 [\bar{E}]_i} \quad (C.30)$$

Equation C.29 can be written in terms of the dimensionless parameters that describe the chemical equilibrium of reaction C.2 and the mass transfer enhancement due to that reaction,

$$\frac{[\bar{F}]_i - [F]_o}{[A]_i - [A]_o} = Ha_2^2 \beta_2 \frac{([A]_i - [\bar{A}]_{eq,rxn2})}{([A]_i - [A]_o)} = Ha_2^2 \beta_2 (1 - \theta_2) \quad (C.31)$$

Equation C.29 indicates that the accumulation of the reaction product F at the interface is directly proportional to the gas-liquid contact time and the reaction rate, i.e.,

$$[\bar{F}]_i - [F]_o \sim t k_{22} [\bar{E}]_i ([A]_i - [\bar{A}]_{eq,rxn2}) \quad (C.32)$$

Equation C.29 is expected to be a better approximation the slower the reaction rate \bar{R}_2 , because under this condition the error introduced taking the average reaction rate would be less significant. Therefore, it is suggested that the approximate solution of the diffusion-reaction equation be performed either for species involved in the slower reaction or for species involved in the faster reaction, but eliminating the fast reaction rate.

In order to illustrate this last point, let us assume that reaction C.1 is a fast reaction and reaction C.2 is a slower reaction. If the reaction-diffusion equation for a component involved in reaction C.1 needs to be solved approximately, the rate for reaction C.1 has to be eliminated. For example, for components C and A:

$$D_c \frac{\partial^2 [C]}{\partial x^2} - \frac{\partial [C]}{\partial t} = -R_1 \quad (C.33)$$

$$D_A \frac{\partial^2 [A]}{\partial x^2} - \frac{\partial [A]}{\partial t} = R_1 + R_2 \quad (C.34)$$

Adding Equations C.33 and C.34,

$$D_A \frac{\partial^2 [A]}{\partial x^2} + D_c \frac{\partial^2 [C]}{\partial x^2} - \frac{\partial [A]}{\partial t} - \frac{\partial [C]}{\partial t} = R_2 \quad (C.35)$$

defining the variable $[Q] = [A] + [C]$, taking the s-multiplied Laplace transform, and considering the time-mean average reaction rate \bar{R}_2 as the average reaction rate through the reaction zone, \bar{R}_2^{av} , the following equation is obtained:

$$\frac{d^2 [\bar{Q}]}{dx^2} - \frac{s}{D_c} ([\bar{Q}] - [Q]_0) - \left(1 - \frac{1}{r_c}\right) \frac{d^2 [\bar{A}]}{dx^2} = \frac{\bar{R}_2^{av}}{D_c} \quad (C.35)$$

Equation C.35 can be solved using the concentration profile for component A (Equation C.10) and the following boundary conditions:

$$\text{at } x \rightarrow \infty, [Q]_0 = [A]_0 + [C]_0 \quad (C.36)$$

$$\text{at } x=0, \left. \frac{d[\bar{Q}]}{dx} \right|_{x=0} = \left. \frac{d[\bar{A}]}{dx} \right|_{x=0} + \left. \frac{d[\bar{C}]}{dx} \right|_{x=0} = -E_A \sqrt{\frac{s}{D_A}} ([A]_i - [A]_0) + 0 \quad (C.37)$$

The solution is:

$$[\bar{Q}] - [Q]_0 = C_1 e^{-\sqrt{\frac{s}{D_p}} x} + C_2 e^{-E_A \sqrt{\frac{s}{D_A}} x} - \frac{1}{s} \bar{R}_2^{av} \quad (C.38)$$

where,

$$\begin{aligned}
C_1 &= \frac{E_A \sqrt{r_{pr}} ([A]_i - [A]_o) (E_A^2 - 1)}{r_{pr} E_A^2 - 1} \\
C_2 &= \frac{\left(1 - \frac{1}{r_{pr}}\right) ([A]_i - [A]_o) E_A^2}{\left(E_A^2 - \frac{1}{r_{pr}}\right)}
\end{aligned} \tag{C.39}$$

Evaluating Equation C.38 at the interface, the following relation results:

$$\frac{[\bar{C}]_i - [C]_o}{[A]_i - [A]_o} = \frac{E_A^2 - 1}{E_A \sqrt{r_{pr}} + 1} - \frac{\bar{R}_{2(i)}}{s([A]_i - [A]_o)} = \frac{E_A^2 - 1}{E_A \sqrt{r_{pr}} + 1} - Ha_2^2 \beta_2 (1 - \theta_2) \tag{C.40}$$

It is important to note that only when the Hatta number is introduced in Equations C.29 or C.40, this development is restricted to second-order reversible reactions; otherwise it is valid for a general reaction kinetics.

In order to calculate the mass transfer enhancement of component A due to reactions C.1 and C.2, Equations C.17, C.21 through C.24 and either Equation C.31 or C.40 are solved simultaneously using Equation C.14 to describe the functionality of the enhancement factor E_A .

In order to illustrate the importance of using the slower reaction when approximating the solution of a diffusion-reaction equation like Equation C.26, the results of Equation C.40 were compared with those obtained when the fast reaction rate is used ,i.e., when Equation C.33 is solved giving:

$$\frac{[\bar{C}]_i - [C]_o}{[A]_i - [A]_o} = Ha_1^2 \beta_1 \frac{([A]_i - [\bar{A}]_{eq,rxn1})}{([A]_i - [A]_o)} = Ha_1^2 \beta_1 (1 - \theta_1) \tag{C.41}$$

The right-hand side of Equations C.40 and C.41 can be considered as the dimensionless interfacial rate of reaction C.1. For the case where $K_1=1000$, $Ha_1=50$, $Ha_2=5$ and K_2 varies from 0.5 to 1000, it was calculated that the

dimensionless interfacial rate of reaction C.1 calculated from Equation C.41 can be as much as 15 to 50 times larger than that calculated from Equation C.40. This leads to a much more significant depletion of reactant B as predicted by Equation C.41. Also, for low values of K_2 , numerical convergence is not achieved or negative concentration are predicted for components F and G when Equation C.41 is used. When Equations C.31 or C.40 are used, convergence is always achieved and when K_2 approaches zero the enhancement factor approaches an asymptote which corresponds to the enhancement due to reaction C.1 alone. The results obtained when Equation C.31 is used are within 2% of those obtained when Equation C.40 is used. These results will be presented in graphical form latter.

Glasscock and Rochelle (1993) proposed the use of a different approximation for predicting enhancement factors in reactive absorption. The proposed approach is based on the assumption that the flux of a given reaction product is proportional to the interfacial reaction rate and that proportionality constant, α , is independent on the reaction rate itself. For the reaction product F, this approximation is expressed as:

$$D_F([F]_i - [F]_o) \approx \alpha R_{F,i} \quad (C.42)$$

In order to avoid the calculation of the constant α , the ratio between the fluxes of different reaction products was calculated. For example, for species C and F, this ratio was expressed as:

$$\frac{D_F([F]_i - [F]_o)}{D_F([F]_i - [F]_o) + D_C([C]_i - [C]_o)} = \frac{R_{2,i}}{R_{2,i} + R_{1,i}} \quad (C.43)$$

This approximation was given the name of modified combined flux (MCFLUX). Equation C.43 would be equivalent to Equation C.31 or C.40

provided that the flux of component C is expressed in terms of the slower reaction rate (R_2 in this case) and the overall enhancement factor (Equation C.40). Otherwise, Equation C.43 will overpredict the depletion of the fast reacting component similarly to Equation C.41. In this work it was found that the use of Equation C.43 without the necessary care to express the faster reaction rate, leads to lack of convergence or negative concentrations as it was described above when Equation C.41 is used.

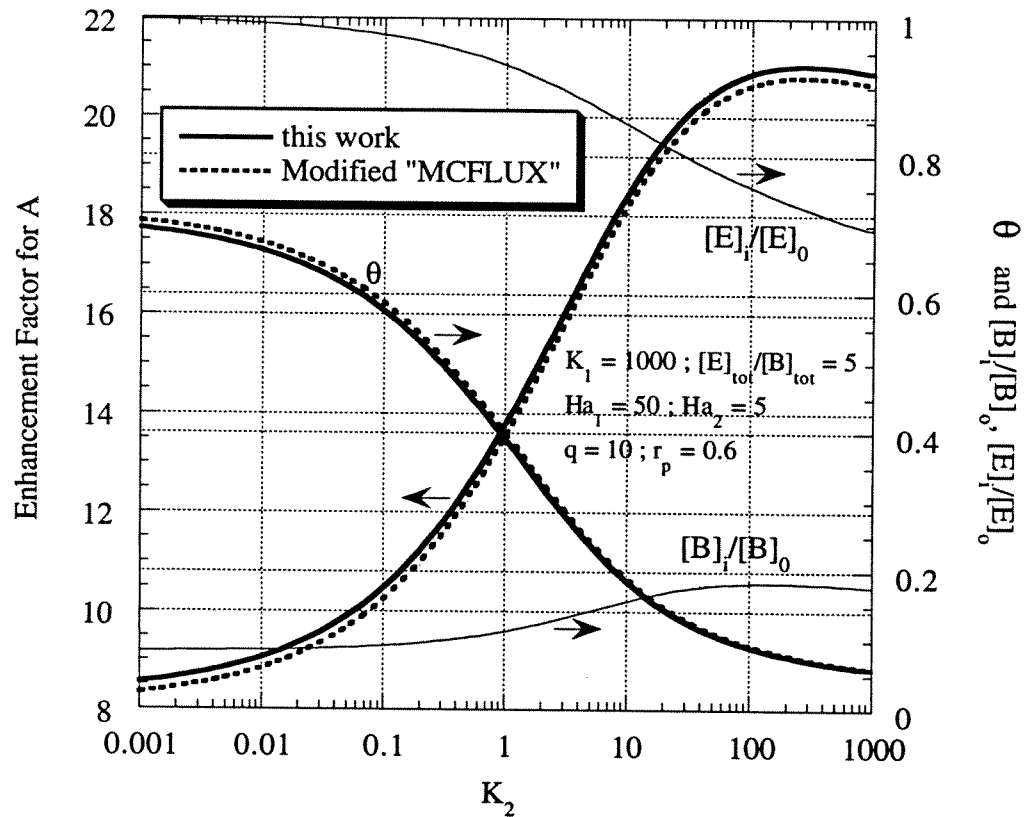


Figure C.1. Predictions of enhancement factors, liquid-phase reactant gradients and approach to equilibrium at the interface.

Considering the development that led to Equation C.31 or C.40, it is important to note that the use of the ratio of fluxes and reaction rates expressed in Equation C.43 appears to be unnecessary because using first principles the functionality of α in Equation C.42 can be determined. However, Equations C.31 or C.40 can be considered as modified forms of the MCFLUX approach because both approaches are based on the description of the fluxes of the reaction products in terms of the interfacial reaction rates.

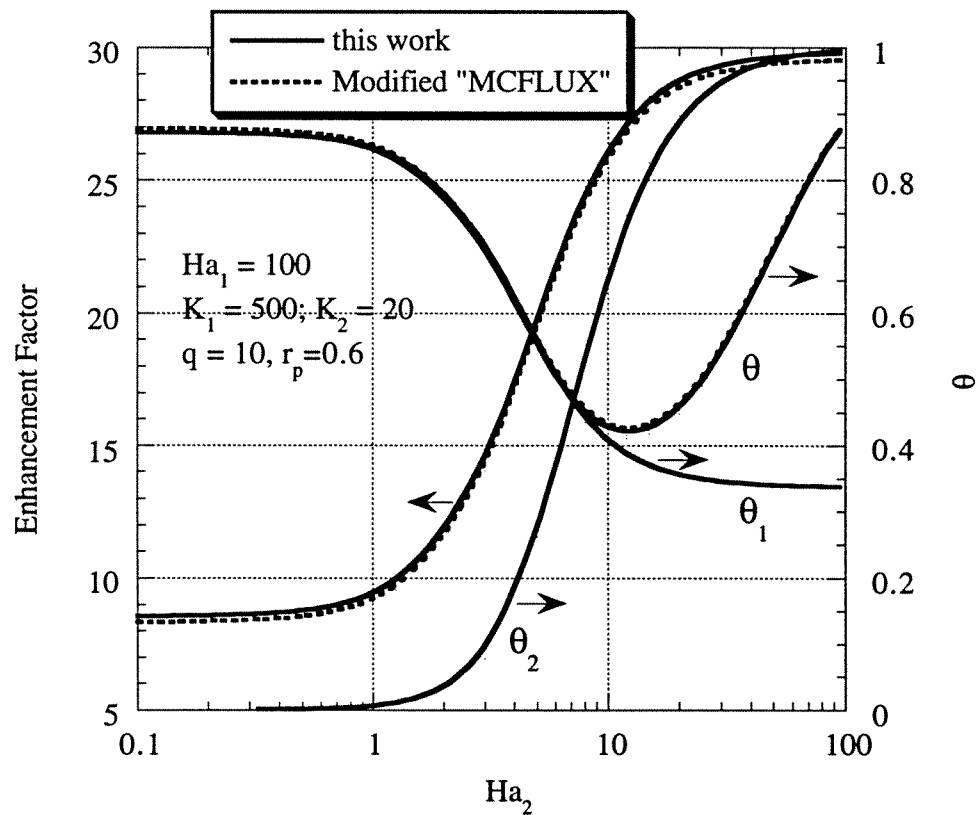


Figure C.2. Effect of the Hatta number for the slower reaction on the mass transfer enhancement and interfacial equilibrium.

In Figures C.1 and C.2 the results labeled as “modified MCFLUX” corresponds to the use of Equation C.31 while those labeled as “this work”

corresponds to the use of Equation C.40. For the example calculations described in Figure C.1, K_2 is varied for a fixed K_1 and the Hatta number for reaction C.1 was given a values ten times larger than that for reaction C.2.

Figure C.1 shows that the predictions of the mass transfer enhancement and equilibrium approach at the interface are quite close when Equations C.31 or C.40 are used. Also, an independent calculation of the mass transfer enhancement due to the single reaction C.1 (in the absence of reaction C.2) indicates that when $K_2 \rightarrow 0$ the predicted enhancement factors asymptotically approach the enhancement factor due to reaction C.1 with $Ha_1=50$ and $K_1=1000$.

Figure C.2 depicts the predicted effects of the Hatta number for the slower reaction on the overall mass transfer enhancement and on the partial and overall equilibria at the interface.

Figure C.2 shows that when Ha_2 approaches zero, the mass transfer enhancement for component A and the approach to equilibrium at the interface tend to asymptotic values corresponding to the case where only reaction C.1 occurs. The approach to equilibrium at the interface represented by the parameter θ shows an interesting behaviour. The minimum of the parameter θ is due to the interaction between the two equilibria. As Ha_2 increases, the accumulation of products of reaction 2 at the interface is more significant, increasing the effect of the reverse reaction and therefore, increasing the value of θ_2 to an asymptotic value of unity. On the other hand, as reaction C.2 becomes more important (Ha_2 increases), it starts to compete with reaction C.1 which leads to a lesser accumulation of products of reaction C.1 at the interface, and therefore, to a decrease of the importance of the reverse reaction (decrease of θ_1).

generally the “shooting” method is the most efficient technique for this type of situations. This method is based on the use of successive approximations to solve for the missing initial condition. This is implemented by initially assuming a value for the missing initial condition(s), solving the initial value problem to estimate the final boundary condition(s), and successively refining this process until the final boundary condition(s) are satisfied. An important advantage of the shooting method is that it can utilize highly efficient initial value algorithms such as LSODE. It is important to note that the missing initial condition for the diffusing gas A is the concentration gradient at the interface, while that for the other reactants and products are the interfacial concentrations.

Four situations were studied for the purpose of comparison of the numerical results and the approximate approach. These situations cover conditions where the reversibility of the chemical reactions and the diffusion of reactants and products significantly control the interfacial mass transfer enhancement for component A. Table C.1 presents the conditions and results for the situations studied.

Table C.1 Comparison between the numerical solution and approximate approach.

Case	Ha_1	Ha_2	K_1	K_2	E_A Numerical	θ Numerical	E_A Approx.	θ Approx.
1	50	10	1000	800	36.85	0.0101	32.82	0.0178
2	50	10	1000	2	21.57	0.155	16.60	0.382
3	100	3	500	20	16.44	0.581	14.28	0.703
4	100	0.2	500	20	9.87	0.754	8.57	0.871

In this work, the concentration of the diffusing gas that would be at equilibrium at the interface is calculated such that overall reaction rate is zero, that is,

$$\bar{R}_{1,i} + \bar{R}_{2,i} = k_{21}[\bar{A}]_{\text{eq},i}[\bar{B}]_i - \frac{k_{21}}{K_1}[\bar{C}]_i[\bar{D}]_i + k_{22}[\bar{A}]_{\text{eq},i}[\bar{E}]_i - \frac{k_{22}}{K_2}[\bar{F}]_i[\bar{G}]_i = 0 \quad (\text{C.44})$$

and Equation C.44 is solved for $[\bar{A}]_{\text{eq},i}$. Considering the definitions of θ , θ_1 , and θ_2 , the following relationship can be found:

$$\theta = \frac{Ha_1^2 \beta_1 \theta_1 + Ha_2^2 \beta_2 \theta_2}{Ha_1^2 \beta_1 + Ha_2^2 \beta_2} \quad (\text{C.45})$$

Equation C.45 describes the equilibrium interaction depicted in Figure C.2.

C.2. COMPARISON BETWEEN NUMERICAL AND APPROXIMATE SOLUTIONS

In order to quantify the accuracy of the approximate approach described in Section C.1 and used for the analysis of the experimental rate data in this dissertation, the system of differential equations represented by Equation C.3 were solved numerically. The s-multiplied Laplace transform was applied to these equations and the resulting differential equations with only the spatial coordinate as independent variable (see Equations C.12 or C.26) were solved numerically. LSODE (Livermore Solver for Ordinary Differential Equations; Hindmarsh, 1983) was used. This solver automatically adjusts the order of the method and step size based on stiffness and estimated local error during the integration.

The diffusion-reaction model to be solved is a boundary value problem where the boundary conditions given by Equations C.7 and C.8 have to be satisfied at the liquid bulk and at the interface. Hanna et al. (1995) indicated that

The results shown in Table C.1 indicate that the approximate approach underpredicts the mass transfer enhancement within 11 to 23%. This can be explained considering that the key assumption in the approximate approach is that the interfacial concentration of the liquid-phase reactants can be estimated using the interfacial reaction rate of the slower reaction (see Equations C.31 or C.40). This approximation leads to a predicted larger depletion of the liquid phase reactants. This in turns underpredicts the parameter $Ha_i\beta_i$ and overpredicts the effect of the reversible reactions (increases θ) in the enhancement factor model.

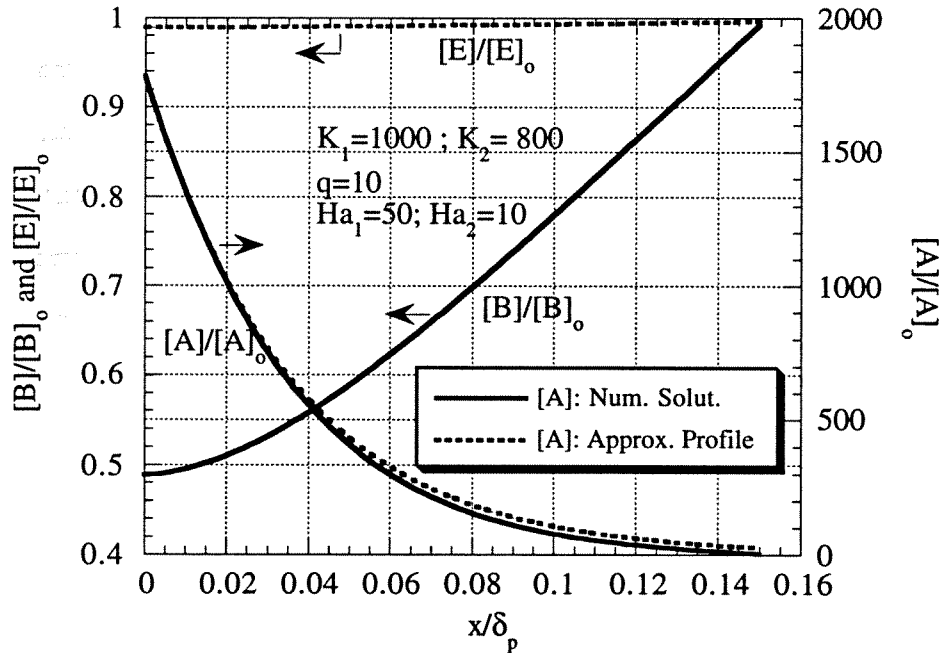


Figure C.3. Concentration gradients obtained from the numerical and approximate solutions. Case 1 presented in Table C.1. $\theta = 0.0101$.

Figure C.3 depicts the concentration profiles of reactants B and E calculated from the numerical solution, and also compares the concentration

profile of the diffusing gas with that predicted by the approximate method (Equation C.10). A dimensionless spatial coordinate was defined by:

$$x^d = \frac{x}{\delta_p} = \frac{x}{\sqrt{r_{pr}} \delta_A} = \frac{x}{\sqrt{r_{pr}}} \sqrt{\frac{s}{D_A}} \quad (C.46)$$

where δ_p is the film thickness for the reactants and products (except the diffusing gas) when it is calculated using film theory. It is important to note that the diffusion-reaction problem was solved using surface renewal theory, but a film thickness obtained from film theory is used to non-dimensionalize the independent variable.

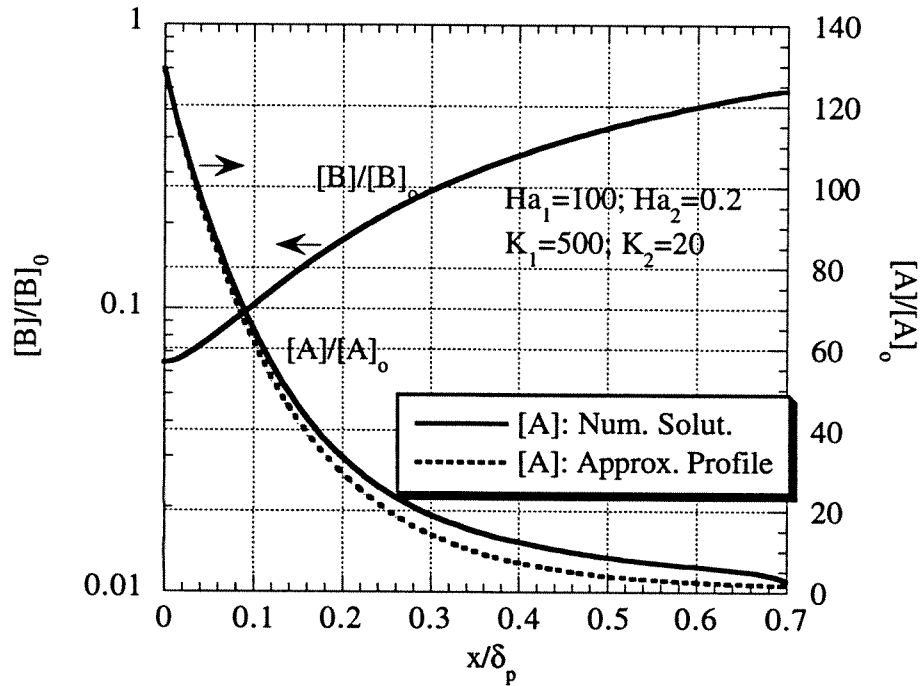


Figure C.4. Concentration gradients obtained from the numerical and approximate solutions. Case 4 presented in Table C.1. $\theta = 0.754$.

Figure C.3 indicates that a significant gradient for the fast reacting component (species B) is predicted. This figure also indicates that the

concentration profile for the diffusing gas estimated using the approximate gradient (Equation C.10) follows closely the profile obtained from the numerical solution.

Figure C.4 shows that for cases where the diffusion limitations and the importance of the reversibility are even more important, the concentration profile given by Equation C.10 is a good approximation of the more exact profile.

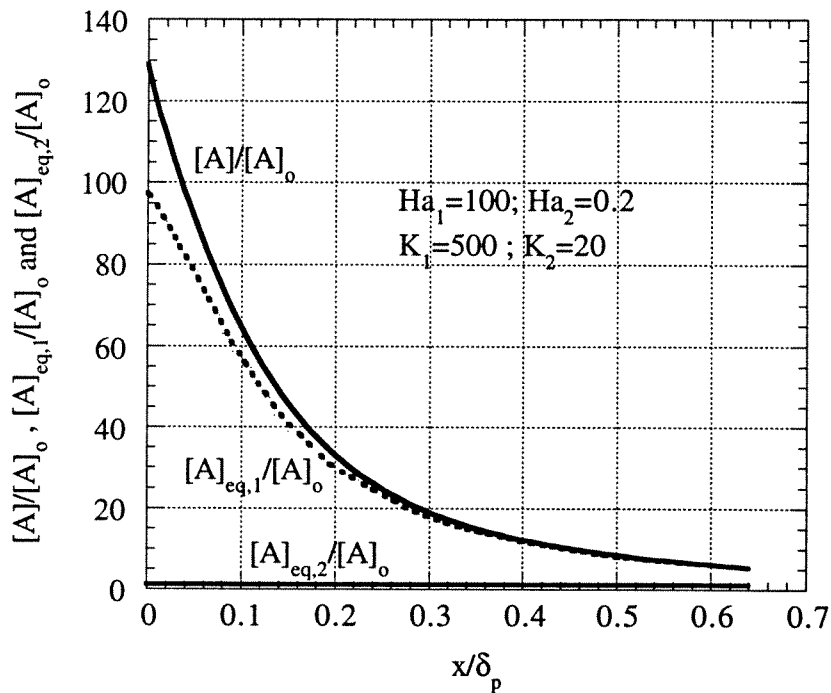


Figure C.5. Concentration gradient for the diffusing gas A and equilibrium concentrations for each reaction obtained from the numerical solution. Case 4 presented in Table C.1. $\theta = 0.754$.

Figure C.5 depicts the concentration profile for component A and the equilibrium concentrations for each reaction. This figure indicates that, for the conditions of Case 4, the approach to equilibrium is governed by the fast reaction while the concentration of component A in equilibrium in the slower reaction is

significantly lower. That is, Case 4 tends to approach the limiting condition of an instantaneous reversible reaction accompanied by a slow reaction. This situation resembles the actual reactive system studied in the present dissertation, the reactive absorption of CO_2 into aqueous mixtures of DGA and MDEA.

Figure C.6 represents the actual concentration profile and equilibrium concentrations for the diffusing gas for Case 2 indicated in Figure C.1. Since the importance of the reverse reaction rate is less significant ($\theta = 0.155$), the equilibrium concentrations are further apart from the actual profile of A and they tend to approach each other only towards the liquid bulk. Even for this case the approach to equilibrium is more significantly controlled by the faster reaction.

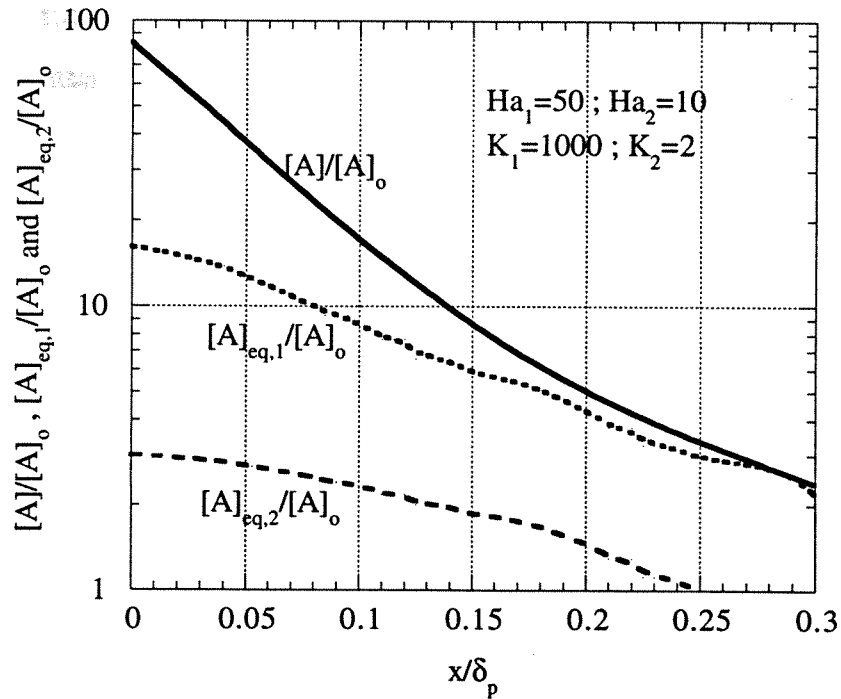


Figure C.6. Concentration gradient for the diffusing gas A and equilibrium concentrations for each reaction obtained from the numerical solution. Case 2 presented in Table C.1. $\theta = 0.155$.

The comparison presented above indicates that the approximate approach implemented in this dissertation to model reactive absorption when parallel reversible reactions take place is a reasonable approximation under a wide range of conditions particularly for the case when one of the reactions is significantly faster. It has been shown that this approach is a good approximation even for the case when the enhancement of the interfacial mass transfer is limited by the diffusion of reactants or the approach to equilibrium.

An important issue when analyzing parallel reversible reactions is the subtle interaction that leads to the regeneration of the faster reactant. Versteeg et al. (1990) addressed this issue showing that due to the presence of the slower reactant E the concentration of the faster reactant B near the interface can increase according to the following reaction that is obtained by combining reactions C.1 and C.2:



According to this reaction, near the boundary layer component B is regenerated by component E from the reaction products C and D leading to the simultaneous formation of the products F and G. This higher concentration of the faster reactant B decreases its diffusion limitation from the liquid bulk to the gas-liquid interface which in turn increases the enhancement of the mass transfer due to the faster reactant. Reaction C.47 is equivalent to the regeneration of free DGA from DGA carbamate that leads to the simultaneous formation of bicarbonate (see Equation 5.36).

Figure C.7 shows the effect of the slower reaction on the concentration of the faster reactant B in the reaction zone. It can be seen that as the Hatta number

for the second reaction increases, the ratio of the interfacial to bulk concentration increases reflecting the regeneration of B. This figure also indicates that as the Hatta number increases, the faster reaction (Equation C.1) is limited by the equilibrium in a lesser extent (θ_1 is closer to zero). This can be explained considering that as the slower reaction becomes more important, the accumulation of the reaction products C and D decreases to regenerate reactant B through Equation C.47.

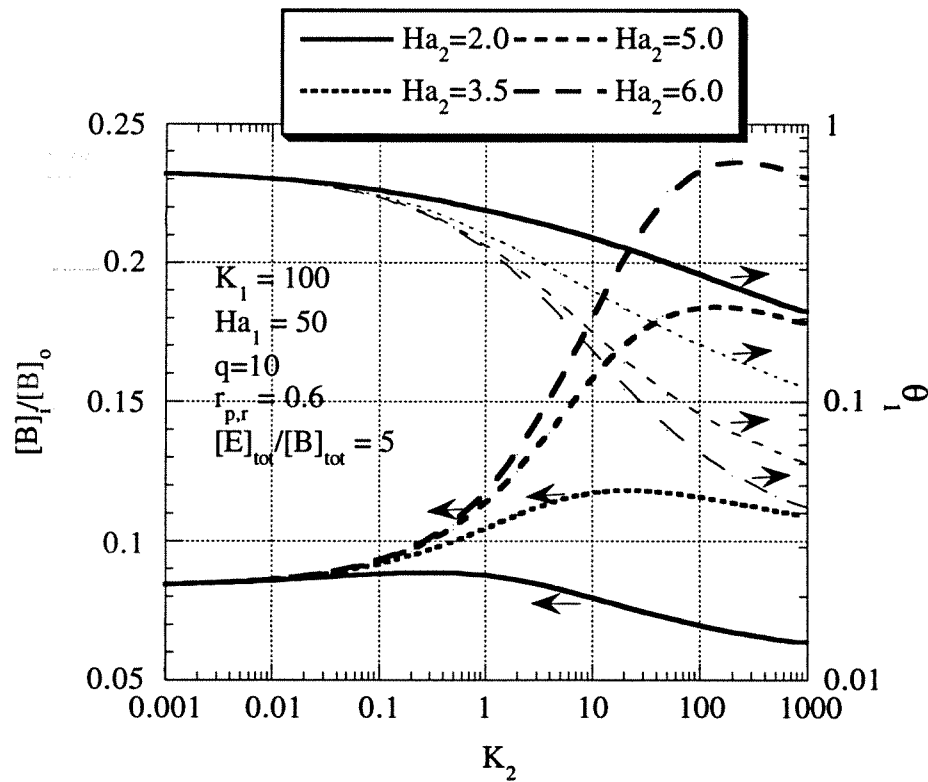


Figure C.7. Effect of the slower reaction on the regeneration of the faster reactant and equilibrium limitation for the faster reaction.

Figure C.8 depicts the enhancement of the interfacial mass transfer of A for the cases shown in Figure C.7. The increasing enhancement factors shown in

Figure C.8 reflects the direct effect of the slower reaction and its effect on the regeneration of B which tend to increase further the mass transfer enhancement.

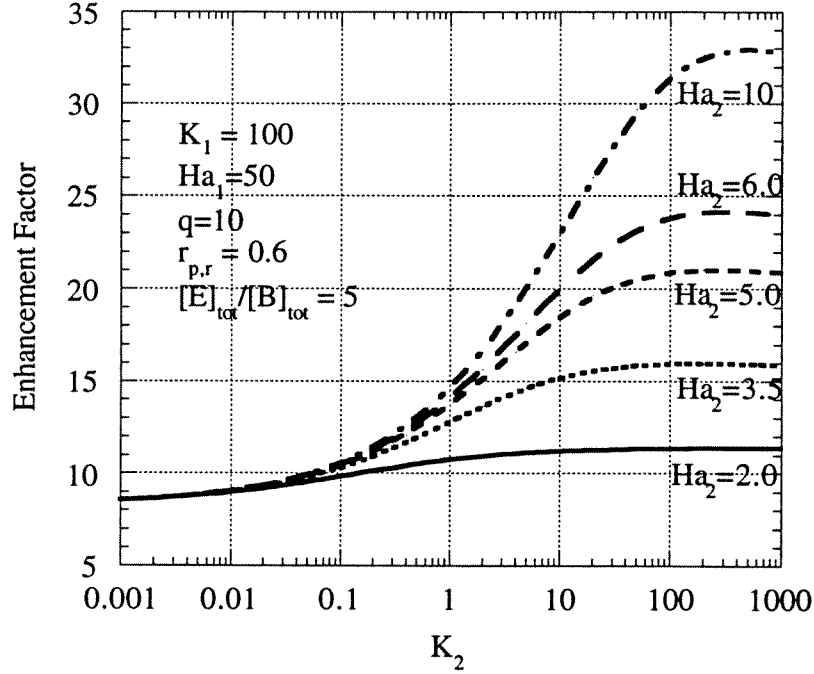


Figure C.8. Mass transfer enhancement of component A predicted by the approximate solution of the diffusion-reaction equations.

C.3. COMPARISON BETWEEN MCFLUX AND THIS WORK FOR THE SYSTEM DGA-MDEA-WATER-CO₂

The carbamate balance used in this work is given by Equation 5.29, which neglecting the CO₂-OH reaction becomes:

$$\frac{\Delta[\overline{RR'NCOO^-}]}{\Delta[\overline{CO_2}]} = \left(\frac{E^2 - 1}{1 + E\sqrt{r_{pr}}} \right) - \frac{1}{s} \{ k_{2t} [\overline{MDEA}]_i (1 - \theta_{MDEA}) \} \quad (C.48)$$

This equation can be written in terms of the flux of carbamate and total flux of CO₂ by multiplying the denominator by the enhancement factor and the proper combination of mass transfer coefficients:

$$\frac{N_{\text{DGACOO-}}}{N_{\text{CO}_2}} \frac{1}{\sqrt{r_{\text{pr}}}} = \frac{1}{E} \left(\frac{E^2 - 1}{1 + E\sqrt{r_{\text{pr}}}} \right) - \frac{1}{sE} \{k_{2t}[\overline{\text{MDEA}}]_i (1 - \theta_{\text{MDEA}})\} \quad (\text{C.49})$$

Considering the interfacial equilibrium, the enhancement factor can be directly expressed in terms of the interfacial reaction rates:

$$1 - \theta = \frac{\overline{R}_{\text{DGA},i} + \overline{R}_{\text{MDEA},i}}{([\text{CO}_2]_i - [\text{CO}_2]_o)(k_{2p}[\overline{\text{DGA}}]_i + k_{2t}[\overline{\text{MDEA}}]_i)} \quad (\text{C.50})$$

Substituting Equation C.50 into Equation 5.15a, the following is obtained:

$$E = \sqrt{1 + \left\{ \frac{\overline{R}_{\text{DGA},i} + \overline{R}_{\text{MDEA},i}}{([\text{CO}_2]_i - [\text{CO}_2]_o)} \right\} \frac{1}{s}} \quad (\text{C.51})$$

When the expression for E given by Equation C.51 is substituted into Equation C.49, the following is obtained upon rearrangement:

$$\frac{N_{\text{DGACOO-}}}{N_{\text{CO}_2}} = \sqrt{r_{\text{pr}}} \left[\frac{k_{2p}[\overline{\text{DGA}}]_i (1 - \theta_{\text{DGA}}) - \sqrt{r_{\text{pr}}} E k_{2t}[\overline{\text{MDEA}}]_i (1 - \theta_{\text{MDEA}})}{E^2 s \sqrt{r_{\text{pr}}} + Es} \right] \quad (\text{C.52})$$

If $E^2 \sqrt{r_{\text{pr}}} \gg E$ and substituting the expression for E² given by Equation C.51 in the denominator of Equation C.52:

$$\frac{N_{\text{DGACOO-}}}{N_{\text{CO}_2}} = \left[\frac{k_{2p}[\overline{\text{DGA}}]_i (1 - \theta_{\text{DGA}}) - \sqrt{r_{\text{pr}}} E k_{2t}[\overline{\text{MDEA}}]_i (1 - \theta_{\text{MDEA}})}{k_{2p}[\overline{\text{DGA}}]_i (1 - \theta_{\text{DGA}}) + k_{2t}[\overline{\text{MDEA}}]_i (1 - \theta_{\text{MDEA}})} \right] \quad (\text{C.53})$$

This form of writing Equation 5.29 resembles the MCFLUX approximation (Glasscock and Rochelle, 1993) which establishes that the ratio of the fluxes is equal to the ratio of the reaction rates:

$$\frac{N_{\text{DGACOO}^-}}{N_{\text{CO}_2}} = \frac{k_{2p}[\overline{\text{DGA}}]_i(1 - \theta_{\text{DGA}})}{k_{2p}[\overline{\text{DGA}}]_i(1 - \theta_{\text{DGA}}) + k_{2t}[\overline{\text{MDEA}}]_i(1 - \theta_{\text{MDEA}})} \quad (\text{C.54})$$

Equation C.54 would tend to overpredict the contribution of the flux of carbamate to the total CO_2 flux with respect to the prediction of Equation C.53.

C.4. SOLUTION OF THE DIFFUSION-REACTION EQUATION ASSUMING INSTANTANEOUS REACTION FOR THE FAST REACTION

When the time-mean concentration of the MDEA reaction given by Equation 5.41 is substituted into the s-multiplied Laplace transform of Equation 5.37, the following relation is obtained:

$$D_p \frac{\partial^2 [\overline{\text{DGACOO}^-}]}{\partial x^2} - s \{ [\overline{\text{DGACOO}^-}] - [\overline{\text{DGACOO}^-}]_0 \} = \lambda [\overline{\text{DGACOO}^-}] - \phi \quad (\text{C.55})$$

where:

$$\lambda = \frac{k_{2t}[\overline{\text{MDEAH}^+}]_i}{K_{\text{DM}}[\overline{\text{DGA}}]_i} \text{ and } \phi = \frac{k_{2t}[\overline{\text{MDEAH}^+}]_i[\overline{\text{HCO}_3^-}]_i}{K_{\text{MDEA,K}}} \quad (\text{C.56})$$

The solution of Equation C.55 is given by :

$$[\overline{\text{DGACOO}^-}] = C_1 \exp\left(-\sqrt{\frac{s+\lambda}{D_p}}x\right) + C_2 \exp\left(\sqrt{\frac{s+\lambda}{D_p}}x\right) + \frac{\phi + s[\overline{\text{DGACOO}^-}]_0}{s+\lambda} \quad (\text{C.57})$$

Since $[\overline{\text{DGACOO}^-}]$ is finite as $x \rightarrow \infty$, $C_2 = 0$. Also, using Equation 5.45 for the gradient of the carbamate concentration at the interface, C_1 can be determined:

$$C_1 = -\frac{\left(\frac{d[\overline{\text{DGACOO}^-}]}{dx}\right)_{x=0}}{\sqrt{\frac{s+\lambda}{D_p}}} \quad (\text{C.58})$$

Therefore, when the DGA-CO₂ reaction is assumed at equilibrium the carbamate concentration can be estimated by:

$$\overline{[\text{DGACOO}^-]}_i = \frac{\phi + s[\text{DGACOO}^-]_o}{s + \lambda} - \frac{\left(\frac{d[\text{DGACOO}^-]}{dx} \right)_{x=0}}{\sqrt{\frac{s + \lambda}{D_p}}} \quad (\text{C.59})$$

C.5. COMPARISON BETWEEN THE ENHANCEMENT FACTOR MODEL USED IN THIS WORK AND THAT USED BY GLASSCOCK AND ROCHELLE (1993)

Glasscock and Rochelle (1993) indicated that for a second order reversible reaction, like Equation C.1, an intuitive enhancement factor model that can be used is as follows:

$$E_A = 1 + \left\{ \sqrt{1 + \beta_1 \text{Ha}_1^2} - 1 \right\} (1 - \theta) \quad (\text{C.60})$$

where β_1 , Ha_1 and θ are given by Equations C.15. When the enhancement factor model represented by Equation C.60 is combined with the appropriate mass balances in the liquid boundary layer, the predicted enhancement factors are given in Figure C.9 for a given set of conditions. This figure compares the predicted enhancement factors for component A with those predicted by the model used in this dissertation (Equation C.14) which, for multiple reactions, constitutes an extension of the work documented by DeCoursey (1992).

Figure C.9 shows that for a wide range of values of the reaction equilibrium constant, the predictions of the two enhancement factor models differ by less than 5%. It is only for the limiting condition where the diffusivity of the reactant (component B) and reaction products is much slower than the diffusivity

of component A (diffusing gas), that the difference in the predictions between the two models become larger.

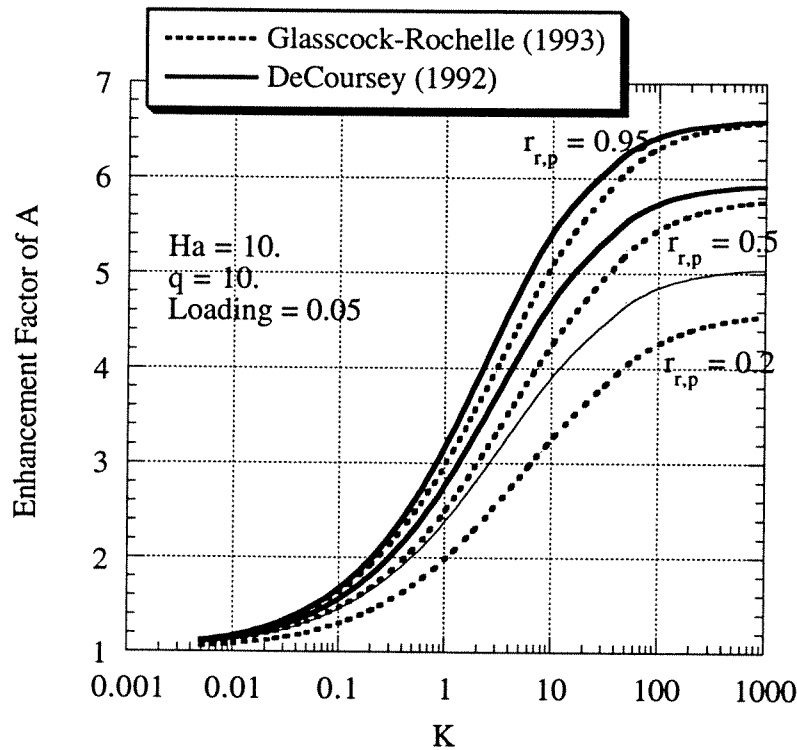


Figure C.9. Enhancement factors for component A predicted using the approach by DeCoursey (1992) and Glasscock and Rochelle (1993) for a second order reversible reaction. Varying equilibrium constant.

Figure C.10 compares the two enhancement factor models for a wide range of Hatta numbers. It shows that not only the enhancement factor, but also the depletion of the liquid phase reactant through the reaction zone (component B) and the approach to equilibrium at the interface (reflected on the parameter θ) are in good agreement between the two models. Figure C.10 also proves that the agreement is valid even for conditions where the reversibility of the reaction controls the mass transfer enhancement, that is when θ approaches unity. This is

an important issue because in this dissertation the enhancement factor model is tested even under the limiting condition where reversibility and diffusion of reactants and products significantly controls the mass transfer enhancement.

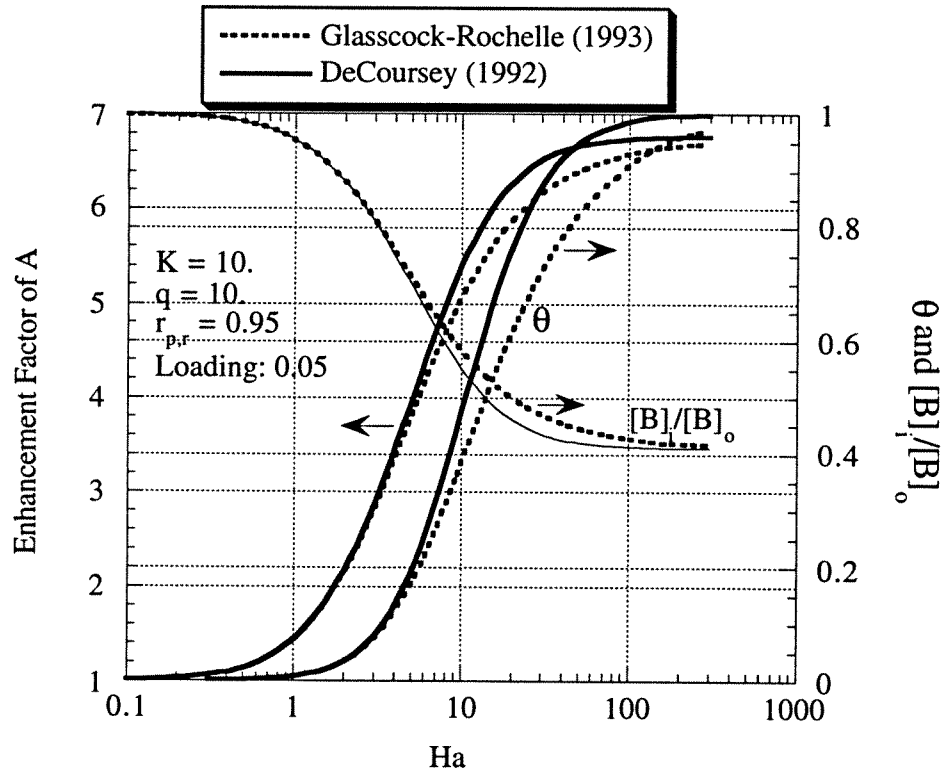


Figure C.10. Enhancement factors for component A predicted using the approach by Decoursey (1992) and Glasscock and Rochelle (1993) for a second order reversible reaction. Varying Hatta number.

C.6. NOMENCLATURE

[J]: Concentration of species J (kmoles/m³).

D: Diffusion coefficient (m²/sec or cm²/sec).

E: Enhancement factor.

Ha_i : Hatta number for reaction i (-).

k_{21} : Forward reaction rate constant for reaction C.1 ($m^3/kmol \text{ sec}$).

k_{22} : Forward reaction rate constant for reaction C.2 ($m^3/kmol \text{ sec}$).

$k_{L,i}^o$: Physical mass transfer coefficient of species i in the liquid phase (m/sec).

K_i : Concentration-based equilibrium constants for reactions i (-).

$$q = [B]_o / ([A]_i - [A]_o)$$

r_{pr} : Ratio of the diffusion coefficient of the reaction products to that of diffusing gas A.

R_i : Rate of reaction i ($kmol/m^3 \text{ sec}$).

s : Parameter in Danckwerts model ($1/sec$).

t : Time (sec).

x : Spatial coordinate in the liquid boundary layer (m).

Greek Symbols:

δ : Film thickness (m).

θ : Parameter in enhancement factor model.

Superscripts:

$[\bar{A}]$: Time-mean concentration of species A.

\bar{R} : Time-mean reaction rate ($kmol/m^3 \text{ sec}$).

Subscripts:

eq,i: In equilibrium at the interface.

eq,rxn1: In equilibrium with reaction C.1.

eq,rxn2: In equilibrium with reaction C.2.

i: For component i .

o: Evaluated at the liquid bulk.

p: Evaluated for the reaction products.

pr: Evaluated for reaction products and reactant (except diffusing gas A).

C.7. REFERENCES

- Danckwerts, P. V., *Gas Liquid Reactions*. McGraw-Hill Inc., New York, 1970.
- DeCoursey, W. J., "A Simpler Approximation for Enhancement of Mass Transfer by Second-Order Reversible Reaction," *ICHEME Symp. Ser.*, **1992**, 128, B269.
- DeCoursey, W. J., Thring, R. W., "Effects of Unequal Diffusivities on Enhancement Factors for Reversible and Irreversible Reaction," *Chem. Engng. Sci.*, **1989**, 44, 1715.
- Glasscock, D. A., Rochelle, G. T., "Approximate Simulation of CO₂ and H₂S Absorption into Aqueous Alkanolamines," *AIChE Journal.*, **1993**, 39, 1389.
- Hindmarsh, A. C., "Odepack, a Systematized Collection of ODE Solvers," *Scientific Computing*, **1983**, 55, Stepleman, R. S. et al. (eds.), North-Holland, Amsterdam.
- Versteeg, G.F., Kuipers, J.A.M., Van Beckum, F.P.H., Van Swaaij, W.P.M., "Mass Transfer with Complex Reversible Chemical Reactions-II. Parallel Reversible Chemical Reactions," *Chem. Engng. Sci.*, **1990**, 45, 183.

Appendix D

Equilibrium Calculations for the System DGA-MDEA-water-CO₂

Figures D.1 and D.2 depict the equilibrium partial pressures of CO₂ over a range of CO₂ loading for the system 50wt% MDEA, 5wt% DGA-45wt% MDEA and 15wt% DGA-35wt% MDEA using the electrolyte NRTL thermodynamic model. The interaction parameter $\tau(\text{water, DGACOO}^-\text{-MDEAH}^+)$ used in the calculations shown in this appendix is that determined in this work given in Figure 5.9.

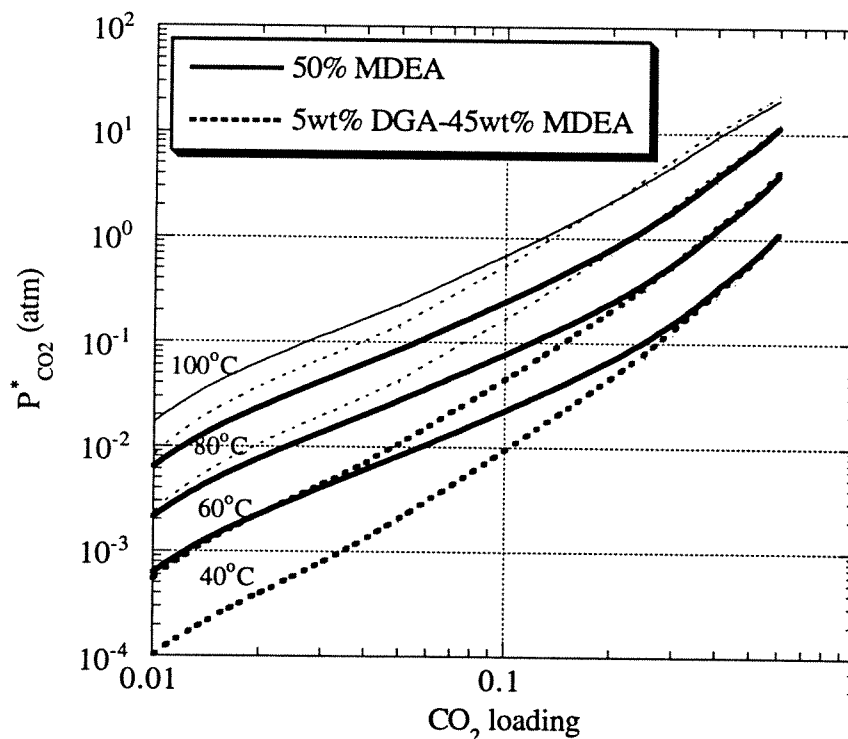


Figure D.1 Comparison between calculated equilibrium partial pressures of CO₂ for the systems 50wt% MDEA and 5wt% DGA-45wt% MDEA.

Figures D.1 and D.2 indicate that as temperature and CO₂ loading increase the effect of the presence of DGA of reducing the equilibrium partial pressure of CO₂ becomes less important. From the discussion given in Section 5.4.7 of Chapter 5 it can be seen that both the non-equilibrium and equilibrium effects of the presence of DGA on the interfacial mass transfer rate of CO₂ tend to decrease with increasing temperature and CO₂ loading.

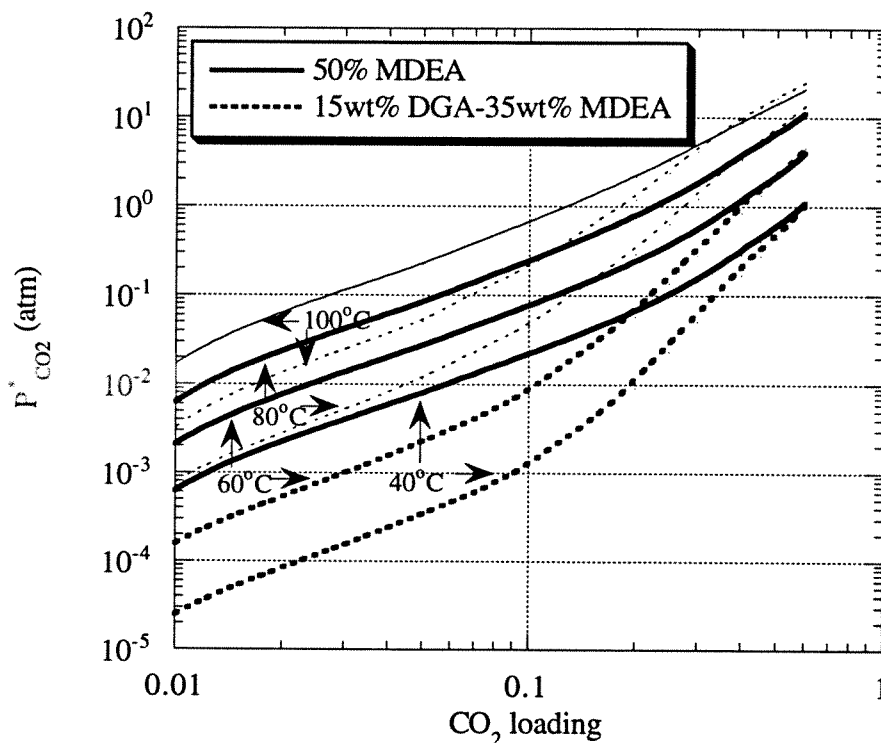


Figure D.2 Comparison between calculated equilibrium partial pressures of CO₂ for the systems 50wt% MDEA and 15wt% DGA-35wt% MDEA.

Figures D.3 and D.4 show the concentrations of free DGA and MDEA, respectively, as predicted by the electrolyte NRTL thermodynamic model for the systems 5 wt% DGA-45 wt% MDEA and 15 wt% DGA-35 wt% MDEA. These figures indicate that both temperature and CO₂ loading have a more pronounced

effect on the depletion of DGA than on that for MDEA. This larger depletion of DGA with respect to MDEA may be due to the more reactive nature of DGA with CO_2 .

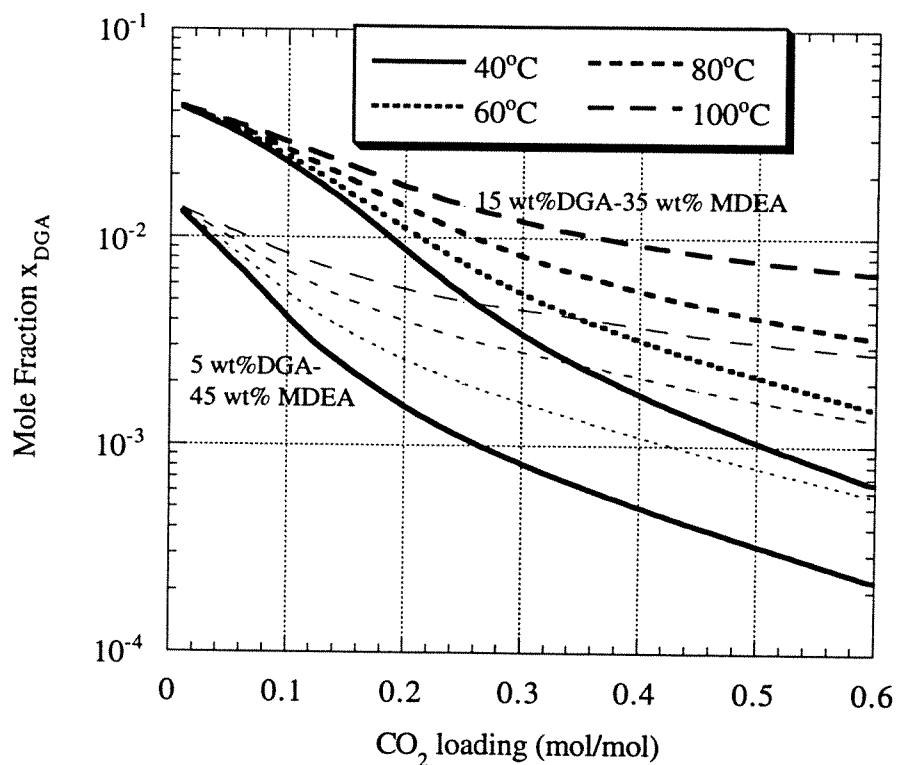


Figure D.3. Concentrations of free DGA for the systems 5 wt% DGA-45 wt% MDEA and 15 wt% DGA-35 wt% MDEA as predicted by the electrolyte NRTL model.

The electrolyte NRTL model also predicts that as temperature increases the depletion of DGA and MDEA is less significant with increasing loading. This is due to the fact that the reactions of DGA and MDEA with CO_2 are exothermic, and therefore the extent of the reactions decreases with increasing temperature leading to a lower depletion of DGA and MDEA.

The effect of temperature on the concentration of free DGA seen in Figures D.3 resembles the non-equilibrium effect represented in Figure 5.15. Since at higher temperature more DGA is in the form of free DGA, there is a tendency to achieve lower DGA gradients through the reaction zone because of the lower diffusion limitations.

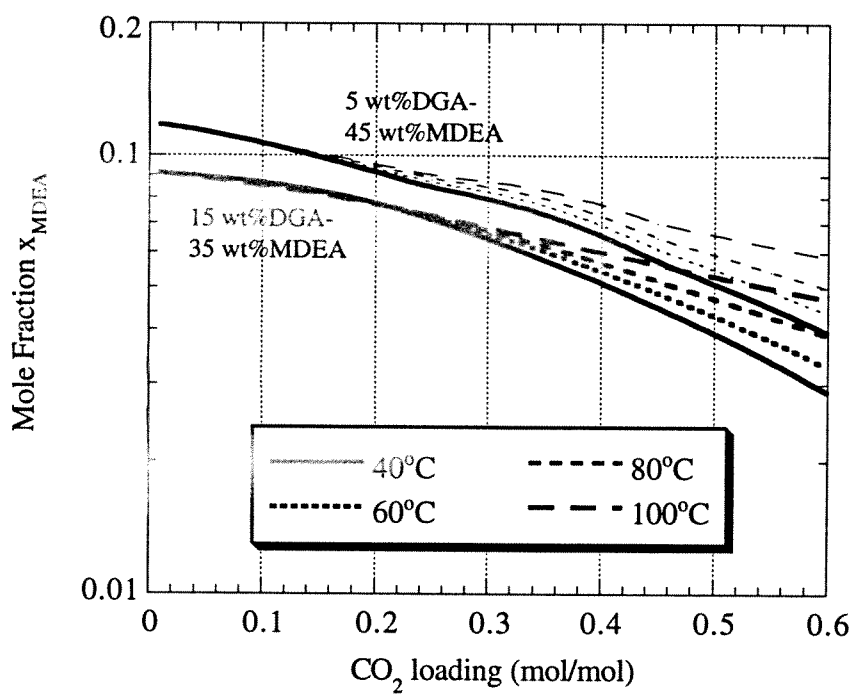


Figure D.4. Concentrations of free MDEA for the systems 5 wt% DGA-45 wt% MDEA and 15wt% DGA-35wt% MDEA as predicted by the electrolyte NRTL model.

References

- Abry, R. G. F., Dupart, M. S., "Amine Plant Troubleshooting and Optimization," *Hydrocarbon Processing*, April **1995**, 41.
- Al-Ghawas, H. A., Hagewiesche, D. P., Ruiz-Ibanez, G., Sandall, O. C., "Physicochemical Properties Important for Carbon Dioxide Absorption in Aqueous Methyldiethanolamine," *J. Chem. Eng. Data*, **1989**, 34, 385.
- Alper, E., "Kinetics of Reactions of Carbon Dioxide with Diglycolamine and Morpholine," *Chem. Engng. J.*, **1990**, 44, 107.
- Alper, E., "Kinetics of Reactions of Carbon Dioxide with Diglycolamine and Morpholine," *Chem. Engng. J.* **1990**, 44, 107.
- American Institute of Chemical Engineers (A.I.Ch.E). "Bubble-Tray Design Manual. Prediction of Fractionation Efficiencies," New York, 1958
- Astarita, G., Savage, D. W., "Gas Absorption and Desorption with Reversible Instantaneous Chemical Reaction," *Chem. Engng. Sci.* **1980**, 35, 10, 1755
- Astarita, G., Savage, D. W., Bisio, A., "*Gas Treating with Chemical Solvents*," Wiley: New York, 1983.
- Austgen, D. M., "A Model of Vapor-Liquid Equilibria for Acid gas-Alkanolamine-water Systems". Ph.D. Dissertation, The University of Texas at Austin, 1989.
- Billet, R. *Packed Towers in Processing and Environmental Technology*. VCH Verlagsgesellschaft: Weinheim, Federal Republic of Germany, 1995.
- Billet, R., Schultes, M. "Fluid Dynamics and Mass Transfer in the Total Capacity Range of Packed Columns up to the flood Point," *Chem. Eng. Technol.*, **1995**, 18, 371.
- Bird, R. B., Stewart, W. E., Lightfoot, E. N., *Transport Phenomena*, Wiley, New York, 1960.
- Blauwhoff, P.M.M., Versteeg, G.F., van Swaaij, W.P.M., "A Study of the Reaction Between CO₂ and Alkanolamines in Aqueous Solutions," *Chem. Engng. Sci.* **1984**, 39, 207. New York, 1960.
- Blauwhoff, P. M. M., Kamphuis, B., van Swaaij, W. P. W., Westerterp, K. R., "Absorber Design in Sour Natural Gas Treatment Plants: Impact of

- Process Variables on Operation and Economics," *Chem. Eng. Process.*, **1985**, 19,1.
- Blauwhoff, P.M.M., Versteeg, G.F., van Swaaij, W.P.M., "A Study of the Reaction Between CO₂ and Alkanolamines in Aqueous Solutions," *Chem. Engng. Sci.* **1984**, 39, 207.
- Blohm, C. L., Riesenfeld, F. C., U.S. Patent 2712978, July 12, 1955.
- Bravo, J. L., Shell Oil Company. Private Communication. 1998.
- Bravo, J. L., Fair, J. R., "Generalized Correlation for Mass Transfer in Packed Distillation Columns," *Ind. Eng. Chem. Process Des. Dev.*, **1982**, 21, 162.
- Brian, P., Vivian, J., Mayr, S., "Cellular Convection in Desorbing Surface Tension-Lowering Solutes from Water," *Ind. Eng. Chem. Fund.* **1971**, 10, 75.
- Browning, G. J., "Physical Solubility of Carbon Dioxide in Aqueous Alkanolamines Via Nitrous Oxide Analogy," Thesis, Department of Chemical Engineering. The University of Newcastle, Australia, 1993.
- Caracotsios, M., "Model Parametric Sensitivity Analysis and Nonlinear Parameter Estimation. Theory and Applications," Doctoral Dissertation, The University of Wisconsin - Madison, 1986.
- Carberry, J. J., *Chemical and Catalytic Reaction Engineering*. McGraw-Hill Inc., New York, 1976.
- Carey, T. R., "Rate-Based Modeling of Acid Gas Absorption and Stripping Using Aqueous Alkanolamine Solutions". M. S. Thesis, The University of Texas at Austin, 1990.
- Carey, T. R., Hermes, J. E., Rochelle, G. T., "A Model of Acid Gas Absorption/Stripping Using Methyldiethanolamine with Added Acid," *Gas Separation and Purification*, **1991**, 5, 95.
- Chakravarty, S., "Absorption of Carbon Dioxide in Aqueous Blends of Diethanolamine and Methyldiethanolamine". M. S. Thesis, The University of Texas at Austin, 1992.
- Chakravarty, T., Phukan, U. K., Weiland, R. H., "Reaction of Acid Gases with Mixtures of Amines," *Chem. Eng. Prog.* April **1985**, 81, 32.
- Chan, H., Fair, J. R., "Prediction of Point Efficiencies in Sieve Trays. 1. Binary Systems," *Ind. Eng. Chem. Process Des. Dev.*, **1984**, 23, 814.

- Chang, C. S., Rochelle, G. T., "Mass Transfer Enhanced by Equilibrium Reactions," *Ind. Eng. Chem. Fundam.* **1982**, 21, 379.
- Critchfield, J. E., "CO₂ Absorption/Desorption in Methyldiethanolamine Solutions Promoted with Monoethanolamine and Diethanolamine: Mass Transfer and Reaction Kinetics". Ph.D. Dissertation, The University of Texas at Austin, 1988.
- Critchfield, J. E., Rochelle, G. T., "CO₂ Absorption into Aqueous MDEA and MDEA/MEA Solutions," Presented at the AIChE National Meeting, Houston, Texas, March 1987.
- Danckwerts, P. V., *Gas Liquid Reactions*. McGraw-Hill Inc., New York, 1970.
- Danckwerts, P. V., "The Reaction of CO₂ with Ethanolamines," *Chem. Eng. Sci.* **1979**, 34, 443.
- Darton, R. C., "Distillation and Absorption Technology: Current Market and New Developments," *Trans. IChemE.* **1992**, 70 (Part A), 435.
- Darton, R. C., Hoek, P. J., Spaninks, J. A. M., Suenson, M. M., Wijn, E. F., "The Effect of Equipment on Selectivity in Amine Treating," I.Chem. E. Symposium Series, **1987**, No.104, A323.
- DeCoursey, W. J., "Enhancement Factors for Gas Absorption with Reversible Reaction," *Chem. Engng. Sci.* **1982**, 37, 1483.
- DeCoursey, W. J., "A Simpler Approximation for Enhancement of Mass Transfer by Second-Order Reversible Reaction," *IChemE. Symp. Ser.* **1992**, 128, B269.
- DeCoursey, W. J., Thring, R. W., "Effects of Unequal Diffusivities on Enhancement Factors for Reversible and Irreversible Reaction," *Chem. Engng. Sci.* **1989**, 44, 1715.
- Dhulesia, H., "Clear Liquid Height on Sieve and Valve Trays," *Chem. Eng. Res. Des.*, **1984**, 62, 321.
- Donaldson, T. L., Nguyen, Y. N., "Carbon Dioxide Reaction Kinetics and Transport in Aqueous Amine Membranes," *Ind. Eng. Chem. Fundam.* **1980**, 19, 260.
- Fair, J. R., "Comparing Trays and Packing," *Chem. Eng. Progress*, **1970**, 66, 45.
- Fair, J. R. "Stagewise Mass Transfer Processes". In "Scaleup of Chemical Processes". Bisio, A., Kabel, R.L. (Ed.), Wiley: New York, 1985.

- Fair, J. R. The University of Texas at Austin. Private Communication, 1997.
- Frank, M. J. W., Kuipers, J. A. M., Versteeg, G. F., Van Swaaij, W. P. M., "Modelling of Simultaneous Mass and Heat Transfer with Chemical Reaction Using the Maxwell-Stefan Theory-I. Model Development and Isothermal Study," *Chem. Engng. Sci.* **1995**, 50, 1645.
- Frank, M. J. W., Kuipers, J. A. M., Krishna, R., Van Swaaij, W. P. M., "Modelling of Simultaneous Mass and Heat Transfer with Chemical Reaction Using the Maxwell-Stefan Theory-II. Non-Isothermal Study," *Chem. Engng. Sci.* **1995b**, 50, 1661.
- Fujinawa, K., Hozawa, M., Imaishi, N., "Effects of Desorption and Absorption of Surface Tension-Lowering Solutes on Liquid-Phase Mass Transfer Coefficients at a Turbulent Gas-Liquid Interface," *J. Chem. Eng. Japan.* **1978**, 11, 107.
- Glasscock, D. A., "Modelling and Experimental Study of Carbon Dioxide Absorption into Aqueous Alkanolamines". Ph.D Dissertation, The University of Texas at Austin, 1990.
- Glasscock, D. A., Rochelle, G. T., "Numerical Solution of Theories for Gas Absorption with Chemical Reaction," *AIChE Journal* . **1989**, 35, 1271.
- Glasscock, D. A., Rochelle, G. T., "Approximate Simulation of CO₂ and H₂S Absorption into Aqueous Alkanolamines," *AIChE Journal*. **1993**, 39, 1389.
- Hagewiesche, D. P., Ashour, S. S., Al-Ghawas, H. A., Sandall, O. C., "Absorption of Carbon Dioxide into Aqueous Blends of Monoethanolamine and N-Methyldiethanolamine," *Chem. Engng. Sci.* **1995**, 50, 1071.
- Hagewiesche, D. P., Ashour, S. S., Sandall, O. C., "Solubility and Diffusivity of Nitrous Oxide in Ternary Mixtures of Water, Monoethanolamine, and N-Methyldiethanolamine and Solution Densities and Viscosities," *J. Chem. Eng. Data*, **1995**, 40, 627.
- Haimour, N., K., Sandall, O. C., "Absorption of Carbon Dioxide into Aqueous Methyldiethanolamine," *Chem. Eng. Sci.* **1984**, 39, 1791.
- Hanna, O., Sandall O., *Computational Methods in Chemical Engineering*. Prentice Hall. New Jersey, 1995.
- Hikita, H., Asai, S., Ishikawa, H., Honda, M., "The Kinetics of Reactions of Carbon Dioxide with Monoisopropanolamine, Diglycolamine and Ethylenediamine by a Rapid Mixing Method," *Chem. Engng. J.* **1977**, 14, 27.

- Hikita, H., Ishikawa, H., Murakami, T., Ishii, T., "Densities, Viscosities and Amine Diffusivities of Aqueous MIPA, DIPA, DGA and EDA Solutions," *Journal Chem. Eng. Japan*, **1981**, 14, 411.
- Hindmarsh, A. C., "Odepack, a Systematized Collection of ODE Solvers," *Scientific Computing*, **1983**, 55, Stepleman, R. S. et al. (eds.), North-Holland, Amsterdam.
- Hobler, T., *Mass Transfer and Absorbers*, Pergamon Press, Oxford, 1966.
- Hofhuis, P.A.M., Thesis (T.U. Delft), 1980. Cited by Zarzycki, R. and Chacuk, A. (1993).
- Hofhuis, P.A.M., Zuiderweg, F. J., "Sieve Trays: Dispersion Density and Flow Regimes," *Inst. Chem. Engrs. Symp. Series.*, **1979**, No. 56, 2.2/1.
- Imaishi, N., Suzuki, Y., Hozawa, M., Fujinawa, K., "Interfacial Turbulence in Gas-Liquid Mass Transfer." *Int. Chem. Eng.* **1982**, 22, 659.
- Jefferson Chemical Company. Technical Service Information, 1970.
- Kister, H. Z., *Distillation Design*, McGraw-Hill Inc., New York, 1992.
- Kister, H. Z., Larson, K. F., Yanagi, T., "Capacity and Efficiency: How Trays and Packings Compare," Presented at the AIChE Spring National Meeting, Houston, Texas, March 31, 1993. Paper 24c.
- Krishna, R., "A Film Model Analysis of Non-Equimolar Distillation of Multicomponent Mixtures," *Chem. Engng. Sci.* **1977**, 32, 1197.
- Krishna, R., Martinez, H. F., Sreedhar, R., Standart, G. L., "Murphree Point Efficiencies in Multicomponent Systems," *Trans. IChemE.* **1977**, 55, 178.
- Krishna, R., Wesselingh, J. A., "The Maxwell-Stefan Approach to Mass Transfer," *Chem. Engng. Sci.* **1997**, 52, 861.
- Krishnamurthy, R., Taylor, R., "Absorber Simulation and Design Using a Nonequilibrium Stage Model," *Can. J. Chem. Eng.* **1986**, 64, 96.
- Kurtz, D. P., McNulty, K. J., Morgan, R. D., "Stretch the Capacity of High-Pressure Distillation Columns," *Chem. Eng. Progress*, February **1991**, 43.
- Licht, S.E., Weiland, R. H., "Density and Physical Solubility of CO₂ in Partially Loaded Solutions of MEA, DEA and MDEA," Presented at the AIChE National Meeting **1989**, Paper No. 57f, Houston, Texas.

- Linek, V., Hrma, P., "Enhancement of Absorption Caused by Density Driven Convection at Gas-Liquid Interface Induced by Absorption with Chemical Reaction." *Chem. Eng. Sci.* **1976**, 31, 97.
- Littel, R. J., "Selective Carbonyl Sulfide Removal in Acid Gas Treating Processes," Doctoral Dissertation. Twente University of Technology. The Netherlands, 1991.
- Littel, R. J., Filmer, B., Versteeg, G. F., Van Swaaij, W. P. M., "Modeling of Simultaneous Absorption of H_2S and CO_2 in Alkanolamine Solutions: The Influence of Parallel and Consecutive Reversible Reactions and the Coupled Diffusion of Ionic Species," *Chem. Engng. Sci.* **1991**, 46, 2313.
- Littel, R. J., van Swaaij, W. P. M., Versteeg, G. F., "Kinetics of Carbon Dioxide with Tertiary Amines in Aqueous Solutions," *AIChE J.* **1990**, 36, 1633.
- Lockett, M.J., "The Froth to Spray Transition on Sieve Trays," *Trans. Inst. Chem. Engrs.*, **1981**, 59, 26.
- Lockett, M. J., *Distillation Tray Fundamentals*, Cambridge University Press, Cambridge, 1986.
- Mackowiak, J., "Determination of Flooding Gas Velocity and Liquid Hold-up at Flooding in Packed Columns for Gas/Liquid Systems," *Chem. Eng. Technol.*, **1990**, 13, 184.
- Martin, J. L., Otto, F. D., Mather, A. E., "Solubility of Hydrogen Sulfide and Carbon Dioxide in a Diglycolamine Solution," *J. Chem. Eng. Data*, **1978**, 23, 163.
- Meissner, R. E., Wagner, U., "Low-energy Process Recovers CO_2 ," *Oil & Gas Journal*, Feb. **1983**, 55.
- Miyahara, T., Asoda, M., Takahashi, T., "Gas-liquid Intrefacial Area and Liquid-phase Mass Transfer Coefficient in Sieve-Plate Columns Having Large Free Areas with Downcomers," *J. Chem. Eng. Japan*, **1990**, 23, 760.
- Mshewa, M., "Carbon Dioxide Desorption/Absorption with Aqueous Mixtures of Methyldiethanolamine and Diethanolamine at 40 to 120°C." Ph.D Dissertation, The University of Texas at Austin, 1995.
- Onda, K., Takeuchi, H., Okumoto, Y., "Mass Transfer Coefficients Between Gas and Liquid Phases in Packed Columns," *J. Chem. Eng. Japan*, **1968**, 1, 56.

- Pigford, R., L., "Counter-Diffusion in a Wetted Wall Column," Doctoral Dissertation, The University of Illinois, Urbana, Illinois, 1941.
- Pinsent, B. R. W., Pearson, L., Roughton, F. J. W., "The Kinetics of Combination of Carbon Dioxide with Hydroxide Ions," *Trans. Faraday Soc.* **1956**, 52, 1512.
- Posey, M. L., "Thermodynamic Model for Acid Gas Loaded Aqueous Amine Solutions." Ph.D. Dissertation, The University of Texas at Austin, 1996.
- Raal, J. D., Khurana, M. K., "Gas Absorption with Large Heat Effects in Packed Columns," *Can. J. Chem. Eng.* August **1973**, 51, 162.
- Rangwala, H. A., Morell, B. R., Mather, A. E. Otto, F. D., "Absorption of CO₂ into Aqueous Tertiary Amine/MEA Solutions," *Can. J. Chem. Engng.* **1992**, 70, 482.
- Reid, R. C., Prausnitz, J. M., Poling, B. E., *The Properties of Gases and Liquids*, McGraw-Hill Inc., Singapore, 1988.
- Rinker, E. B., Ashour, S. S., Sandall, O. C., "Kinetics and Modeling of Carbon Dioxide Absorption into Aqueous Solutions of N-methyldiethanolamine," *Chem. Eng. Sci.* **1995**, 50, 755.
- Rinker, E.B., Oelschlager, D.W., Colussi, A.T., Henry, K.R., Sandall, O.C., "Viscosity, Density, and Surface Tension of Binary Mixtures of Water and N-Methyldiethanolamine and Water and Diethanolamine and Tertiary Mixtures of These Amines with Water over the Temperature Range 20-100°C," *J. Chem. Eng. Data.* **1994**, 39, 392.
- Sandall, O. C., Rinker, E. B., Ashour, S., "Acid Gas Treating by Aqueous Alkanolamines," Annual Report for the Gas Research Institute, **1993**.
- Scheffe, R. D., Weiland, R. H., "Mass Transfer Characteristics of Valve Trays," *Ind. Eng. Chem. Res.*, **1987**, 26, 228.
- Seader, J. D. "The Rate-based Approach for Modeling Staged Separations," *Chem. Eng. Prog.* **1989**, 85, 41.
- Sivasubramanian, M. S., "The Heat and Mass Transfer Rate Approach for the Simulation and Design of Acid Gas Treating Units". Ph.D. Dissertation. Clarkson University. December, 1985.
- Snijder, E. D., te Riele, M. J. M., Versteeg, G. F., van Swaaij, W.P.M., "Diffusion Coefficients of Several Aqueous Alkanolamine Solutions," *J. Chem. Eng. Data.* **1993**, 38, 475.

- Spekuljak, Z., "A Criterion to Determine the Occurrence of the Marangoni effect in a Thin Liquid Film," *Chem. Engng. Sci.* **1987**, 42, 163.
- Subawalla, H. E., "Modeling, Simulation and Design of Reactive Distillation Columns," Ph.D Dissertation, The University of Texas at Austin, 1997.
- Tamimi, A., Rinker, E. B., Sandall, O.C., "Diffusion Coefficients for Hydrogen Sulfide, Carbon Dioxide, and Nitrous Oxide in Water over the Temperature Range 293-368K," *J. Chem. Eng. Data.* **1994a**, 39, 330.
- Tamimi, A., Rinker, E. B., Sandall, O.C., "Diffusivity of Nitrous Oxide in Aqueous Solutions of N-methyldiethanolamine and Diethanolamine from 298 to 368 K," *J. Chem. Eng. Data.* **1994b**, 39, 396.
- Taylor, R., Krishna, R., *Multicomponent Mass Transfer*. Wiley, New York, 1993.
- Thomas, W. J, Nicholl, E., "Interfacial Turbulence Accompanying Absorption with Reaction," *Trans. Instn. Chem. Engrs.* **1969**, 47, p. T325.
- Tomcej, R. A., Otto, F. D., "Improved Design of Amine Treating Units by Simulation Using Personal Computers," Presented at the World Congress of Chemical Engineering, Tokyo, Japan, 1986.
- Tomcej, R. A., Otto, F. D., Rangwala, H. A., Morrell, B. R., "Tray Design for Selective Absorption," Presented at the Gas Conditioning Conference. **1987**. Norman, Oklahoma, USA.
- Valerio, S., Vanni, M., "Interfacial Mass Transfer and Chemical Reaction in Non-Ideal Multicomponent Systems," *Chem. Engng. Sci.* **1994**, 49, 3297.
- Vanni, M., Baldi, G., "Mass Transfer and Chemical Reaction with Multicomponent Diffusion," *Chem. Engng. Sci.* **1991**, 46, 2465.
- van Swaaij, W. P. W., Versteeg, G. F., "Mass Transfer Accompanied with Complex Reversible Chemical Reactions in Gas-Liquid Systems: An Overview," *Chem. Engng. Sci.* **1992**, 47, 3181.
- Versteeg, G. F., Kuipers, J. A. M., van Beckum, F. P. H., van Swaaij, W. P. M., "Mass Transfer with Complex Reversible Chemical Reactions-I. Single Reversible Chemical Reaction," *Chem. Engng. Sci.* **1989**, 44, 2295.
- Versteeg, G. F., Kuipers, J. A. M., van Beckum, F. P. H., van Swaaij, W. P. M., "Mass Transfer with Complex Reversible Chemical Reactions-II. Parallel Reversible Chemical Reactions," *Chem. Engng. Sci.* **1990**, 45, 183.

- Versteeg, G. F., van Swaaij, W. P. M., "Solubility and Diffusivity of Acid Gases (CO_2 , N_2O) in Aqueous Alkanolamine Solutions," *J. Chem. Eng. Data*, **1988**, 33, 29.
- Versteeg, G. F., van Swaaij, W. P. M., "On the Kinetics Between CO_2 and Alkanolamines both in Aqueous and non-Aqueous Solutions-II. Tertiary Amines," *Chem. Engng. Sci.* **1988b**, 43, 587.
- Zarzycki, R., Chacuk, A., *Absorption, Fundamentals and Applications*. Pergamon Press. Oxford, Great Britain, 1993.
- Zheng, Y., Xu, X., "Study of Catalytic Distillation Processes. Part II. Simulation of Catalytic Distillation Processes-Quasi Homogeneous and Rate-Based Model," *Trans. IChemE.*, **1992**, 70, Part A, 465.
- Zuiderweg, F. J., "Sieve Trays, A View on the State of the Art," *Chem. Eng. Sci.*, **1982**, 37, 1441.
- Zuiderweg, F. J., Hofhuis, P.A.M., Kuzniar, J., "Flow Regimes on Sieve Trays: The Significance of the Emulsion Flow Regime," *Chem. Eng. Res. Des.*, **1984**, 62, 39.
- Warmuzinski, K., Tanczyk, M., "Marangoni Instability During Absorption of Carbon Dioxide into Aqueous Solutions of Monoethanolamine," *Chem. Eng. Process*, **1991**, 30, 113.
- Winkelman, J.G.M., Brodsky, S. J., Beenackers, A.A.C.M., "Effect of Unequal Diffusivities on Enhancement Factors for Reversible Reactions: Numerical Solutions and Comparison with DeCoursey's Method," *Chem. Engng. Sci.* **1992**, 47, 485.

Vita

Manuel Antonio Pacheco was born in Barcelona, Venezuela, on February 20, 1971, the son of Manuel Pacheco and Maria Gonzalez de Pacheco. After completing his studies in Italo Venezolano High School, Puerto la Cruz, Venezuela, in 1987, he attended Universidad Metropolitana in Caracas, Venezuela, from 1988 to 1992. As a partial requirement for the bachelor degree, he joined a project at the Center for Research and Development of the Venezuelan Oil Industry (Intevep) where he worked for ten months in the area of modeling and simulation of etherification reactors. After receiving the Bachelor of Science degree in Chemical Engineering in October 1992, he was temporarily employed as an instructor in Universidad Metropolitana where he taught a basic Chemical Engineering course for one semester. In August 1993, he entered The Graduate School at the University of Texas at Austin under the supervision of Dr. James R. Fair. In May 1995, he completed a Master in Chemical Engineering and soon after he started the Ph.D. program under the supervision of Dr. Gary T. Rochelle.

Permanent address: Las Acacias Avenue, Res. El Amanecer, Piso 3-C. La
Florida, Caracas 1050. Venezuela.

This dissertation was typed by the author.